NASA CR-120787
71-AEG-297

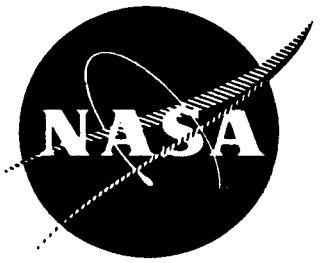

LF460 DETAIL DESIGN

GENERAL ELECTRIC COMPANY

prepared for

NATIONAL AERONAUTICS AND SPACE ADMINISTRATION

NASA-Lewis Research Center

Contract NAS3-6056

Laurence W. Gertsma, Project Manager

Requests for copies of this report should be referred to

National Aeronautics and Space Administration
Scientific and Technical Information Facility
P. O. Box 33
College Park, Maryland 20740

1. Report No.	2. Government Accession No.	3. Recipient's Catalog No.
NASA CR-120787		

4. Title and Subtitle	5. Report Date
LF460 DETAIL DESIGN	September, 1971
	6. Performing Organization Code

7. Author(s)	8. Performing Organization Report No.
	71-AEG-297
	10. Work Unit No.

9. Performing Organization Name and Address	11. Contract or Grant No.
General Electric Company Aircraft Engine Group Cincinnati, Ohio 45215	NAS2-6056
	13. Type of Report and Period Covered
12. Sponsoring Agency Name and Address	Contractor Report
National Aeronautics and Space Administration Washington, D.C. 20546	14. Sponsoring Agency Code

15. Supplementary Notes

Project Manager - Laurence W. Gertsma, Fluid System Components Division, NASA Lewis Research Center, Cleveland, Ohio

16. Abstract

This is the final technical report documenting the detail design of the LF460, an advanced turbotip lift fan intended for application with the YJ97-GE-100 turbojet gas generator to a V/STOL transport research aircraft. Primary objective of the design was to achieve a low noise level while maintaining the high thrust/weight ratio capability of a high pressure ratio lift fan. Report covers design requirements and summarizes activities and final results in the areas of aerodynamic and mechanical design, component and system performance, acoustic features and final noise predictions.

17. Key Words (Suggested by Author(s))	18. Distribution Statement
Turbotip Lift Fan Tip-Turbine Lift Fan Lift Fan Detail Design of a Turbotip Lift Fan	Unclassified - Unlimited

19. Security Classif. (of this report)	20. Security Classif. (of this page)	21. No. of Pages	22. Price*
Unclassified	Unclassified	242	$3.00

* For sale by the National Technical Information Service, Springfield, Virginia 22151

TABLE OF CONTENTS

TABLE OF CONTENTS

TABLE OF CONTENTS

TABLE OF CONTENTS

TABLE OF CONTENTS

LIST OF TABLES

LIST OF TABLES

LIST OF FIGURES

LIST OF FIGURES

LIST OF FIGURES

LIST OF FIGURES

LIST OF FIGURES

LIST OF FIGURES

SECTION I

SUMMARY

This report is the final technical report documenting the results of the LF460 turbotip lift fan detail design, carried out during the period from April, 1970 to May, 1971 under Contract NAS2-6056.

The LF460 is a 60 inch (fan) diameter advanced turbotip lift fan with a fan aerodynamic design pressure ratio of 1.35 and a fan tip speed of 1125 feet per second. The fan turbine is designed to accept the full exhaust flow of the General Electric YJ97-GE-100 turbojet gas generator.

The LF460 lift fan is designed to satisfy the requirements of a projected V/STOL transport research aircraft which will provide technology information required for the design of future commercial V/STOL transports.

The final fan layout is shown on the following page. As indicated by the layout, the LF460 is designed primarily for a shallow inlet installation where the upper aircraft structure blends into the inlet bellmouth provided with the fan system. Optional installation with a deep inlet, or as a cruise fan is possible providing the inlet diameter at the juncture with the bellmouth is at least 69 inches in diameter in order to minimize changes in the flow conditions at the fan tip.

The exhaust system of the fan is designed for operation in combination with thrust vectoring louvers, although the louvers are not provided as an integral part of the fan system, nor is the structure designed to permit direct mounting of a louver system to the fan. Similarly, the fan front frame has not been designed to accept an inlet closure system because of the dependency of a closure system on a particular aircraft system. Should it be desirable to mount an inlet closure system directly to the fan structure, the effects on front frame design and weight would have to be determined.

The LF460 is designed for application in a multiple fan installation

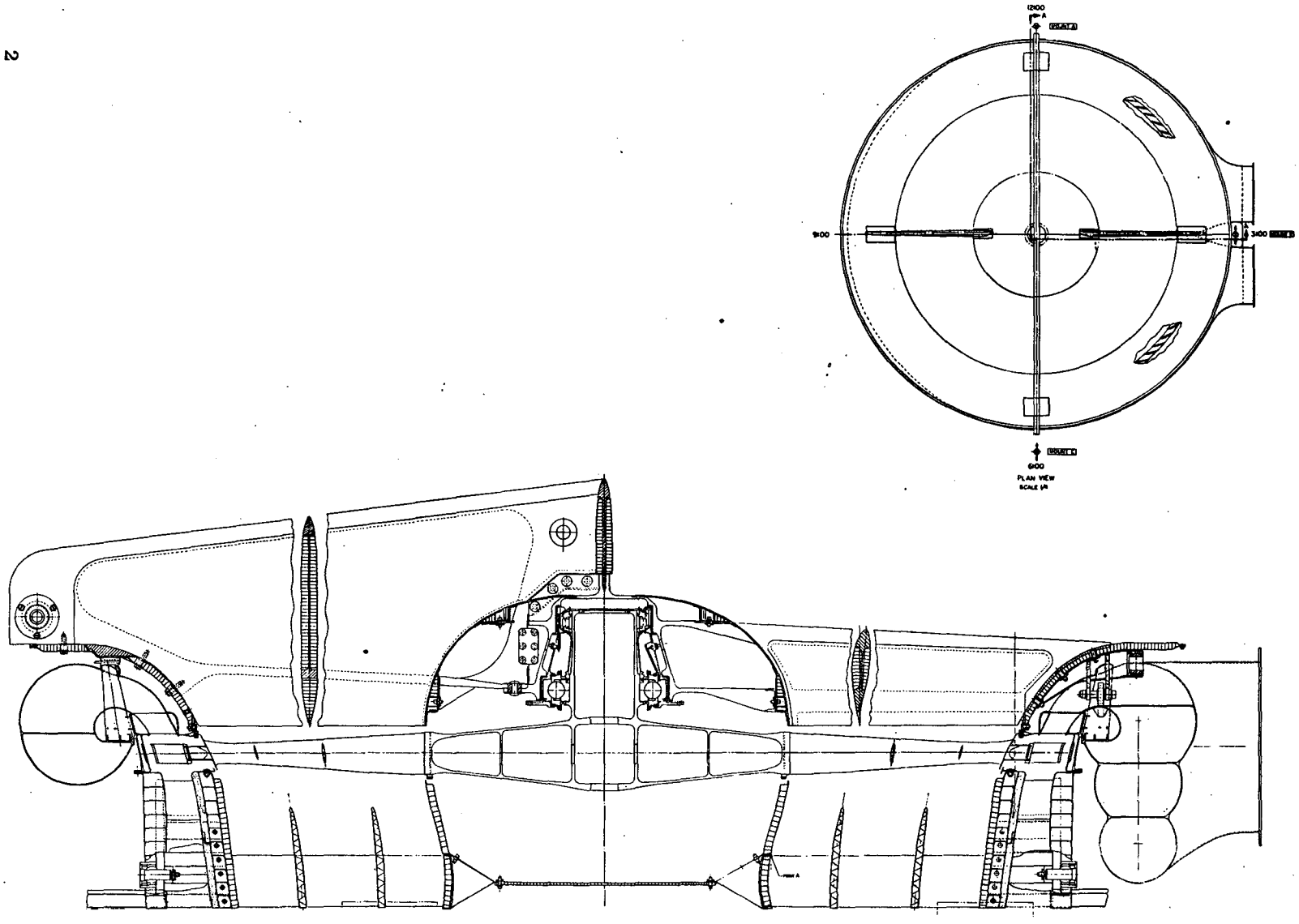

LF460 Lift Fan Layout

with the fans and gas generators interconnected to provide for aircraft attitude control and to meet engine or fan-out operating requirements with a minimum number of propulsion units. Use of the lift unit for lift and aircraft control requires a different approach in the fan design. During V/STOL operation, the lift from individual fans will continually vary to satisfy the aircraft control requirements. To establish the design requirements of the LF460, a representative V/STOL transport research aircraft mission was assumed, and a duty cycle was defined relating fan operating conditions (speed, inlet pressure, inlet temperature) to the percent time required at the given operating condition to satisfy the mission and aircraft control requirements. This represents one of the first attempts at designing an integrated propulsion system for a V/STOL aircraft. Additional analysis and further study of V/STOL systems will be required to refine and optimize this approach.

Utilizing the established duty cycle, each of the fan components was designed for a given life without repair and an ultimate life with repair as specified in the following table:

Component	Minimum Life Without Repair	Ultimate Life With Repair
Front Frame	2400 hours	6000 hours
Scroll	600	1200
Rear Frame	2400	6000
Fan Honeycomb Seals	600	1200
Fan Blades	600	1200
Fan Disk	2400	6000
Buckets and Carriers	600	1200
Bearings and Seals	600	600
Sump Components	600	600

It should be noted that the life values shown correspond to total aircraft flight hours. The ultimate life is divided into the following categories:

% of Ultimate Life	Aircraft/Fan Operational Mode
35	V/STOL (Duty Cycle applies)
44	Cruise: Speed < 250 knots Altitude < 5000 feet
5	Cruise - Ferry mission
16	Idle

If the fan is used to provide thrust during the cruise modes, its operational life and design life coincide. However, if the fan is not used to provide cruise propulsion, the fan operational life required is considerably shorter than the design life which is based on aircraft flight hours.

Propulsion systems for V/STOL aircraft will be subjected to higher rates of cyclic exposure than conventional propulsion systems. Assuming 6 start-stop cycles for each 33-minute mission, and allowing for ground start-stop cycles, a requirement of 12 start-stop cycles per hour was established for the fan design. For the fan hot parts having an ultimate life of 1200 hours, this results in a total requirement of 14,400 start-stop cycles. In addition to start-stop cycles, V/STOL propulsion units utilized for aircraft attitude control will be subjected to a large number of short duration cyclic changes due to control system inputs. Helicopter and V/STOL aircraft operating experience was used to establish the short time cyclic exposure design criteria for the LF460. Other factors included in the definition of the overall design requirements were: the flight envelope; maneuver loads; engine-out operation; and operation in crossflow.

Referring again to the fan layout, the major geometry features are summarized in the following table:

	Fan	Turbine
Tip Diameter (in)	59.95	66.65
Radius Ratio	0.454	0.94
No. of Rotor Blades	88	264
Rotor Blade Aspect Ratio	5.84	1.43
No. of Stator Vanes	56	157
Stator Vane Aspect Ratio	3.99	0.65-1.04 (3 families)
Turbine Bucket Height (in)	-	2.06
Turbine Admission Arc (°)	-	360

The basic fan aerodynamic design parameters are:

Corrected Air Flow - 617 lb/sec	Total Pressure Ratio - 1.35
Specific Flow - 39.65 lb/sec/ft^2	Static Pressure Ratio - 1.025
Corrected Tip Speed - 1125 ft/sec	Efficiency - 80.3%
Rotor Tip Rel. Mach No. - 1.262	Hub Work Coef. - 2.14 ($2gJ\Delta h/U^2$)

The fan airflow is established by the available turbine energy, fan pressure ratio and fan efficiency. Previous experience has shown that for fans with pressure ratios above 1.3 specific flows greater than 40 lb/sec/ft^2 require extremely thin airfoils (not consistent with tip turbine fan design requirements) and/or high incidence angles to pass the flow without choking. The fan airflow and selected specific flow establish the rotor inlet annulus area.

Rotor tip speed was selected to provide adequate stall margin for a given number of rotor blades without excessive hub solidity. The selection of the numbers of blades and vanes was primarily defined by mechanical and acoustic considerations.

The minimum radius ratio was dictated by the combination of rotor tip speed, fan pressure ratio and the selected maximum permissible hub work coefficient. The radius ratio in combination with the rotor inlet annulus area establish the fan tip diameter.

In the selection of the fan static pressure ratio, consideration was given to the effects of possible thrust vectoring systems which create fan back pressure. A representative exit louver system was used to establish the 1.025 design exit static pressure ratio.

A large number of high aspect ratio rotor blades are required to achieve an acceptable rotor polar moment of inertia, and a high blade passing frequency. The selected aspect ratio (5.84) requires that two part-span dampers be used to meet system dynamic requirements.

The 56 fan stator vanes are leaned 18° in the direction of rotation at the hub. The introduction of stator lean is based on acoustic considerations. To prevent choking at the stator hub, it was necessary to contour the stator flowpath walls to permit the flow to curve radially outward, as can be seen in the fan layout. Two stator part-span splitters are included based on mechanical and acoustic considerations. Splitter losses were added to produce a 2% fan efficiency decrement for each splitter.

It is noted that the selection of the fan rotor and stator aspect ratios and solidities are based on extrapolations of General Electric solidity/aspect ratio correlations. However, the absolute values are beyond General Electric experience for aerodynamic loadings of this level. Fan aerodynamic tests are required to substantiate the design.

The turbine aerodynamic design point parameters are summarized in the following table:

Inlet Total Temperature (°R) - 2060	Design Energy (Btu/lb) - 115.3
Inlet Total Pressure (lb/in^2) - 54.74	Exit Axial Mach Number - 0.6
Inlet Gas Flow (lb/sec) - 76.22	Overall Efficiency - 0.832
Total to Static Pressure Ratio - 3.85	Stage Velocity Ratio U/Vo - 0.42
Total to Total Pressure Ratio - 3.05	Stage Work Function - 0.991 ($gJ\Delta h/2U^2$)

The LF460 turbine is a 360° admission turbine fed by two independent 180° admission scrolls. The flowpath at the rotor centerline has a 15° inward slope to be compatible with the fan outer flowpath. The turbine is basically of the axial flow type and has been designed according to axial flow principles.

It is important that the turbine bucket be kept as short as possible to minimize rotor weight and polar moment of inertia. This dictated the use of a high turbine exhaust Mach number. A Mach number of 0.6 was selected as the maximum that could be used with assurance of good performance. A high area ratio diffuser is used at the discharge from the turbine rotor to (a) provide a low static pressure at turbine discharge to assure that flow leakage will always be from the fan stream to the turbine stream, (b) to provide a low pressure sink for the rear frame mid-box cooling air, and (c) reduce the turbine stream discharge velocities to minimize the overall jet noise floor.

One of the most significant turbine design parameters affecting the design is the high stage total to static pressure ratio (3.85). The pressure ratio combined with the impulse design approach results in a high stator discharge Mach number. Using available cascade data, it was estimated that a simple converging nozzle design operating at this pressure ratio would have an efficiency approximately 4 percent lower than a converging-diverging nozzle. However, analyses indicated that if the convergent-divergent nozzle were designed for the full 3.85 pressure ratio, the turbine part-speed performance would be poor due to overexpansion in the nozzle. A compromise design was selected where the nozzles were designed for a total to static pressure ratio of 2.8. This corresponds to an exit to throat area ratio of 1.071. Available data indicated that with this design losses due to underexpansion at the turbine design pressure ratio would be quite small.

The diverging portions of the nozzle passages are all geometrically similar; however, the converging portions of the three nozzle families differ depending on their location in the scroll and their corresponding design inlet flow angles.

Although the bucket inlet relative Mach number is quite high (0.94), previous design and cascade test experience with a nearly identical bucket section has shown that reasonably good performance can be obtained with inlet Mach numbers of this level if the profile is properly designed.

The turbine exit diffuser contains eight equally-spaced struts which are staggered 7° from axial to line up with the turbine exhaust swirl at the design point.

The major fan components shown in the fan layout are the front frame, scroll, rotor and rear frame.

The front frame is the main structural support of the lift fan assembly. It transfers all rotor loads (gyroscopic moments, inertia forces and lift), as well as bellmouth - scroll lift and rear frame axial loads to the main airframe mounts. The front frame components include: a continuous 360° steel honeycomb bellmouth; an aluminum (bonded structure) major strut; two aluminum minor struts cast integrally with the center hub structure; and a fiberglass dome. The front frame also supports the forward air seal assembly, which minimizes hot gas leakage from the turbine stream to the fan stream.

The triple bubble scroll concept was selected to minimize both fan depth and diameter. The scroll assembly is divided into two independent 180° admission scrolls to permit fan operation under engine-out conditions when only one half of the flow of a gas generator is available to the fan. Each 180° scroll is divided into three separate ducts in the scroll inlet section. The flows in the three ducts are not kept separate for the entire length but are merged again at locations just upstream of the scroll struts. Flow enters the scroll at a 0.3 flow Mach number and is accelerated to approximately 0.35 Mach number in the circumferential passages. The scroll is fabricated from René 41 and can operate at temperatures to a maximum of 1600°F in accordance with the selected duty cycle.

The rotor is an overhung single stage fan with a concentric tip turbine drive. There are 88 high aspect ratio fan blades which have two part-span shrouds to control torsional flutter and other blade vibrations. The fan blades are made from high strength René 95. The turbine consists of 88 sectors, each containing three shrouded, Udimet 700 buckets. Each of the three bucket turbine sectors is brazed to a fan blade to form an integral fan blade/tip turbine component. This design approach results in a significant weight savings and reduction in polar moment of inertia when compared with previous lift fan designs where a mechanical joint (clevis with a bolt) was used to attach the turbine to the fan blade. The turbine is designed to allow use of a single braze cycle compared to the multiple braze cycles required for previous carrier fabrication.

A René 95 material/braze joint data development program is currently in process to define the properties of René 95 under the required heat treat conditions, select the best available braze and braze techniques, and establish braze joint properties. This program is scheduled for completion in December, 1971 with a final report to be submitted by mid-January, 1972.

The rotor disk utilizes twin web geometry, similar in concept to that used on previous lift fans. The two-piece titanium disk is electron beam welded at the rim and brazed at the spacers.

The bearings have inner-race rotation similar to the LF1 lift fan utilized in the XV-5 aircraft. Silverplated bronze cages are used to minimize power loss. Vacuum melt M50 bearing material is used in the races, rollers and balls. The roller bearing employs an out-of round inner ring which loads the rollers to prevent skidding.

The bearings are lubricated with Unitemp 500 grease. A regrease system is included in the design to permit regrease of the bearings from external fittings on the bearing housing. A similar regrease system was recently added to one of the LF336 fans. Regrease interval requirements can be estimated as LF336 test experience is accumulated.

The LF460 has a common bearing housing not used on previous lift fans. This packaged self-contained bearing sub-assembly can be removed as a unit, and permits the rotor to be balanced on its own bearings prior to fan assembly.

The fan rear frame consists of: a composite aluminum/titanium/fiberglass hub assembly; 56 hollow titanium fan stator vanes; two part-span titanium/fiberglass acoustic splitters; a titanium/steel/fiberglass midbox; eight titanium turbine struts with steel heat shields; steel turbine exhaust liners; and a René 41 casing. The turbine struts and the midbox are cooled with air taken from the aircraft cavity and exhausted from the turbine struts into the turbine discharge stream. The casing transfers the rearframe loads to the scroll.

Component and total fan system weights are summarized in the following table:

	Weight (lbs)
Front Frame	127.0
Scroll	267.5
Rotor	230.8
Rear Frame	129.7
Sub-Total	755.0
Development Margin	34.0
Total	789.0

The final calculated rotor polar moment of inertia (Ip) is 18.6 lb/ft/sec^2 versus the original objective of 22.5. An Ip value of 19.5 lb/ft/sec^2 will be used for quotation purposes.

Preliminary performance estimates for the LF460/YJ97-GE-100 system were made during the first quarter of 1971 to support transport research aircraft concept definition studies conducted by the aircraft companies. These data were published in the LF460/YJ97-GE-100 PRELIMINARY PERFORMANCE

AND INSTALLATION DATA bulletin dated March 1, 1971.

Final performance data for the LF460/YJ97-GE-100 system are being prepared in the form of a customer computer deck for use on the IBM 360.

Static performance at the noise rating point and maximum control point are presented in the following tabulation:

	Sea Level Static, Nominal Rating*	Standard Day Maximum Control
YJ97-GE-100 EGT (°R)	1835	2060
Fan Airflow (lb/sec)	568	628
Fan Pressure Ratio	1.29	1.36
Fan RPM (%)	93.0	103.9
Turbine Inlet Pressure (psia)	47.2	54.7
Gas Generator RPM (%)	101.5	101.5
Bypass Ratio	8.17	8.24
Thrust (lbs)	12,216	15,057
SFC	0.389	0.413

* Noise rating point

The data shown represent installed data for a typical aircraft installation. Performance of the LF460 at the noise rating point is based on the flow of a single YJ97-GE-100 engine operating at its rated exhaust gas temperature (EGT). Operation at the maximum control point can only be achieved by operating the engine at a short-time overtemperature condition with flow addition from a second cross-coupled engine.

The objective in the design of the LF460 was to achieve a low noise level consistent with the high thrust/weight ratio capability of a high pressure ratio turbotip lift fan. The final noise level of the LF460 was achieved by (a) reducing fan generated noise, and (b) applying acoustic suppression.

Reduction of fan generated noise was accomplished by application of several design techniques. A large number of fan rotor blades (88) was selected, resulting in a puretone frequency of 6300 Hz, which is well above the 2828 to 4480 Hz band width most heavily weighted for PNdB calculations. The high puretone frequency also takes advantage of higher atmospheric and ground attenuation levels available at higher frequencies. A two chord spacing is used between the fan rotor and stator. With a rotor tip solidity of 1.32, the fan generated wakes which interact with the stator to produce the major noise are significantly attenuated. The high aspect ratio, short chord rotor blades result in minimum fan depth for the selected two chord spacing criteria. The stator configuration was selected to provide minimum noise through proper vane number selection and application of leaned stator vanes to reduce the interaction effect of the rotor wakes. The jet noise floor was kept well below the fan generated noise by diffusing the turbine exhaust flow to a low velocity, providing a good balance between the fan jet and turbine jet noise levels.

The fan noise was suppressed by the use of acoustically treated fan exhaust duct splitters in addition to hub and outer wall treatment. Application of acoustically treated exhaust louvers was also included in the noise predictions.

The final total noise prediction is 99.5 PNdB without exit louvers and 97.3 PNdB with acoustically treated exit louvers. These noise levels are for the LF460 noise rating point (1835°R YJ97-GE-100 exhaust gas temperature), 500 ft sideline, single fan, and standard day conditions. The maximum noise occurs at an altitude of 200 feet, which results in an acoustic angle of 113 degrees.

A reduction of installed fan noise can be accomplished through the use of additional acoustic treatment in the aircraft installation, particularly in those cases where the fan is mounted in the fuselage or as a cruise fan. It is estimated that with installation treatment

the noise of a six fan transport research aircraft will be in the range of 100 to 103 PNdB at a 500 ft sideline.

No credit has been assumed for possible reduction of aircraft noise levels due to tailored aircraft flight paths, thrust scheduling and vectoring of the lift and cruise engines. Noise contour studies for CTOL and STOL aircraft have shown appreciable improvements in the ground noise contours. These effects for VTOL aircraft should be evaluated as a part of the aircraft system studies.

SECTION II

INTRODUCTION

For the past five years, the General Electric Company has been actively engaged in a joint effort with the NASA to define, through studies and demonstration programs, advancements in component and system technology which will lead to advanced lift fan systems applicable to V/STOL flight research and transport aircraft. Specific objectives of these programs include improvements in the areas of performance, weight, size, time response, reliability and maintainability, and evaluation of acoustic features which will permit development of quiet lift fan systems.

The NASA-sponsored LF336 lift fan program, initiated early in 1967, included the design and development of two advanced turbotip lift fan aerodynamic and acoustic test vehicles. An extensive series of test programs have been conducted in the NASA, Ames 40 x 80 wind tunnel and at the GE Edwards acoustic test facility, utilizing the LF336 test vehicle to evaluate aerodynamic and acoustic design features applicable to advanced lift fan systems. This program, which is a continuing technology research program, is currently funded through December, 1972.

Studies were initiated by the NASA and the General Electric Company in 1968 to define an advanced, high pressure ratio, turbotip lift fan system which would take advantage of available higher energy gas generator power sources, with potential application to a modified XV-5 aircraft for flight test research. The LF446, a 1.35 pressure ratio, 46 inch diameter turbotip lift fan was designed for future application with a projected advanced engine cycle (GE1/10); however, recognizing that this advanced cycle would not be available in time for the planned LF446 flight demonstration, the YJ97-GE-100 turbojet gas generator was selected as the most promising candidate for the XV-5 flight demonstration program.

In late 1969, the program was redirected by the NASA toward a research aircraft that would provide flight technology information that would be required in the design of future V/STOL commercial transports. The LF446 lift fan utilized only part of the available flow from the YJ97-GE-100 gas generator. With the change in direction of the research aircraft program, the LF446 was scaled-up in size to take advantage of the full flow capability of the YJ97 engine. The resulting 60 inch lift fan configuration was called the LF460 advanced turbotip lift fan.

Preliminary design studies of the LF460/YJ97-GE-100 system were conducted in the late 1969, early 1970 time-period to define an advanced lift fan which would satisfy the requirements of a V/STOL transport research aircraft. Strong emphasis was placed on achieving low fan noise while maintaining the high thrust/weight capability of the high pressure ratio lift fan system. Results from the LF336C acoustic test program were used as they became available to modify or refine the LF460 design, including such features as rotor blade-stator spacing, stator lean and acoustic treatment.

Detail design of the LF460 was initiated in April, 1970, under contract to NASA, Ames. The major requirements of this program were: completion of detail design, including manufacturing drawings; development of preliminary design and off-design system performance; prediction of fan noise characteristics; and, preparation of manufacturing cost estimates.

Program responsibility was transferred from Ames to the Lewis Research Center, effective September 30, 1970. The contract was modified in the early part of 1971, deleting the requirement for manufacturing drawings, but adding two technical tasks: (1) Preparation of final LF460/YJ97-GE-100 performance data, and (2) René 95 material/brazed joint data development.

Detail design of the LF460 lift fan was completed in May, 1971. The final fan layout is shown in Figure 1. This report documents the fan detail design activity and program results.

A customer performance deck, being prepared for use on the IBM 360 computer, should be available the latter part of July, 1971. A user's manual will be prepared as a part of the deck construction activity.

Current plans call for completion of the René 95 material/brazed joint data development program in December, 1971. A separate final report covering this phase of the work will be issued in January, 1972.

SECTION III

DESIGN REQUIREMENTS

A. GENERAL SYSTEM REQUIREMENTS

The LF460 remote lift fan is designed to meet the anticipated requirements of a typical V/STOL transport research aircraft. To establish design requirements, certain assumptions concerning the system must be made to define the operating environment of the propulsion systems. For example, it has been assumed that the aircraft attitude control system will use modulation of fan thrust to obtain control moments in the VTOL operating regime. In addition, the requirement for control from the lift units will be programmed proportional to aircraft flight speed. These assumptions are only two of the many required in the definition of a realistic set of design requirements. In the following discussion, the assumptions used in the analysis will be presented.

The procedures developed and used in the definition of the LF460 Duty Cycle represent a first attempt at designing for the integrated propulsion system requirements of a V/STOL aircraft. Additional analysis and further study of V/STOL systems are required to refine and optimize the integrated design approach. The requirements established by the procedures and analysis to be described should provide a lift fan unit optimized to the V/STOL system. This trend was obvious during the design of the LF460, where considerable weight reductions were accomplished for certain components, primarily those subjected to the high temperature discharge flow of the gas generator.

B. THE V/STOL MISSION

The V/STOL mission selected was based on numerous V/STOL system studies and an estimation of the probable type of flight test programs that would be conducted using the transport research aircraft.

For example, it is reasonable to assume that the research aircraft will operate in the V/STOL mode for longer duration than an operational aircraft; that is, the cruise mode of operation will be relatively short and at low speed and attitude. Also, it is reasonable to assume that several take-off and landings will occur during a particular flight, based on the estimated fuel loads of the aircraft. Using these assumptions, the V/STOL mission defined in Table I was selected as a basis for establishing the fan design requirements.

During this mission, there are three phases where the propulsion system is required to provide all or part of the aircraft control moments. These three phases are take-off, decent and landing. Since the attitude control requirements imply a continuously time-varying thrust level, some type of statistical analysis was required to describe the LF460 duty cycle for these three parts of the mission. The idle and cruise phases represent relatively steady-state operation and can be treated in the conventional manner for CTOL propulsion systems.

C. DUTY CYCLE ANALYSIS

During the V/STOL mode of flight, the attitude control of the aircraft is assumed to result from a combination of lift unit thrust modulation and conventional aerodynamic control. The effectiveness of the conventional aerodynamic controls was assumed to increase, with flight speed dynamic pressure, with only conventional control required at the maximum transition speed of 150 knots. To maintain a constant total control power at all speeds between hover and maximum transition speeds, the levels of lift unit modulation are required to vary from maximum at hover to complete phase-out at transition speed. The maximum total control requirements were assumed to be equal to the capability designed into the LF460/YJ97 system, that is plus or minus about 25 percent lift change. This level is typical of the requirements of a V/STOL aircraft system.

A second major input required for the duty cycle analysis is a definition of the V/STOL flight path. The assumed power-speed-time

spectrum for the V/STOL mission is presented in Figure 2.

One of the most significant parameters required for the establishment of the LF460 duty cycle, is the control utilization requirements as shown in Figure 3. This characteristic is based on a statistical approach to control level probability. For example, if the control power level is adequate for the system, the 100 percent control requirement will never be utilized. Secondly, the neutral or zero percent control level will always be exceeded. These two conditions establish the two end points of the curve in Figure 3. The third point on the curve was established by assuming 50 percent control will be required only 25 percent of the total operating time. This assumption agrees with typical control requirements of helicopters and experience gained during XV-5A flight testing. A probability curve was then drawn through these three points as shown in the figure.

Another assumption that has a secondary effect on the analysis, is that the LF460 fan unit's constant power overspeed due to crossflow distortion will be 5 percent at 150 knots aircraft speed.

The most significant assumption used in the analysis (later verified by additional studies) is that the total thrust variation for control will be 25 percent of the maximum neutral control lift of the LF460. Cycle analysis of the LF460 showed a total lift variation of 22 percent based on YJ-97 engine cycle restrictions as will be discussed later. The additional three percent control was assumed to occur with a slight loss in total system lift.

The control system for the LF460 assumes some method of power transfer to produce the approximate fan unit operating conditions shown in Figure 4. These are only approximate performance parameters used in the duty cycle analysis. As the design of the LF460 progressed, minor changes in performance occurred due to design modifications such as the addition of stator lean and acoustic splitters. Because of the approximate nature of this analysis, the redefinition of the

LF460 duty cycle to reflect these changes was not warranted.

A time share computer program was developed to integrate the individual time intervals of operation in the various phases of the mission. The duty cycle was then established for two significant design parameters, fan rotational speed and hot gas total pressure for selected ranges of gas generation discharge total temperature. The fan rotational speed along with gas temperature establish the criteria for rotor and cold static structure design. The pressure-temperature duty cycle applies primarily to design of hot gas ducting such as the scroll system. The duty cycle that was established by this procedure and used as a basis for the LF460 design is summarized in Figures 5 and 6. The increments shown in the graphical presentations integrate to a total of 100 percent time. This integrated time applies only to those phases of the mission when the system is in the V/STOL mode, or a total of about 37 percent of total design life. The remaining component life applies to the CTOL cruise mode (46 percent) and engine idle (17 percent).

D. FERRY MISSION

The need for ferry capability for the V/STOL transport was also included in the design of the LF460. Since the fan unit is capable of operating as a cruise fan unit, the system design requirements include consideration of the ferry mission shown in Table II.

It was assumed that the ferry mission accounted for 5 percent of the total component design life; thus, the remaining 95 percent of the design life is based on the V/STOL mission previously defined.

E. DESIGN LIFE REQUIREMENTS

The components of the LF460 were designed for a minimum life without repair and an ultimate life with repair as specified in Table III.

The total life of the system was divided into the following general categories.

- 35% of total life in the V/STOL mode with a duty cycle as defined in Figures 5 and 6.

- 44% of total life cruising at speeds less than 250 knots and altitudes less than 5000 feet.

- 5% of total life operating in the cruise mode as defined by the ferry mission.

- 16% of total life at idle conditions.

The fan design life essentially represents total aircraft flight hours. If the fans are used to provide thrust during the cruise mode the fan operational life and design life are the same. However, if the fans are inoperative during the cruise mode, the fan operational life is considerably shorter than its design life (aircraft flight hours).

F. CYCLIC REQUIREMENTS

Propulsion components and systems for V/STOL aircraft are subjected to a higher rate of cyclic exposure than a conventional propulsion system. In addition, a research V/STOL transport will require a more severe cyclic design requirement because of the large percentage of operation in the V/STOL mode versus the conventional cruise mode.

The number of start-stop cycles is based on the mission shown in Table I. For this mission, the propulsion units will be subjected to a total of 6 cycles for a 33-minute mission. Allowing for additional ground start-stop cycles, a design requirement of 12 cycles per hour of operation was included in the LF460 design. The number of cycles applies to the total design life of the components.

In addition to start-stop cycles, propulsion systems for V/STOL aircraft are subjected to a large number of cyclic changes due to attitude control system inputs. A survey of existing helicopter and

V/STOL control experience shows that the average frequency for aircraft control inputs is between 0.5 and 1.5 excursions per minute. Using this criteria, and the V/STOL mission requirements, a control cyclic exposure criteria was established for the LF460 system. The cyclic requirement is presented in Table IV. The number of design cycles per hundred hours of life are shown for the significant duty cycle parameters of speed, temperature and pressure. The cyclic requirement for each parameter is presented as a mean or average value and the level (single amplitude or mean to peak) of the vibratory or cyclic component.

These two criteria imply a low and high cycle design criteria for the components of the LF460 lift system.

G. FLIGHT ENVELOPE

The flight envelope established for the LF460 is shown in Figure 7. This envelope applies to the LF460 when operating in either the V/STOL or CTOL (cruise) modes. The engine power spectrum for the V/STOL mode of operation is as shown in Figure 8.

H. MANEUVER LOADING

Maneuver load requirements for the LF460 are divided into categories depending on the particular mode of operation. The maneuver loads for operation in the V/STOL mode are presented in Figures 9 through 11. These loads can occur simultaneously with the aerodynamic loading due to scroll piston forces, and forces due to crossflow. The design criteria for the loads are as follows:

- Steady Flight - Continuous application of the maneuver loads in Figure 9 plus the aerodynamic loading due to operation in the V/STOL mode for a range of power settings as defined by the V/STOL duty cycle.

- Landing - Simultaneous application of the maneuver loads of Figure 10 plus the aerodynamic loading for the range of zero

to maximum fan lift with or without control inputs. The occurrence rate is once every 0.15 hours of operation for two seconds.

- Transitional Flight - Simultaneous application of the aerodynamic loadings at maximum power and 150 knots transitional speed plus the maneuver loads in Figure 11. It is assumed that this condition, which provides the design criteria for rotating component clearances, occurs once each ten hours of operation for a duration of five seconds each occurrence during the life of the components.

The maneuver load criteria for operation of the LF460 as a cruise propulsion unit during CTOL flight is defined by Figures 9, 12 and 13. The criteria for application of these loads are as follows:

- Steady Flight - Continuous application of the maneuver loads in Figure 9 and the propulsion system loads at any power setting within the CTOL flight envelope shown in Figure 7.

- CTOL Landing - Application of the maneuver loads of Figure 12 with fan power off but with all components at their respected rated operating temperature.

- Unpowered Flight - Application of the maneuver loads of Figure 13 with fan power off but with all components at their respected rated operating temperature.

I. ENGINE OUT OPERATION

The LF460 design is capable of engine-out operation, or operation using 50 percent of the flow from a single gas generator. This requirement establishes the need for the double entry scroll with two separated flowpaths, each covering an 180 degree arc.

Operation in the engine-out mode is considered an emergency situation and not a normal operating procedure. The duration of single engine operation was established at a maximum of three minutes per event. In addition, it is reasonable to assume that the engine failure that requires this mode of operation will occur in flight; thus, steady state operation (essentially) has been established prior to the failure. This requirement plus the relatively short duration of operation relieves the thermal stress problem in the static structure components which develop when half of the fan is subjected to high temperature gas flows while the remaining half of the system is inactive.

The effects of this mode of operation are included in the analysis of the rotating and static components of the fan system.

J. OPERATION IN CROSSFLOW

One of the principal considerations included in the LF460 design is the requirement for operation in the flow environment established by the crossflow effects on a shallow inlet system. When a shallow inlet operates in the V/STOL transition envelope, there is a flow underturning effect that develops a large assymmetrical loading of the fan components. These variations of aerodynamic loading were factored into the LF460 design by considering two extreme operating conditions:

- Operation at 150 knots with the lift units at 100 percent design speed. It should be noted that this speed level exceeds the maximum power capability of the gas generator and thus represents a conservative design criteria.

- Operation at 150 knots following an engine failure. For this case, the fan unit was assumed to be operating with 50 percent flow from a single engine at a fan rotational speed of 70 percent of design.

The radial and circumferential aerodynamic load distributions

were estimated for these cases based on test experience obtained for shallow lift fans in crossflow. These load distributions will be presented later, and will be the basis for design of the LF460 to fulfill transition requirements.

SECTION IV

ACOUSTIC DESIGN AND ANALYSIS

A. DESIGN FEATURES

A primary objective of the LF460 design was to provide low noise levels consistent with the requirements of a high thrust/weight lift fan system for V/STOL transport research aircraft. To achieve low noise, the LF460 was designed to have: (a) a low level of noise generated without external suppression devices, and (b) the application of acoustic suppression as an integral part of the fan aerodynamic and mechanical design. These areas of noise reduction are summarized in the following paragraphs.

1. SOURCE REDUCTION

Fan generated noise was reduced through the use of high aspect ratio, short chord blades with moderate solidity. The blade number was relatively high (88) which resulted in a puretone frequency of 6300 Hz. The high frequency is well above the 2828 to 4480 Hz band width most heavily weighted for PNdB calculations, and also takes advantage of higher atmospheric and ground attenuation levels available at the higher frequencies.

The short chord blades result in minimum depth for a fan designed with two chord spacing between the fan rotor and stator. With a rotor tip solidity of 1.32, the fan generated wakes which interact with the stator to produce the major noise are attenuated significantly in the length provided by the two chord spacing.

The stator configuration was selected to provide minimum noise through the proper vane number selection consistent with 88 rotor blades. Significant reduction was also obtained by circumferentially leaning the stator vanes to reduce the interaction effect with the rotor wakes.

Jet noise was kept as low as possible by diffusing the turbine exit flow, reducing the turbine jet velocity. This provides a balance between the fan jet and turbine jet noise levels and keeps the jet noise floor well below the fan generated noise. For the current configuration, this allows the suppression devices to be more effective and also leaves room for additional suppression when the engine is installed in an aircraft. If the jet noise floor were not reduced, the allowable suppression would be greatly reduced.

2. SUPPRESSION

Fan noise was suppressed by the use of acoustically treated fan exhaust duct splitters and vectoring louvers. Both the treated splitters and exit louvers were selected to provide suppression at the critical frequencies in the noise spectrum. A scale model test of the exhaust splitters confirmed the suppression spectrum which was applied to the unsuppressed fan noise. The splitters were designed as an integral part of the fan duct flowpath from both an aerodynamic and mechanical viewpoint. The exit louvers were selected on the basis of solidity and blockage limitations in the fan flowpath.

B. SUMMARY OF LF460 ACOUSTIC PREDICTIONS

Initially, the LF460 was evaluated acoustically at the design point (100% fan speed, 1.35 p/p) and estimates were made as to the suppression obtainable from acoustically treated exhaust splitters and exit louvers. A source noise reduction due to stator lean was also estimated utilizing test results obtained from the LF336/C Modification and Acoustic Test Program.[1] On the basis of these assumptions, the noise level prediction for one fan at 500 ft sideline was 101.6. A summary of the approach and a list of values used in this prediction are presented in Table V.

Studies sponsored by NASA Lewis of advanced VTOL propulsion systems resulted in the definition of a noise rating point at 80% of design point thrust. This fan power setting is considered as the nominal

rated lift point, allowing 25% increase in lift for aircraft attitude control. Using this approach as a guide, subsequent LF460 acoustic predictions were based on the following assumptions:

- 500 ft sideline
- Takeoff power at 1835°R YJ97-GE-100 (nominal rated lift) EGT
- Single engine
- Standard day

After development of an analytical prediction technique for stator lean (Section IV.C) and completion of the exhaust splitter tests (Section IV.D), the LF460 was re-evaluated at the noise rating point using estimated part power cycle data. These results are shown in Table VI. During this time period an additional modification was made to the LF460 noise estimates. Testing of fan engines at NASA Lewis had indicated that the fan jet noise was significantly lower than the level predicted by an extrapolation of the standard SAE method to low jet velocities. Analysis of the data and additional data from GE cold jet tests resulted in a reduction of the cold, low velocity fan jet noise estimates by approximately 5 PNdB. The fan jet noise number shown on Table VI includes this modified cold jet noise prediction.

Utilizing finalized fan part power performance and design characteristics, another estimate was made for the LF460 at the noise rating point. These results are presented in Table VII. The fan noise and fan jet noise increased slightly while a significant reduction in turbine jet noise was achieved due to a modification in the turbine exit flowpath. The net result was a slight decrease in total noise due primarily to the reduction in the jet noise floor. As part of the final noise predictions, an estimate of the tip turbine generated broadband and puretone noise was made. Due to the high blade number, the puretone is beyond the PNdB spectrum but the broadband noise is still contributing to the floor noise. The results of this analysis indicated that the LF460 total noise level was 98.1 PNdB.

All acoustic predictions presented in Tables V through VII were based on a technique which utilizes a simulated VTO flight path. The simulation is accomplished by treating the 500 ft sideline distance as an altitude for a normal flyover case. Figure 14 shows the simulated case as compared to a true VTO. A difference of 1 to 2 PNdB can be expected for the two analysis techniques. The simulation is utilized for initial design comparisons and to arrive at a desired acoustic configuration. After the configuration is defined, a more elaborate prediction technique is used to calculate the noise for a true VTO flight path. Using the noise constituents as defined in Table VII the total engine noise was predicted for the true VTO case. The result of these predictions is shown on Table VIII. Included in these predictions was a final exit louver suppression spectrum. The final LF460 noise estimate was 97.3 PNdB at the noise rating point. Presented in Section IV.G are predictions with variation in altitude, sideline distance and power setting.

C. OGV LEAN ANALYSIS

The level of puretone or blade passing frequency noise is a function of the interaction between the wake from the rotor and the stator (OGV). By circumferentially leaning the OGV, the rotor wake becomes oblique to the OGV, thus producing a slicing type interaction as opposed to a more uniform or radial, simultaneous interaction.

An analytical technique for calculating the puretone power level which results from the viscous wake interaction between a rotor and a tangentially leaned stator was developed from basic assumptions, and the results of this analysis were compared to experimental data. The analytical technique was based upon the premise that the sound field of the duct in which the rotor and stator are located can be described in terms of a velocity potential, ϕ. The field ϕ is governed by the wave equation which, when solved with the boundary conditions at the plane of noise generation and at the inner and outer walls of the duct, determines the velocity potential uniquely. The velocity and the

pressure in the duct are functions of the velocity potential. From these two expressions, the total acoustic power for the blade-vane viscous wake interaction can be mathematically formulated.

Experimental data available from Reference 1, for ROTOR-OGV geometry with 30° stator lean and a two-chord spacing was used to evaluate the analysis. For this configuration, the difference between the predicted and the measured fundamental, puretone power levels is less than 1 dB.

In the analysis, the puretone noise is determined using the basic geometric and aerodynamic parameters which define the fan stage. The approach is based on an earlier analysis of the puretone noise resulting from the viscous wake interaction. This earlier theory, which culminated in the computer program FAINT [2] is based on the assumption that the geometries of both the viscous wake and the downstream blade row are radial. This constraint introduced a known approximation in that the viscous wake off of the upstream blade is not radial at the leading edge of the downstream blade. Also, since the stators were required to be radial, a possible variable was eliminated from noise reduction studies. The present analysis accounts for non-radial viscous wakes and allows the stators in a ROTOR-OGV fan system to be leaned.

1. GENERAL SOLUTION AND BOUNDARY CONDITIONS

The calculation of the puretone noise power level generated by a ROTOR-OGV viscous wake interaction utilizes both a mathematical description of the noise generating mechanism and of the wave propagation. Both of these mathematical descriptions are functions of the radial phase relationship of the disturbance.

The solution for the power level of the puretone noise is accomplished in the following way. The velocity potential in an annular duct is determined from the wave equation with boundary conditions at the plane of noise generation and at the inner and outer walls of the duct.

Since the radial phasing in the wave equation is a function of the noise generating mechanism, the viscous interaction mechanism of the blade rows is considered first in this analysis.

2. NOISE GENERATING MECHANISM

One of the boundary conditions for the wave equation is the tangential velocity distribution at the plane of noise generation ($z = 0$). This velocity distribution is a function of the disturbance which is a result of the interaction of the rotor wake with the OGVs. This disturbance, for a particular harmonic number, is actually the superposition of an infinite number of rotating lobe patterns. The number of lobes in each pattern is given by the succession values of n, which are generated as the index K ranges over all positive and negative integers in the expression: $n = n'B+KV$.[3] Each lobe pattern rotates at a different speed; however, the lobe passing frequency for each pattern is equal to the blade passing frequency of the rotor. Therefore, the angular velocity of a lobe pattern, in terms of the blade passing frequency is: $\omega_n = \omega/n$.

As an approximation, the tangential velocity is defined such that discontinuities are located at the rotating lobes. Referring to Figure 15, it will be noted that one disturbance, with phase angle $\epsilon(r)$ rotates with angular velocity ω_n.

The tangential velocity at an angle θ is zero until the disturbance is at that angle. When the lobe coincides with the angle at some radius, the tangential velocity jumps to a value f(r). This relationship can be expressed mathematically as:

$$V_\theta(r) = f(r) \cdot \delta[\theta-\omega_n t-\epsilon(r)] \qquad \text{Equation 1}$$

where f(r) is the radial distribution of the tangential velocity. By using the definition of the circulation (Reference 4, Appendix A), the above equation can be rearranged into the non-dimensional expression:

$$V_\theta(r) = \frac{\Gamma(r)}{C.r.Ro}\ \delta[\theta - \omega_n t - \epsilon(r)] \qquad \text{Equation 2}$$

If there are "M" rotating line disturbances, the velocity field at the plane of noise generation can be described for the following limits:

$$\left\{\omega_n t - \epsilon(r_{tip})\right\} \leq \theta(r) \leq \left\{\omega_n t\right\}$$

$$\left\{\omega_n t + \frac{2\pi}{M} - \epsilon(r_{tip})\right\} \leq \theta(r) \leq \left\{\omega_n t + \frac{2\pi}{M}\right\}$$

$$\left\{\omega_n t + 2\,\frac{2\pi}{M} - \epsilon(r_{tip})\right\} \leq \theta(r) \leq \left\{\omega_n t + 2\,\frac{2\pi}{M}\right\}$$

$$\vdots$$

$$\left\{\omega_n t + (M-1)\,\frac{2\pi}{M} - \epsilon(r_{tip})\right\} \leq \theta(r) \leq \left\{\omega_n t + (M-1)\left(\frac{2\pi}{M}\right)\right\}$$

with the corresponding velocity field equations:

$$V_\theta(r) = \frac{\Gamma(r)}{C.r.Ro}\ .\ \delta[\theta - \omega_n t - \epsilon(r)]$$

$$V_\theta(r) = \frac{\Gamma(r)}{C.r.Ro}\ .\ \delta[\theta - \omega_n t - \epsilon(r) - \frac{2\pi}{M}]$$

$$V_\theta(r) = \frac{\Gamma(r)}{C.r.Ro}\ .\ \delta[\theta - \omega_n t - \epsilon(r) - 2\,\frac{2\pi}{M}$$

$$\vdots$$

$$V_\theta(r) = \frac{\Gamma(r)}{C.r.Ro}\ .\ \delta[\theta - \omega_n t - \epsilon(r) - (M-1)\,\frac{2\pi}{M}] \qquad \text{Equation 3}$$

In addition, for any angle, $\theta(r)$, not defined above - $V_\theta(r) = 0$.

The phase relationship, $\epsilon(r)$, is a function of both aerodynamic and geometric parameters. The terms used to describe these two parameters are the effective and physical lean angles, respectively. The effective lean angle is a result of the non-flat velocity profile of the rotor wake at the leading edge of the OGVs. In Reference 4, Appendix B, an equation for effective lean is determined from the aerodynamic data of the ROTOR-OGV stage. The expression is in the form of the quadratic equation

$$\theta_e(r) = b_0 + b_1 r + b_2 r^2 \qquad \text{Equation 4}$$

where b_0, b_1, b_2 are constants.

The physical lean angle is the result of the tangential (non-radial) lean of the OGVs. This angle can be explicitly determined from the geometry of the stator blade row (Reference 4, Appendix C). The expression for the physical lean angle is:

$$g(r) = \alpha(r) - \text{SIN}^{-1}\left\{\frac{r_{hub}}{r}\ \text{SIN}\left[180 - \alpha(r)\right]\right\} \qquad \text{Equation 5}$$

This equation applies to both curved and straight OGVs.

The formulation of the overall angular displacement, as a function of radius, is a combination of both the effective and physical lean angles. In terms of these angles, the angular displacement is:

$$G(r) = g(r) - \theta_e(r) \qquad \text{Equation 6}$$

The angular displacement, G(r), is used in the calculation of both the angular and the time phase shifts which have been summarily expressed as $\epsilon(r)$. To explicitly determine the phase relationship, it is necessary to consider the angle and the time in Equation 2 as functions of radius.[5] Incorporating this radial dependency into the tangential velocity expression, Equation 2 becomes:

$$V_\theta = \frac{\Gamma(r)}{C.r.Ro} \cdot \delta\left[\left\{\theta - G(r)\right\} - \omega_n \left\{t - \frac{G(r)}{\frac{2\pi N}{60} \cdot \frac{Ro}{C}}\right\}\right] \qquad \text{Equation 7}$$

The preceding equation reduces to:

$$V_\theta = \frac{\Gamma(r)}{C.r.Ro} \cdot \delta\left[\theta - \omega_n t - G(r) \cdot \left\{1 - \frac{n'.\ B}{n}\right\}\right] \qquad \text{Equation 8}$$

Thus, for the case where there are "M" rotating line disturbances, the velocity field at the plane of noise generation can be described for the following limits:

$$-G(r_t)\left\{1 - \frac{n'B}{n}\right\} \leq [\theta - \omega_n t] \leq 0$$

$$\frac{2\pi}{M} - G(r_t)\left\{1 - \frac{n'B}{n}\right\} \leq [\theta - \omega_n t] \leq \frac{2\pi}{M}$$

$$2\left(\frac{2\pi}{M}\right) - G(r_t)\left\{1 - \frac{n'B}{n}\right\} \leq [\theta - \omega_n t] \leq 2\left(\frac{2\pi}{M}\right)$$

$$\vdots$$

$$(M-1)\left(\frac{2\pi}{M}\right) - G(r_t)\left\{1 - \frac{n'B}{n}\right\} \leq [\theta - \omega_n t] \leq (M-1)\left(\frac{2\pi}{M}\right)$$

with the corresponding velocity field equations:

$$V_\theta = \frac{\Gamma(r)}{C.r.Ro} \cdot \delta\left[\theta - \omega_n t - G(r)\left\{1 - \frac{n'B}{n}\right\}\right]$$

$$V_\theta = \frac{\Gamma(r)}{C.r.Ro} \cdot \delta\left[\theta - \omega_n t - G(r)\left\{1 - \frac{n'B}{n}\right\} - \frac{2\pi}{M}\right]$$

$$V_\theta = \frac{\Gamma(r)}{C.r.Ro} \cdot \delta\left[\theta - \omega_n t - G(r)\left\{1 - \frac{n'B}{n}\right\} - 2\left(\frac{2\pi}{M}\right)\right]$$

$$\vdots$$

$$V_\theta = \frac{\Gamma(r)}{C.r.Ro} \cdot \delta\left[\theta - \omega_n t - G(r)\left\{1 - \frac{n'B}{n}\right\} - (M-1)\left(\frac{2\pi}{M}\right)\right] \qquad \text{Equation 9}$$

The above velocity field is used as a boundary condition in the solution of the wave equation.

3. NOISE PROPAGATION

In this analysis, it is assumed that the noise field is generated in the cross-sectional plane Z = 0 by the interaction of the rotor viscous wake with the downstream OGVs and that this field can be described in terms of the velocity potential ϕ (r, θ, z, t). The velocity field is governed by the wave equation, which for zero Mach number may be written in the form:

$$\frac{\partial^2\phi}{\partial r^2} + \frac{1}{r} \cdot \frac{\partial\phi}{\partial r} + \frac{1}{r^2}\frac{\partial^2\phi}{\partial\theta^2} + \frac{\partial^2\phi}{\partial z^2} - \frac{\partial^2\phi}{\partial t^2} = 0 \qquad \text{Equation 10}$$

Where the coordinates (r, θ, z, t) are nondimensionalized with respect to the tip radius, Ro, and the speed of sound, C. The derivation and nondimensionalization of the above equation is found in Reference 4, Appendix D.

Solving the wave equation by the method of separation of variables (Reference 4, Appendix E) yields, as a particular solution for the velocity potential, the following:

Equation 11

$$\phi(r, \theta, z, t) = C_n e^{in\theta_r} \cdot e^{-in\omega_n t_r} [K_1 e^{i\gamma z} + K_2 e^{-i\gamma z}] R_n(\lambda_n r)$$

where

$$\gamma = \sqrt{n^2 \omega^2 - \lambda_n^2}$$ Equation 12

$$R_n(\lambda_n r) = E_n \cdot J_n(\lambda_n r) + F_n \cdot Y_n(\lambda_n r)$$ Equation 13

The angle and the time in Equation 11 are, like their counterparts in the definition of the velocity field at Z = 0, phased in the radial direction. The angular and the time phase relationships are:

$$\theta_r = \theta - G(r) \quad \text{and} \quad t_r = t - \frac{G(r)}{\frac{2\pi N}{60} \cdot \frac{Ro}{C}}$$ Equations 14 and 15

Substituting the above results into Equation 11, yields the following:

Equation 16

$$\theta(r, \theta, z, t) = C_n e^{in\left\{\theta - \omega_n t - G(r)\left[1 - \frac{n'B}{n}\right]\right\}} [K_1 e^{i\gamma z} + K_2 e^{-i\gamma z}] R_n(\lambda_n r)$$

Equation 16 is the form of the velocity potential to which the boundary conditions are applied.

By combining the wave equation, velocity potential and boundary conditions, a solution for amplitude is obtained which varies with OGV physical and aerodynamic lean. The complete solution of these equations is given in Reference 4.

4. COMPARISON WITH TEST DATA

The verification of the preceding analytical technique lies, in the final analysis, in the degree of agreement between the predicted and the measured numerical results. The experimental data which is used for this purpose is from the LF336 lift fan. The blade passing frequency power levels of the ROTOR-OGV interaction for the LF336 were measured from both probe and arc data. These PWLs are presented in Table IX.

The power levels presented in the aforementioned table cannot be directly compared to the calculated PWLs; for the planes at which the puretone power levels were experimentally measured are upstream of the rotor and downstream of the OGV. Correction terms must be applied to the experimentally measured power levels in order to have the PWLs at the plane of noise generation, which is the leading edge of the OGVs. From tests, it has been found that the attenuations through a stator and a rotor blade row are 2.5 and 3.5, respectively.[6]

After applying the correction factors to the experimental data, a comparison of the predicted and the corrected measured, fundamental puretone, total acoustic power levels can be made. These results are presented in Table X and from them, it can be seen that the agreement between the arc and probe corrected data is 0.3 dB. The analytical total PWL is within 1 dB of either of the measured power levels.

D. ACOUSTIC SPLITTER DESIGN AND TESTS

Installation of acoustically treated fan flowpath splitters is limited by the physical dimensions of the rotor and the open area required to pass the fan flow. As more splitters are added, the tip and hub diameters increase and decrease respectively. For the rotor dimensions selected on the basis of fan aerodynamic and mechanical considerations, this creates more turning at the rotor exit due to more distortion of the flowpath around the splitters. An objective suppression level of

2.5 PNdB was set for the splitter arrangement. This appeared to be achievable using two splitters with a maximum thickness of 0.5 inches for each splitter. The number of splitters and splitter dimensions were also compatible with the selected fan flowpath geometry. Several types of acoustic splitters were evaluated through a series of tests. The test objective was to determine the most suitable geometry for matching the splitter suppression characteristics to the LF460 spectrum.

1. ACOUSTIC SPLITTER GEOMETRY

Shown in Figure 16 are the three different types of treatment considered for the acoustic splitters. These design approaches can be described as follows:

- One-Half Inch Total Thickness
  Treated on one side only, this type of geometry can be tuned to lower frequencies than the other two types, and has a broader suppression band width. However, acoustic splitters are much more effective if both sides can be treated.

- One-Half Inch Total Thickness With Septum and Both Sides Treated
  This type of configuration is desirable since both sides are treated. However, due to the decrease in depth, the resonance of the configuration is increased to a much higher frequency and the absorption and band width is decreased.

- One-Half Inch Triangular Core With Both Sides Treated
  This type of core configuration is more applicable for acoustic splitter configurations than the septum configuration, since both sides are treated without a sacrifice in panel thickness.

2. WEIGHTED SPECTRUM

Given in Figure 17 are the PNdB weighting values added to the LF460 spectrum for PNdB. For the weighted LF460 spectrum, the optimum tuning frequency for maximum PNL reduction was located between 2500 Hz and 6300 Hz. Thus, for the treatment to be most effective, the peak suppression was designed to correspond to this frequency band. The weighted spectrum also showed that broadband suppression is a requirement since the difference in noise level is small from approximately 2000 Hz to 6000 Hz. This is due to the weighting values at the lower frequencies increasing the spectrum level to that of the levels near the blade passing frequency.

3. TESTS

Shown in Figure 18 are four candidate fan acoustic treatment systems. Half of each configuration was tested in an acoustic duct facility (Figure 19), where transmission loss measurements were obtained. Results are presented in Figure 20 for a flow Mach number of 0.4. The triangular core configuration gives the maximum PNdB suppression when used with the LF460 spectrum. This splitter configuration was therefore utilized in the LF460 design. Details of the tests are given in Reference 7.

E. EXIT LOUVER DESIGN

On the basis of the acoustic splitter tests, the exit louvers were assumed to have the same design cross-section and the corresponding suppression characteristics. The primary aerodynamic parameters were solidity and blockage, which could be converted to a distance between exit louvers and a length for a given number of louvers. For this spacing and length, an approximate ΔPNdB could be established. A parametric curve was defined as shown in Figure 21. The configuration selected for an objective suppression of 2.5 PNdB was as follows:

Max $t/_c$	0.05
Solidity	2.4
Blockage	12%
No. of Louvers	17
Thickness	0.5 inches
Length	10 inches

Using these physical values and the splitter test results for suppression bandwidth, the LF460 noise was calculated with exit louvers. The net suppression effect of the louvers was 2.2 PNdB compared to the objective of 2.5 PNdB.

F. NOISE PREDICTION TECHNIQUE OUTLINE

The LF460 has several noise sources which must be evaluated to obtain the total system noise. Each source is predicted separately and a noise spectrum defined. The spectra are then added together to arrive at the total noise. As suppression methods are defined, the suppression levels are applied to the particular spectra affected. The following summarizes the methods for predicting the noise constituents:

- Fan

  This is the major noise source in the LF460 and is made up of a puretone at the blade passing frequency and broadband noise. The puretone level is predicted analytically from the physical and aerodynamic fan characteristics. It is based on the interaction of the fan rotor wakes with the outlet guide vanes. Reference 2 describes the analysis in detail. Directivity patterns for the puretone are based on CF6 measured levels.

  The broadband noise is based on CF6 measurements correlated with rotor tip relative Mach number for level and tip physical Mach number for directivity.

- **Fan Jet**

  NASA large scale fan test acoustic data and GE scale model cold jet data were used to define a level of overall sound power level as a function of jet velocity. This curve was approximately 5 dB below the SAE line for jet noise extrapolated to velocities below 1000 ft/sec. The SAE spectrum shape was used along with GE cold jet directivity indices to define the noise at each angle.

- **Turbine Jet**

  The SAE jet noise curve was extrapolated to velocities below 1000 ft/sec for the hot turbine jet predictions. As with the cold fan jet, the SAE spectrum and GE directivity indices were used to define the noise at each angle.

- **Turbine**

  A puretone level is defined using the same type rotor-stator interaction as used in the fan noise analysis. The directivity indices are based on Rolls Royce and GE data. The associated broadband noise was also estimated from Rolls Royce and GE engine data.

Figure 22 shows graphically the procedure used in defining the spectrum for each noise source and the summation to obtain total system noise.

G. FINAL LF460 NOISE PREDICTIONS

Presented in Figures 23 through 29 are the LF460 single engine noise levels as a function of altitude, sideline distance and cycle parameters. Data are shown for both hot and standard day conditions. The noise rating point level is indicated on each standard day curve. The predictions include the effects of OGV lean (18 degrees), acoustic splitters and exit louvers. As shown in Figure 23, the maximum noise for the LF460 occurs at an altitude of 200 feet which corresponds to an acoustic angle of 113 degrees.

The spectrum shape of the LF460 at the noise rating point is shown in Figure 30. Levels below 300 Hz are dominated by jet noise while those above 300 Hz are fan broadband noise. The large drop-off in noise between 2000 Hz and 4000 Hz is a result of the acoustic splitter and exit louver suppression. The puretone is still evident at 6300 Hz. It was not suppressed as much as the 3000 Hz band due to the PNdB weighting with frequency being less.

SECTION V

AERODYNAMIC DESIGN

A. FAN

1. FAN DESCRIPTION

The significant design parameters which describe the LF460 fan are presented in Table XI. The values of many of these parameters were chosen during preliminary design studies and, in some cases, are the result of compromises made in an attempt to obtain the best combination of low noise, high thrust and low weight. Selection of fan airflow and pressure ratio were based primarily on installation requirements and available gas generator power. Aerodynamic design considerations strongly influenced the selection of values of the remaining parameters.

The selection of inlet specific flow for fans with pressure ratios above approximately 1.3, is controlled by blade row choking considerations. Previous experience indicates that specific flows greater than 40 $lb/sec/ft^2$ require extremely thin airfoils and/or high incidence angles to pass the flow without choking. This was an important consideration in the LF460 fan design since it must be capable of operating off-design at greater than design flow. The selection of flow and specific flow established the rotor inlet annulus area.

The minimum rotor radius ratio was dictated by the combination of rotor tip speed, fan pressure ratio and the selected maximum permissible hub work coefficient.

Rotor tip speed was selected to provide adequate stall margin for a given number of rotor blades without excessive hub solidity. The selection of the numbers of blades and vanes was primarily controlled by mechanical and acoustic considerations.

In the selection of fan static pressure ratio for a fan such as the LF460 consideration must be given to the effects of the associated thrust vectoring system, which creates the fan back-pressure. The predicted thrust vectoring (louvers) performance map, in terms of inlet total to ambient pressure ratio as a function of inlet flow function for various louver settings, is presented in Figure 31. Also shown is the predicted LF460 100% speed, fan characteristic. The fan design point was selected near the 0° louver setting rather than the maximum louver setting of 30°, since fan performance is expected to deteriorate more rapidly with flow increase than flow decrease. The fan design point was thus selected to have an exit static pressure of 1.025 of ambient.

The rotor contains two part-span dampers at stream functions of 0.378 and 0.723. The stator contains acoustic splitters at stream functions of 0.200 and 0.600.

The fan design point efficiency (80.3%), shown in Table XI, includes consideration of the effects of rotor shock loss, two rotor part span dampers, tip hot gas leakage, two acoustic splitters, and the high rotor solidities.

2. AERODYNAMIC DESIGN PROCEDURE

The detail design of the LF460 fan flowpath was accomplished using the General Electric Wing Fan Flow computer program (WFF). The WFF program numerically solves the axisymmetric differential equations of compressible fluid flow along desired calculation lines within axisymmetric boundaries. The theory is a modification and extension of the equations derived by Theodore Katsanis[8]. The program is capable of handling flows with or without blade rows, variable total pressure loss profiles and leaned and/or swept blade rows. Recent program modifications permit design with loaded or unloaded splitters.

The detail design of the blade rows was accomplished using the Air Foil Analysis computer program (AFAP). This program uses the air angles and streamline inclination angles generated by WFF along with

airfoil definition data to generate airfoil coordinates. Using air pressure and temperature data from WFF, blade stall and choke margins along with other important parameters necessary for evaluation of the blade design are then calculated.

The AFAP program generates airfoil coordinates in the following manner. Using the cylindrical projections of the leading and trailing edge blade angles of a streamline, an airfoil is constructed on a plane according to a specified chord, maximum thickness, etc. This planar blade is then positioned such that a radial line from the fan axis is normal to the planar blade at the blade mid-chord. The planar blade is then projected along parallel rays to the streamtube surface. The airfoil used for the rotor in the LF460 is a multiple circular arc airfoil on the construction plane. The stator airfoil is a double circular arc on the construction plane. As illustrated in Figure 32, the meanline is composed of two circular arcs and its shape is controlled by the leading and trailing edge angles along with two other parameters called arc-length-ratio (ALR) and arc radius ratio (ARR). ALR is the ratio of the arc length of the leading meanline arc to the total meanline length. ARR is the ratio of the radius of curvature of the trailing meanline arc to the radius of curvature of the leading meanline arc. By varying incidence, ARR and ALR, the chordwise camber distribution may be varied to obtain the desired choke margin.

Final airfoil coordinates are generated for use by mechanical designers by the Spline Blade Stack (SBSTAK) computer program. This program stacks the three-dimensional blade coordinates and interpolates the coordinates to obtain cylindrical section coordinates at desired radii.

3. AERODYNAMIC DESIGN DETAILS

The predicted LF460 fan map shown in Figure 33 was generated using an analytical-empirical technique based on test results of previous General Electric fans.

The fan exit total and static pressure ratio (to ambient) profiles are presented in Figure 34. The dips in the profiles are caused by the acoustical splitters.

Shown in Figure 35 are the wall absolute Mach numbers as a function of wall surface distance. A maximum Mach number of 0.855 occurs aft of the rotor hub trailing edge.

The rotor absolute total pressure ratio profile is presented in Figure 36. The hub design pressure ratio was set low to maintain an acceptable level of hub work coefficient. The high total pressure loss in the rotor tip region, which is due to the presence of the tip turbine, causes the rotor tip D-factor to be rather high. To keep the rotor tip D-factor at an acceptable level, the rotor tip pressure ratio must be made lower than average. The dips in the profile shown in Figure 36 are due to the rotor part-span damper losses.

Figure 37 describes the assumed rotor relative total pressure loss coefficient profile. This profile is established by calculating loss coefficients based on the rotor D-factors, as described in NASA SP-36[9]. The calculated loss was increased by 10%, and additional losses were added at particular streamlines to account for wall boundary layers, part-span dampers, turbine leakage effects, and shock loss. The shock loss was assumed to be 150% of the loss associated with a normal shock at the inlet relative Mach number. The loss peaks in the mid portion of the loss profile are due to the two part-span dampers. The part-span damper loss coefficients were calculated based on a General Electric correlation obtained from cascade tests of vanes with various types of part-span dampers.

Presented in Figure 38 are the absolute and relative Mach number profiles at the rotor leading edge.

Figure 39 is a plot of the cylindrical projections of the leading and trailing edge rotor air and blade angles.

Rotor incidence, deviation and "X" angles from hub to tip are shown in Figure 40. Incidence angle was first estimated based on a General Electric minimum loss correlation which considers camber and solidity. Incidence was then modified to smooth the inlet blade angle radially and/or to provide proper choke margin. The deviation angle was calculated from the camber of an equivalent two-dimensional cascade using Carter's Rule with an additive empirical adjustment, "X", which is based on General Electric experience.

The total aerodynamic load exerted on all the rotor blades is shown in Figure 41 in terms of axial and tangential components.

Figure 42 is a plot of rotor blade meanline arc length ratio (ALR) and meanline arc radius ratio (ARR) versus radius. At the hub, ARR and ALR were selected to provide a double-circular-arc airfoil. At the tip, ALR was selected to keep the junction of the meanline arcs downstream of the blade throat. ALR was then varied approximately linearly from hub to tip. ARR was varied from hub to tip in a manner to provide the proper local and rotor average choke margins.

The LF460 rotor blade geometry is summarized in Figure 43 The sudden increase in chord and t_m/c near the tip are the result of mechanical requirements for attachment of the tip turbine bucket carriers. The waviness of the camber and stagger curves is due to the part-span dampers.

The stator inlet Mach number profile is presented in Figure 44. The stator vanes in the LF460 are leaned from hub to tip in the direction of rotor rotation (-18° measured at the hub) and impart a radially outward force to the airflow in the stator vane row. To prevent choking at the stator hub, it was necessary to contour the stator flowpath walls to permit the flow to curve radially outward,

as can be seen in the fan flowpath drawing (Figure 45). The hub of the stator was placed radially inward relative to the rotor hub to permit an outward curvature in the stator hub and tip flowpath walls while maintaining the exit flow as near axial as possible. This created the hub wall curvature between the rotor and stator, producing the stator inlet Mach number profile shown.

Cylindrical projections of the stator leading and trailing edge air and vane angles are shown in Figure 46.

The relative total pressure loss coefficients calculated for the stator are presented in Figure 47. The two peaks are caused by the two acoustic splitters. Splitter losses were added to produce a 2% fan efficiency decrement for each splitter.

Shown in Figure 48 are the stator incidence and deviation angles used from hub to tip. Incidence angles were estimated from the General Electric minimum loss-incidence angle correlation and were modified to produce a smooth radial vane angle variation from hub to tip. No "X" adjustment was used in the stator design.

Presented in Figure 49 is a plot of the radial variation of total tangential and axial aerodynamic load exerted on all the stator vanes. The dips in the curves are the result of the two acoustic splitters.

The stator vane geometry is defined in Figure 50. Chord, maximum thickness and edge thicknesses are radially constant. Aerodynamic values are called out since mechanical values are slightly different due to the -18° lean angle (measured at the hub).

Presented in Figure 51 are rotor and stator D-factor variations from hub to tip. The rotor part-span dampers and the stator acoustic splitters cause local increases in D-factor as shown in the

plot. The inboard rotor part-span damper increased the local rotor D-factor to a value of 0.52. Though high, this D-factor is within General Electric experience (refer to Comparison with Other Tip-Turbine Fans) and the inboard damper is located in a region of relatively "clean" inlet flow.

Static pressure rise coefficient profiles for the rotor and stator are shown in Figure 52. Again, the influence of the rotor part-span dampers and stator acoustic splitters can be seen, causing peaks for the rotor and dips in the stator. These profiles are not considered high in comparison with previous General Electric fan design experience (refer to Comparison with Other Tip-Turbine Fans).

Figure 53 is a plot of the ratio of the throat flow function to the choke flow function (FFTC) profiles for the rotor and stator. The rotor was designed to have a maximum local FFTC of 0.96 and a flow weighted average value of 0.949. Past experience has shown that fan efficiency decreases when the average FFTC exceeds 0.96 due to choking and decreases when FFTC is less than 0.96 due to high shock losses associated with high leading edge suction surface Mach numbers. The mid-span dampers in the LF460 rotor create an effective annulus blockage of 0.011; thus, the average value of rotor FFTC is 0.949. Since the stator is completely subsonic, an average value of stator FFTC less than 0.960 is acceptable. Effect of the acoustic splitters was accounted for by blockage in the WFF program.

Presented in Figure 54 are the variations of rotor and stator solidities from hub to tip. The given solidity levels were selected to provide adequate stall and choke margins, as well as mechanical strength.

The relationship of stream function, which is the common aerodynamic parameter used in presenting design data, to radius at the blade row edges is shown in Figure 55.

4. COMPARISON WITH OTHER TIP-TURBINE FANS

Table XII presents a comparison of several LF460 fan aerodynamic parameters with those of other General Electric tip-turbine lift fans that have been tested. All values shown are design values. The most significant departures from previous fan designs are the LF460 rotor and stator aspect ratios and solidities. The low pressure ratio LF1 fan is the only fan which utilized aspect ratios as high as those of the LF460.

Additional comparative data are presented in Figures 56 through 63. As shown in Figure 56, the LF460 rotor relative Mach number is higher than previous fans at the hub and tip. Also, the rotor part-span shrouds cause locally higher static pressure rise coefficients (Figure 58) and D-factors (Figure 60) than have been present in previous tip-turbine fan designs. With these exceptions, the design parameters in general fall within the range of previous fan design experience.

B. TURBINE AND SCROLL

1. GENERAL DESIGN FEATURES

The LF460 turbine is a 360° admission impulse turbine fed by two independent 180° admission scrolls. The flowpath at the rotor center line has a 15° inward slope to be compatible with the fan outer flowpath. Thus, the turbine is basically of the axial flow type and has been designed according to axial flow principles.

The scrolls are based on a "triple bubble" design approach intended to minimize overall fan depth and diameter. In this design, the flow into each scroll is divided into three separate ducts at the scroll inlet flange. Each duct then supplies flow to a portion of the turbine admission arc. The flow in these three ducts is not kept completely separate for their entire length but is merged again at a point just upstream of the scroll struts.

The turbine exhausts into a diffuser section which serves to reduce the turbine exhaust gas velocity. Since the static pressure at the diffuser inlet is below ambient, this also serves as sink for small quantities of cooling and leakage air. This section also contains eight radial struts which carry the fan stator loads through the turbine exhaust stream.

The turbine is driven by the exhaust gas of the J97 engine and, therefore, must have inlet conditions compatible with this engine. Design point turbine inlet conditions were selected corresponding to the nominal maximum, SLS, standard day exhaust conditions of the J97 with an assumed 11% total pressure drop in the ducting and scroll. These basic design conditions are listed in Table XIII. It is noted that the 2060°R turbine design point corresponds to the fan maximum control thrust point. At this operating condition, the turbine receives about 9% of its flow from a second interconnected YJ97 gas generator.

A rotational speed of 4300 RPM was selected during preliminary design studies based on combined fan aero, turbine performance and mechanical design considerations.

It is important that the bucket length be kept as short as possible to minimize rotor weight and polar moment of inertia. This dictated the use of a high turbine exhaust Mach number. An exhaust Mach number of 0.6 was selected as being the maximum which could be used with assurance of reasonably good aerodynamic performance. A low static pressure is required at turbine rotor exit: (a) to assure that flow leakage will always be from the fan stream to the turbine stream to prevent the impingement of hot gas on the rear frame titanium components, and (b) to provide a low pressure sink for the mid-box cooling flow. Also, a low Mach number at the discharge from the turbine stream is necessary to minimize the overall fan jet noise floor. These requirements dictated the use of a fairly high area ratio diffuser at turbine rotor discharge.

Large thermal growth of the turbine casing and relatively small growth of the rotor tip diameter result in running tip clearances

of 0.5 inch. This large running clearance dictates the use of tip shrouded buckets and impulse staging in order to minimize the tip leakage losses.

A listing of a number of significant turbine design point parameters is given in Table XIII. The gas conditions at several stations through the turbine flowpath are defined in Figure 64. Shown in Figure 65 is the turbine mean velocity diagram in a view looking normal to the flow direction.

Probably one of the most significant design features of this turbine is the relatively high Mach number at the nozzle exit and bucket entrance. This is the result of the high stage total to static pressure ratio (3.85) in combination with the impulse velocity diagram. As a result, the nozzles have been designed with converging-diverging passages in order to achieve the higher efficiency associated with internal expansion.

Tip turbines of this type lend themselves to a design approach which has been used successfully on all previous General Electric lift fans. This approach features a zero static pressure gradient in the radial direction, at least in the vicinity of the nozzles and buckets which is in contrast to the more usual positive static pressure gradient utilized in most conventional turbines. To accomplish this, the flowpath is designed with an outward curvature which cancels the effect of the circumferential curvature of the turbine annulus. A design of this type results in a nearly constant velocity diagram from hub to tip and makes possible the use of constant section buckets and nozzles. Lift fan tip turbines lend themselves to this design approach because of their large diameter, high radius ratio, and need for a general outward curvature of the flowpath to fit within the fan tip flowpath.

2. DESIGN DETAILS

a. Scroll

1. Flowpath

The general configuration of the scrolls is shown in Figure 66. Flow enters radially into the two inlets at a Mach number of approximately 0.3. The major portion of the flow is then turned in the circumferential direction, divided into three ducts on each side, and accelerated to a Mach number of approximately 0.35. The flow in each duct remains at a constant 0.35 Mach number until it passes through a cascade of struts, which serve primarily to reduce the tangential velocity before the flow enters the nozzle vanes through an axisymmetric gooseneck section. The three ducts are composed essentially of three intersecting circular ducts of varying radii. The intersections are connected by separator plates to form separate passages. The separator plates do not extend the full length of the scroll, stopping somewhat short of the scroll struts to allow the flow in the three ducts to merge before entering the struts. The separator plates have a row of small circular holes down their length to allow static pressure equalization between the ducts.

Details of the scroll cross-sections are shown in Figures 67a, 67b and 67c. As indicated in the figures, the scroll cross section is constant from the 150° location to the 180° location. Thus, the flow in the last 30° of admission arc on each side is gradually decelerated from a circumferential Mach number of 0.35 to 0. The reason for maintaining a constant scroll cross-section in this area is to provide adequate mechanical strength.

In the vicinity of the gooseneck and scroll struts, flow velocity components in a radial plane become significant and are of interest in determining flow angles relative to the struts and nozzle leading edges. Shown in Figure 68 is the streamline pattern in a

radial plane resulting from an incompressible, two-dimensional potential flow analysis. Use of this analysis with a correction for the gross effect of compressibility defined velocity components in the radial plane which were then used in the strut and nozzle designs. The analysis was performed with the separator plate at its lowest position on the top bubble, and was then repeated with the separator plate in its highest position. Results indicated very little difference in the velocities at the strut leading edges and downstream of the struts.

2. Struts

The function of the struts is both structural and aerodynamic. Aerodynamically, they serve to reduce the circumferential velocity component and to turn the flow to a constant angle in the nozzle leading edge plane. The strut geometry is defined in Figures 69 and 70. A spacing of 2.5 inches was selected for mechanical considerations. A chord varying from 3.0 inches at the upper end to 2.5 inches at the lower end was found to be desirable from both aero and mechanical considerations. This results in a solidity of 1.2 at the upper end and 1.0 at the lower end.

A double circular arc profile was selected rather than a NACA series profile because of the very high inlet angles. The thinner forward portion of the double circular arc section was preferred. Maximum thickness of the strut was tapered from 11% of the chord at the upper end to 9% at the lower end. This was done to allow the struts to be inserted from the upper end during assembly of the scroll.

Except in the vicinity of the inlets and the 180° locations, the struts were designed to produce a flow angle in the nozzle leading edge plane whose projection on a cylinderical surface was radially constant. This was desirable from the standpoint of using untwisted nozzle vanes and also resulted in a nearly uniform spanwise aerodynamic loading of the struts. This angle was selected as ± 60°

when measured from axial, the direction being with rotation in the 6:00 o'clock scroll half and against rotation in the 12:00 o'clock scroll half. In the vicinity of the scroll inlets and the 180° locations, the tangential velocity of the flow is substantially less than in the rest of the scroll and this angle varies down to 0°.

Flow angles at the strut leading and trailing edges were obtained by superimposing the meridianal velocities obtained from the potential flow analysis in the radial plane on the tangential velocities. At the strut leading edge, a constant tangential velocity corresponding to 0.35 Mach number was used. At the strut trailing edge, the tangential velocity was selected to provide the desired flow angle at the nozzle leading edge plane, assuming a constant tangential velocity along stream surfaces between the strut trailing edge and nozzle leading edge.

Deviation angles for the struts were calculated using Carter's Rule. The resulting strut angles were then transferred to sections in planes normal to the strut axis.

b. Nozzles

There are three different nozzle vane profiles designed for three different inlet flow angles (+60°, 0°, and -60°). The nozzle profiles, shown in Figure 71, are located about the scroll in groups according to the local inlet flow angle, as shown in Figure 69.

At the turbine design point, the nozzle total to static pressure ratio is 3.85. Using available cascade test data, it was estimated that with this pressure ratio a simple converging nozzle design would have an efficiency approximately 4 percent lower than a converging-diverging nozzle. In addition, the velocity profile exiting from a converging nozzle would be much more nonuniform than for a converging-diverging nozzle. Thus, the bucket would see even

larger variations in relative flow angles and velocities, and present the possibility of additional losses in turbine efficiency. For these reasons, it was felt necessary to design the supersonic portion of the nozzles with at least some internal expansion and area divergence.

Analysis indicated that if the convergent-divergent nozzle were designed for a pressure ratio of 3.85, the turbine part speed performance would be poor due to overexpansion in the nozzle. A compromise design was selected where the divergent portions of the nozzles were designed for a total to static pressure ratio of 2.8. This corresponds to an exit to throat area ratio of 1.071. Available cascade data indicated that with this design the nozzle efficiency loss due to underexpansion at the turbine design pressure ratio would be quite small. A nozzle efficiency of 95% was used in the turbine design and analysis.

The diverging portion of all the nozzle passages, which are geometrically similar, are described in Figure 72. Basically, the supersonic portion of the passage is designed as a Prandtl-Meyer expansion from an assumed uniform sonic velocity across the throat to the design Mach number at the exit.

The converging portion of each nozzle family is different depending on the design inlet angle. The nozzles were analyzed by means of an incompressible potential flow computer program. An approximate correction for compressibility was made on these results up to the throat location. Downstream of the throat, the flow velocities and pressures were analyzed by the method of characteristics. The results of these analyses are shown in Figure 73 where surface static pressures and velocity ratios (M^*) are shown as a function of axial distance downstream of the leading edge. The converging portion of each nozzle family was modified several times until reasonably smooth and accelerating velocities were obtained over each surface.

The axial width of the nozzle partitions was chosen to be 1.5 inches based on mechanical design requirements. The axial width

of all three families was held constant, but the spacing of each family was selected to give a Zweifel aerodynamic loading parameter of approximately 0.46. As a result, the nozzle vane family doing the most turning has a much higher solidity than the family doing the least turning.

c. Buckets

The bucket profile is shown in Figure 74. This section is constant from hub to tip. From the vector diagram shown in Figure 65, it may be seen that the bucket entering relative Mach number is quite high (0.94). Previous design and cascade test experience with a nearly identical bucket section has shown that reasonably good performance can be obtained with inlet Mach numbers of this level if the profile is properly designed. Figure 75 shows the cascade efficiencies obtained on a bucket section of the same solidity and aspect ratio but with about 2° less camber. This bucket was operating at near impulse conditions and the efficiencies shown are averaged across the span.

In both the cascade profile and the LF460 bucket profile, the design procedure employed was identical. An inlet Mach number of 1.00 was assumed for design purposes. A Prandtl-Meyer expansion to a Mach number of 1.18 was taken around the leading edge suction surface, which has an incidence angle of 3.9° relative to the upstream flow. The flow was then assumed to go through a normal shock just upstream of the inlet throat and then reestablish itself as a free vortex flow in the channel which is designed as two concentric arcs. The convex surface within the channel was designed to have a Mach number of 1.20 and the concave surface a Mach number of 0.58. The two concentric arcs forming the channel are simply blended by smooth curves to the inlet and exit throat areas. A flow coefficient of 0.96 was used in sizing the channel and throat flow areas. The profile was made completely symmetrical about the mid-chord point as this was found to result in impulse operating conditions in the cascade test. The calculated M* and static pressure distributions about the bucket profile are shown in Figure 76.

d. Exhaust System

An exit diffuser system is located downstream of the turbine buckets as shown in Figure 45. This system includes an expanding flowpath with an area ratio of about 1.5 and eight equally-spaced struts. The struts serve as structural members to carry stator loads in addition to providing a path to bring cooling air into the mid-box and to exhaust the cooling air into the turbine exit stream.

The diffusing flowpath is provided to diffuse the turbine stream exit velocity to a level consistent with low turbine jet noise levels. A high level of turbine bucket exit velocity is desired for minimum rotor weight and polar moment of inertia. The diffusion system also develops a low turbine bucket exit static pressure to insure that hot turbine gases do not enter the fan stream flowpath at the rotor exit location. Since this leakage is from the fan stream into the diffuser inlet, the effectiveness of the diffuser system will be influenced by the levels of leakage flow. The estimated performance of the diffusion process with leakage is shown in Figure 77. This characteristic was derived from tests of a similar diffuser configuration both with and without leakage. In addition to these effective area ratio corrections, a diffuser and strut loss coefficient of 0.15, based on inlet gas condition, was also applied for the complete exhaust system.

3. PERFORMANCE

a. Scroll Pressure Loss Estimate

Previous cold airflow tests of several tip turbine scroll models have provided a reasonable basis for estimating the scroll pressure loss. In these tests, it was possible to segregate the total scroll loss into the following elements:

1. Entrance turn loss

2. Skin friction

3. Struts

4. Gooseneck

Total pressure loss for the present scroll has been estimated by adjusting the skin friction loss to account for the increased surface area of the "triple bubble." In addition, all the above losses were adjusted for small differences in local Mach numbers and were recombined to obtain a new scroll total loss. Table XIV summarizes these calculations.

Because the turbine nozzles are choked over nearly all of the normal fan operating range, the scroll loss would not be expected to vary significantly.

b. Off-Design Performance

Figure 78 shows the estimated turbine performance map. This map was generated by a computer program designed specifically for high pressure ratio, impulse tip turbines. Basically, this program performs a pitch line analysis over a range of speeds and bucket inlet relative angles and defines the resulting performance at each point. Bucket efficiency and deviation angles are varied as a function of bucket inlet Mach number and inlet relative flow angle. Nozzle efficiency and exit flow angle are varied with nozzle pressure ratio to account for over and under expansion effects of the convergent-divergent passage design.

4. COMPARISON WITH OTHER TIP TURBINES

Table XV shows a comparison of the LF460 turbine with several other General Electric tip turbine designs.

SECTION VI

AERODYNAMIC LOADING

The LF460 lift fan system is designed to withstand the aerodynamic forces representative of operation at static or hover conditions and in the estimated cross-flow environment of transitional flight. The following discussion presents the aerodynamic loading criteria established for the design. All data will be presented for operation at 100 percent of the design rotational speed. The aerodynamic loading for part power operating conditions, as required for mechanical design analyses, was obtained using the loading factors presented in Figure 79. The parameter shown represents the ratio of part power loading to the design point loading at static operating conditions.

A. HOVER OPERATION

At near zero flight speed or hover, the lift fan is the major source of aircraft control; thus, fan thrust and speed are time varying functions. The previously described duty cycle was established to introduce the effects of these variations into the design. The following airloads were corrected to the appropriate speed levels for use in the fan mechanical design.

Presented in Figure 80 are the air loads which act on the front frame system including the bulletnose and bellmouth surfaces. The forces shown are a result of the aerodynamic surface pressure distribution established during the aerodynamic design. The vent or reference pressures for the bulletnose and bellmouth were established as rotor hub inlet static pressure and ambient static pressure, respectively.

Axial and tangential air loads for the complete rotor system are shown in Figure 81. These loads are presented as a function of radial location along the rotor blade centerline. All rotor loads including the fan hub and carrier surfaces are included in this combined load distribution.

Rear frame air loads are presented in Figure 82. Loads due to base pressures and the turbine diffuser are included in the load distributions.

Using the loads described above, the integrated forces acting on each component were obtained. The results are presented in Table XVI. The sum of these axial forces compares favorably with the total force as obtained by the overall cycle calculations.

B. TRANSITION OPERATION

The LF460 is required to operate in the environment established by transitional flight of the aircraft. Testing of other lift fan units in transition has shown that significant changes in fan air loading will occur. The experience gained from the actual test programs was used to estimate the load distributions for the LF460 lift fan system.

The most severe loading condition was found to occur at the maximum transitional or conversion speed of the aircraft system. Maximum speed was established at 150 knots with the fan operating at its design rotational speed. The loading parameters in transition or cross-flow are presented using a cross-flow ratio (ratio of flight speed to fan tip speed). At the design flight speed of 150 knots, or 253 feet per second and a design tip speed of 1125 feet per second, the cross-flow ratio becomes 0.225. This point is identified on the data to be presented. Operation above this level can only be accomplished at reduced power settings.

Presented in Figures 83 through 87 are the variations of system forces and related factors affecting design during cross-flow conditions. The effects of cross-flow on the three major lift components are shown in Figure 83. All data are based on a reference lift level of the fan system at static condition and the same fan speed used to determine the cross-flow ratio. At static conditions and design fan speed, this reference lift is 13,680 pounds. It is noted that the reference value

is the momentum lift of the fan only.

Shown in Figure 84 are the variations in inlet, rotor and total system drag or crosswise loading on the fan system in transitional flight. These two force components represent the total momentum drag of the fan inflow, and based on the analysis are almost equally divided between the rotor and fan inlet system.

Presented in Figure 85 are the variations in rotor and stator torque during cross-flow operation. A slight increase in rotor torque occurs, with a significant reduction in stator torque, the difference being a torque developed on the fan rotor due to a skewed inlet flow distribution that occurs with cross-flow. The slight increase in rotor torque indicates a required fan rotor power increase. Fan power measurements in cross-flow testing indicated a small fan overspeed or power reduction. This difference in test and analysis can be attributed to bellmouth leading edge separation which occurred during the test, but was not considered in the analysis.

The changes in the centers of lift for the rotor and stator in cross-flow are shown in Figures 86 and 87. This center of lift translation, plus the lift variation from Figure 83 establish the cross-flow moments for the system.

Inlet system airloads in transitional flight were also estimated based on test results obtained for lift fans in cross-flow. These airloads, used in the design of the front frame system, are presented in Figures 88 through 90. Shown in Figure 88 are the load distributions around the bellmouth structure. The radial distributions of loading for the inlet bellmouth and bulletnose are shown in Figures 89 and 90.

The distribution of tangential and vertical loading on the rotor and stator systems, as used in the development of the total loads, are presented in Figures 91 and 92.

SECTION VII

MECHANICAL DESIGN

A. FRONT FRAME

1. GENERAL DESCRIPTION

The front frame layout is presented as Figure 93. The frame is composed of a center hub structure for mounting the rotor, a major strut which provides structural support between the fore and aft airframe mounts, and two minor struts which restrict the relative deflections between the rotor and adjacent structure. The inboard minor strut also includes an airframe mount between the scroll inlets. The front frame is the main structural support of the lift fan assembly. It transfers all rotor loads, gyroscopic moments and inertia forces, as well as bellmouth-scroll lift and exit stator vane axial loads through the front frame structure to the main airframe mounts.

2. DESIGN REQUIREMENTS

In addition to the general design requirements defined in Section III, the following requirements are specifically applicable to the front frame:

- Maintain adequate clearance and required stability of static components to prevent interference with rotating parts during all fan operating conditions.
- Adequately seal between the turbine and fan inlets to preclude adverse hot gas injection into the fan.

3. LOADING ASSUMPTIONS

The fan system is subjected to aerodynamic, maneuver and cross-flow loading conditions. The front frame is designed to transfer all rotor, scroll and rear frame loads to the airframe mounts.

a. Aerodynamic Loads

The following is a summary of the resultant static forces due to aerodynamic loads at 100% fan speed:

Component	Axial Force (Pounds)	Torque (Inch-Pounds)
Bellmouth	+3753	0
Bulletnose	-1196	0
Struts	-22	0
Rotor Hub	+1878	0
Rotor Blades	+7016	176,000
Turbine Carriers and Buckets	+180	176,000
Stator Hub and Inner Wall	+560	0
Fan Stators and Splitters	+2240	176,000
Stator Mid-Box and Outer Wall	+84	0
Scroll Nozzles	+2096	186,700*

* Turbine Residual Swirl = 10,700 inch-pounds

Air loads on the struts are due to aerodynamic drag only and are assumed negligible during hover operation.

b. Maneuver Loads

The front frame and mounts are designed to withstand maneuver loads as defined in Section III when applied simultaneously with the aerodynamic loading. Maneuver loads can be applied during conventional flight or in a crossflow environment.

c. Crossflow Conditions

The front frame is designed to withstand aerodynamic loads experienced during transitional flight when installed with a shallow wing fan inlet. The design point for crossflow operation, as defined in Section III, is 100% fan speed at a flight speed of 150 knots.

4. COMPONENT DESIGN DESCRIPTION

a. Major Strut

The major strut spans the 12:00 to the 6:00 o'clock positions, providing the primary support for the rotor thrust and maneuver loads and transferring them to the 12:00 and 6:00 o'clock airframe mounts. Maneuver loads which would produce torsion in the main strut are reacted by a couple formed in conjunction with the 3:00 and 9:00 o'clock minor struts. The major strut also provides a rigid radial support for the bellmouth at the 12:00 and 6:00 o'clock positions. As shown in Figures 93 and 94, the strut is a structural spar utilizing top and bottom cap strips integrally connected to a continuous shear web. The general shape of the structural spar is similar to a tapered I-beam being symmetrical to either side of the hub center. The strut is a modified NACA 16-015 airfoil having a maximum thickness of 1.2 inches and a chord that tapers from the center hub to the end mounts. The major strut uses a honeycomb filler between the cap strips to form the required airfoil contour. The honeycomb is adhesive-bonded to the center shear web and the 0.010 inch aluminum face sheets. Honeycomb filler is also used between face sheets for that part of the airfoil beneath the bottom cap strip.

The bending stiffness of the strut is of prime importance. The strut is designed to limit hub axial deflection, caused by rotor lift, to less than 0.15 inches. This limited axial deflection at the midspan of the strut is required to retain axial clearance between the turbine and forward air seal.

As shown in the frame layout (Figure 93), the bottom cap strip transitions to a rectangular section at the hub to provide efficient load transfer to the hub. The bottom cap strip normally experiences compressive loads and has, therefore, been designed with a slight interference fit with the hub to provide a bearing surface for distribution of these loads. The slight interference fit assures

contact of these surfaces at all times. Two 0.375 inch shear rivets shouldered by 0.75 inch diameter steel inserts are used to attach each of the bottom cap strips to the hub. These rivets incur small shear loads because of the prevailing compressive loads and the interference assembly. All rivet holes are match drilled with the hub to assure proper load transmission. The strut shear web is stepped to a 0.25 inch thickness in the area where it is attached to the hub. The shear web fits snugly into the hub vertical attachment clevis and is secured by eight 0.375 inch rivets. Additional shear plates sandwich the center shear web and the hub gussets at the 12:00 and 6:00 o'clock positions to insure low shear stresses in the hub clevis rivets during maneuver loading conditions. The shear plates are riveted to the strut shear web and hub gusset with six 0.25 inch rivets on each side.

The fiberglass dome is mechanically attached by two 0.1875 inch bolts (per side) at the mounting pads located on each side of the strut bottom cap at a radius of 12.6 inches.

The scroll is supported by the major strut at two 36.5 inch radial locations. At the attachment point, the bottom cap strip transitions to a rectangular "ear", which is 5 inches wide and follows the contour of the bellmouth (Figure 95). Four 0.5 inch holes are counterbored in each ear, two on each side of the major strut. This permits the mounting bolts to be recessed below the flow surface.

The outer ends of the strut are solid to provide adequate material thickness for attachment of the bellmouth and to transfer the cap strip loads to the airframe mounts at the 6:00 and 12:00 o'clock positions. A unibal mount is provided at each end of the major strut to facilitate the different airframe installations.

b. Hub

The hub provides a load-carrying structure to transfer all the rotor loads directly to the major and minor struts. It is a

stiff structure in the radial direction to insure proper support for the outer bearing races and to provide an efficient load path to the major and minor struts. Since the hub and minor struts are cast as an integral component, the selection of material is of prime importance. Cast aluminum alloy A357 was selected because of its low density (0.1 lbs/in^3) and adequate fatigue strength (31 KSI). To preclude damage to the hub during assembly and disassembly of the bearings, two steel inserts are provided as an integral part of the hub. These inserts are machined to the required O.D. of the outer bearing races. Eight equally-spaced holes are provided through the bottom hub disk to mount the rotor shaft retaining plate.

The hub bottom disk is machined locally at the 6:00 and 12:00 o'clock positions to provide a smooth bearing surface for the major strut bottom cap strip attachment flange.

A 0.1 inch recession is machined on the top of the hub to provide a smooth mounting surface for the hub dome. The dome is mechanically attached to the hub by eight 0.1875 inch flat head machine bolts. Eight anchor nuts are provided on the inside of the hub.

c. Minor Strut

The minor struts span the 3:00 and 9:00 o'clock positions and provide the necessary structure to react the torsional-producing crossflow and gyroscopic loads. They also provide a rigid radial support for the bellmouth at the 3:00 and 9:00 o'clock positions. As stated previously, the minor struts are cast integrally with the hub from A357 aluminum. As shown in Figure 96, the minor struts are structural spars utilizing top and bottom cap strips supported by a continuous shear web. The shape of each strut resembles a tapered I-beam, having a maximum chord of 7.5 inches at the hub and 6.0 inches at the bellmouth. Both top and bottom cap strips transition from the required airfoil contour in the fan flow area to disks which transfer loads around the hub. This is illustrated in Figure 96. A rectangular

flange is provided around the minor strut at the intersection of the strut with the dome (Figure 96 Section J-J). This allows the dome to be fabricated in two pieces, each having a rectangular cutout around the minor struts.

The minor strut top and bottom cap strips transition to a solid airfoil section approximately one inch from the bellmouth. The solid airfoil then transitions to a rectangular flange four inches wide and having a constant thickness of 0.2 inches. This flange follows the bellmouth contour and is positioned within a recess in the bellmouth. The minor struts are attached to the bellmouth by six 0.25 inch flat head machine bolts per strut.

The minor struts use a honeycomb filler between the cap strips to form the required airfoil contour. The honeycomb is adhesive-bonded to the center shear web and the 0.010 inch aluminum face sheets in a manner similar to the major strut construction.

Both minor struts are NACA 63-618 airfoils and are designed as left and right hand struts. As shown in the frame layout (Figure 93), both struts are staggered 4° from the vertical facing in the aircraft flight direction (12:00 o'clock direction). The struts are designed so that the scroll inlets can be turned 180° for installation flexibility.

d. Bellmouth

The bellmouth forms the aerodynamic flowpath at the fan inlet. It also positions the forward air seal assembly, provides a mounting attachment for the scroll at each strut, and includes an airframe mount at the 3:00 o'clock position.

Since the bellmouth must limit the relative radial deflections between the forward air seal and the rotor seal lip to preclude adverse hot gas leakage, it is designed to provide a high level of stiffness in the radial direction. To meet the stiffness requirements with minimum weight, the bellmouth structure is a continuous

360° honeycomb structure utilizing 0.010 inch face sheets resistance welded to a 0.0035 inch foil forming a 0.25 inch core. The panel has a uniform thickness of 0.5 inches except for local crushing.

At the inner diameter of the bellmouth (30.75 inch radius) the panel is crushed to form a vertical concentric inner surface which is the mounting surface for the forward air seal assembly. A series of locally crushed areas are also required on the outer side of the panel at the bellmouth inner diameter to provide sufficient space to attach forty-eight 0.1875 inch anchor nuts.

At the outer diameter of the bellmouth (42.5 inch radius) the panel is crushed to a uniform minimum thickness. This is necessary to provide a recession for the airframe installation cover. Forty-eight equally spaced 0.1875 inch anchor nuts are provided on the underside of the bellmouth panel for mounting the aircraft installation cover.

The bellmouth is mechanically attached to the major and minor struts. At the 6:00 and 12:00 o'clock positions, four mechanical inserts are pressed into the panel; these inserts act as shoulders for four 0.25 inch bolts which are used to attach the bellmouth to the major strut. At the 3:00 and 9:00 o'clock positions, the bellmouth panel is locally crushed to a 0.25 inch thickness to provide a recess for the minor strut attachment flange. Six mechanical inserts are pressed into the panel to provide shoulders for the six minor strut attachment bolts. Two additional mechanical inserts are pressed into the panel directly above the 3:00 and 9:00 o'clock scroll to front frame mounting brackets (at a radius of approximately 39 inches). These inserts act as shoulders for the two 0.25 inch flat head bolts which position the scroll mounting bracket.

At the 6:00 and 12:00 o'clock positions, a rectangular section of the panel (approximately 5 inches x 3 inches) is removed. A machined insert is welded to the inner and outer edges which are

crushed together. This local deformity is necessary to provide a recess for the major strut to scroll attachment "ear" and to allow sufficient material for accurately machining a surface for the scroll mount.

At the 3:00 and 9:00 o'clock positions, the scroll mount brackets are line drilled at final assembly to assure correct positioning of the scroll to the front frame. The 3:00 o'clock mount bracket also supports a 1.25 inch unibal, mounted with the bore in the radial direction. This unibal provides the required front frame to airframe mount.

e. Dome

The dome which forms the flowpath at the fan inlet in the hub region, is designed in two halves, each half separated by the major strut. Minor strut cut-outs are provided, to allow the dome halves to straddle the minor strut flanges. The dome is a fiberglass laminate outer skin bonded to an internal load-carrying network of ribs. The ribs carry the loads to aluminum inserts which provide the required bolt bearing surfaces and transmit the dome loads from the outer skin and ribs to the mounting bolts. The dome is bolted to the hub and to each strut flange.

f. Forward Air Seal Assembly

The forward air seal is attached to the aft inner surface of the bellmouth. The purpose of this seal is to minimize the hot gas leakage from the turbine stream to the fan stream, and to direct the leakage flow into the fan rotor. A radial slip seal also restricts hot gas leakage from the turbine to the cavity between the bellmouth and scroll. An exploded view of this area of the fan is shown in Figure 97.

The forward air seal consists of thirty 12° segments (Figure 98). Each segment consists of a backing plate, 0.050 inch thick,

and a strip of honeycomb 0.2 inch thick by 0.5 inch wide brazed to the backing plate. The ends of the backing plate are machined to provide a 0.25 inch overlap from segment to segment. The honeycomb seal utilizes 0.0625 inch cell size, with 0.0025 inch foil. Each seal sector is supported by the bellmouth with two 0.1875 inch bolts.

The bellmouth to scroll slip seal (Figure 99) also consists of 12° segments. Each segment includes two 0.010 inch sheets laminated to form an overlap at each end, thus providing an "interlock" between segments. The slip seal is supported by the same bolts that support the forward air seal sectors.

The air deflector (Figure 100) consists of four 90° segments. Each segment is mechanically attached to the bellmouth at six locations. The air deflector directs the hot gas leakage into the rotor in a manner to minimize leakage effects on fan airflow and performance.

5. DESIGN STRESS LEVELS

The results of the front frame structural analyses are presented in Figure 101. Stress levels shown are the maximum which will occur under combined steady state, crossflow and maneuver conditions.* As indicated, the stress levels are fairly low since the frame design is deflection limited. The material selections and component weights for the frame and associated hardware are shown in Table XVII.

B. SCROLL

1. GENERAL DESCRIPTION

A general description of the scroll concept was presented previously (Section V, AERODYNAMIC DESIGN). The initial design requirements established by the NASA called for a minimum depth fan configuration.

---

* The fan mounting arrangement and loading levels are discussed in Section IX, INSTALLATION.

On the basis of this ground-rule, a triple-bubble scroll concept was selected over a single-bubble arrangement to provide a reduced installed fan diameter.

The scroll, which is illustrated in Figures 66 and 67 provides a load path to transfer all rear frame (stator) loads to the front frame. The scroll also includes two airframe mount points - one between the scroll inlets (0°) to transfer all fan side inertia loads and the scroll piston load to the airframe, and a second mount (drag link at 180°) which, in combination with the first mount, cancels any torque imbalance.

The final scroll design is based on application of René 41 material.

2. DESIGN REQUIREMENTS

The scroll is designed to satisfy the design life, cyclic and engine-out requirements defined in Section III. In addition, the scroll is capable of accepting all rear frame loads and transferring them to the front frame.

3. COMPONENT DESCRIPTION

a. Flowpath

As illustrated in Figure 102 the flowpath consists of: an inlet pipe; upper, middle and lower bubbles; and a gooseneck. All of the bubble skins are stretch-formed in the right-hand and left-hand sections. To achieve minimum weight while providing the necessary weld joint thickness and good formability, the bubble skins are masked and chem-milled to minimum thickness after the forming operation. The remaining sheet metal parts (covers, fairings and plates, etc.) are die stretch formed in segments and then processed in a manner similar to the bubble skins.

The "gooseneck" flowpath, which directs the flow to the turbine nozzle, is formed from a constant section of a torus. This toroidal section is made in segments and butt welded together to form a complete ring. One edge of the torus is welded to a 0.060 inch hat section that forms a ring for the upper bubble and "gooseneck" intersection. The other edge of the torus is welded to a 0.040 inch "V" shaped section that forms a ring (nozzle hat) to which the nozzle partitions are brazed. The flowpath from 0° (between the inlets) to 23° is defined as the inlet region. The inlet structure is designed as an investment cast framework. The scroll transitions from the circular inlet configuration to the three toroidal shaped bubbles at the 23° location.

The adjacent bubbles intersect each other to form cusp lines. Plates 0.040 inches thick extend between the cusp lines separating the adjacent bubble passages, and forming the internal scroll structure.

The plates are continuous from the inlet pipes, where they are welded to the inlet skins, to the termination of the cusp points in the scroll arms. From 23° to 60° the middle and lower bubbles rise axially with the upper cusp migrating along the upper bubble contour. As shown in Figure 103 at 60° the middle bubble has been superimposed onto the upper bubble, forming a two-bubble scroll. At this location, the upper plate is terminated. From 60° to 98° the lower bubble rises axially and blends into the upper bubble. At the 98° location the scroll becomes a single bubble configuration (Figure 104) and the lower plate is terminated. Between the 98° and 150° locations the upper bubble is reduced in diameter to 5.3 inches. From 150° to the 180° location this cross-section is held constant. The "Y" joint that is formed at the intersection of adjacent bubbles (cusp) is cast with a stock thickness of 0.060 inches. The "Y" joints change in angular orientation as they move circumferentially around the scroll.

b. Torque Tube

The torque tube (Figures 102 and 105) is a machined and welded structure, forming the backbone of the scroll. The machined ring which makes up the inside portion of the torus from the struts to the nozzle partitions is integral with the rear frame support flange. All portions of this ring are machined to a 0.030 inch thickness. Two horizontal flanges 0.040 inches thick and 0.6 inches long extend from the ring and, after eloxing, are brazed to the struts. The torque tube bottom plate is a 360° section varying in thickness from 0.060 to 0.030 inches. It has two vertical flanges 0.060 inches thick which, after eloxing, are brazed to the ends of the struts. These flanges also provide the necessary rigidity for the bottom plate from 110° to 180° to react the pressure gradient as the lower end of the bubble migrates to its final position at 180° as shown in Figure 105. A third flange is also machined into the bottom plate. This flange provides a structural continuation of the lower end of the bubble for the necessary structural attachment to the struts. Completing the torque tube is a 0.020 inch thick close-out section, which is welded in place after braze inspection of the struts and nozzle partitions.

c. Nozzle and Strut Hat Sections

Both the nozzle and strut hat sections (Figure 102) are 0.028 inch machined channels which provide a torque box for the outside ends of the strut and nozzle partitions. The nozzle hat also has the three-leaf slip seal attached to its lower end.

d. Nozzle

Variation of the gas flow angles inside the scroll requires the use of three different families of nozzle partitions to turn the gas and provide a constant nozzle discharge angle. Each nozzle has a 0.005 inch protuberance on the pressure side which forms the throat area of the convergent-divergent nozzle. Each nozzle is a hollow casting with a wall

thickness of 0.040 inches, and a projected axial chord of 1.50 inches. The nozzle is brazed to the "V" shaped nozzle hat section and the torque tube. The average length of the nozzle is 3.5 inches. There are 42 Family I, 38 Family II and 77 Family III nozzles.

e. Strut

The strut is a hollow casting with a wall thickness of 0.040 inches. Each strut has a non-uniform twist which results in a requirement for a three inch chord with 11% tm/c at the top and 2½ inch chord with 9% tm/c at the torque tube. The average length of these struts is 5.5 inches. A total of 86 struts are required.

The upper and lower plates have entrance and exit struts (stiffeners) having a 2.5 inch chord and 10% tm/c. These cast struts are welded to the plates and brazed into the bubbles. The entrance struts on the upper plates of the two-scroll inlets form a single continuous strut which extends across the two scroll inlets, forming a load path for one airframe mount.

f. Scroll/Front Frame Mounts

The scroll is attached to the front frame at the 0° (inlet), 90°, 180° and 270° locations. The 90° and 270° (Major Strut) ties (Figure 106) use a lift pad to transfer the scroll loads to the front frame. These pads also position the front frame during thermal growth so that the front frame and scroll are always concentric. The male parts are 4 x 1.25 x 0.150 inch pads welded directly to the 6:00 and 12:00 o'clock gooseneck struts. The female portions consist of an integral machined part that bolts to the major strut and hooks over the strut pad.

The 0° and 180° (inboard and outboard) mounts have a 0.25 inch thick plate welded to the torque tube with a 0.75 inch diameter unibal insert to preclude adverse bending loads.

g. Scroll/Airframe Mounts

The airframe mount between scroll inlets is a welded structure consisting of a 4 inch diameter pipe with a structural center plate. The material thickness is 0.125 inches. The structural plate has a short extension in the center with a 1 inch diameter unibal insert. The pipe is welded to the scroll inlet pipes while the center plate is an integral part of the upper plate leading edge strut.

The outboard mount clevis (Figure 107) attaches to a 1 inch outer diameter tube 30 inches long having a 0.040 wall thickness with a unibal mount point at each end. The clevis is welded to the torque tube and drilled to accept a body-bound 0.1875 inch diameter bolt.

h. Inlet Flange

The scroll inlet flanges are one inch high and have an inside diameter of 12.26 inches. Twenty-one 0.203 inch drilled holes are provided on a bolt circle diameter of 13.32 inches for flange to flange attachment.

i. Insulation

The outer surface of the scroll is covered with 0.25 inch Min-K insulation bagged in a quartz cloth insulation blanket. It is attached at the nozzle hat near the slip seal, around the scroll, and at the aft end of the rear frame casing.

4. DESIGN RESULTS

a. Stress Summary

Shown in Figure 108 are the maximum stresses experienced by various portions of the scroll. These stresses do not include the engine-out condition which requires that only one-half of the scroll receive hot gas. Analysis of the engine-out condition shows no

adverse structural effects, provided the duration of the engine-out condition is of moderate duration (3 minutes or less per event).

b. Life Analysis

Due to the duty cycle necessary for aircraft attitude control, the scroll experiences high cyclic loading imposed over the steady state loading. The scroll is, therefore, analyzed as a "Time and Cycle - Dependent Structure." Using the assumption that a linear combination of creep damage and fatigue damage is valid for design purposes, the equation:

$$\sum_{n=1}^{n} \frac{t'_n}{t_n} + \sum_{k=1}^{k} \frac{N'_k}{N_k} \leq 1.0 \qquad \text{Equation 1}$$

represents an acceptable structural design. Equation 1 can be separated into the time dependent part,

$$\sum_{n=1}^{n} \frac{t'_n}{t_n} = R \qquad \text{Equation 2}$$

and the cycle dependent part,

$$\sum_{k=1}^{k} \frac{N'_k}{N_k} \leq K \qquad \text{Equation 3}$$

1. Time Dependent Part (Equation 2)

Life expectancy (t_n) of the scroll can be determined for each component of the duty cycle based on an assumed stress using the "Larson-Miller" parameter,

$$P = T \quad (C + \log_{10} t) \times 10^{-3} \qquad \text{Equation 4}$$

For the temperature and assumed stress allowable, the life t_1, t_2, ... t_n is determined. With t_1', t_2', ... t_n' representing the corresponding times specified in the duty cycle, the summation R is the part of total life consumed.

As shown previously, the maximum scroll stress levels range from 13,500 to 25,200 lb/in^2. Using a stress level of 26,000 lb/in^2, a value for P (Larson-Miller parameter - Equation 4) of 43.4 is obtained (Figure 109) for 0.2% plastic creep. Use of 80% of Master Rupture as the design criteria and 26,000 lb/in^2 (actual) stress would result in a value for P essentially the same as that obtained using 0.2% plastic creep design criteria.

Using a value for P of 43.4 in combination with the duty cycle summarized in Table XVIII application of Equation 2 results in:

$$\sum_{n=1}^{n} \frac{t'_n}{t_n} = 0.66$$

2. Cycle Dependent Part (Equation 3)

For missions in which fatigue and load conditions must be combined, a linear damage approach is again recommended for the fatigue part. If Condition 1 is repeated N_1' times and would produce failure in N_1 cycles, Condition 2 is repeated N_2' times and would produce failure in N_2 cycles, etc, then,

$$\frac{N_1'}{N_1} + \frac{N_2'}{N_2} + \cdots + \frac{N_k'}{N_k} = \sum_{k=1}^{k} \frac{N_k'}{N_k} = K$$

The scroll mission life requirement is 1200 hours; however, all of the scroll life will be consumed in the V/STOL portion of the mission, which accounts for only 35% (420 hours) of the mission life. For a creep limited life of 420 hours and a Larson-Miller parameter (P) value of 43.4, the temperature would be approximately 1450°F. The 1450°F value simply represents that level of steady state metal temperature that would provide 420 hours of creep limited life at a stress level of 26,000 lb/in^2. Using this level of temperature, and assuming an alternating stress level of 40,000 lb/in^2, a fatigue life of 700,000 cycles is obtained from Figure 110.

The required number of mission cycles is 12 per hour or 14,400 for 1200 hours life: with N_k representing the fatigue life and N_k' the number of start-stop cycles, then:

$$\sum_{k=1}^{k} \frac{N_k'}{N_k} = \frac{14,400}{700,000} = 0.0206$$

and for the life criteria (Equation 1):

$$\sum_{n=1}^{n} \frac{t_n'}{t_n} + \sum_{k=1}^{k} \frac{N_k'}{N_k} = 0.66 + 0.02 = 0.68,$$

which satisfies the design criteria.

The assumptions and procedures used in this analysis are quite conservative, such as: the use of the maximum stress (26,000 lb/in^2) at all duty cycle operating conditions; the use of maximum instead of average temperature for calculating the "time at temperature"

for each portion of the duty cycle; and the assumption that the metal temperature closely follows the gas temperature under the rapid response conditions associated with the control requirements.

Results indicate that the final scroll design should be more than adequate to satisfy the 1200-hour mission life requirement.

c. Weight Summary

Summarized in Table XIX are final wall thicknesses and scroll component weights.

C. ROTOR

1. GENERAL DESCRIPTION

The LF460 rotor, shown in Figure 111 is an overhung single stage fan with an integral concentric tip turbine drive. There are 88 high aspect ratio fan blades which have two part-span shrouds to control torsional flutter and other blade vibration. The part-span shrouds are located in the mid-portion of the blade near the 1/3 and 2/3 span points, and are aerodynamically contoured to reduce flow disturbance.

The turbine consists of 88 sectors, each containing three shrouded buckets. A three-bucket turbine carrier assembly is integrally attached to each blade tip. This design approach results in a large weight saving when comparison is made with previous lift fans, where a mechanical joint (clevis with a bolt) was used to attach the turbine to the fan blade.

The disk utilizes the twin web geometry proven by operation on previous lift fans. The two-piece disk is electron beam (EB) welded at the rim and brazed at the spacers. This eliminates the need for bolts and results in minimum weight. The stub shaft is integral with the disk, eliminating another mechanical joint.

The LF460 bearings have inner race rotation similar to the LF1 lift fan utilized in the XV-5 aircraft. Silverplated bronze cages are used to minimize power loss. Vacuum melt M50 bearing material is used in the races, rollers and balls to improve bearing fatigue life. The roller bearing employs an out-of-round inner ring which loads the rollers to prevent skidding.

a. Design Features

The LF460 rotor offers the following features not found on previous General Electric turbotip fans:

- Integral blade and tip turbine sector.
- New high strength blade alloy (René 95).
- Torque transmission by two blade part-span shrouds and a blade tip lockup.
- One-piece turbine bucket and tip shroud.
- Buckets designed for improved FOD resistance.
- High temperature bucket alloy, Udimet 700.
- Turbine assembly requires only one braze cycle.
- Electron beam welded disk with integral shaft and integral webs.
- Sump is a self-contained removable subassembly.
- Rotor can be balanced on its own bearings prior to fan assembly.

Other design features include:

- Eighty-eight high-aspect ratio fan blades each integrally joined to three low-aspect ratio turbine buckets.

- Single-hook blade dovetail design.
- Dovetail contact surfaces coated with copper-nickel-indium and Aquadag to minimum fretting and galling.
- Part-span and tip lockup contact surfaces hard-coated to minimize wear.
- Overhung disk.
- Hub flowpath formed by integrally contoured disk platform.
- Rotor supported by two grease-packed bearings (one angular-contact thrust bearing and one pre-loaded roller bearing).

b. Weight and Inertia

During the preliminary design studies which preceded this program, weight and polar moment of inertia goals of 230 lbs and 22 lb/ft/sec^2, respectively, were established for the rotor. The final calculated rotor weight is 230.8 lbs and the rotor polar moment of inertia (I_p) is 18.6 lb/ft/sec^2. An I_p value of 19.5 lb/ft/sec^2 will be used for quotation purposes. The rotor component weights are summarized in Table XX.

c. Assembly

An exploded view of the rotor is presented in Figure 112 The rotor assembly procedure is as follows:

- Assemble the sump subassembly and install on the disk shaft.
- Pan weigh and moment balance each blade-turbine integral assembly. Number the blades in order of assembly for best rotor balance.
- Place blades in an assembly fixture which pretwists the blades. This pretwist is required for proper contact between the blade part-span shrouds and tip lockups.

- Place the disk in position by engaging all of the blade dovetails in the disk slots simultaneously. Install the blade retainer ring.
- Balance the rotor and install on the front frame.

d. Dynamics

Lift fan rotors exhibit dynamic characteristics similar to gas generator rotors, in that both are susceptible to coupled blade-disk vibrations. The rotor dynamic requirement is that no detrimental vibratory mode of the coupled blade-disk be present in the fan operating speed range of 70% to 100% rpm. The design criteria are:

- The coupled blade-disk two-wave vibratory mode should be at least 15% higher in frequency than the 2/rev excitation at 100% rpm.
- The coupled blade-disk three-wave critical speed should be below 70% rpm.
- The rotor must withstand a 1 rad/sec gyroscopic angular velocity at a crossflow velocity of 150 knots.

The results of the axial vibratory analyses are shown in Figure 113. The two-wave resonance has a margin of 14.8% compared to an objective margin of 15%. The differences between the calculated value and the objective is within the accuracy of the analysis. The three-wave resonance occurs at 72% rpm, compared to an objective of 70% rpm. A reduction to the 70% level would not be desirable since any decrease in the three-wave critical rpm would also decrease the 14.8% margin of the two-wave resonance. Design and test experience have shown that placement of the two-wave mode above the 2/rev excitation is more important that having the three-wave mode at the bottom of the operating range. The LF336 has a three-wave resonance at 74% rpm, yet has experienced no blade stress build-up. The results obtained are therefore considered completely acceptable.

e. Deflections

The selected minimum axial clearance between the rotor and stator is 0.60 inches, 0.40 inches for front frame deflection and 0.20 inches for rotor deflection. The rotor deflections for cross flow and gyroscopic loading are shown in Figure 114. The calculated blade tip deflection under combined gyroscopic and cross flow loading is 0.171 inches, compared to the design allowable value of 0.20 inches.

f. Analysis of Low-Cycle Fatigue

All rotor components were assumed to be subject to 12 start-stop cycles per hour. The stress range for the low-cycle fatigue analysis was defined as the difference between the stresses at the 0% speed and 104% overspeed conditions. Half of this stress range was considered to be mean stress and the other half was considered to be alternating stress, as illustrated in Figure 115. A stress concentration factor was applied to both alternating and mean stresses. Table XXI summarizes the results of the analysis. For each major rotor component, the stress range, stress concentration factor and the number of allowable cycles are given.

g. Limiting Stress and Life

A summary of limiting stresses and life for all major rotor components is given in Table XXII. This table lists the material, design temperature, type of loading, and criteria for limiting stress. Comparisons are made between calculated and allowable stresses and calculated and required lives. Margins of safety are given for the limiting stress, either yield, rupture, low- or high-cycle fatigue. All margins of safety are positive. In summary, all rotor components meet the objective levels of allowable stress and required life.

2. BLADE

The blade configuration is shown in Figure 116. The fan contains

88 René 95 blades. Each blade has an integrally attached turbine sector at its tip, two part-span shrouds on the airfoil, and a single hook dovetail at the blade root for disk attachment. The fan blades are multiple circular arc airfoils. Blade geometry is defined in Figure 117. The inner fan flowpath is established by the integral platforms on the blade root and the adjacent disk dovetail posts. The outer fan flowpath is defined by the fan blade tip shroud. Blade rigidity for frequency control and torque transmission is provided at the root by the dovetail, along the airfoil by part-span lockups near the 1/3- and 2/3-span points, and at the tip by the tip shroud lockup. Axial blade retention is provided in the forward direction by an integral hook on the dovetail aft face and in the aft direction by a blade retainer ring.

The YJ97-GE-100 exhaust gas temperature produces metal temperatures in the blade-turbine attachment region above the maximum design allowable temperature of any titanium alloy. For this reason, the blades are made of René 95, a relatively new nickel-base alloy. René 95 offers strength margins higher than other candidate blade materials at room temperature and at elevated temperatures.

a. Design Requirements

The blade has been designed to meet the life and cycle requirements defined in Section III. These requirements include:

- Minimum life of 1200 hours.
- Capable of withstanding 14,400 start-stop cycles.

b. Design Criteria

The blade design criteria are:

- In the fan operating range (70% to 100% rpm), there must be a margin of at least 15% between any blade natural frequency and any per rev excitation frequency from the front frame and stators.

- Blade flutter must not occur prior to fan stall.
- All blade stresses must be less than:
  - 80% of ultimate tensile strength
  - 0.2% minimum yield strength
  - Minimum rupture strength
  - 10^7 cycles on the stress range diagram
- The disk dovetail post must be stronger than the blade dovetail.
- The blade dovetail must be stronger than the blade root.

c. Dovetail

The blade root attachment to the disk is made using a straight, single-hook dovetail with a 55° flank angle. Straight, single-hook dovetails are employed for ease of manufacture and reliability. Strength levels even at overspeed conditions are adequate, as shown in Figures 118 and 119. The dovetail and the dovetail shank extension to the airfoil are progressively stronger than the blade root, as desired.

d. Airfoil

Airfoil centrifugal stress levels at 100% rpm are shown in Figure 120. The distribution of airfoil centrifugal stress plus bending and twisting effects are shown in Figures 121 and 122. The airfoil peak local stress occurs near the hub on the concave surface, as shown in Figure 122.

The alternating stress margin for the peak stress point is shown in the airfoil stress range diagram, Figure 123. All airfoil cross-sections except at the peak stress point have alternating stress margins greater than that shown in Figure 123.

Blade vibration from aeromechanical flutter and strut-induced flow distortion is avoided. Resonant frequencies of the blade

panels are shown in the blade frequency-speed diagram of Figure 124. All blade natural frequencies are safely more than 15% above both the 4/rev excitation of the front frame struts and the 56/rev excitation of the rear frame stators.

Analysis of blade torsional flutter indicates that the three blade panels have the following flutter margins:

Panel	Percent of Flutter Margin at Fan Stall
1	22%
2	21%
3	36%

e. Part-Span Shrouds and Tip Lockup

The blade part-span shrouds (Figures 111, 116 and 125) are triangular platform extensions from the airfoil surface. The shrouds are located near the 1/3 and 2/3 span blade locations. Cross sections through the shroud taken along flow streamlines are elliptical to reduce flow losses. The shroud plan view presented in Figure 125 shows the blade-to-blade fitup. Flat contact surfaces provide lockup between adjacent blades. The contact faces are set at 40 degrees from tangential to balance steady state and dynamic loading. A hard coating will be flame-sprayed onto the contact surface for long life.

Torque transmission is provided by the part-span shrouds and the tip lockups during crossflow and one-engine-out operation. Contact is assured between the blades at all times by installing the blades with pre-twist at assembly, as defined in Table XXIII. Figure 125 illustrates the superposition of loading due to assembly, steady state operation, crossflow and one-engine-out operation. Fan steady state operation increases the assembly contact forces and twist moments. Crossflow and one-engine-out operations cause alternating forces and moments which are always less than those due to assembly and steady state operation, as shown in Table XXIV.

The upper part-span shroud is more highly stressed than the lower shroud. The combined stress in the upper shroud under total loading (centrifugal bending, assembly preload, airload untwist and torque transmission) is relatively low as shown in Figures 126 and 127. As can be seen in Figure 127 at the peak steady state stress of 94.1 KSI, the margin of safety for alternating stress is 0.70.

The blade tip section transitions from an airfoil into the blade tip shroud and siderails as shown in Figures 116 and 128. The blade tip shroud forms the fan tip flowpath and supports the seal. The siderails support the turbine buckets and transmit bucket loads to the blade. The tip shroud and the siderails are machined as integral parts of the blade.

f. Tip Shroud and Seal

The blade tip shroud, like the siderails, is tapered for better utilization of the René 95 material. This taper can be seen in Figure 129. Also shown in Figure 129 is the stress distribution in the shroud under centrifugal loading at 100% rpm. No rupture life is consumed in the blade shroud; therefore, the limiting design criteria is fatigue. The stress range diagram (Figure 130) shows that with a criterion of 10 KSI alternating stress, there is an alternating stress margin of 1.2 at the peak steady state stress point.

The seal (Figure 128) is 0.015 inches thick and is formed from René 41 sheet. This single-tooth running seal rubs the stationary honeycomb seal strip on the front frame-bellmouth assembly, blocking hot gas leakage from the tip turbine into the fan. This seal supports only its own weight and is, therefore, not highly stressed. The seal is brazed to the fan tip shroud, and is replaceable.

g. Siderails

The siderails, shown in Figure 129 and Table XXV are tapered along the tangential surface to obtain maximum material

utilization and to reduce weight. The upper part of the siderails is in the same temperature environment as the braze. At these temperatures, only 25% of rupture life is consumed; therefore, fatigue is the limiting design criteria for the siderails. The siderail vibratory stress limit is 10,000 psi. The siderail stresses and margins of safety are shown in Table XXV.

3. TURBINE

The turbine contains 264 hollow uncooled buckets, arranged into 88 sectors of three buckets each. Each sector is an integral part of one fan blade. The integral blade-turbine eliminates the clevis and bolt connection used on previous lift fans, resulting in a light-weight low inertia rotor system.

A blade-turbine sector, shown in Figure 128, consists of:

- Three buckets, each with integral internal stiffener and integral tip shroud.
- A two-piece sheet metal box section.
- A one-piece sheet metal forward air seal tooth.
- One fan blade with integral siderails, part-span shrouds, blade tip shroud and tip lockup.

The buckets are equally spaced over the blade, with the center of gravity of the center bucket in line with the blade stacking axis. The box section (Figure 128) positions the buckets and adds structural rigidity by absorbing bucket gas bending loads. The siderails are integral parts of the blade. The attachment of the buckets and box section to the siderails is the only structural braze joint in the blade-turbine sector assembly.

a. Design Requirements

The turbine has been designed to satisfy the life and cyclic requirements defined in Section III. These include:

- 1200 hours life.
- Capability of withstanding 14,400 start-stop cycles.

In addition, the rotor system is designed to provide:

- Minimum axial clearance of 0.60 inches between the turbine and any stationary fan component.

b. Design Criteria

The following criteria have been established:

- All stresses must be less than:
  - 0.02 minimum yield strength
  - Minimum rupture strength derated for thin wall high temperature effects
  - 10^7 cycles on the stress range diagram
- Bucket uncorrected gas bending stress must be less than 10,000 psi. This is a criterion which regulates the bucket stiffness for acceptable vibratory stress.
- Gas bending stress during one engine-out must be less than twice the gas bending stress during normal operation.
- The endurance limit of all thin-wall high-temperature components must be no more than 70% of the material minimum endurance limit.
- All calculated turbine natural frequencies must be at least 15% higher than any known per-rev excitation frequency in the operating range of 70% to 100% speed.

The turbine mechanical design is based on the metal temperatures shown in Figure 131. These temperatures were calculated based on LF336 turbine carrier heat transfer data measured during recent fan tests, adjusted for the exhaust gas temperature of the YJ97-GE-100 gas generator.

c. Bucket

The bucket cross section is shown in Figure 132. The one-piece bucket and tip shroud (Figure 133) is manufactured from a Udimet 700 forging. Electric Chemical Machining (ECM) and Electric Discharge Machining (EDM) are used to generate the external contours and surfaces. The inside cavities with integral stiffeners are formed by ECM. This manufacturing process eliminates critical leading and trailing edge welding, brazing, and bend-forming problems. The leading edge suction surface wall thickness is twice as thick as the other walls (Figure 132). This added thickness and the solid leading edge provide added resistance to foreign object damage compared to previous bucket designs.

The turbine frequency-speed diagram is shown in Figure 134. As indicated, no critical excitations exist throughout the turbine operating range of 70% to 100% rpm. The smallest frequency margin, between the first torsional frequency and the 16/rev excitation frequency, is 30% at 100% rpm, which is well above the established criterion.

The buckets are tilted one degree from the radial direction. The restoring moment due to the centrifugal force cancels 70% of the bucket gas bending stress. The bucket steady state stresses, given in Table XXVI indicate that the bucket uses no appreciable amount of its rupture life during its operation. Fatigue is the limiting design criteria for the bucket. Figure 135 is the stress range diagram for Udimet 700 at 1400°F, which is the predicted bucket metal temperature when the YJ97-GE-100 is operating at 2060°R EGT. As shown in Figure 135 and in Table XXVI the bucket meets the requirements of both the steady state and the one engine-out operating conditions.

d. Bucket Tip Shroud

Based on a 35,700 psi maximum stress at 100% rpm, the bucket shroud uses only 4% of its rupture life during operation. Fatigue is, therefore, the limiting design criteria for the shroud.

Figure 136 shows the stress distribution in the shroud under centrifugal loading at 100% rpm. Figure 137 is the stress range diagram for Udimet 700 at 1400°F. As indicated in Figure 137, there is adequate alternating stress margin for the fatigue sensitive area of the shroud.

e. Box Section and Braze Joint

The buckets are held by the siderails and by the vertical walls of the box section. The horizontal box members and the braze fillets are conservatively considered as having no major load carrying ability. A rupture stress limit of 9,000 psi at 100% rpm, based on a 100% life consumption, was set for the braze. The braze area was selected so that the stress level was within this rupture life requirement. The box section vertical walls are brazed to the siderails. The maximum shear stress in this joint is 4000 psi, well below the allowable braze stress limit of 9,000 psi.

4. DISK AND SHAFT

The disk and shaft transmit blade and bucket loads to the bearings, and must have sufficient strength to limit rotor tip deflection to reasonably small clearance variations with the non-rotating parts.

The fan has a titanium integral shaft and disk arrangement utilizing an electron beam welded disk assembly. The LF460 and the LF1 used in the XV-5 aircraft both have an overhung disk and a rotating shaft, but are quite different, as shown in the comparison given in Table XXVII.

a. Design Requirements

The disk and shaft are designed to satisfy the following requirements:

- Design speed of 100% rpm (4300 rpm)
- Burst speed not less than 122% rpm
- Design life of 2400 hours

- Able to withstand at least 28,800 start-stop cycles.

b. Design Criteria

The following criteria have been established:

- The steady state meanline stress must be less than the material 0.02% yield strength.
- The steady state bore stress and the maximum maneuver surface stress must be less than the material 0.2% yield strength
- Minimum material properties.

c. Disk

The disk halves are welded together using electron beam welding. The stub shaft is integral with the forward disk. The disk rim is contour-machined to form the hub flowpath. The blade retainer hooks are located on the aft face of the rim. The disk material (titanium 6-4) was chosen for its machineability and weldability. The welded joint properties of titanium 6-4 are greater than 90% of those of the parent material.

The disk forward web meanline stress distribution is shown in Figure 138. The disk forward web surface steady state stress distribution is shown in Figure 139. All calculated stresses are within the allowable values. The disk is stiffness-limited rather than stress-limited due to system dynamic requirements.

Figure 140 is the stress range diagram for the disk dovetail. At the peak steady state stress point, the margin of safety for alternating stress is 0.3.

d. Shaft

The shaft steady state stress distribution is shown in Figure 141. The shaft maximum bending stress during a gyroscopic

maneuver is 6600 psi/radian. The shaft stresses are safely below the 0.2% yield criterion.

5. BEARINGS AND SUMP

The bearings and sump maintain rotor concentricity and alignment with non-rotating parts with minimum friction loss. The bearings and sump transmit rotor thrust, maneuver loads, and other dynamic loads to the fan frame.

The LF460 bearing arrangement (Figures 111 and 112) is similar to the LF1 installation, consisting of one deep-groove angular-contact, split-inner-ring ball bearing and one light-weight roller bearing. The bearings are grease-lubricated (Unitemp 500) as are all other General Electric lift fan bearings. The bearings are sealed by four radial lip seals.

The LF460 has a common bearing housing not used on previous General Electric lift fans. This packaged bearing concept offers the following advantages:

- Bearings are sealed from the environment.
- Improved maintainability of bearings and seals.
- Sump hardware can be assembled on the disk shaft and stored until needed.
- Rotor assembly onto the frame is facilitated.
- The rotor can be balanced on its own bearings.

a. Design Requirements

The bearings and sump have been designed to meet the following requirements:

- Minimum life of 600 hours.
- Minimum regrease cycle of 10 hours.
- Ability to withstand a minimum of 7200 start-stop cycles.

b. Ball Bearings

The ball bearing is a split inner ring, deep groove, angular-contact bearing. There are puller grooves in the inner and outer rings to facilitate disassembly. The balls and rings are M50 steel. The bearing has the maximum ball complement, retained by a precision-machined one-piece silicon-iron-bronze cage. The basic dimensions of the ball bearing are given in Table XXVIII.

c. Roller Bearings

The roller bearing uses cylindrical rollers and a separable inner ring. The precision-machined one-piece cage permits a maximum roller complement. There are puller grooves in the inner and outer rings to facilitate disassembly. The rollers and rings are M50 steel and the cage is silicon-iron bronze. This bearing has an initial load (preload) to prevent skidding. This preload is obtained by using an out-of-round inner ring. This concept has been successfully demonstrated on the LF336 lift fan. The basic dimensions of the roller bearing are given in Table XXIX.

d. Temperatures

The bearings are cooled by airflow through the hollow shaft. This airflow is caused by the pressure gradient which exists across the rotor. The results of the heat transfer analysis for the hover design point are shown in Figure 142. Although the bearing ring steady state temperatures are 300°F, transient temperatures during transition may go up to 600°F. The analysis indicates that the disk, shaft and sump temperatures are all safely within material property limits.

e. Lubrication

The bearings are lubricated with Unitemp 500 grease. This grease has limited service life above 400°F. Data are being accumulated on the LF336 bearings, which use Unitemp 500 grease and which have temperatures between 500° and 600°F during crossflow operation. Regrease

intervals for the LF460 can be estimated as additional LF336 test experience is accumulated.

The bearings can be regreased using the external grease fittings on the bearing housing, as shown in Figure 111. The grease is directed to each bearing through internal passages. Each bearing has its own distribution system. Grease is maintained in the bearings by spring-loaded radial lip seals using metallic-filled teflon seal lips.

f. Life

The bearings are designed in accordance with AFBMA and General Electric design practices. The calculated bearing fatigue lives, including the effects of crossflow, are 369 hours for the ball and 249 hours for the roller. Adjusting these lives per General Electric design practices for material improvements (5X for M50) and for grease lubrication ($\frac{1}{2}$X), the calculated bearing fatigue lives become 620 hours for the roller and 920 hours for the ball.

D. REAR FRAME

1. GENERAL DESCRIPTION

The rear frame (Figure 143) is designed to turn the fan flow in the axial direction. Air and maneuver loads induced on the fan stators are transferred to the mid-box and then through the eight turbine stators to the rear frame casing which transfers the loads to the scroll. The rear frame is also designed to provide noise suppression through the use of leaned stators, two chord rotor-stator spacing, and acoustically treated splitters and flowpath walls.

2. DESIGN REQUIREMENTS

The rear frame is designed to satisfy the design requirements defined in Section III. The following requirements are specifically applicable to the rear frame.

- Operate for a minimum average life of 2400 hours without repair and an average of 6000 hours with repair.
- Accept a maximum of 80,000 start-stop cycles.

In addition, the rear frame is designed to:

- Maintain adequate clearance during all fan operating conditions to prevent interference with rotating parts.
- Accurately regulate the design gap of the aft air seal to minimize leakage flow from the fan stream to the turbine stream.

3. COMPONENT DESIGN DESCRIPTION

The major rear frame components are shown in Figure 144 and discussed in the following paragraphs.

a. Hub Disk

The hub disk provides radial stiffness through the center of the rear frame and allows access to the instrumentation at the hub of the rotor. The disk is formed from two 0.010 inch aluminum 6061T6 face sheets bonded to an aluminum 5052 honeycomb core. The core has 0.25 inch cells with a height of 0.23 inch. The disk is bolted to the hub with sixteen 0.1875 inch bolts.

b. Hub

The hub assembly retains the inboard end of the fan stator vanes and provides frame structural stiffness at the hub. A Y-shaped transition section extends from the hub disk to the hub structural box section at the inner fan flowpath. The transition section has 0.010 inch aluminum 6061T6 sheets which are bonded together forming a flange at its inner diameter for attachment to the hub disk. The transition section is also bonded to the circumferential box section at its outer diameter. Sixteen 0.1875 inch anchor nuts are riveted

to the transition section at the forward side of the attachment flange.

Three sides of the circumferential box section are formed from 0.020 inch sheet 6-2-4-2 (6Al-2Sn-4Zr-2Mo) titanium. The fan stator vanes are brazed into the box section. The inner fan flowpath contour (the fourth side of the box) is formed by fifty-six individual fiberglass inserts which are placed between the fan stator vanes. The stock thickness of the fiberglass is 0.030 inches. The 0.5 inch box section is filled with 0.375 inch cell size fiberglass honeycomb. The fiberglass sheets and honeycomb are bonded in place between the fan stator vanes.

The inner fan flowpath between the rotor and the rear frame structure is established by a bonded fiberglass honeycomb box section which is bolted to the transition section of the hub with eight 0.1875 inch bolts. The two fiberglass face sheets are 0.030 inch thick and are separated 0.5 inches by 0.375 cell size fiberglass honeycomb. The inner fan flowpath is acoustically treated through the use of 0.0625 inch diameter holes and a hole porosity of 22 percent.

c. Fan Stator Vanes

The fan stator vanes turn the fan flow in the axial direction, inducing a lift and circumferential torque load into the rear frame. A total of 56 hollow 6-2-4-2 titanium fan stator vanes are incorporated into the rear frame. The vanes are double circular arc airfoil sections with a thickness/chord ratio (tm/c) of 4.755%. The actual vane chord is 3.83 inches. The vanes have 6 degrees of twist and an overall length of 17.72. The camber angle varies linearly from hub to tip, with an average value of 39.6 degrees.

The stator vane skin thickness is 0.020 inches between the outer splitter and the mid-box, locally at the inner

splitter and hub, and along the leading and trailing edges. The remaining portion of the vane skin is 0.010 inches thick. The increased stock thickness locally at the hub and inner splitter, and the leading and trailing edges is to facilitate brazing of the stator vanes. Shown in Figure 145 are the die formed 0.005 inch thick internal stiffeners which are brazed into each hollow vane. The two full span hat sections provide stability for the vane skins to preclude panel buckeling failures, while the corrugated portions of the stiffener which covers the full chord provide a load path across the vane at each of the structural boxes. The portion of each vane that is inside the mid-box has four 0.3 inch diameter eyeletted holes to allow cooling air to flow circumferentially around the mid-box.

d. Acoustic Splitters

Two splitter rings are included in the fan flowpath to reduce the noise level of the fan and to provide aero-elastic stability for the fan stator vanes.

Both the inner and outer splitter are of similar construction. The inner acoustic splitter is located at an average radius of 16.76 inches (in the vane trailing edge plane) and the outer acoustic splitter is located at an average radius of 22.61 inches. The leading edges of both splitters are positioned four inches aft of the rotor centerline. The splitter face sheets are fabricated from 0.020 inch sheet titanium (6-2-4-2) and 0.030 inch sheet fiberglass. The splitters have a constant thickness of 0.54 inches from the leading edge to the trailing edge of the vane. The 0.010 inch thick internal wiggle strip is fabricated from C.P. titanium. Forward of the stator vane leading edge the inner 0.020 inch thick splitter face sheet is titanium. The 0.030 inch thick outer face sheet and the 0.020 inch thick wiggle strip are a fiberglass fabrication. The titanium portion of the splitter is brazed to the stator vanes and the fiberglass is bonded to the titanium. A 0.010 inch thick AMS 5510 stainless steel leading edge is bonded to each splitter for added F.O.D. resistance.

Both sides of the acoustic splitters are perforated with 0.0625 inch diameter holes, with a 22% hole porosity.

e. Mid-Box

The mid-box transfers the stator vane loads to the eight turbine struts and supports the acoustically treated outer fan flowpath. It is a brazed circumferential box section fabricated from 6-2-4-2 titanium. Aft of the turbine strut leading edge, the inner and outer face sheets are 0.020 inches thick while the forward portion of the face sheets are chem-milled to a 0.010 inch thickness. At the aft end of the inner face sheet, a channel is formed inward that becomes the aft end close-out for the acoustic panel. At the aft end of the outer face sheet, a channel is formed outward to support the aft insulation blanket and to provide a slip-fit attachment for the exhaust liner. Four and one-half inches forward, another channel is welded to the outer face sheet which supports the forward insulation blanket and provides an additional slip-fit attachment to support the middle of the exhaust liner. Eleven "U" channels (0.010 inch thick and 0.93 inch wide) are brazed between the face sheets providing the required panel stiffness. The mid-box cooling flow is directed through eyeletted 0.375 inch diameter metering holes in the channels. Each channel which is penetrated by a turbine strut or a fan stator vane is brazed to that strut or vane. The mating of the channels and vanes is accomplished by brazing a 6-2-4-2 titanium angle piece (0.010 inch thick with 0.2 inch legs) at each joint. This assures continuity of the load paths and efficient load transfer. Riveted anchor nuts (0.1875 inch) are used on the forward end of the mid-box closeout channel to retain the aft air seal and the exhaust liners.

Bonded to the fan side of the mid-box is the acoustically treated, fiberglass outer fan flowpath section. A circumferential honeycomb panel made in eight sections is utilized in this flowpath section forward of the fan stator vanes. Through the stator vane row, individual

acoustic panels are placed between the vanes. The honeycomb panels have 0.03 inch face sheets with 0.375 inch fiberglass honeycomb core. Overall thickness of the panels is 0.53 inch. The panels are bonded to the mid-box inner face sheet and the titanium closeout.

f. Exhaust Liner

The exhaust liners (Figures 144 and 146) form the inner flowpath contour through the turbine exhaust section and protect the insulation from the 1200°F high velocity exhaust gas. Hastelloy X material (0.015 inch thick) was selected for the sixteen liner segments. The liners are assembled in pairs and then inserted between the eight turbine struts. On the insulation side of the liner, at the middle and aft end, are extensions which "fishmouth" over two circumferential support channels attached to the mid-box. The sides of each pair of liners also have overlap (fishmouth) connections which fit around a flange provided by the turbine strut heat shield. The heat shield is shown in phantom in Figure 146. The forward end of each liner is flanged inward and bolted with two 0.1875 inch bolts to the forward side of the mid-box.

g. Turbine Strut

The eight turbine struts transfer the rear frame loads to the casing. The unibal connection between the struts and the casing assure that only axial and tangential loads (no moments) are transferred into the casing, while the sliding pin allows unrestricted radial growth.

The struts also function as ducts to pass cavity purge air to the mid-box. The structural portion of the turbine strut is shaped like an isosoceles trapezoid. The hollow strut is fabricated from 0.03 inch 6-2-4-2 titanium. Within the strut are five "U" channels with stock thicknesses of 0.010 inches. The channels provide added strength and stabilize the thin strut skins. The turbine strut, which

has an overall length of 5.25 inches, is brazed to the mid-box.

At the pinned connection, the turbine strut has a solid block of 6-2-4-2 titanium brazed between two of the stiffeners. After brazing has been completed, a 0.2 inch diameter hole is drilled through to the block with a 0.75 inch diameter spotface. The spotface provides the cavity for the 0.75 inch diameter pin which is torqued to a 0.25 inch anchor nut attached to the back side of the block.

The aft two stiffeners and close-out for each turbine strut extend into the fan cavity through a cutout in the casing. This duct provides the inlet for the cavity purge air used to cool the mid-box.

h. Heat Shield

The turbine strut heat shield (Figure 147) protects the insulation and the titanium structural portion of the turbine strut from the high velocity 1200°F turbine stream. The aerodynamic contour of the turbine strut is defined by the heat shield, with the maximum thickness occurring in the fan exit plane.

The heat shield, which is fabricated from 0.015 inch Hastelloy X sheet, extends from the mid-box into the turbine strut housing in the casing. At the inner turbine flowpath the heat shield is flanged to provide a slip-fit connection with the exhaust liner. A close out which is welded to the outer end of the heat shield, connects the cover and cap. In the final assembly, the cover protects the strut insulation which incases the strut.

The cap (Figure 147), which is fabricated from 0.015 inch Hastelloy X sheet, provides a passage for the cooling flow as it exits from the mid-box and enters the turbine stream. Internally, two channel sections are used to stiffen the structure and control the cooling air distribution. In order to maintain the proper exit area for the cooling air, a corrugated strip is welded between the cap and the heat shield.

i. Casing

The casing (Figure 148), which transfers the rear frame loads to the scroll, is a circumferential stiffened box section. For thermal compatibility with the scroll, the entire casing is fabricated from the same material as the scroll (René 41). Two vertical face sheets, 0.02 inches thick, are separated by nine "U" channels, which act as stiffeners and closeouts for the structural box. The channels are corrugated on the outside leg to provide passage for the hot gas flow which is required to heat the outer face sheet. Fifty equally spaced 0.5 inch diameter holes are located on the inner face sheet 0.5 inches forward of the fan exhaust plane to provide entrance for the exhaust gas, while fifty equally spaced 0.375 inch diameter holes, located 0.5 inches aft of the casing leading edge, are used to eject the hot gas back into the exhaust stream. In eight positions, the inner face sheet and channels form a pocket to allow access for the eight turbine struts. The recess is 0.8 inches deep, and is sealed with a 0.020 inch thick closeout.

The unibal housing between the closeout and the outer face sheet of the casing is formed from a two inch diameter by 1.2 inch thick René 41 bar brazed in place and machined to accept a 0.75 inch unibal. A threaded retainer screws into the housing to hold the unibal in place, and a snap ring is used to lock the retainer.

The forward two and one-half inches of the inner face sheet are contoured slightly outward. With a 0.25 inch radius, the leading edge, which has a 0.25 inch radius, is formed outward and butt welded to a 0.020 inch disk, which with the outer casing face sheet and a 0.060 inch thick machined strip are welded together to form a flange. Eighty 0.2 inch diameter bolt holes on a 69.36 inch diameter bolt circle are used to mount the scroll.

j. Mid-Box Insulation Blanket

Sixteen Dyna Flex insulation blankets (0.5 inches thick)

insulate the mid-box structure from the 1200°F turbine exhaust gas. Two blankets are located between each pair of struts and are contained between the exhaust lines and the mid-box. The two channel supports (at the middle and the aft end of the mid-box) position the blankets, while the forward end of the forward blanket is bolted between the exhaust liner and the mid-box.

The insulation selected has a density of 12 lbs/ft^3 and a thermal conductivity of 0.7 Btu in/(sq ft-hr-°F) at 1200°F. The blanket is bagged in 0.003 inch quilted AMS 5510 stainless steel foil.

k. Turbine Strut Insulation

The turbine strut insulation provides thermal protection for the structural portion of the strut.

A layer of Dyna Flex insulation separates the Hastelloy X heat shield from the titanium structure. The insulation has a density of 12 lbs/ft^3 and a thermal conductivity of 0.7 Btu in/(sq ft-hr-°F) at 1200°F. The insulation is bagged in 0.003 inch quilted AMS 5510 stainless steel foil.

l. Aft Air Seal

The aft air seal restricts the flow of air from the fan stream to the turbine stream. This concept, which differs from the approach used on previous lift fans, provides for removal of a portion of the fan boundary layer (forward air seal leakage). This results in the exposure of the mid-box to lower temperatures. The aft air seal, which bolts to the forward end of the mid-box, is fabricated from Hastelloy X in 22.5° segments (16 pieces). The seal has two slotted holes per segment which allow for radial seal clearance adjustment.

4. MID-BOX COOLING

Because of the large temperature difference that exists between the turbine and fan streams, it is necessary that the mid-box be either insulated and cooled, or fabricated in segments, accepting the thermal stresses induced between the stator vanes and the mid-box. The use of insulation and cooling air results in a lower component system weight; this approach was therefore selected for the LF460 design. After consideration of several cooling air sources, the decision was made to use air taken from the aircraft cavity surrounding the fan. This approach provides air at an acceptable temperature and pressure, and eliminates the need for blowers in the aircraft (as were used in the XV-5 aircraft) to remove the warm air surrounding and receiving heat from the fan.

The selected mid-box cooling scheme is illustrated in Figure 149. Cooling air is ducted from the aircraft cavity surrounding the fan through the eight turbine struts. As shown in the figure, the air is directed through the structural portion of the turbine strut in a manner to provide effective cooling. The cooling air enters the mid-box through air passages inside of the strut and flows circumferentially. Mid-way between adjacent turbine struts the air is turned 90° flowing into the forward portion of the mid-box, and is then turned an additional 90° flowing back to the struts. The air is ducted back into the eight turbine struts through the false leading edge (cap) and is ejected into the turbine stream.

Estimates indicate that a cooling flow rate of 0.8 lbs/sec is sufficient to cool both the turbine struts and the mid-box and to maintain the aircraft cavity at a temperature below 125°F (Standard Day Conditions).

5. DESIGN RESULTS

Results of design analyses are presented in Figure 150. The stress levels shown represent the maximum values under combined

loading conditions. As shown, the maximum stress occurs in the fan stator vane at the point of attachment to the mid-box. All stress levels are within allowable limits.

A summary of final rear frame component materials and weights is presented in Table XXX.

SECTION VIII

PERFORMANCE

Performance of the LF460 lift system was obtained using the gas discharge conditions of the YJ97-GE-100 turbojet engine. The performance of the basic engine was calculated using the estimated performance data deck [10] provided for the engine. Minor modifications of the performance deck to provide the necessary gas generator data included a revision of the exhaust system to eliminate the nozzle included in the turbojet engine system and an increase of the fuel flow limits to permit operation at overtemperature conditions.

The gas conditions obtained from the engine deck were then used as input to the LF460 fan off-design performance deck. The LF460 off-design calculation was based on the estimated fan and turbine maps and characteristics of the fan inlet and exhaust systems. Using this approach, a preliminary performance bulletin [11] was prepared for the use of the NASA and the aircraft companies in research aircraft concept definition studies.

As a part of the modified contract, a customer performance deck suitable for use on the IBM 360 computer is being prepared. The result of these efforts will be a combined fan/gas generator system performance deck which will integrate the performance of the YJ97-GE-100 gas generator and the LF460 lift fan. The deck will include provisions for applying installation effects such as ducting performance, lift control method, engine and fan inlet recoveries and fan exhaust performance. Options will also be provided for operating the lift fan unit as a conventional fan-in-wing (shallow inlet), as a fuselage fan (deep inlet) or as a cruise fan with inlet nacelle and exhaust nozzle. Since these data will be available for detailed performance calculations, only basic design point and static performance data will be presented in this report.

A. DESIGN POINT PERFORMANCE

The LF460 lift fan is sized to operate using the exhaust gases of a single YJ97-GE-100 engine. Operation at the fan aerodynamic design point can only be achieved by operating the engine at a short-time over-temperature condition with some flow addition from a second cross-coupled engine.

Design point and off-design performance presented herein is based on an assumed lift fan installation typical of a shallow inlet system. Thus, design point performance in this case represents installed performance versus the usual approach for turbojet or turbofan engines to present design point performance on an uninstalled basis. This installed systems approach is required since the lift fan aerodynamic design is dependent on the installation assumptions, and operation at the design point cannot be achieved in the uninstalled condition. The installation assumptions used in calculating the performance are summarized in Table XXXI.

Performance of the LF460 at the Nominal Rated and Maximum Control settings at sea level static, standard day conditions is given in Table XXXII.

B. OFF-DESIGN PERFORMANCE

Off-design performance at sea level static conditions is presented for the LF460 over a range of engine power settings. Standard day performance data are presented for the gas generator and fan in Figures 151 and 152 respectively. Corresponding data for a hot day (90°F) are presented in Figures 153 and 154. These data are based on the assumption that the lift fan is supplied by gas from a single gas generator. The engine discharge and fan scroll nozzle flow functions are sized for rated temperature operation of the engine on a standard day.

C. PERFORMANCE WITH CONTROL

Modulation of the thrust levels of the LF460, as required for aircraft attitude control, is accomplished by short-time overtemperature operation of the YJ97-GE-100 engine with flow augmentation from the interconnected engine. Component and system performance characteristics are presented in Figures 155 through 158 for sea level static standard and hot day conditions. Performance is presented at the maximum power setting of the engine with overtemperature levels not exceeding the short time limit (2060°R), as established for the fan design. Operation of the fan in this control mode results in a fan thrust increase of 23 percent on the standard day and 19 percent on the hot day.

D. SINGLE ENGINE OPERATION

Two LF460 lift fans are capable of operating on the gas flow from a single gas generator by virtue of the double entry, split scroll. Estimated performance for operation of the fan system in this mode can be obtained by multiplying the appropriate performance parameter by the correction factors given in Table XXXIII.

E. TRANSIENT PERFORMANCE

LF460 transient response was calculated for the gas conditions defined previously. Fan speed and thrust time constants were obtained for step changes in the gas conditions; thus, the data represents the fan alone response. The time constant is defined as the time, in seconds, required for the fan to reach 63.2 percent of a commanded step change.

Shown in Figure 159 are the LF460 thrust and speed time constants versus gas generator speed. Response for changes of 20 percent thrust and about 10 percent speed are given. The fan thrust time constant of the LF460 is 0.21 seconds at 101.5% gas generator speed (1835°R EGT).

SECTION IX

INSTALLATION

The LF460 lift fan combined with the YJ97-GE-100 turbojet engine gas generator represents the basic V/STOL propulsion system. The LF460 was designed to operate primarily in a shallow inlet installation where the upper structure surface blends into the inlet bellmouth provided with the lift fan. The exhaust system of the fan was designed for operation in combination with thrust vectoring louvers, although the louvers are not provided as an integral part of the lift fan structure. Optional installation of the LF460 as a deep inlet fuselage fan or as a cruise fan is possible providing the restrictions discussed in subsequent paragraphs are considered.

A. LIFT FAN INSTALLATION

The LF460 lift fan system was designed to accept the exhaust gas from the gas generator through a double entry scroll. The fan installation drawing is presented as Figure 160. Each of the two bolted inlet flanges is designed for attachment to a free bellows that will be a part of the aircraft ducting system; thus, the forces transmitted to the scroll inlet are limited to the pressure-area (piston) force and shear forces, as established by system deflections and the nominal spring rate of the bellows system.

The attachment of the structure surrounding the fan bellmouth shall be accomplished using an airframe-furnished flexible seal. A bolted flange is provided around the periphery of the bellmouth for attachment. Sufficient radial clearance shall be provided to insure at least a quarter of an inch minimum clearance in both the cold and normal hot running conditions. The seal arrangement shall have sufficient flexibility to absorb all airframe deflection while imposing negligible loads on the fan inlet.

Although presently not defined, because of the dependency on the particular aircraft installation, a seal shall also be provided around the periphery of the fan discharge plane. This seal must absorb both the thermal and structural deflections with adequate sealing to prevent hot gas leakage into the fan-aircraft structural cavity. Careful attention in the design of this aft seal is required to prevent the flow of the fan exhaust gases into the aircraft cavity during fan throttling. This has been a problem in previous fan installations.

Provision must also be made in the installation for a free flow-path for the aircraft cavity air that is used to cool the mid-box.

Possible application of an exit louver system has been considered in the fan aerodynamic design. The effective area of the louver system must be equal to or greater than 1750 square inches. This requirement infers a dropped louver cascade if thrust vectoring angles in excess of 35 degrees and/or thrust spoiling in excess of 15 percent are required. It should be noted that attachment of a louver system directly to the fan has not been considered in the fan structural design.

Similarly, the fan structure has not been designed to accept an inlet closure system primarily because of the dependency of a closure system on a particular aircraft system. If it is desirable to mount an inlet closure system directly to the fan structure, the effects on front frame structural design and fan weight must be evaluated.

B. WEIGHTS AND INERTIAS

The weights and inertia data for the basic fan system are presented in Table XXXIV. These data are applicable for evaluation of the particular mount reactions under maneuver load conditions.

C. MOUNTING SYSTEM

The LF460 lift fan mounting system incorporates five separate mounting point locations. Presented in Figure 161 is a schematic of

the recommended types of restraint at each mount location. With the exception of the stabilizing link at mount location E, the system is a conventional non-redundant structure. The additional restraint at E is required to maintain structural stability of the free quadrant of the bellmouth and scroll system relative to the rotational axis of the fan, particularly during engine-out conditions when only 180 degrees of the scroll will remain active.

Mount reactions for the recommended mounting system are tabulated in Table XXXV. Forces for static and crossflow operations are given along with reactions experienced under conditions of unit maneuver loading.

D. CRUISE AND FUSELAGE INSTALLATION

The fan unit may be installed and operated as a cruise or deep inlet fan providing the inlet diameter at the juncture to the fan bellmouth is large enough to minimize changes in the flow conditions at the fan tip. The aerodynamic design of the rotor blading was established based on high velocities adjacent to the bellmouth. An inlet system with a flow diameter less than 69 inches will produce flow changes significant enough to affect fan stall margin.

E. YJ97 INSTALLATION

Installation requirements and descriptive information for the YJ97-GE-100 engine are given in the engine model specification.[10] Modification of the engine to meet the requirements of the LF460/YJ97-GE-100 lift fan system is accomplished by removal of the tailpipe and exhaust diffuser cone normally provided for the turbojet configuration. The airframe ducting system will attach directly to the engine turbine frame flange in place of the removed components.

The ducting system downstream of the engine flange shall not transmit any loads to the engine other than the axial force due to the pressure-area (piston) force of the ducting and the spring rate of the ducting bellows system.

SECTION X

DISCUSSION OF RESULTS

The basic program requirement was the detail design of the LF460 turbo-tip lift fan for application to a V/STOL transport research aircraft. The major objective was to achieve low fan noise while maintaining the high thrust/weight capability of a high pressure ratio lift fan system.

The final estimated noise level of a single fan is 97.3 PNdB at a 500 ft sideline, when the fan is used in combination with acoustic exit louvers. Assuming reasonable installation acoustic treatment, a total aircraft noise level in the range of 100 to 103 PNdB should be possible for a six fan research transport configuration.

The objective fan weight of 789 lbs was achieved with a margin of 34 lbs for fan development. This results in a fan thrust/weight ratio of 19.1 at the maximum control thrust point and 15.5 at the nominal (noise rating) point, based on representative installed performance.

The rotor polar moment of inertia (Ip) objective of 22.5 $lb/ft/sec^2$ was bettered, with a calculated value of 18.6. An Ip level of 19.5 $lb/ft/sec^2$ will be used for quotation purposes, allowing approximately 5% margin for development and fan to fan variation.

The rotor design is based on estimated René 95 material properties and braze joint strengths. A material technology program, scheduled for completion in December, 1971, will provide substantiation of the design and/or identify areas requiring modification.

The LF460 contains a number of new features that provide significant improvements over previous lift fan designs. These features include:

- Integral turbine bucket with wall thickness control for FOD protection.

- Single turbine carrier braze cycle versus multiple cycles required for previous assemblies.

- Self-contained, removable sump assembly that permits the rotor to be balanced on its own bearings prior to assembly.

- Tri-lobe roller bearing to eliminate bearing skid-design approach substantiated in recent LF336 fan tests.

- Bearing regrease system that permits addition of grease without fan disassembly - design to be evaluated in the LF336 fan in near future tests.

- Turbine exit diffuser to reduce turbine jet velocity and jet noise floor while maintaining a small bucket height based on a high turbine discharge Mach number. The diffuser also provides a low static pressure at turbine discharge to assure leakage flow from the fan stream to the turbine stream at rotor exit.

- Mid-box and turbine strut cooling system that uses cooling air taken from the aircraft cavity. The use of cavity air for cooling eliminates the need for aircraft blowers that would otherwise be required to remove air surrounding and receiving heat from the fan high temperature structure.

- Low noise features: high number of fan rotor blades, resulting in a high puretone frequency; two chord rotor/vane spacing; stator vane lean; hub and outer wall acoustic treatment; and acoustic splitters.

The fan and turbine aerodynamic designs represent reasonable extensions of established turbotip fan technology. The fan aerodynamic design is based on General Electric solidity/aspect ratio correlations; however, the absolute values of aspect ratio exceed General Electric Company experience for the levels of aerodynamic loading used in the design. Manufacturing tolerances on the two part-span dampers must be tight to achieve a satisfactory aerodynamic design.

The high pressure ratio turbine incorporates converging-diverging nozzles (new to turbotip lift fans) and increased bucket relative Mach numbers. These design features are necessary to achieve good fan performance, but add increased risk to the design.

One component area requiring possible future attention is the scroll. The triple bubble concept used in the LF460 design was selected to meet the NASA requirement of minimum installed fan diameter and fan depth. The resulting design meets the objective, but is complex and will be a high cost item. Studies of other scroll concepts indicate that if minimum fan depth is not a requirement substantial savings in weight may be possible with a simpler and lower cost scroll.

SECTION XI

CONCLUSIONS

1. The LF460 YJ97-GE-100 turbotip lift fan system will meet the requirements of a V/STOL transport research aircraft, and will provide the capability of attaining a total aircraft noise level of 100 to 103 PNdB at 500 ft sideline for a six fan aircraft.

   No credit has been assumed for possible reduction of aircraft noise levels due to tailored aircraft flight paths, thrust scheduling and vectoring of the lift and cruise engines. Noise contour studies for CTOL and STOL aircraft have shown appreciable improvements in the ground noise contours. These effects for VTOL aircraft should be evaluated as a part of the aircraft system studies.

2. Detail design analysis indicates that the objective weight can be achieved, and the objective rotor polar moment of inertia can be substantially bettered, providing results of the René 95 material and braze property data program are favorable.

3. Scroll modifications to reduce weight, complexity and cost should be evaluated if aircraft studies do not indicate a need for a minimum depth fan.

4. Fan full scale or model aerodynamic tests are considered mandatory to substantiate the design and/or provide necessary direction for modification prior to proceeding with a fan development program.

5. Turbine cold flow rig tests are desirable prior to proceeding with fan development. Such tests are currently planned at the Lewis Research Center for the last quarter of 1971.

NOMENCLATURE

SYMBOL	DEFINITION	UNITS
A/C	Aircraft	-
$A_{ll_{eff}}$	Effective exit area of lift unit fan stream	sq in
ALR	Arc length ratio	-
Alt	Geopotential altitude	ft
A.R.	Aspect ratio	-
ARR	Arc radius ratio	-
B	Blade number	-
C	Constant in Larson-Miller parameter ... or	-
	Speed of sound	ft/sec
c	Chord	in
C_n	Constant in velocity potential	-
C_p	Specific heat	Btu/lb-°R
D-Factor	Diffusion factor	-
e	Natural log base	-
EGT	Exhaust gas temperature	°R or °F
E_n	Constant in cylinder function	-
FFTC	Ratio of throat flow function to choke flow function	-
F_N	Net thrust	lbs
F_n	Constant in cylinder function	-
f(r)	Radial distribution of tangential velocity at Z=0	-
g	Gravitational acceleration (32.174)	ft/sec^2
G(r)	Radial variation of phase angle for the disturbance	-
g(r)	Radial variation of angle for a stator	-
h	Enthalpy	Btu/lb
i	(subscript) Ideal	-

Note: Where more than 1 set of units is shown, refer to specific use of symbol.

NOMENCLATURE

SYMBOL	DEFINITION	UNITS
J	Joule's constant (778.16)	ft-lb/Btu
$J_n(\lambda_{nr})$	Bessel function of the first kind	-
K	Integer index	-
K_1, K_2	Constants determined from boundary conditions	-
L	Lift	lbs
L.E.	Leading edge	-
M	Number of rotating line sources	-
M*	Ratio of local velocity to velocity of sound when Mach number is equal to 1	-
Mo	Aircraft flight Mach number	-
M_1	Mach number entering blade row	-
M_2	Mach number at exit to blade row	-
MR_1	Relative Mach number entering blade row	-
MR_2	Relative Mach number at exit to blade row	-
N	Rotor speed	% or rpm
n	Number of circumferential lobes	-
n'	Harmonic number	-
N_e	Engine speed	% or rpm
N_F	Fan speed	% or rpm
OGV	Outlet guide vane	-
P	Pressure ... or	Atmospheres or psia
	Larson-Miller parameter, $P=T(c = \log_{10}t) \times 10^{-3}$	-
PNdB	Perceived noise level	decibels
P_S	Static pressure	psia
$P_{S\ 5.5}$	Static pressure, lift unit turbine discharge	psia
P_t	Total pressure	psia

NOMENCLATURE

SYMBOL	DEFINITION	UNITS
$P_{T\ 5.4}$	Total pressure, lift unit turbine inlet	psia
PWL	Sound power level	-
$P_{5.1}$	Total pressure, gas generator turbine discharge	psia
$P_{5.4}$	Total pressure at lift unit turbine inlet	psia
r	Non-dimensional radial coordinate ... or	-
	(subscript) radial variation	-
$R_n(\lambda_{nr})$	Cylinder function	-
R_o	Outside radius	in
r_t	Non-dimensional tip radius	-
R_1	Relative velocity entering blade row	ft/sec
R_2	Relative velocity leaving blade row	ft/sec
S.L.	Side load	-
T	Temperature	°R or °F
t	Non-dimensional time ... or	-
	Time ... or	sec or hrs
	Thickness	in
T.E.	Trailing edge	-
T_m	Maximum thickness	in
T_t	Total temperature	°R or °F
$T_{5.1}$	Total temperature, gas generator turbine discharge	°R
$T_{5.4}$	Total temperature, lift unit turbine inlet	°R
U	Velocity	ft/sec
U_T	Tip velocity	ft/sec
V	Vane number	-
V_o	Aircraft flight velocity	ft/sec or knots
V_1	Velocity entering blade row	ft/sec

NOMENCLATURE

SYMBOL	DEFINITION	UNITS
V_2	Velocity leaving blade row	ft/sec
V_θ	Tangential velocity	ft/sec
W	Weight flow	lbs/sec
W_{FT}	Fuel flow	lb/hr
$W_{5.1}$	Weight flow at gas generator turbine discharge	lb/sec
$W_{5.4}$	Weight flow at lift unit turbine entrance	lb/sec
W_{10}	Fan inlet flow	lb/sec
$Y_n(\lambda_{nr})$	Bessel function of the second kind	-
z	Non-dimensional axial coordinate	-
α	Angle of gas flow leaving turbine nozzle (relative to circumferential direction)	degrees
$\alpha(r)$	Physical lean angle from hub	degrees
β_1, β_{1c}	Angle of gas entering blade row	degrees
β_2, β_{2c}	Exit angle of gas leaving blade row	degrees
β_{1c*}	Blade leading edge angle	degrees
β_{2c*}	Blade trailing edge angle	degrees
β_V	Vane angle	degrees
Γ	Angle of gas flow leaving turbine (relative to axial direction)	degrees
$\Gamma(r)$	Circulation	-
δ	Ratio of total pressure to standard total pressure (14.696 psia) ... or	-
	Impulse function	-
$\epsilon(r)$	Phase relationship	-
θ	Ratio of total temperature to standard total temperature (518.7°R) ... or	-
	Angular coordinate	-

NOMENCLATURE

SYMBOL	DEFINITION	UNITS
$\dot{\theta}$	Pitch velocity	rad/sec
$\ddot{\theta}$	Pitch acceleration	rad/sec^2
$\theta_{e(r)}$	Radial variation of the viscous wake	-
ϕ	Velocity potential	-
$\dot{\phi}$	Roll velocity	rad/sec
$\ddot{\phi}$	Roll acceleration	rad/sec^2
$\dot{\Psi}$	Yawing velocity	rad/sec
$\ddot{\Psi}$	Yawing acceleration	rad/sec^2
ω	Blade passing angular velocity	-
$\bar{\omega}$	Ratio of total pressure loss to velocity head	-
ω_n	Mode angular velocity	-

LIST OF REFERENCES

(1) Kazin, S.B. and Volk, L.J.: LF336 Lift Fan Modification and Acoustic Test Program. General Electric Company, NASA CR Under Review, April 16, 1971.

(2) Phipps, W.H. and Kazin, S.B.: FAINT - A Computer Program to Predict Fan Aerodynamically Induced Noise Transmission, Programming and Users' Manual. General Electric Company, TIS R69AEG129, February, 1969.

(3) Tyler, J.M. and Sofrin, T.G.: Axial Flow Compressor Noise Studies. Pratt & Whitney Aircraft, Division of United Aircraft Corporation.

(4) Schloemer, J.J.: An Analysis for Calculating the Blade Passing Frequency Acoustic Power of a Turbomachinery Stage with a Tangentially Leaned Vane Row. General Electric Company, TM 71-519, June 21, 1971.

(5) Nemec, J.: Noise of Axial Fans and Compressors - Study of its Radiation and Reduction. National Research Institute for Machine Design, Bechovice, Praque, Czechoslovakia.

(6) Kazin, S.B. and Jutras, R.R.: A Systematic Study of the Effect of Fan Compressor Stage Design on Blade Passing Frequency Noise Generation. General Electric Company, TM 69-202.

(7) Clemons, A.: LF460 Acoustic Treatment Design Study. General Electric Company, Acoustic Technology Memo, January 6, 1971.

(8) Katsanis, J.: Use of Quasi-Orthogonals for Calculating Flow Distribution in the Meridional Plane of a Turbomachine. NASA TN D-2546, Washington, D.C., December, 1964.

(9) Robbins, W.H., Jackson, R.J. and Lieblein, S.: Aerodynamic Design of Axial-Flow Compressors, NASA SP-36, National Aeronautics and Space Administration, Washington, D.C., 1965, page 248.

LIST OF REFERENCES

(10) Model Specification E-1155. Engine, Aircraft, Turbojet, YJ97-GE-100, dated October 15, 1969. General Electric Company, Lynn, Massachusetts, page 30.

(11) LF460/YJ97-GE-100 Preliminary Performance and Installation Data. Contract NAS2-6056, dated March 1, 1971. General Electric Company, Cincinnati, Ohio, page 5.43.

TABLE I, V/STOL MISSION FOR LF460

Power Setting	Alt	Speed (knots)	% Engine RPM	Time for Each Occurrence	Number of Occurrences	Mode
Idle	0	0	70	3 min	1	CTOL
Idle & Check-out	0	0	70	3 min	1	V/STOL
Take-off	0	0-150	101.5**	1 min	3*	V/STOL
Cruise	5K	250	93.6	5 min	3	CTOL
Decent	0	70-150	95**	2 min	3	V/STOL
Landing	0	0-70	97.5**	1 min	3	V/STOL

TOTAL TIME FOR MISSION: 33 MINS.

* Three V/STOL take-off and landing maneuvers will be accomplished for each complete flight for a total flight time of 27 minutes excluding ground idle and checkout.

** During V/STOL flight mode, aircraft control augmentation is obtained from the propulsion system. The control duty cycle requirements for this phase of the mission are defined in SECTION III-C.

TABLE II, FERRY MISSION FOR LF460

Power Setting	Alt	M_o	% Engine RPM	Time For Each Occurrence
Idle	0	0	70	10 min
Take Off	0	0	101.5	5 min
Max Cont.	10K	0.4	99.1	5 min
Cruise	30K	0.6	93.6	5 hrs
Flt Idle Descent	10K	0.5	80	10 min
Landing	0K	0.2	90	5 min

TOTAL TIME FOR MISSION: 5 hrs, 35 mins.

TABLE III, COMPONENT DESIGN LIFE REQUIREMENTS

Component	Minimum Life Without Repair (1)	Ultimate Life With Repair (1)
Front Frame	2400	6000
Scroll	600	1200
Rear Frame	2400	6000
Fan Honeycomb Seals	600	1200
Fan Blades	600	1200
Fan Disk	2400	6000
Buckets and Carriers	600	1200
Bearings and Seals	600	600
Sump Components	600	600

(1) These life requirements refer to those units operative for both V/STOL and cruise. If units are used exclusively for V/STOL, a reduced total life capability will exist of about 35% of the design life.

TABLE IV, CYCLE EXPOSURE CRITERIA FOR AIRCRAFT CONTROL INPUTS

Fan Speed		Temperature		Pressure		No. of Cycles per
Mean	± S/A	Mean	± S/A	Mean	± S/A	100 hrs Ult Life
91.8	0.7	1849	14	55.0	0.5	2,100
92.6	1.4	1860	25	55.6	1.0	3,200
93 3	2.1	1872	37	56.1	1.5	26,000
94.0	2.8	1885	50	56.6	2.0	33,000
94.7	3.5	1900	65	57.2	2.6	18,000
95.4	4.2	1918	83	57.8	3.2	11,000
96.1	4.9	1933	98	58.4	3.8	6,000
96.9	5.7	1937	112	59.0	4.4	9,000

S/A = Single Amplitude Cyclic Variation

TABLE V - DESIGN POINT ESTIMATES, 1.35 FAN P/P

- PNdB 500 ft sideline
- Single Fan
- Standard Day
- 2060°R YJ97-GE-100 EGT

UNSUPPRESSED	110.9 PNdB	Extrapolated SAE Jet Noise
WITH STATOR LEAN	107.1	From LF336 Results -3.8 PNdB
WITH EXHAUST DUCT SPLITTERS	104.1	Estimated -3 PNdB
WITH EXIT LOUVERS	101.6	Estimated -2.5 PNdB

TABLE VI - NOISE RATING POINT - PRELIMINARY CYCLE DATA

- PNdB 500 ft sideline
- Single Fan
- Standard Day
- 1835°R YJ97-GE-100 EGT

FAN WITH LEAN AND EXHAUST DUCT SPLITTERS	99.1	Lean Analytical Program Complete Exhaust Duct Splitter Design Complete
FAN JET	84.8	Modified Cold Jet Prediction. V_F = 660 ft/sec
TURBINE JET	87.4	V_T = 874 ft/sec
TOTAL JET NOISE FLOOR	89.4	
TOTAL NOISE W/O EXIT LOUVERS	100.8	
TOTAL NOISE WITH EXIT LOUVERS	98.3	Estimated - 2.5 PNdB

TABLE VII - NOISE RATING POINT - FINAL CYCLE DATA

- PNdB 500 ft sideline
- Single Fan
- Standard Day
- 1835°R YJ97-GE-100 EGT

FAN WITH LEAN AND EXHAUST DUCT SPLITTERS	99.5	
FAN JET	85.4	New Cycle Point V_F = 682 ft/sec
TURBINE JET	75.4	V_T = 678 ft/sec
TOTAL JET NOISE FLOOR	85.9	
TURBINE MACHINERY NOISE	78.6	
TOTAL FLOOR NOISE (JETS AND TURBINE)	87.3	
TOTAL NOISE W/O EXIT LOUVERS	100.6	
TOTAL NOISE WITH EXIT LOUVERS	98.1	Estimated - 2.5 PNdB

TABLE VIII - NOISE RATING POINT WITH ACTUAL VTO

TOTAL NOISE W/O EXIT LOUVERS	99.5	
TOTAL NOISE WITH EXIT LOUVERS	97.0	Estimated Reduction 2.5 PNdB
TOTAL NOISE WITH EXIT LOUVERS	97.3	Calculated Reduction With Final Louver Design - 2.2 PNdB

TABLE IX

LF336 EXPERIMENTAL RESULTS

PHYSICAL LEAN ANGLE α (DEGREES)	INTERBLADE ROW SPACING BP (CHORDS)		POWER FORWARD PWL_F (dB)	POWER REAR PWL_R (dB)	TOTAL POWER PWL_T (dB)
30	2.0	P	146.6	136.9	147.0
		A	146.5	140.6	147.5

P = Probe Data

A = Arc Data

TABLE X

COMPARISON OF PURETONE PREDICTION RESULTS WITH EXPERIMENTAL DATA

PHYSICAL LEAN ANGLE α (DEGREES)	INTERBLADE ROW SPACING BP (CHORDS)		TOTAL ACOUSTIC POWER EXPERIMENTAL (Z=0) PWL_E (dB)	TOTAL ACOUSTIC POWER PREDICTED PWL_P (dB)
30	2.0	P	150.5	150.0
		A	150.8	

P = Probe Data

A = Arc Data

TABLE XI

LF460 FAN DESIGN PARAMETERS

Total Pressure Ratio		1.350
Static Pressure Ratio		1.025
Corrected Air Flow		617 lb/sec
Efficiency		80.3
Corrected Tip Speed		1125 ft/sec
Tip Diameter		59.95 in
Radius Ratio		.454
Specific Flow		39.65 lb/sec/ft^2
Rotor Tip Relative Mach Number		1.262
Hub Work Coefficient ($2gJ\Delta h/U^2$)		2.14
Number of Blades		88
Number of Vanes		56
Aspect Ratio		
Rotor		5.84
Stator		3.99 [1/]
Solidity	Hub	Tip
Rotor	3.160	1.320
Stator	2.785	1.240

[1/] Does not include effects of acoustic splitters.

TABLE XII

LIFT FAN COMPARISONS

	LF460	MF415	LF336	CF380	LF1
Pressure Ratio	1.35	1.40	1.30	1.313	1.115
Tip Speed, fps	1125	1125	950	969	720
Radius Ratio	0.454	0.435	0.50	0.48	0.40
Specific Flow	39.65	37.3	39.0	40.4	29.8
Hub Loading Coef.	2.14	2.00	2.03	2.23	2.01
Tip Loading Coef.	0.705	0.773	0.798	0.645	0.481
Rotor A.R.	5.84	4.9	3.72	3.8	5.92
Stator A.R.	3.99	3.5	3.66	1.16	12.0
Solidity					
Rotor Tip	1.320	1.1	1.0	0.91	0.59
Rotor Hub	3.160	2.46	1.83	1.78	1.43
Stator Tip	1.240	0.89	0.99	0.89	0.71
Stator Hub	2.785	1.66	1.54	1.53	1.76

TABLE XIII

TURBINE DESIGN POINT PARAMETERS

Inlet Total Temperature, ^{o}R	2060
Inlet Total Pressure, lb/in^2 absolute	54.74
Inlet Gas Flow, lb/sec	76.22
Inlet Flow Function, $W_{5.4}\sqrt{T_{5.4}}/P_{5.4}$	63.20
Total to Static Pressure Ratio	3.85
Total to Total Pressure Ratio	3.05
Exhaust Static Pressure	14.22
Exhaust Total Pressure	17.96
Speed, RPM	4300
Design Power, HP	12,431
Design Energy, Btu/lb	115.3
Exit Axial Mach Number	0.6
Overall Efficiency	0.832
Pitch Wheel Speed, ft/sec	1212
Stage Velocity Ratio, U/V_o	0.42
Stage Work Function, $gJ\Delta h/2U^2$	0.991
Turbine Tip Diameter, inches	66.65
Turbine Hub Diameter, inches	62.54
Bucket Length, inches	2.06
Admission Arc, degrees	360
Bucket Aspect Ratio	1.43

TABLE XIV

SCROLL LOSS ESTIMATE

	$\bar{\omega}$	% $\Delta P_t/P_{t\ in}$
Entrance and Turning Loss	0.200	1.12
Skin Friction	0.120	1.03
Strut Loss	0.100	0.86
Gooseneck Loss	0.260	2.24
Total		5.25

TABLE XV

TIP TURBINE COMPARISONS

	LF460	LF336	CF380	LF1
Inlet T_T, °R	2060	1711	1637	1653
Inlet P_T, psia	54.74	31.84	41.12	30.27
Inlet Flow	76.22	44.12	169.5	42.92
Pressure Ratio	3.85	2.34	2.69	2.05
Enthalpy, Δh, Btu/lb	115.3	58.4	75.1	58.1
Exit Mach Number	0.60	0.551	0.460	0.346
Velocity Ratio	0.42	0.584	0.471	0.411
Work Function ($gJ\Delta h/2U^2$)	0.991	0.645	0.833	1.16
Admission Arc	360°	346°	360°	158°
Bucket Aspect Ratio	1.43	1.61	2.54	2.65
Bucket Solidity	1.85	1.97	1.85	2.08
Efficiency	0.832	0.818	0.875	0.824
Bucket Relative Mach No.	0.94	0.70	0.73	0.66

TABLE XVI

STATIC FORCE SUMMARY

	Axial Force (Pounds)	Torque (Inch-Pounds)
Front Frame		
Bellmouth	+3753	0
Bulletnose	-1196	0
Struts	- 22	0
Rotor		
Hub	+1878	0
Blades	+7016	176,000
Buckets and Carrier	+ 180	176,000
Rear Frame		
Hub and Inner Flowpath	+ 560	0
Stators and Splitters	+2240	176,000
Mid-box and Outer Flowpath	+ 84	0
Scroll		
Nozzles	+2096	186,700*

* Turbine Residual Swirl = 10,700 inch-pounds of torque

TABLE XVII

FRONT FRAME WEIGHT SUMMARY

COMPONENT	MATERIAL	WEIGHT	TOTAL WEIGHT
MAJOR STRUT			34.20 lbs
Structural Spar	Aluminum (2219-T81)	29.30	
Honeycomb	Aluminum (5052)	1.84	
Sheet Skins	Aluminum (2219-T81)	1.55	
Mount Uniballs	Steel	0.49	
Adhesive	Metalbond 328	1.02	
MINOR STRUT (3:00)			8.85
Structural Spar*	Aluminum (A357)	8.25	
Honeycomb	Aluminum (5052)	0.17	
Sheet Skins	Aluminum (2219-T81)	0.21	
Adhesive	Metalbond 328	0.22	
MINOR STRUT (9:00)			8.85
Structural Spar*	Aluminum (A357)	8.25	
Honeycomb	Aluminum (5052)	0.17	
Sheet Skins	Aluminum (2219-T81)	0.21	
Adhesive	Metalbond 328	0.22	
HUB			19.58
Structural Casting*	Aluminum (A357)	15.65	
Bearing Race Inserts	Stainless Steel (321)	3.93	
DOME	Fiberglass Aluminum (5052)		6.00
BELLMOUTH			38.83
Honeycomb Panel (0.012 face sheets)	Steel (15-7 PH)	30.83	
Insulation Tape	Min-K	1.00	
Inserts, Fasteners, Nut Plates		3.00	
Scroll Mounting Bracket	Steel (15-7 PH)	4.00	
FORWARD AIR SEAL ASSEMBLY			10.78
Scroll Slip Seals	Inconel-X	4.00	
Seal Sectors	Hastelloy-X	4.36	
Cooling Air Deflector	Steel (15-7 PH)	2.42	
TOTAL WEIGHT			127.00 lbs

* Structural hub casting is integral with minor strut structural spars.

TABLE XVIII

LF460 - YJ97-GE-100 DUTY CYCLE

	TEMPERATURE (DEGREES RANKINE)				
PRESSURE	1600-1700	1700-1800	1800-1900	1900-2000	2000-2100
	Time	Time	Time	Time	Time
43.7	30.93	0.63			
44.6	9.65	0.69	0.01		
45.6	3.06	3.07	1.94		
46.5	1.19	8.42			
47.5		6.34			
48.5		4.86			
49.4		2.06		0.17	0.2
50.4		0.2	10.88	2.14	
51.3			7.25		
52.3			2.60		
53.2			1.21	0.5	
54.2				0.9	
55.1				0.47	
56.0				0.31	
57.0				0.12	0.11
58.4					0.09
% Time	44.83	26.27	23.89	4.61	0.40

TABLE XIX

SCROLL WEIGHT SUMMARY

COMPONENT	DESCRIPTION	WEIGHT
Torque Tube	t = 0.030 (0.060 Bottom Plate)	37.2 lbs
Inlet	t = 0.030	25.5
Rear Frame Flange	t = 0.028 and 0.080	9.2
Upper Bubble	t = 0.025	21.9
Middle Bubble	t = 0.018	2.1
Lower Bubble	t = 0.018	6.8
Upper Plate	t = 0.040	3.3
Lower Plate	t = 0.040	6.0
Gooseneck	t = 0.036	10.8
Strut Hat	t = 0.028 (0.040 and 0.060)	10.9
Nozzle Hat	t = 0.028 (0.040)	7.2
Braze		10.0
Insulation	$\frac{1}{4}$" Min K (bagged in Microquartz)	26.0
Nozzles	0.040 Wall	34.0
Struts	0.040 Wall	29.0
Inlet Flange, Bolts and Nuts	42 Bolts	6.0
Inlet and Outboard Mounts		7.0
Finger Seal (Forward Air Seal)		1.5
Plate L.E. Airfoils	$t_m/c = 0.1$, C = 2.5	2.9
Plate T.E. Airfoils	$t_m/c = 0.1$, C = 2.0	1.2
Other Components	(0.010 false flowpath)	9.0
		267.5 lbs

TABLE XX

ROTOR WEIGHT SUMMARY

COMPONENT	WEIGHT, LB.
Turbine	31.5
Blade	106.9
Disk	62.1
Bearings and Sump	30.3
TOTAL ROTOR WEIGHT	230.8

TABLE XXI - ROTOR LOW CYCLE FATIGUE ANALYSIS

COMPONENT	RANGE OF STRESS, KSI	STRESS CONCENTRATION FACTOR	CALCULATED ALLOWABLE CYCLES
Disk	0-86.5	1.0	$> 3 \times 10^4$
Blade Mid-Span	0-101.8	1.75	$> 1 \times 10^5$
Blade Tip Shroud	0-90.9	1.0	$> 1 \times 10^5$
Blade Siderails	0-73.4	2.0	$> 1 \times 10^5$
Bucket & Tip Shroud	0-30.9	1.7	$> 1 \times 10^5$

TABLE XXII

LIMITING STRESS AND LIFE SUMMARY OF ROTOR COMPONENTS

COMPONENT	MATERIAL	DESIGN TEMPERATURE, °F	LOADING	CRITERIA FOR LIMITING STRESS	CALCULATED STRESS, KSI	ALLOWABLE STRESS, KSI	LIFE FACTOR	LIFE CONSUMED, HOURS	TOTAL REQUIRED LIFE, HRS	CALCULATED LCF LIFE, CYCLES	TOTAL REQUIRED LIFE, CYCLES	MARGINS OF SAFETY
DISK												
Shaft	Ti 6-4	225		0.02% Yield	50.0	81.0	-	-		$> 1 \times 10^5$		0.6
Bore	Ti 6-4	120	Steady State Plus Maneuver	0.2% Yield	70.0	108.0	-	-		$> 5 \times 10^4$		0.5
Webs	Ti 6-4	100		LCF	84.8	-	-	-	2400	3.0×10^4	28,800	0.04
Dovetail	Ti 6-4	80		HCF	42.5	-	-	-		$> 1 \times 10^5$		0.3
Spacers	Ti 6-4	100		0.2% Yield	52.0	108.0	-	-		$> 1 \times 10^5$		1.0
BLADE												
Dovetail	R-95	150			45.2	-	-	-				0.73
Airfoil - Root	R-95	150	Steady State		85.0	-	-	-				0.26
- Pitch	R-95	150	Plus		78.0	-	-	-				0.33
- Tip	R-95	150	Maneuver	HCF	58.0	-	-	-	1200	$> 1 \times 10^5$	14,400	0.83
Mid-Spans	R-95	150			94.1	-	-	-				0.16
Tip Shroud	R-95	1000	Centrifugal Bending		84.0	-	2	-				1.2
Siderails	R-95	630/1240	Centrifugal Bending & Shear		57.1	-	2	300				0.2
TURBINE												
Braze Joint	CM50	630-1240	Shear	Rupture	9.0	-	2	1200				-
Bucket	U-700	650-1300	Centrifugal Bending	HCF	21.9	-	2	-	1200	$> 1 \times 10^5$	14,400	0.22
Tip Shroud	U-700	700-1460			35.7	-	2	48				0.4

DEFINITIONS:

LCF = Low-Cycle Fatigue

HCF = High-Cycle Fatigue

MARGINS OF SAFETY:

Rupture Life MS = (Calculated Life/2 x Required Life) -1

Stress MS = (Allowable Stress/Calculated Stress) -1

HCF MS = (Allowable Alternating Stress/Alternating Stress Criterion) -1

LCF MS = (Calculated Cycles/Required Cycles) -1

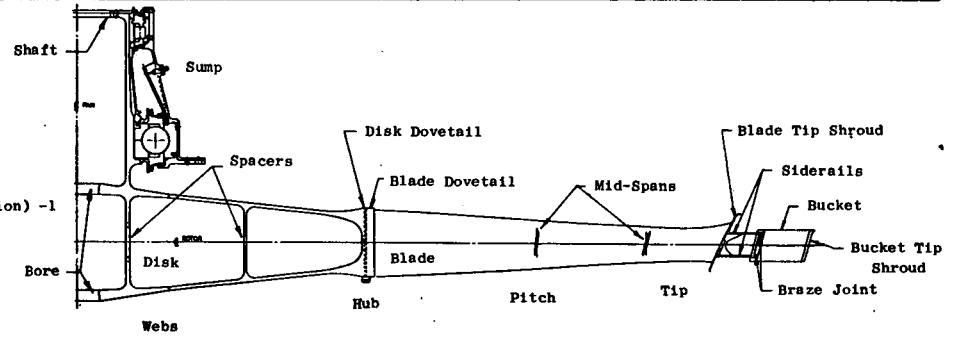

TABLE XXIII - BLADE TWIST ANGLES

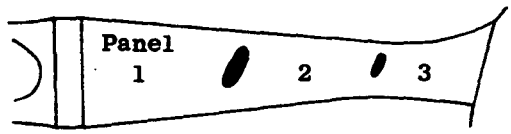

BLADE PANEL	BLADE TWIST ANGLES, DEGREES		
	PRETWIST	MFG. TOLERANCE	TOTAL TWIST
1	4.300	-0.500	3.800
2	4.460	+0.100	4.560
3	3.260	+0.042	3.302
TOTAL	12.020		11.662

TABLE XXIV - BLADE TWIST LOADS & MOMENTS

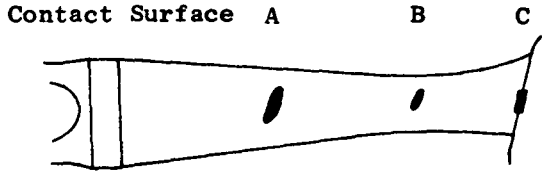

	CONTACT SURFACE	ASSEMBLY		OPERATION			TOTAL	
		PRETWIST	MFG. TOL.	STEADY STATE	CROSSFLOW	ONE-ENGINE OUT	MAXIMUM	MINIMUM
CONTACT FORCE, LB.	A	61	-7	548	±466	0	1068	136
	B	49	1	128	±109	0	287	69
	C	44	1	29	± 25	1015	1114	49
TWIST MOMENT, IN-LB.	A	70	-8	630	±535	0	1227	157
	B	70	1	183	±155	0	409	99
	C	70	1	47	± 40	0	158	78

TABLE XXV - SIDERAIL STRESSES

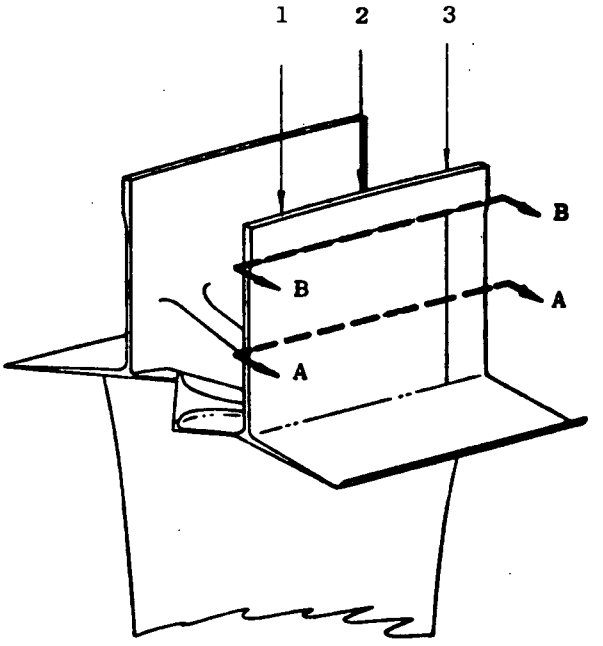

BUCKET LOCATIONS	THICKNESS, IN.	SECTION A-A 100% Speed, 1000°F, 1200 Hrs.		SECTION B-B 100% Speed, 1200°F, 1200 Hrs.	
		MAX. EFFECTIVE STRESS, PSI	MARGIN OF SAFETY	MAX. EFFECTIVE STRESS, PSI	MARGIN OF SAFETY
1	0.0154	45,500	4.0	42,000	1.8
2	0.030	58,600	3.5	51,000	0.9
3	0.045	67,900	3.0	57,100	0.2

$$\text{MARGIN OF SAFETY} = \frac{\text{Allowable Alternating Stress}}{\text{Alternating Stress Criterion}} - 1$$

TABLE XXVI - BUCKET STRESSES

	Normal Operation	One-Engine-Out
Mean Stress, KSI	21.9	13.6
Alternating Stress, KSI	10.0	20.0
Margin of Safety	0.75	0.22

$$\text{Margin of Safety} = \frac{\text{Allowable Alternating Stress}}{\text{Alternating Stress Criterion}} - 1$$

TABLE XXVII

LF460 & LF1 ROTOR DISK COMPARISONS

	LF460	LF1
Shaft/Disk Arrangement	Integral	Separate
Shaft/Disk Material	Ti 6-4	4340 Steel
Disk Assembly	E.B. Weld	Bolted

TABLE XXVIII

BASIC BALL BEARING DIMENSIONS

Basic Bearing Size	226
Inside Diameter	130 mm
Outside Diameter	230 mm
Width	40 mm
Number of Balls	16
Diameter of Balls	1.25 inch
Contact Angle	30 degrees
Specific Dynamic Capacity	35,400 Lbs.

TABLE XXIX

BASIC ROLLER BEARING DIMENSIONS

Basic Bearing Size	1924
Inside Diameter	120 mm
Outside Diameter	165 mm
Width	22 mm
Number of Rollers	30
Specific Dynamic Capacity	25,000 Lbs.

TABLE XXX

REAR FRAME WEIGHT SUMMARY

COMPONENT	MATERIAL	WEIGHT	
Hub			
Disk	Aluminum 6061T6	1.12	lbs.
Transition Section	Aluminum 6061T6	0.55	
Structural Box	Titanium 6-2-4-2	2.4	
	Fiberglass		
Flowpath	Fiberglass	2.61	
Inner Splitter	Titanium 6-2-4-2 & C.P.	5.41	
	Fiberglass		
	Stainless Steel AMS 5510		
Outer Splitter	Titanium 6-2-4-2 & C.P.	7.69	
	Fiberglass		
	Stainless Steel AMS 5510		
Stator Vane		19.56	
Skins	Titanium 6-2-4-2		
Insert	Titanium C.P.		
Mid-box			
Acoustic Flowpath	Fiberglass	5.16	
Structural Box	Titanium 6-2-4-2	13.2	
Exhaust Liner	Hastelloy X	11.12	
Aft Air Seal	Hastelloy X	4.5	
Insulation	Dyna Flex	10.1	
Turbine Strut			
Structure	Titanium 6-2-4-2	7.8	
Heat Shield	Hastelloy X	1.3	
Insulation	Dyna Flex	0.5	
Casing	Rene' 41	36.7	
		129.72	lbs.

TABLE XXXI

INSTALLATION PARAMETERS USED IN LF460 PERFORMANCE

Engine Inlet recovery @ 100%	0.985
Customer Bleed	1.0%
Horsepower Extraction	25
Ducting Pressure Loss, including scroll	11%
Fan Inlet loss coefficient (1)	0.04
Fan Stream Velocity Coefficient (2)	0.98
Turbine Stream Velocity Coefficient (2)	0.98
Fan Stream Exit Flow Coefficient (2)	0.987
Turbine Stream Exit Flow Coefficient (2)	0.994

(1) Typical of shallow inlet system with low loss closure system.

(2) Typical for exit louver cascade at zero thrust deflection angle.

TABLE XXXII

LF460 PERFORMANCE (SEA LEVEL STATIC, STANDARD DAY)

	Nominal Rating*	Maximum Control
Fan Pressure Ratio	1.29	1.36
Fan Tip Speed, Ft/Sec	1046	1168
Fan Efficiency, Percent	80.2	80.0
Fan RPM	4000	4467
Fan Stream Thrust, Pounds	11760	14379
Turbine Stream Thrust, Pounds	1436	1895
Fan Airflow, Lb/Sec	568	628
Fan Horsepower	9393	12727
Scroll Flow Function	63.2	63.2
Fan Stream Discharge Velocity, Ft/Sec	682	759
Turbine Stream Discharge Velocity, Ft/Sec	678	816
Fan Discharge Temperature, °R	568	579
Turbine Discharge Temperature, °R	1488	1639
Turbine Weight Flow, Lb/Sec	69.56	76.22
Turbine Inlet Temperature, °R	1835	2060
Turbine Inlet Pressure, PSIA	47.15	54.74
Total Adjusted Net Thrust (Including Base Drag)	12216	15057
SFC, Lb/Hr/Lb	0.389	0.413

* Noise rating point

TABLE XXXIII

CORRECTION FACTORS FOR PARTIAL ADMISSION OPERATION

Thrust	0.54
Airflow	0.78
RPM	0.75
P/P - 1	0.51

TABLE XXXIV

LF460 WEIGHTS AND INERTIA

Fan Weight	789 pounds
Mass Moments of Inertia	
About major strut axis	56.4 lb-ft-sec^2
About minor strut axis	64.3 lb-ft-sec^2
About vertical axis through fan	116.8 lb-ft-sec^2
Rotor Polar Moment of Inertia	19.5 lb-ft-sec^2
Location of Center of Gravity	
Vertical	0.3 inches above rotor centerline
Fore-Aft	on axis of rotation
Sidewards	3.2 inches towards scroll inlet

TABLE XXXV

LF460 MOUNT LOAD TABLE

TYPE LOAD	LOAD DIRECTION	MOUNT (A)	MOUNT (B)	MOUNT (C)	MOUNT (D)	MOUNT (E)
Steady State	X	---	-200	900	---	-700
Thrust at	Y	---	---	---	13,000	---
100% Speed	Z	-8196	- 95	-8109	---	---
Crossflow at	X	---	-38	-1374	---	-523
150 Knots	Y	---	---	---	14,711	---
	Z	-8034	-2032	-9149	---	---
Gyro Acting	X	---	-57	120	---	-63
Over Minor Struts	Y	---	---	---	0	---
(1 Radian)	Z	$\mp$ 1538	± 3080	$\mp$ 1542	---	---
Gyro Acting	X	---	0	0	---	0
Over Major Strut	Y	---	---	---	0	---
(1 Radian)	Z	± 1395	0	$\mp$ 1395	---	---
g - Loads (1 g)	X	---	---	±380	±240	±170
(1 g)	Y	---	---	---	±790	---
(1 g)	Z	±360	±70	±360	---	---

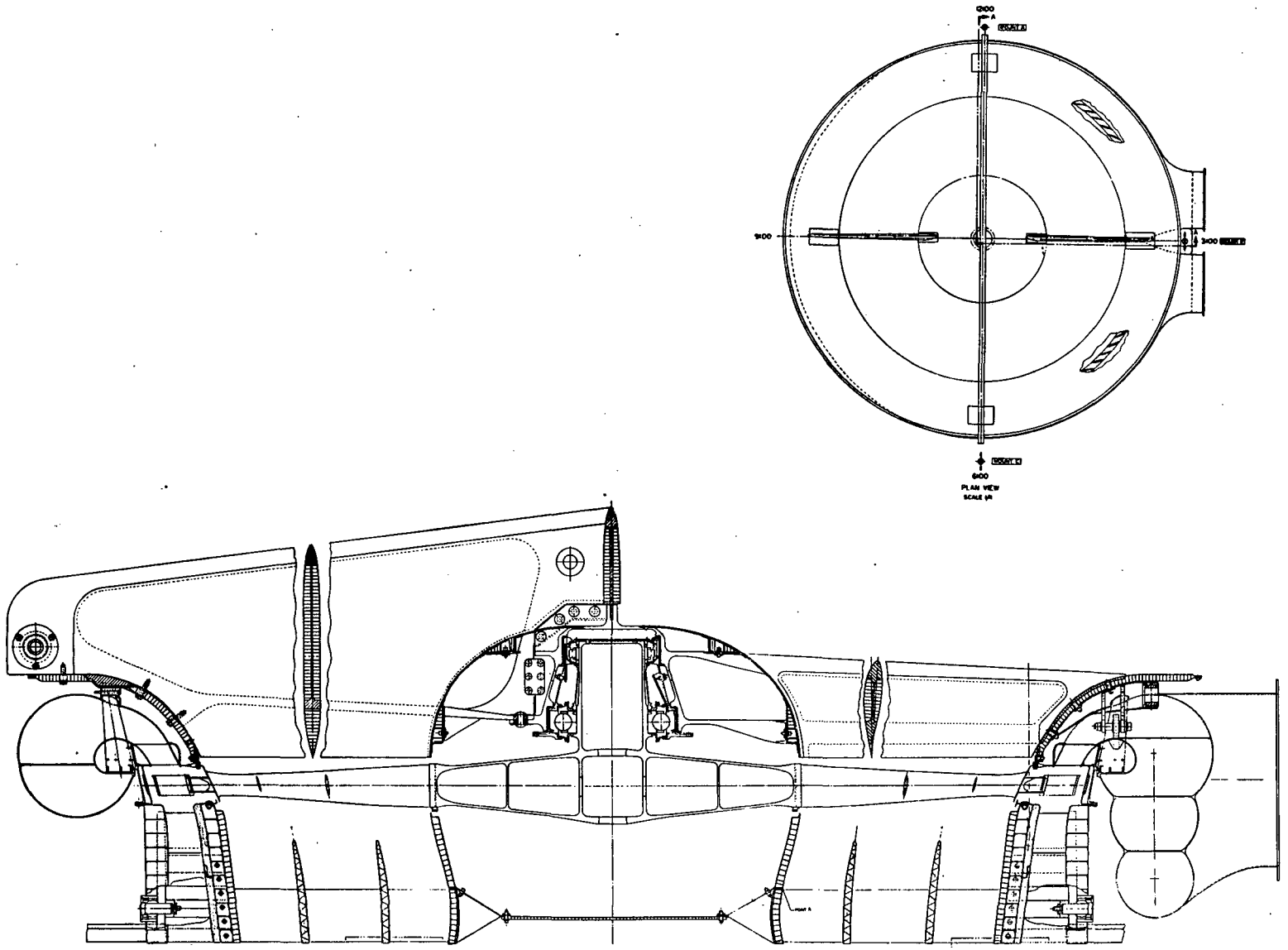

Figure 1 - LF460 Lift Fan Layout

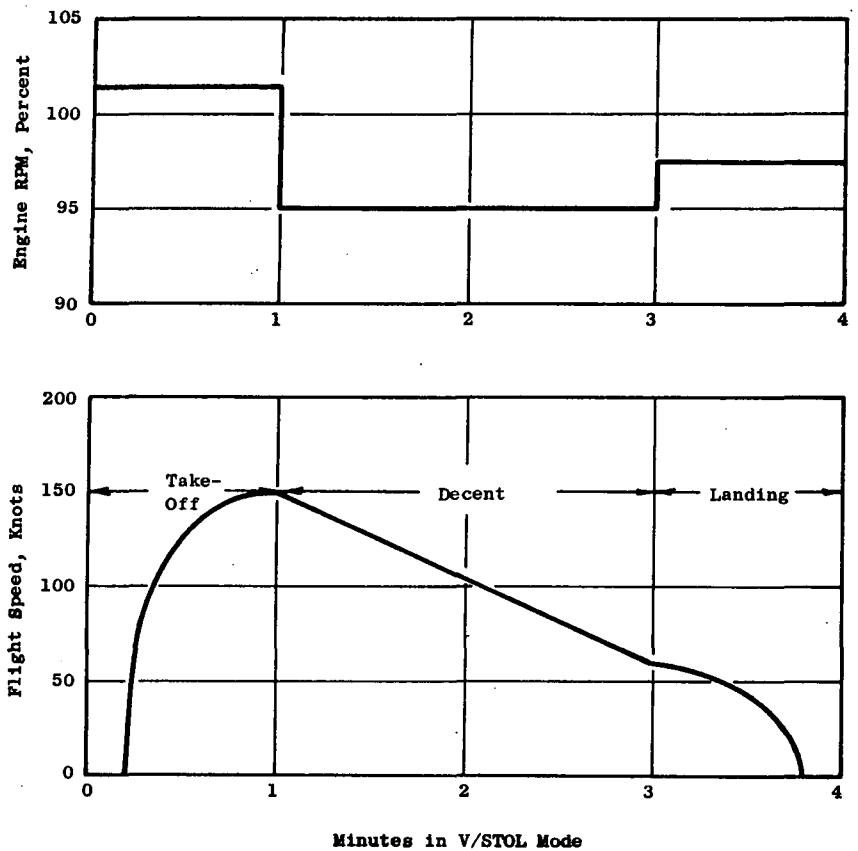

Figure 2 - LF460 V/STOL Mission Definition

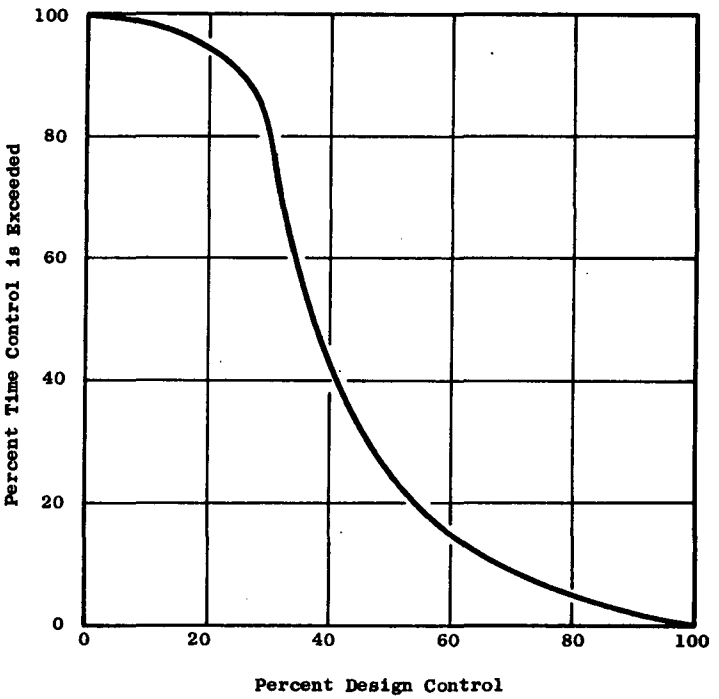

Figure 3 - LF460 Control Utilization

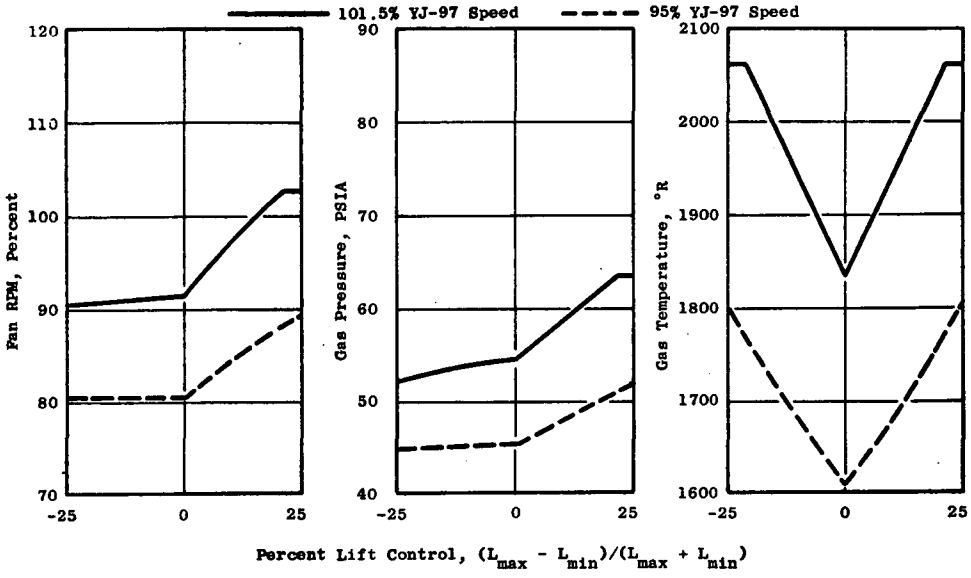

Figure 4 - Control Parameters Used In LF460 Duty Cycle Analysis

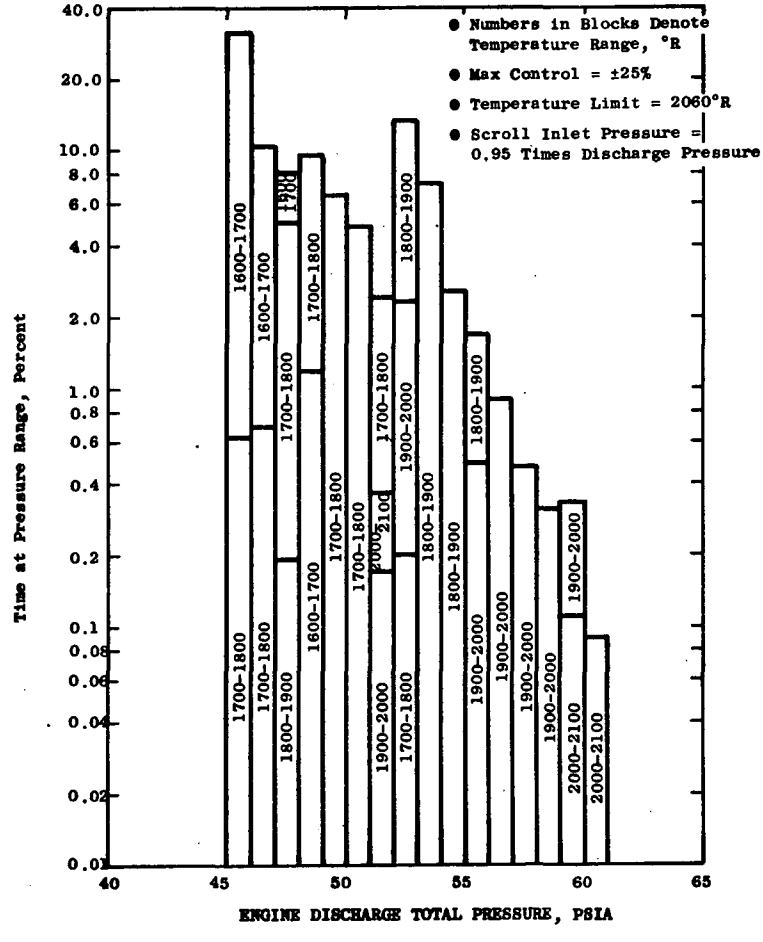

Figure 5 - LF460 Discharge Pressure Duty Cycle

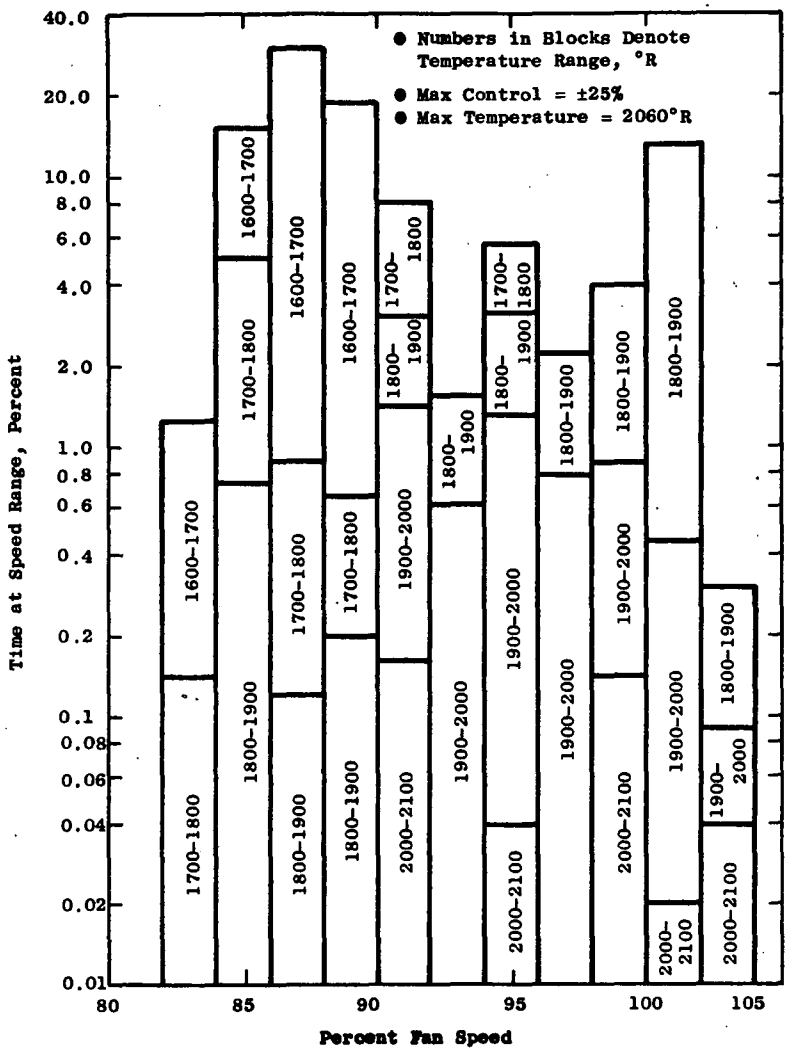

Figure 6 - LF460 Fan Speed Duty Cycle

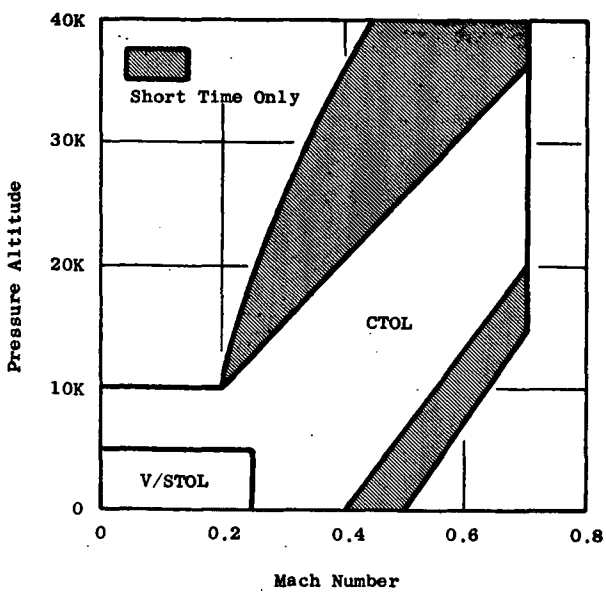

Note: In CTOL Mode, Units Used For V/STOL only will be exposed to Ambient Air Temperatures and Pressures while not operating.

Figure 7 - LF460 Flight Limit Map (ICAO Standard Day)

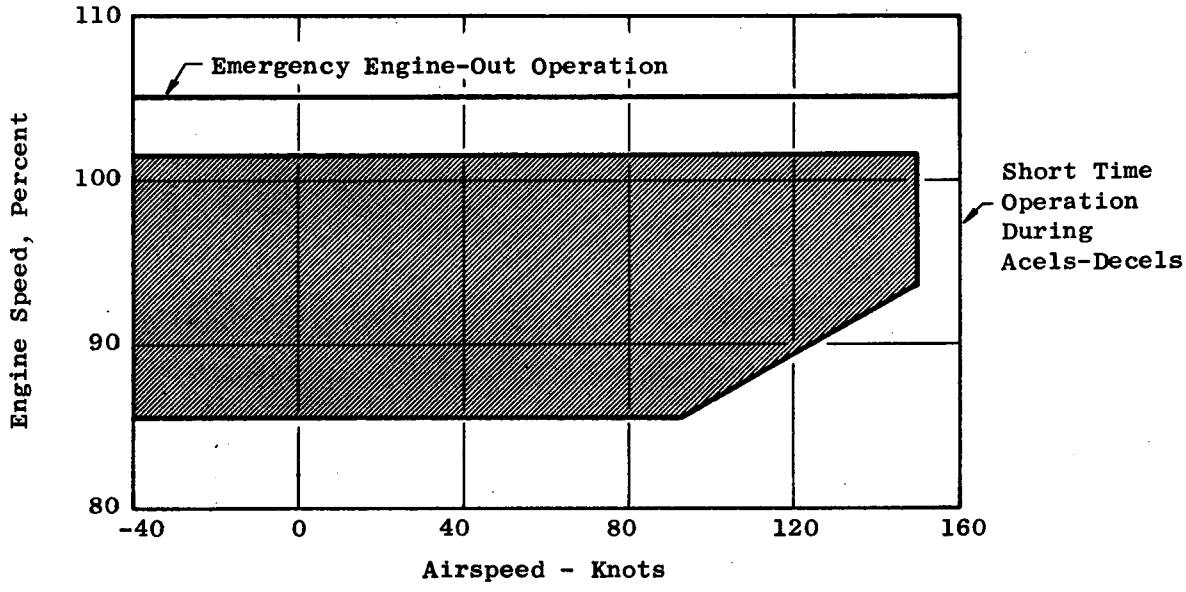

Figure 8 - Power Speed Envelope for LF460 in V/STOL Mode

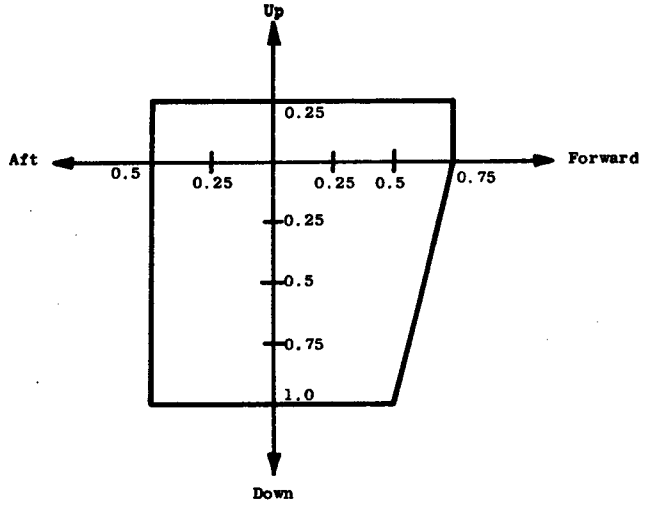

Side Load = ±0.5 g

$\dot{\theta}$ Pitch Velocity = 0.1 rad/sec

$\ddot{\theta}$ Pitch Acceleration = 0.5 rad/sec^2

$\dot{\phi}$ Roll Velocity = 0.1 rad/sec

$\ddot{\phi}$ Roll Acceleration = 1.0 rad/sec^2

Can Occur in any Combination

Notes:
1) Load factors, angular velocities and accelerations to be taken about the C.G. of the fan.
2) Side load factors act to either side.
3) Side loads and gyro loads do not act simultaneously.

Figure 9 - LF460 Steady Maneuver Load Requirements

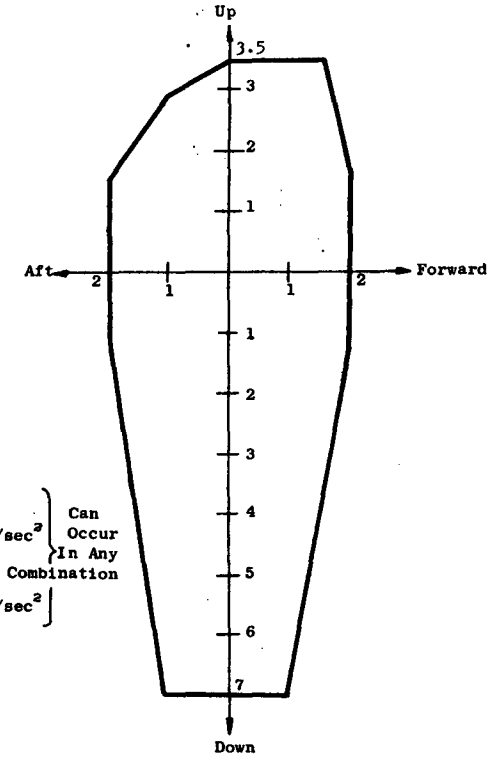

Side Load = ±2.0 g

$\dot{\hat{a}}$ Pitch Velocity = 0

$\ddot{\theta}$ Pitch Acceleration = ±7 rad/sec^2

$\dot{\phi}$ Roll Velocity = 0

$\ddot{\phi}$ Roll Acceleration = ±12 rad/sec^2

} Can Occur In Any Combination

Notes: 1) Load factors, angular velocities and accelerations to be taken about the C.G. of the fan.
2) Side load factors act to either side.
3) Side loads and gyro loads do not act simultaneously.

Figure 10 - LF460 Vertical Landing Maneuver Load Requirements

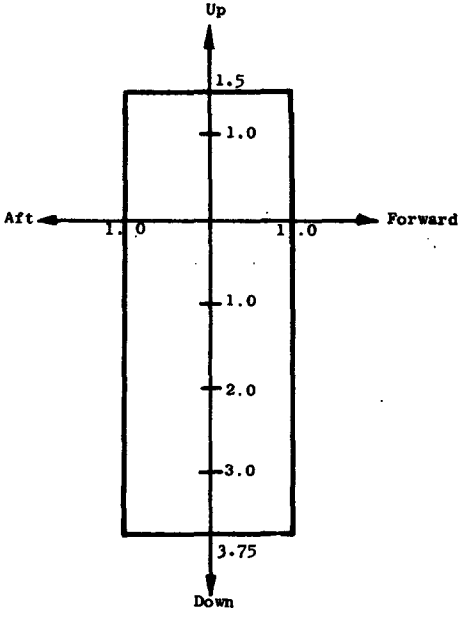

Side Load = ±1.0 g

$\dot{\theta}$ Pitch Velocity = 1.0 rad/sec

$\ddot{\theta}$ Pitch Acceleration = 1.0 rad/sec^2

$\dot{\phi}$ Roll Velocity = 1.0 rad/sec

$\ddot{\phi}$ Roll Acceleration = 3.0 rad/sec^2

} Maximum Combined Velocity = 1.0 rad/sec

Notes: 1) Load factors, angular velocities and accelerations to be taken about the C.G. of the fan.
2) Side load factors act to either side.
3) Side loads and gyro loads do not act simultaneously.

Figure 11 - LF460 Infrequent Maneuver Load Requirements

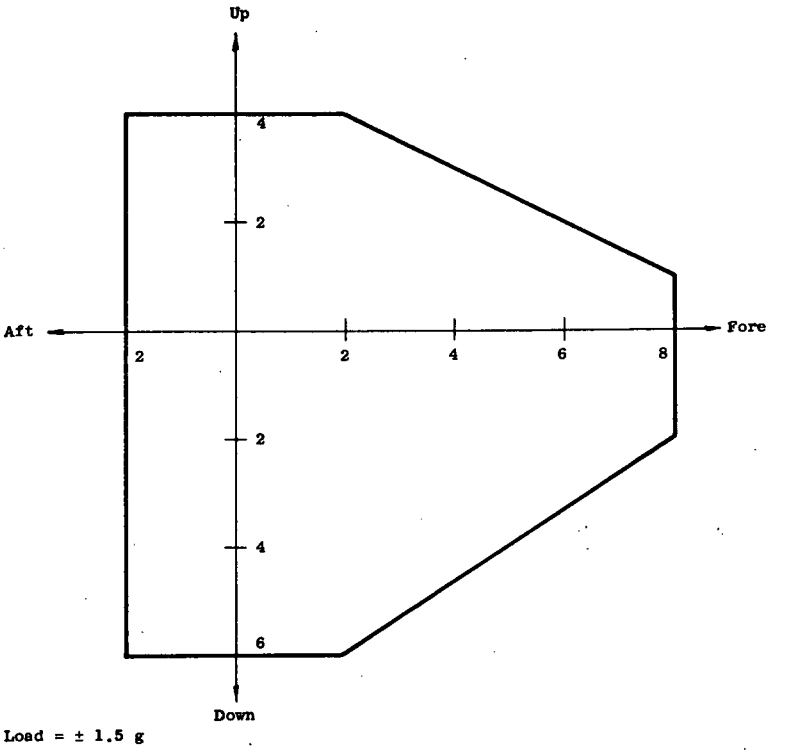

Side Load = ± 1.5 g

$\dot{\theta}$, Pitch Velocity = 0

$\dot{\Psi}$, Yaw Velocity = 0

$\ddot{\theta}$, Pitch Accel = 12 Rad/Sec^2

$\ddot{\Psi}$, Yaw Accel = 6 Rad/Sec^2

Figure 12 - LF460 - CTOL Landing Maneuver Load Requirements

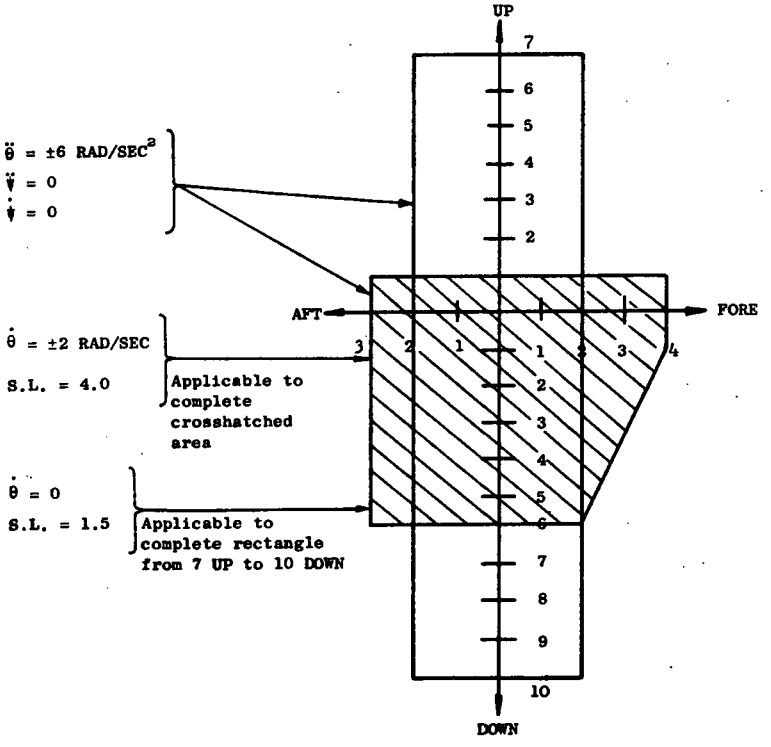

1. Load factors and angular velocities and accelerations should be taken at or about the C.G. of the fan.
2. Side load factors (S.L.) act to either side
3. $\dot{\theta}$ and $\ddot{\theta}$ are pitching velocity and acceleration.
4. $\dot{\Psi}$ and $\ddot{\Psi}$ are yawing velocity and acceleration.
5. Down loads occur during pull out.
6. Fore loads occur during arrested landing.

Figure 13 - LF460 Unpowered Flight Maneuver Loads

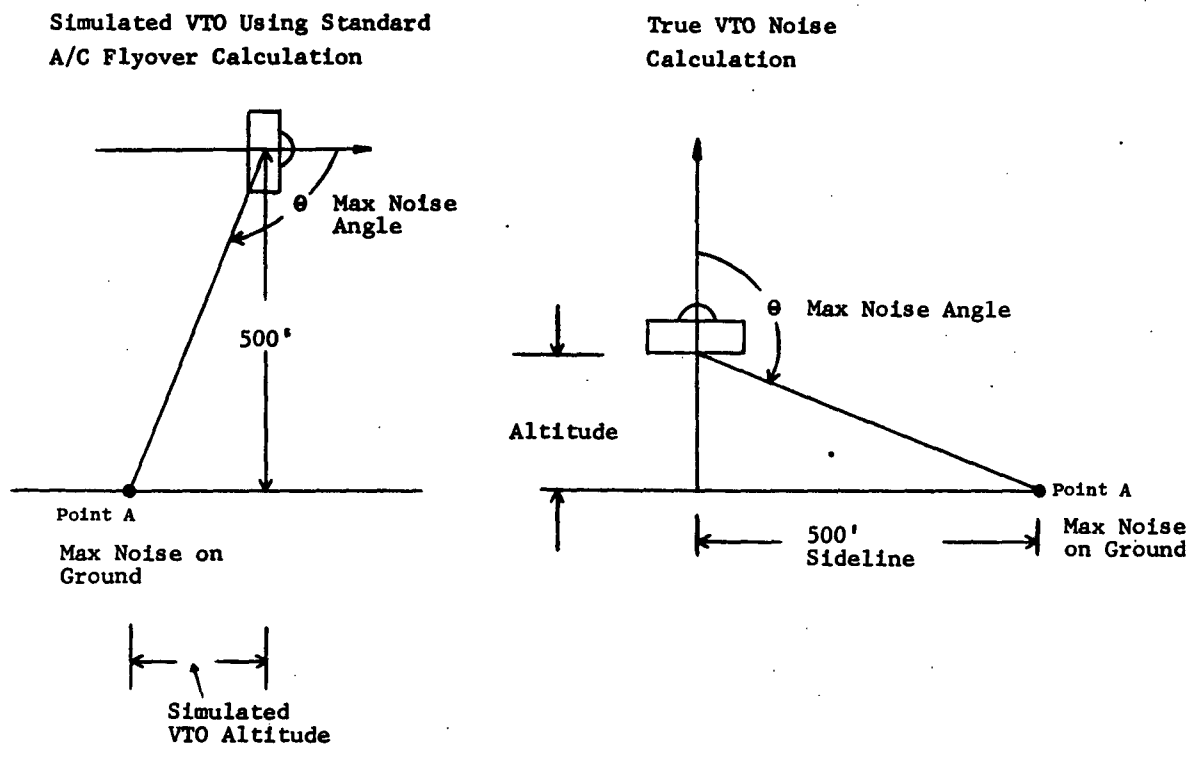

Figure 14 - Comparison of Simulated and True VTO Noise Estimates

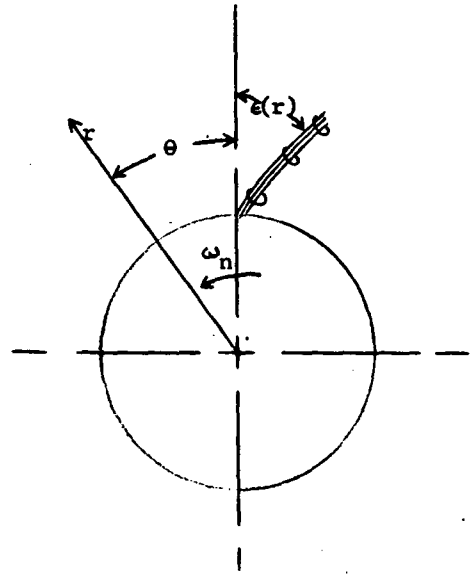

Figure 15 - Noise Source Model

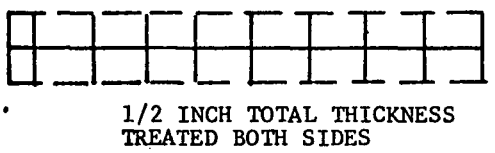

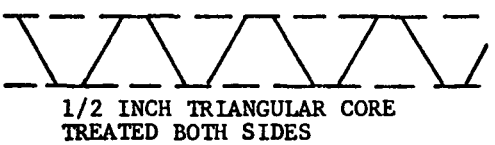

Figure 16 - LF460 Splitter Design Configurations

* Weighting Levels Added to LF460 Fan Spectrum
* Weighting Factors Relative to 50 HZ

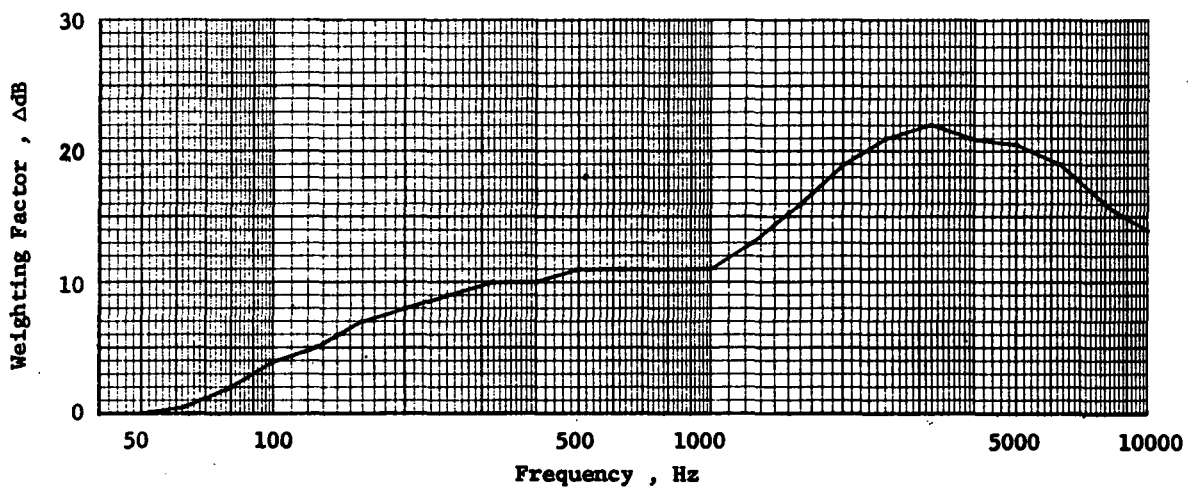

Figure 17 - PNdB Weighting Factors for LF460 Spectrum

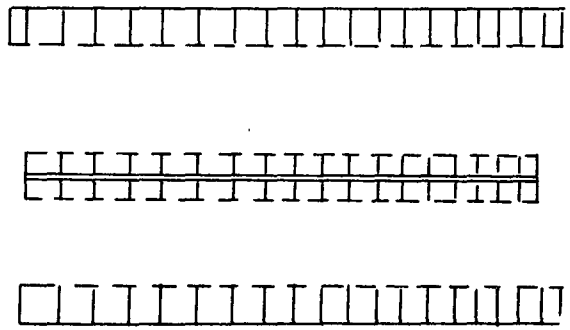

CONFIGURATION #1

1 Acoustic Splitter 1.0" Thick
Treated on Each Side.
Walls 1.0", 10% Porosity for Both
Splitter and Wall.

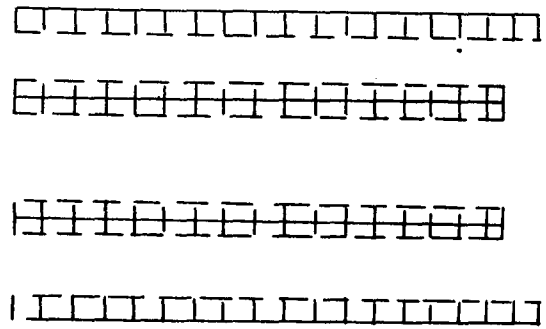

CONFIGURATION #2

2 Acoustic Splitters 0.5" Total
Thickness, Treated on Each Side.
1/4" Walls, 10% Porosity.

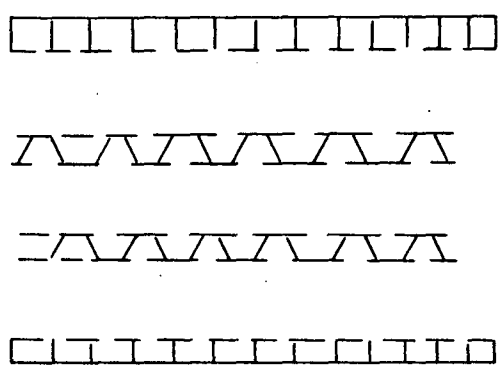

CONFIGURATION #3

2 Acoustic Splitters, 0.5" Total
Thickness. Triangular Core
Splitter Treated on Each Side.
0.5" Walls, 14.5% Porosity
Splitter 10% Porosity

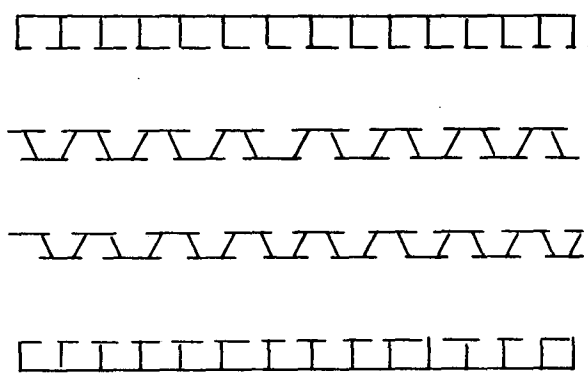

CONFIGURATION #4

2 Acoustic Splitters, 0.5" Total
Thickness. Triangular Core Splitter
Treated on Each Side.
0.5" Walls, 22% Porosity
Splitter 22% Porosity

Figure 18 - Splitter Test Configurations

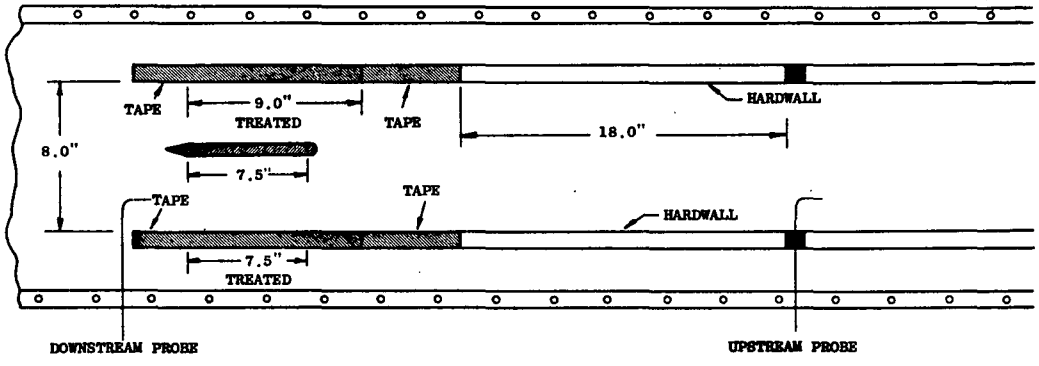

Figure 19 - LF460 Test Program Acoustic Duct

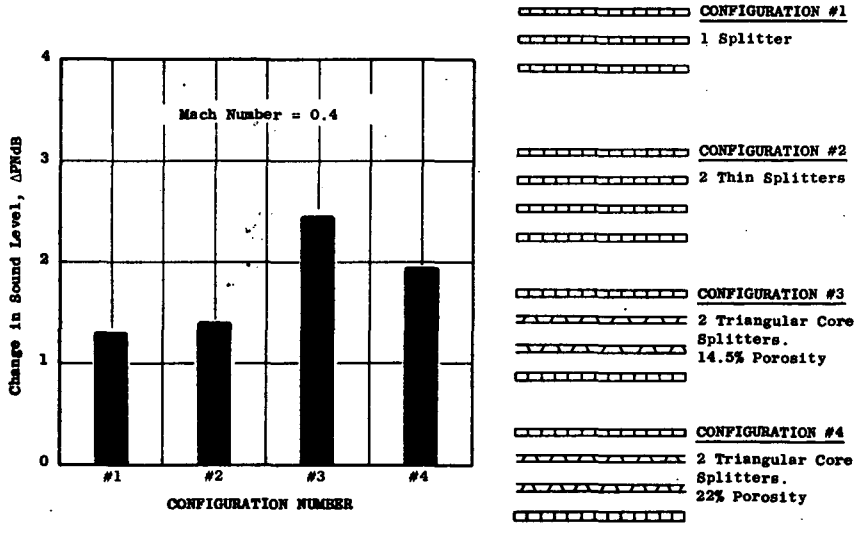

Figure 20 - Splitter Test Results

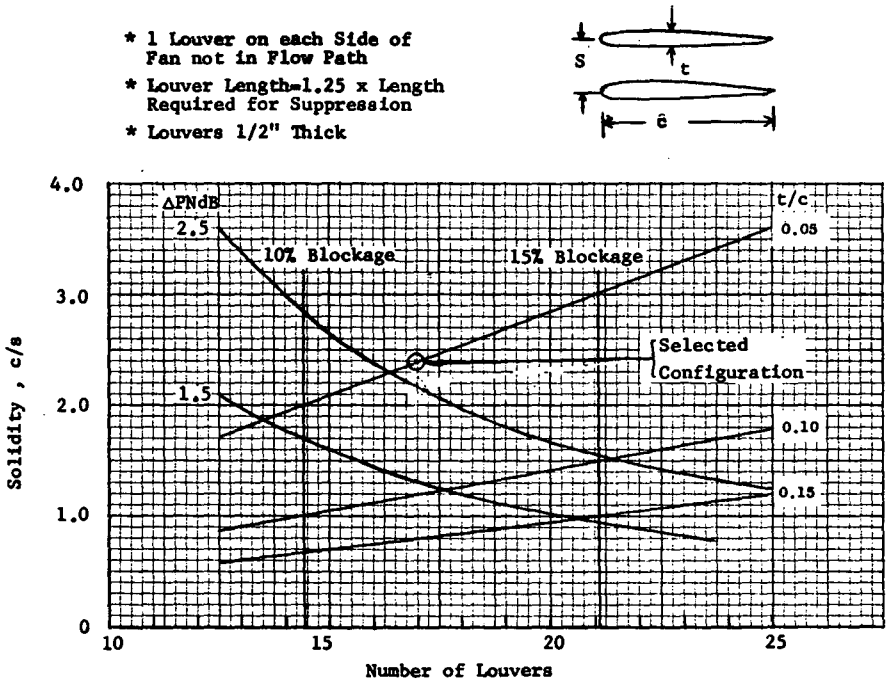

Figure 21 - Exhaust Louver Design Parameters

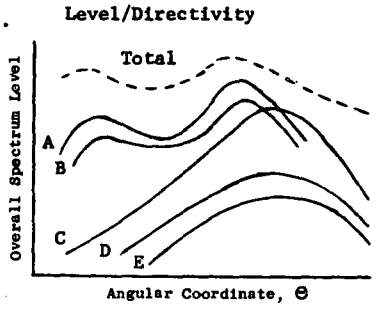

	LEVEL	DIRECTIVITY
A. Fan Puretone	Analytical	Emperical CF6
B. Fan Broadband	Emperical CF6, QEP	Emperical CF6 and QEP
C. Jet Noise	GE/NASA for Fan. SAE Extrapolated below 1000Ft./Sec. Velocity for Turbine	Emperical GE data
D. Turbine Puretone	Analytical	Emperical ROLLS ROYCE and GE
E. Turbine Broadband	Emperical ROLLS ROYCE and GE	Emperical ROLLS ROYCE and GE data

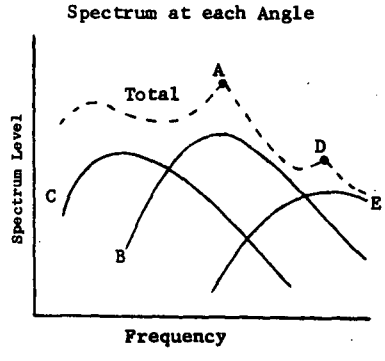

	SPECTRUM
A. Fan Puretone	One Cycle by Definition
B. Fan Broadband	Emperical CF6 and QEP
C. Jet Noise	SAE(Strouhal Number)
D. Turbine Puretone	One Cycle by Definition
E. Turbine Broadband	Emperical ROLLS ROYCE and GE data

Figure 22 - Schematic of Noise Constituent Prediction and Summation

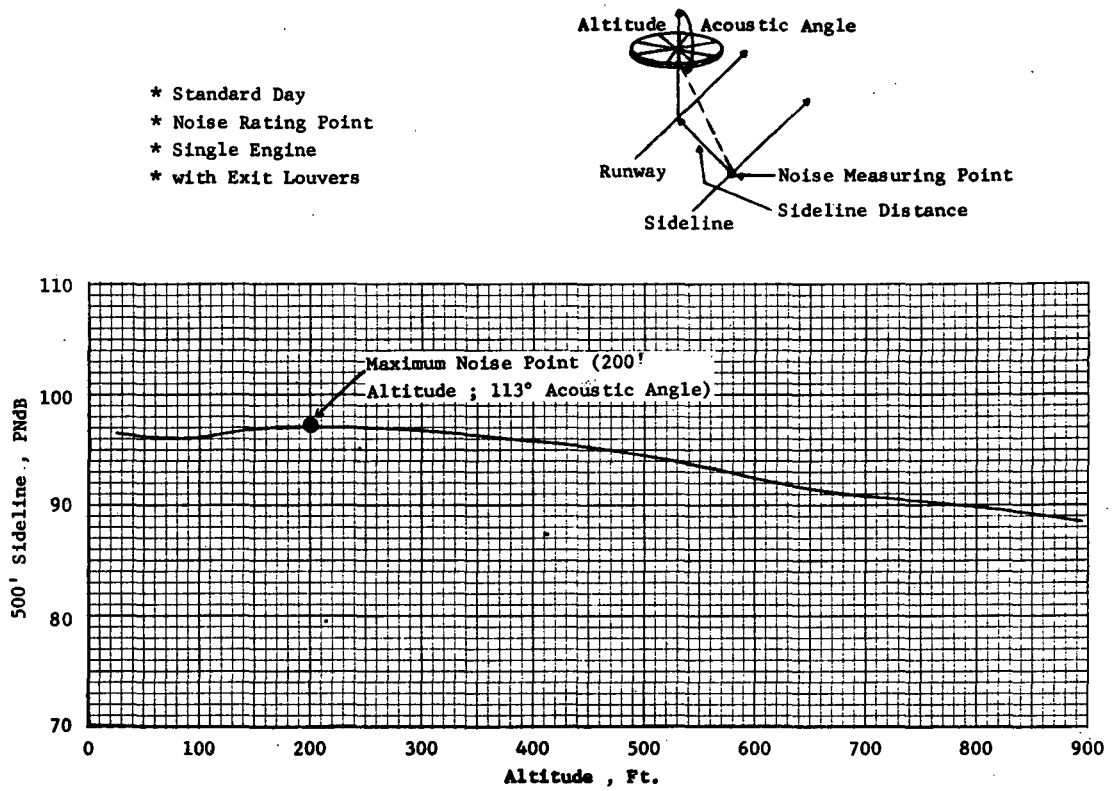

Figure 23 - LF460 Noise on 500' Sideline During Vertical Takeoff

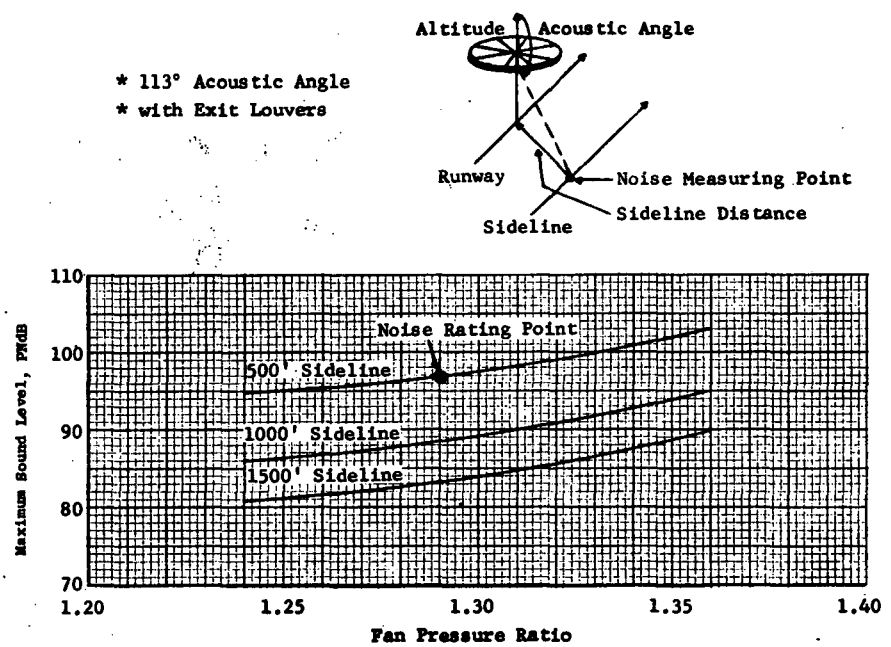

Figure 24 - Variation in Maximum LF460 Noise with Fan Pressure Ratio - Standard Day -

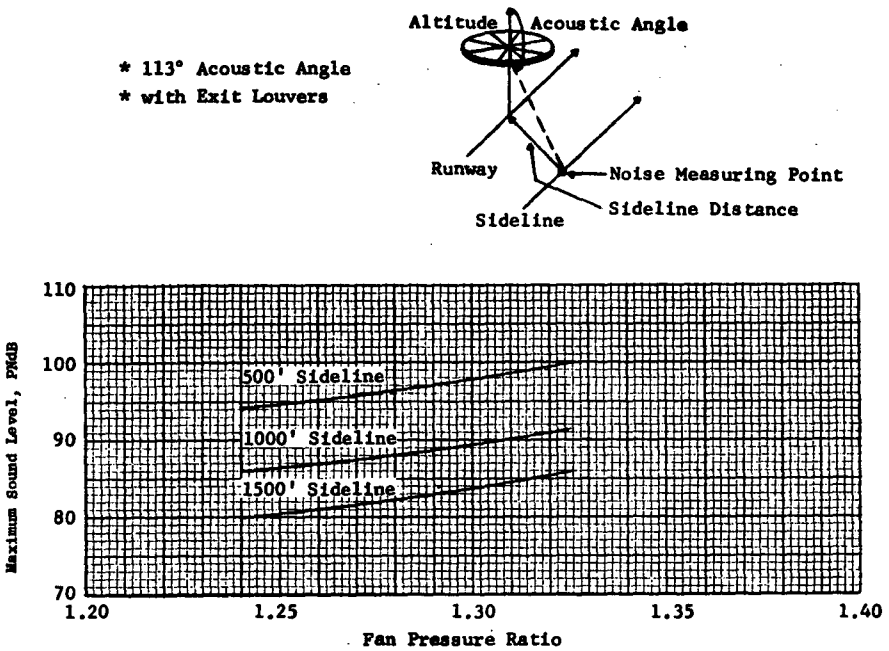

Figure 25 - Variation in Maximum LF460 Noise with Fan Pressure Ratio - Hot Day -

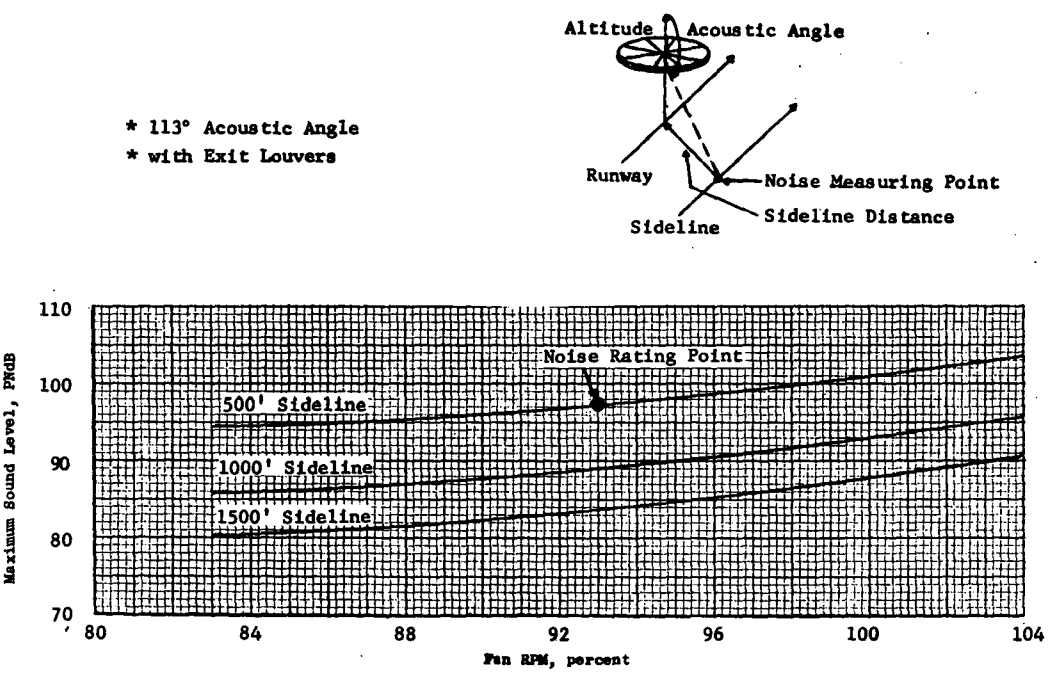

Figure 26 - Variation in Maximum LF460 Noise with Fan RPM - Standard Day -

* 113° Acoustic Angle
* with Exit Louvers

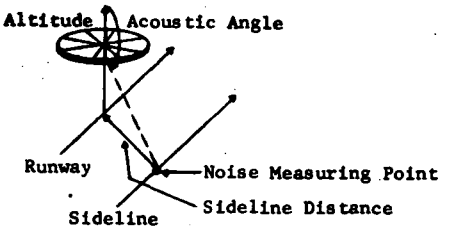

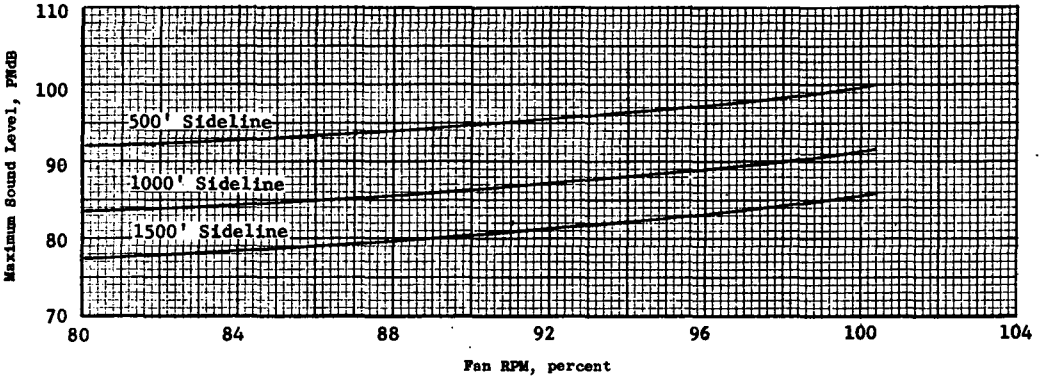

Figure 27 - Variation in Maximum LF460 Noise with Fan RPM - Hot Day -

* 113° Acoustic Angle
* with Exit Louvers

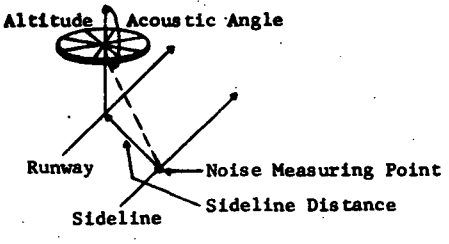

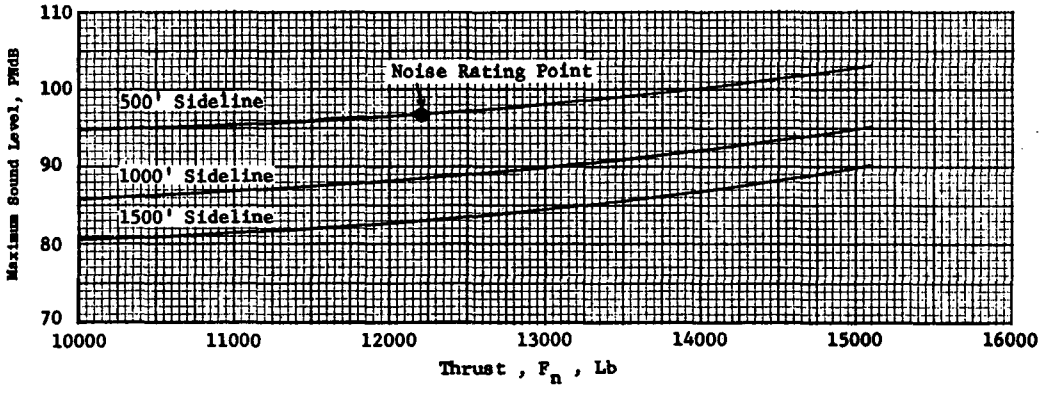

Figure 28 - Variation in Maximum LF460 Noise with Thrust - Standard Day -

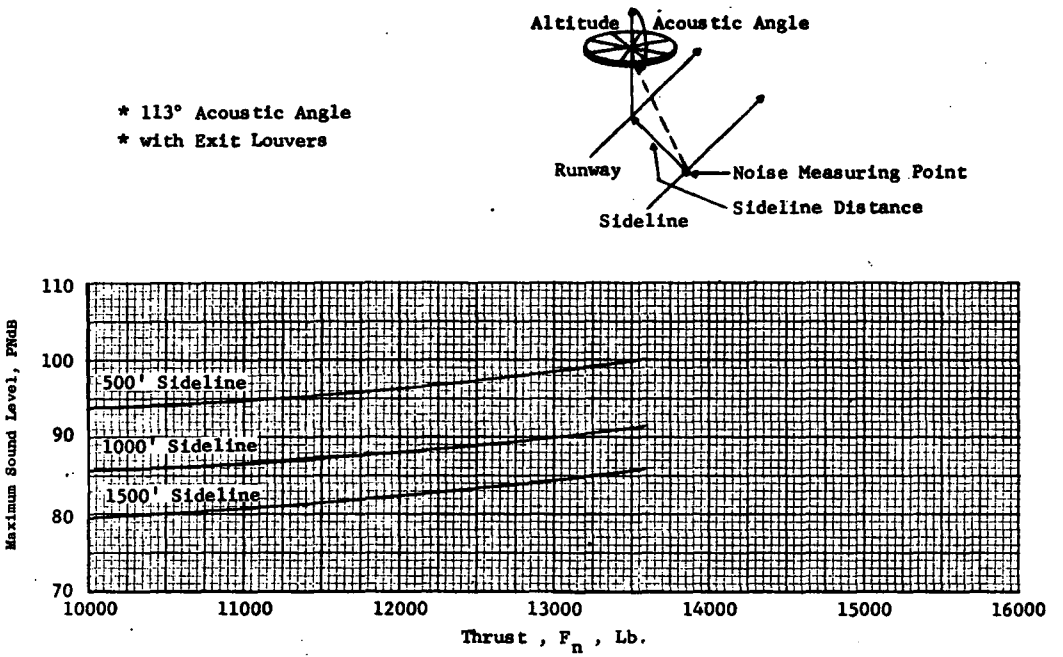

Figure 29 - Variation in Maximum LF460 Noise with Thrust - Hot Day -

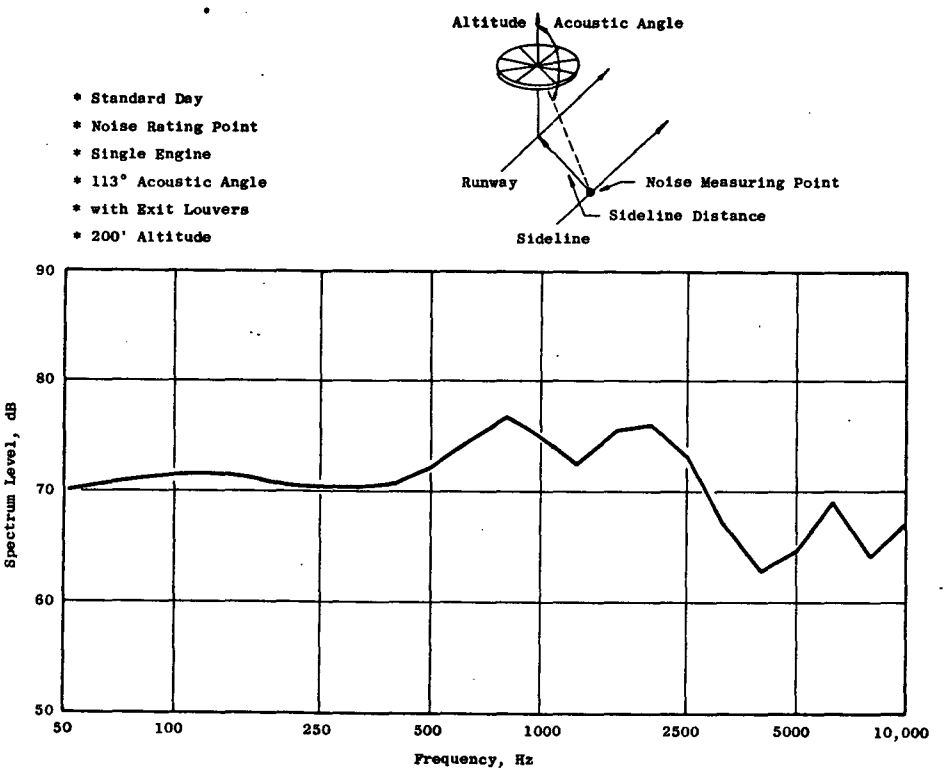

Figure 30 - LF460 Spectrum on 500' Sideline During Vertical Takeoff

40

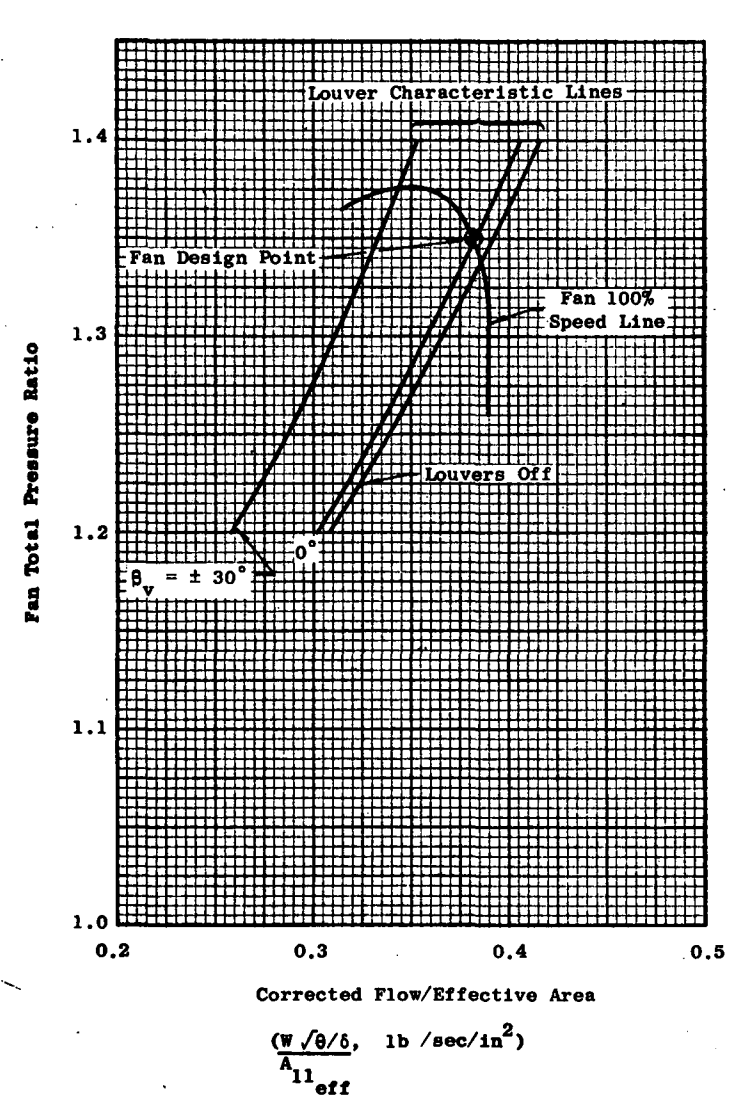

Figure 31 - LF460 Louver and Fan 100% Speed Characteristics

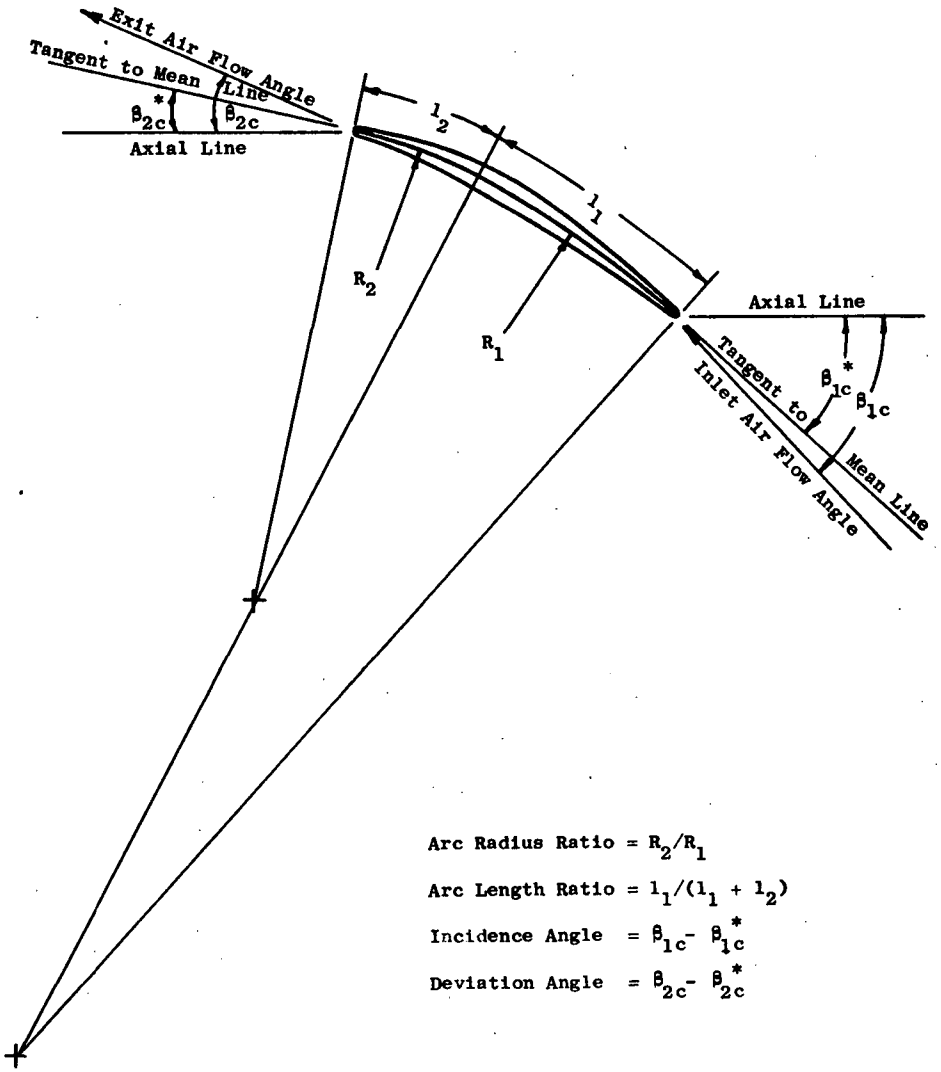

Figure 32 - Multiple Circular Arc Airfoil Definition

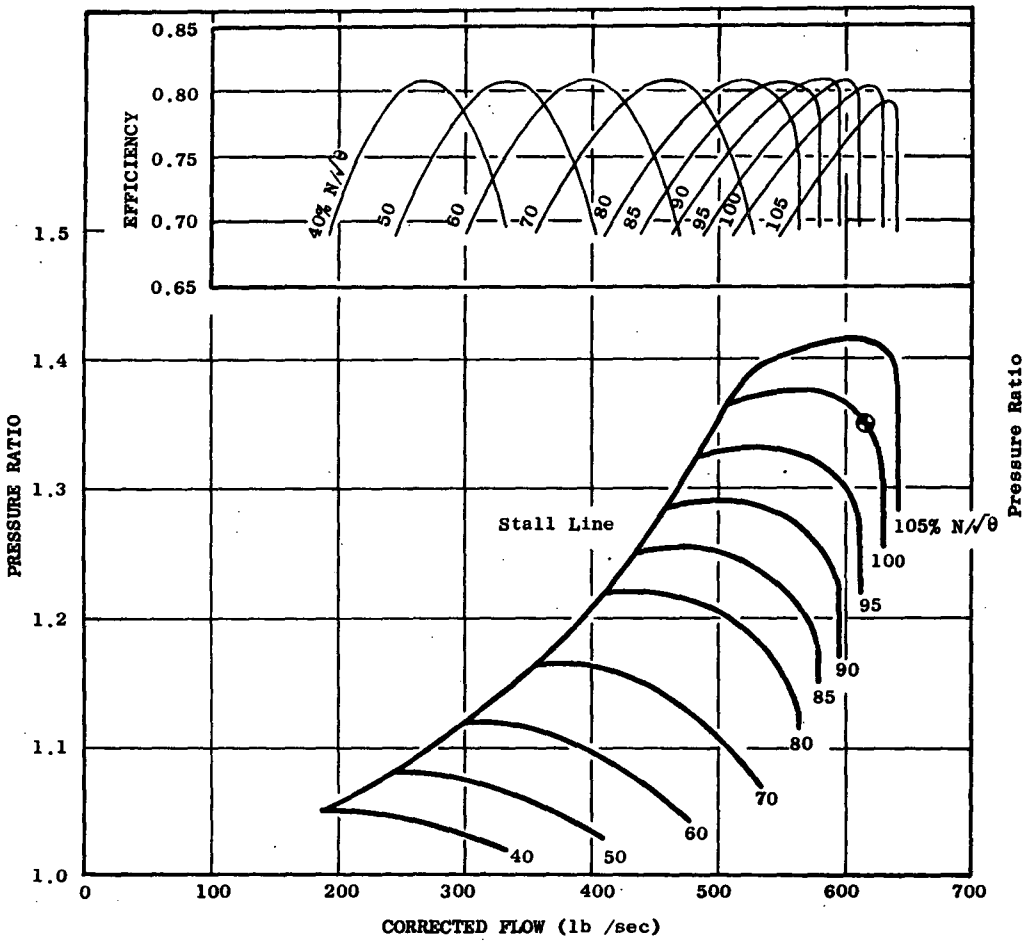

Figure 33 - LF460 Predicted Fan Performance

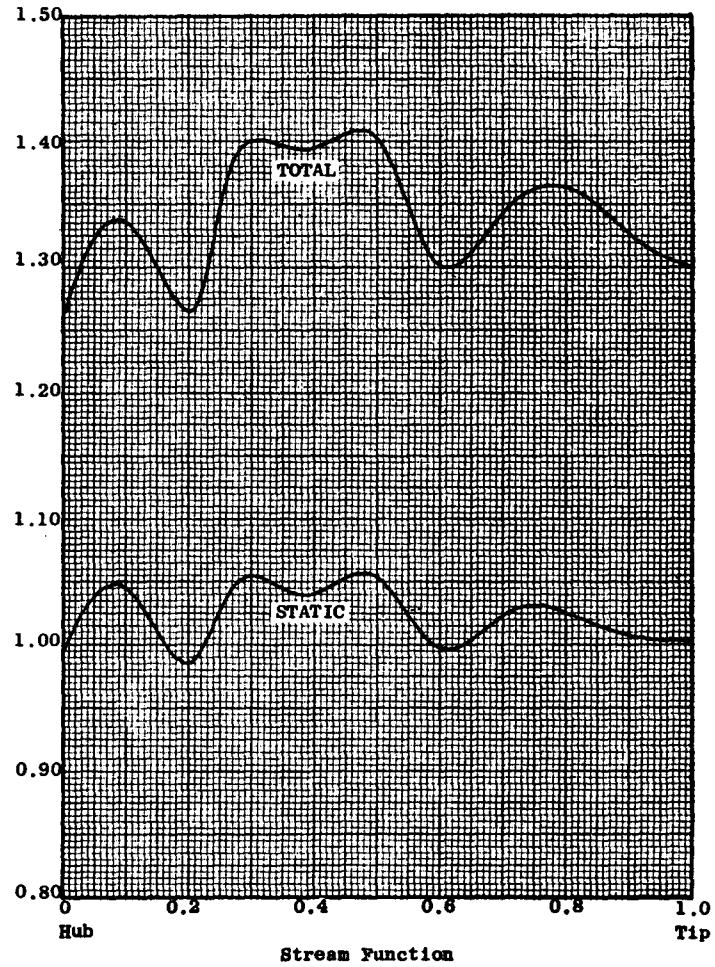

Figure 34 - LF460 Fan Pressure Ratio

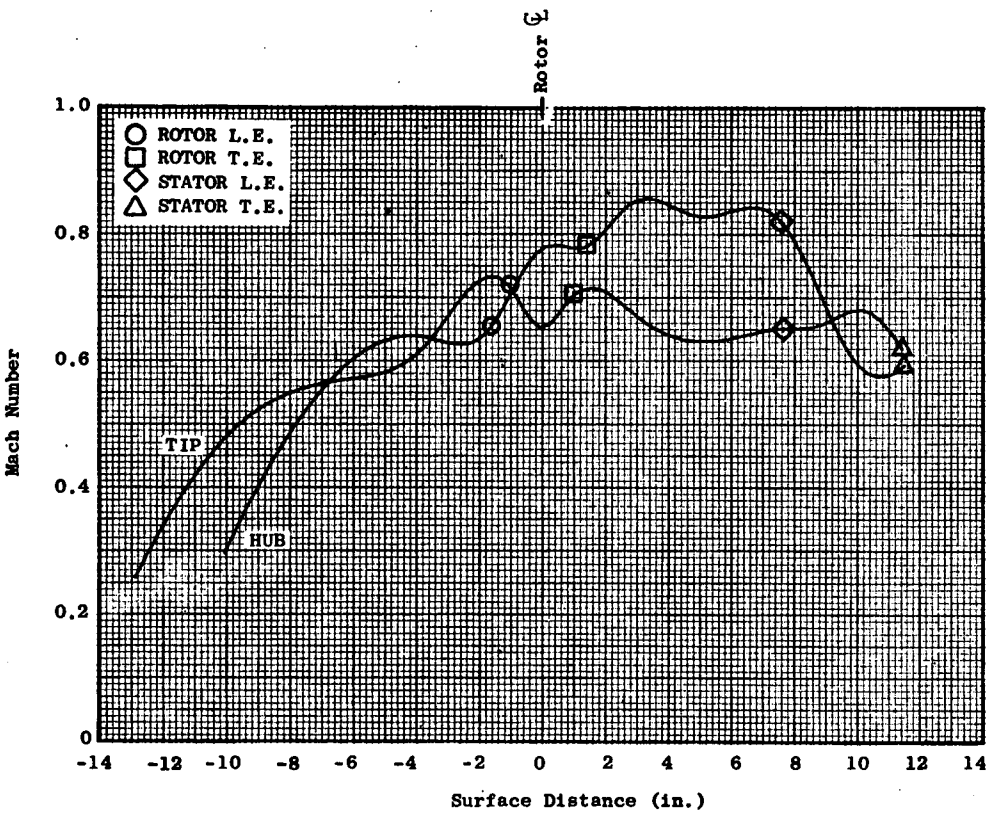

Figure 35 - LF460 Hub and Tip Wall Mach Numbers

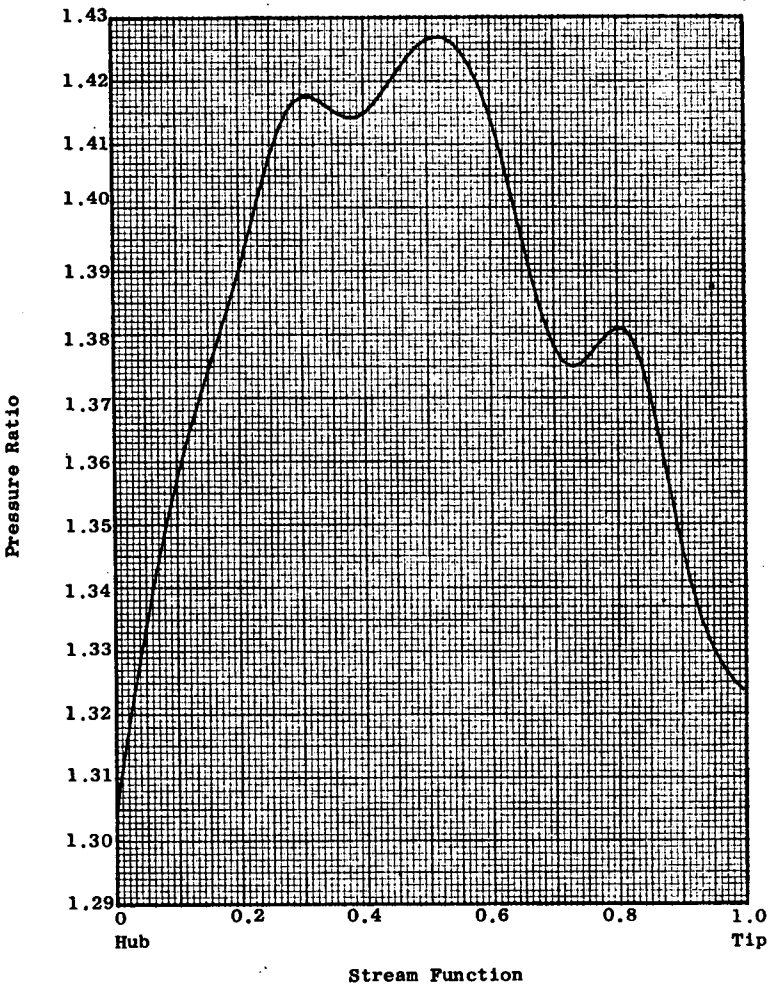

Figure 36 - LF460 Rotor Pressure Ratio

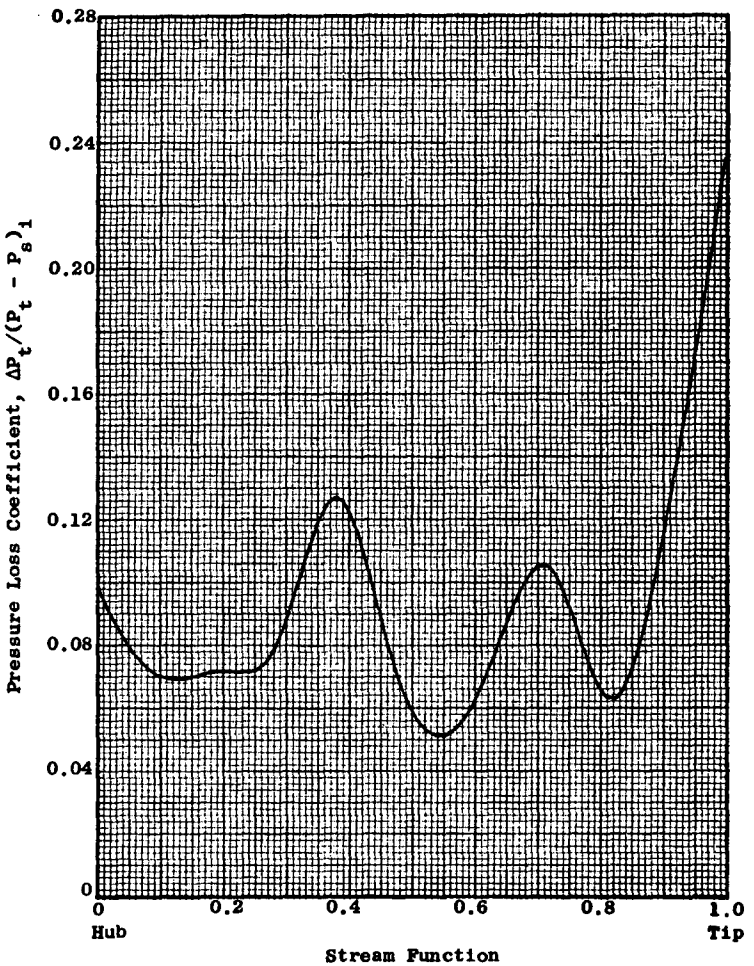

Figure 37 - LF460 Rotor Total Pressure Loss Coefficients

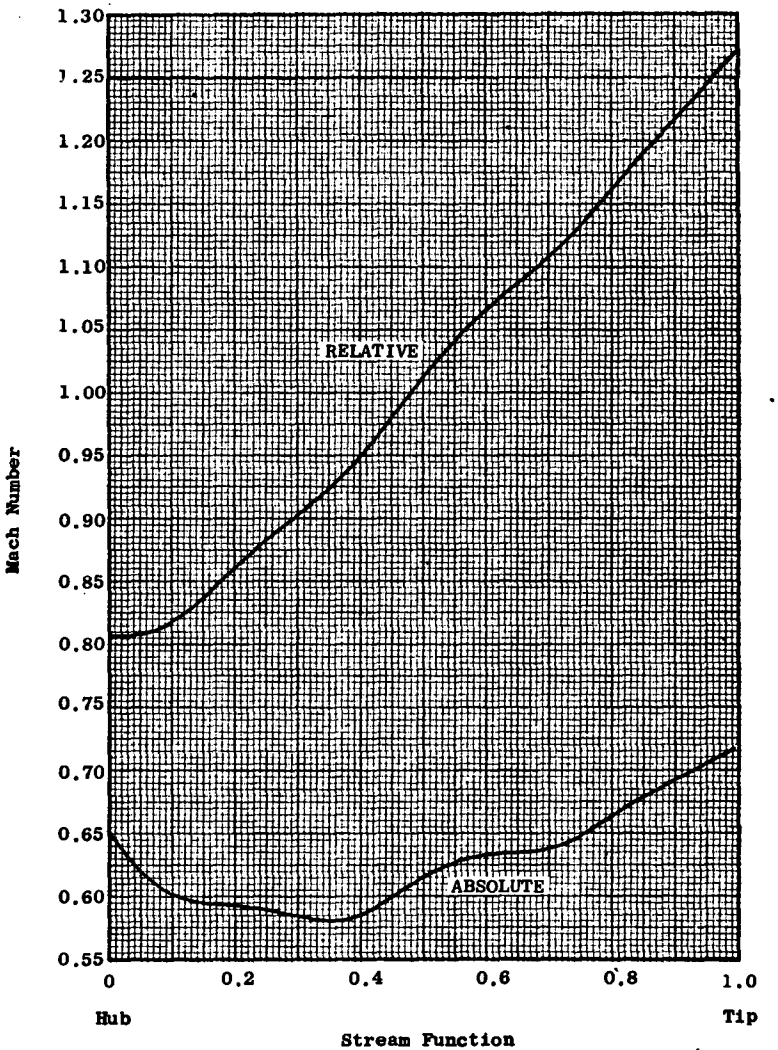

Figure 38 - Rotor Inlet Mach Number

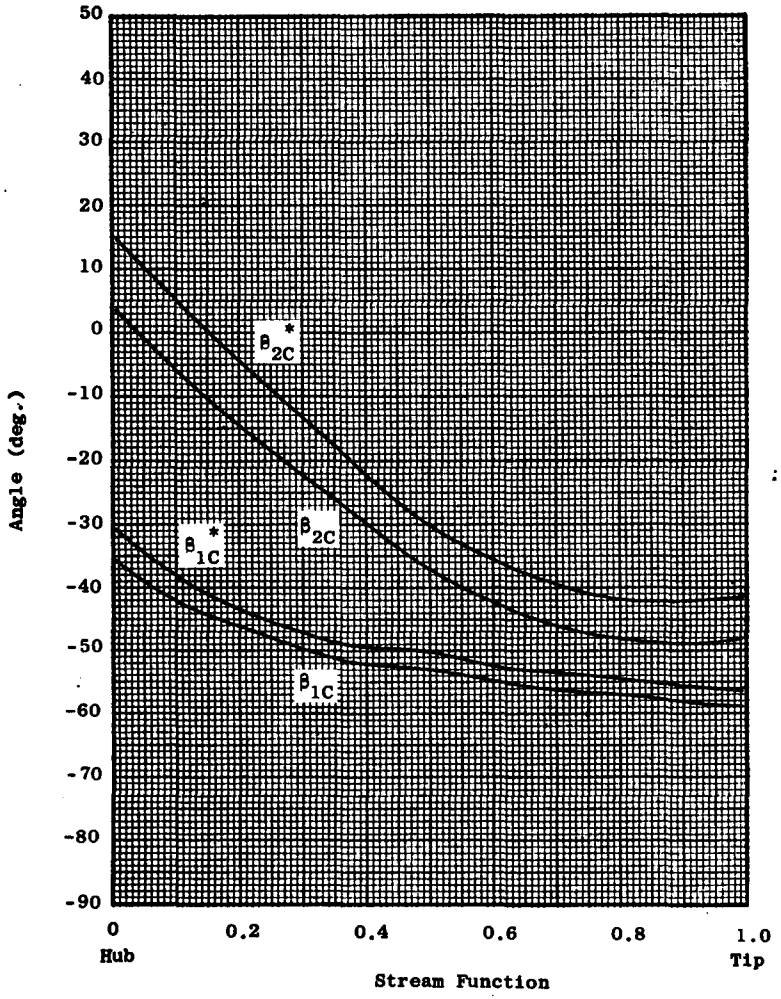

Figure 39 - Rotor Air and Blade Angles

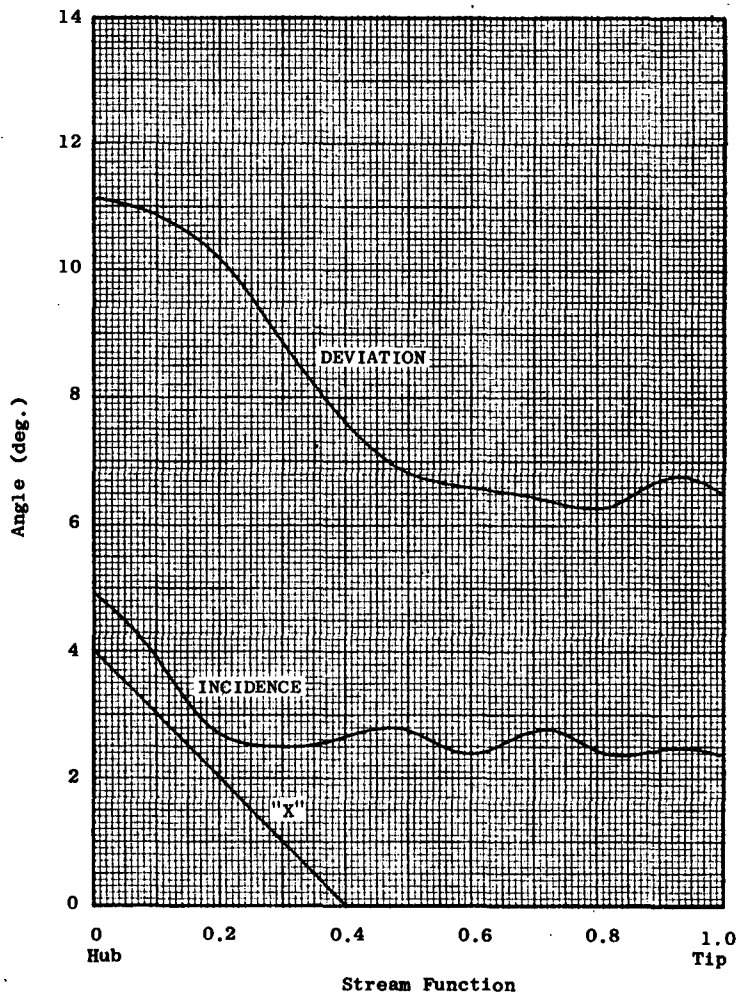

Figure 40 - Rotor Incidence and Deviation Angles

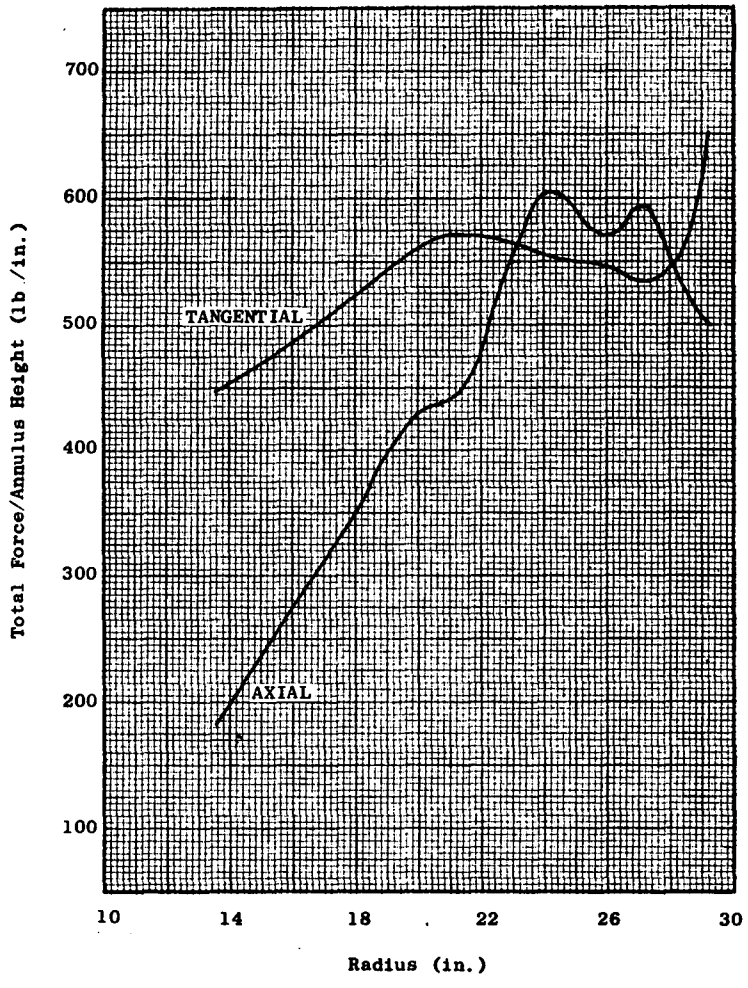

Figure 41 - Rotor Blade Air Loads

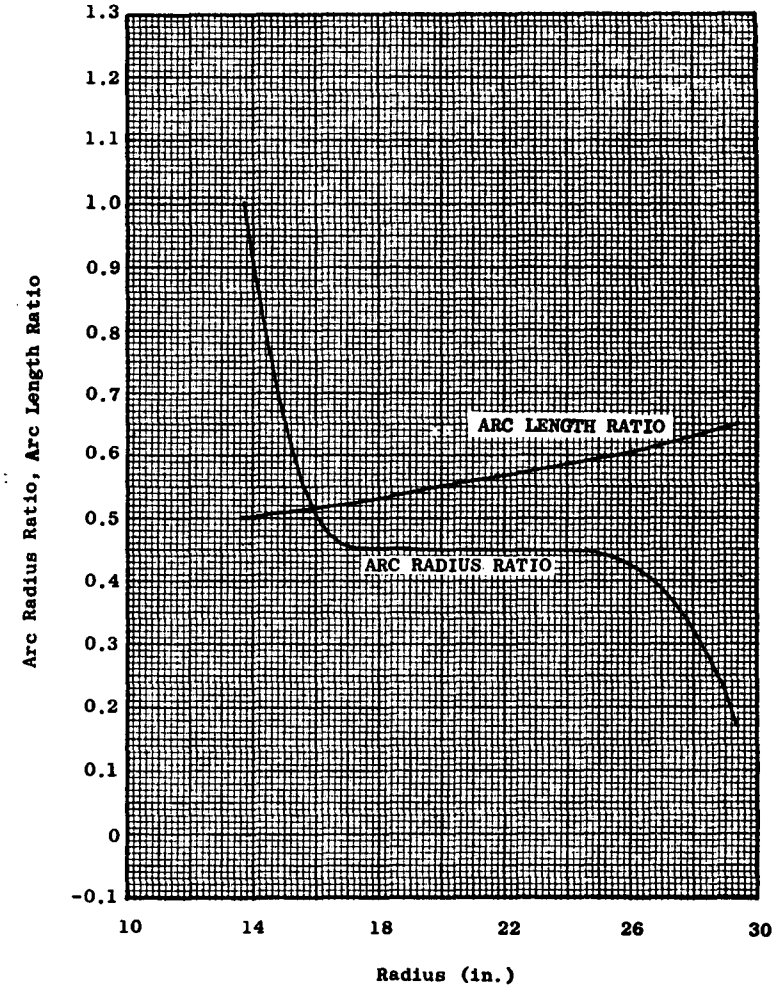

Figure 42 - Rotor Blade Meanline Arc Radius Ratio and Arc Length Ratio

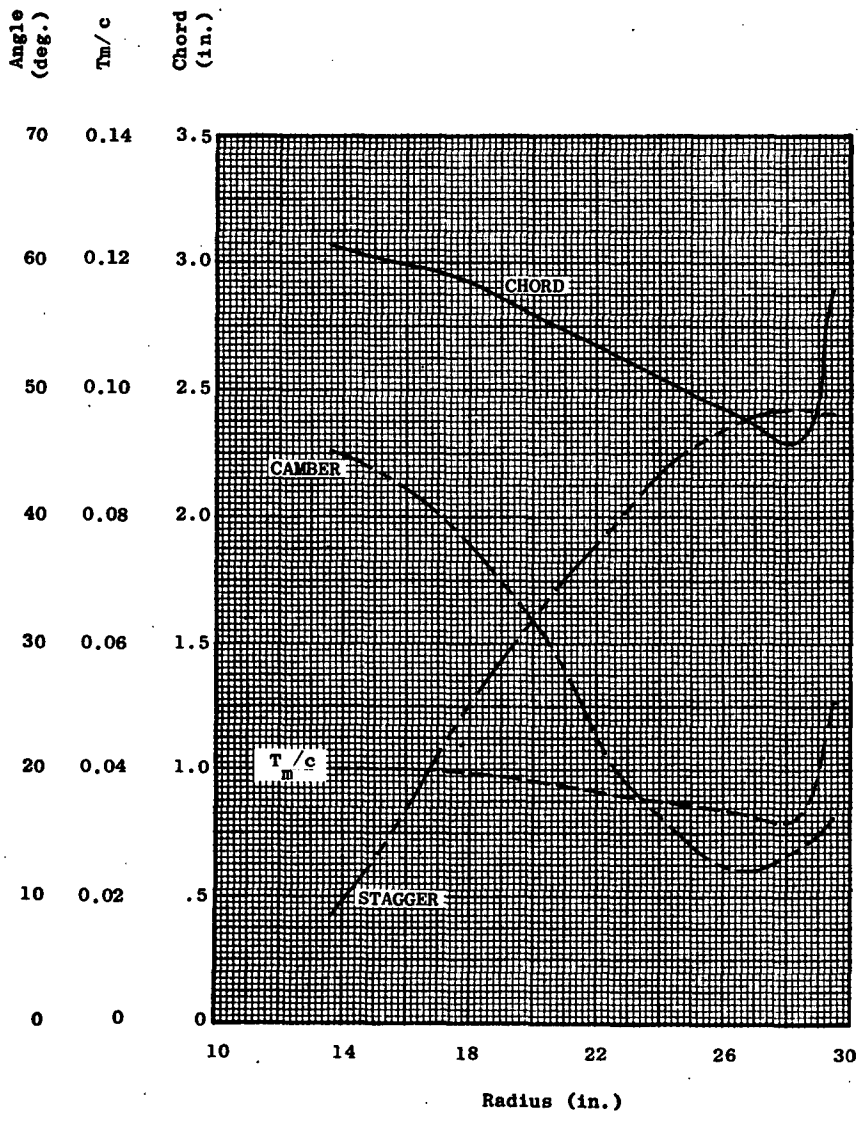

Figure 43 - LF460 Rotor Blade Geometry

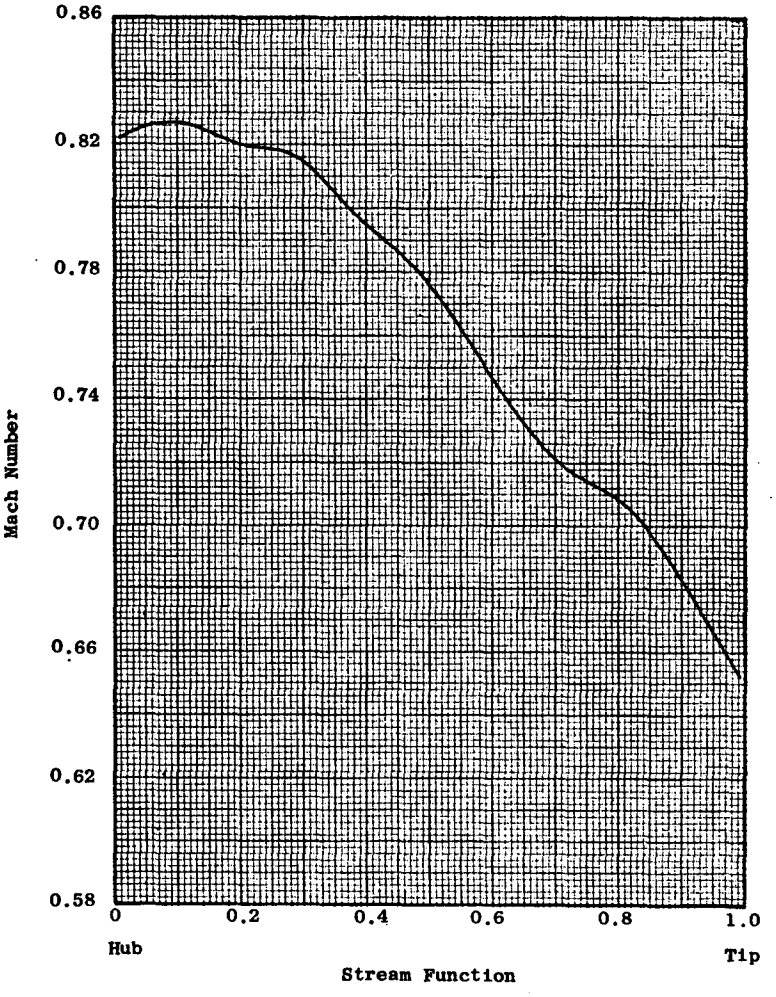

Figure 44 - Stator Inlet Mach Number

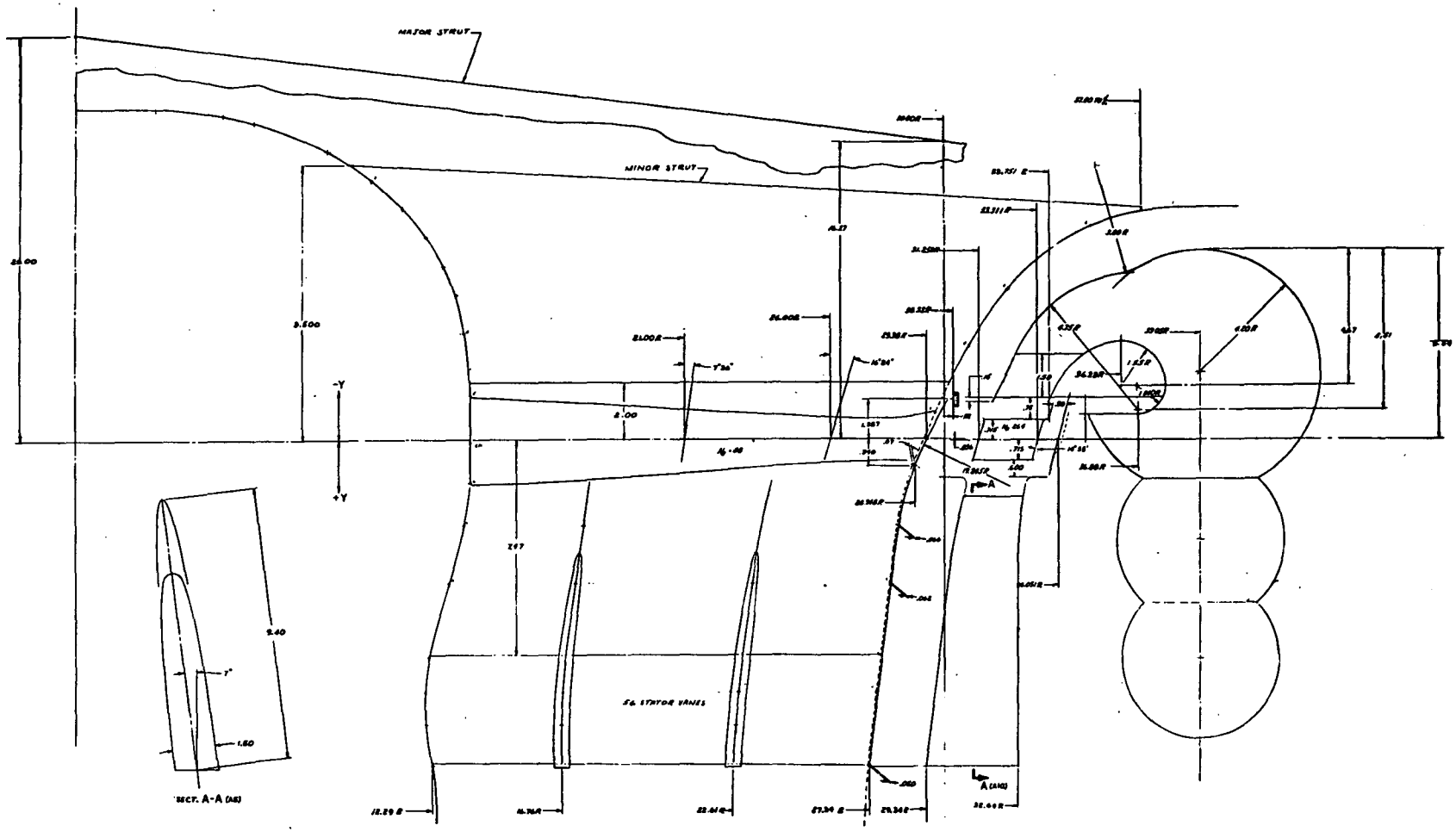

Figure 45 - LF460 Flowpath

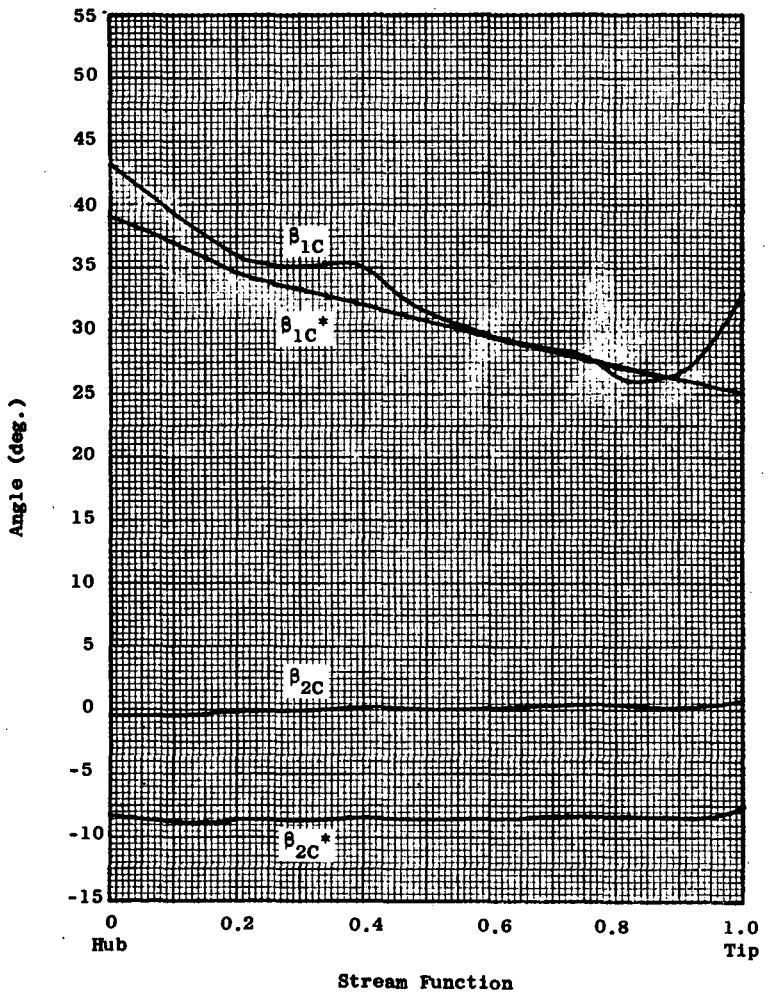

Figure 46 - LF460 Stator Air and Vane Angles

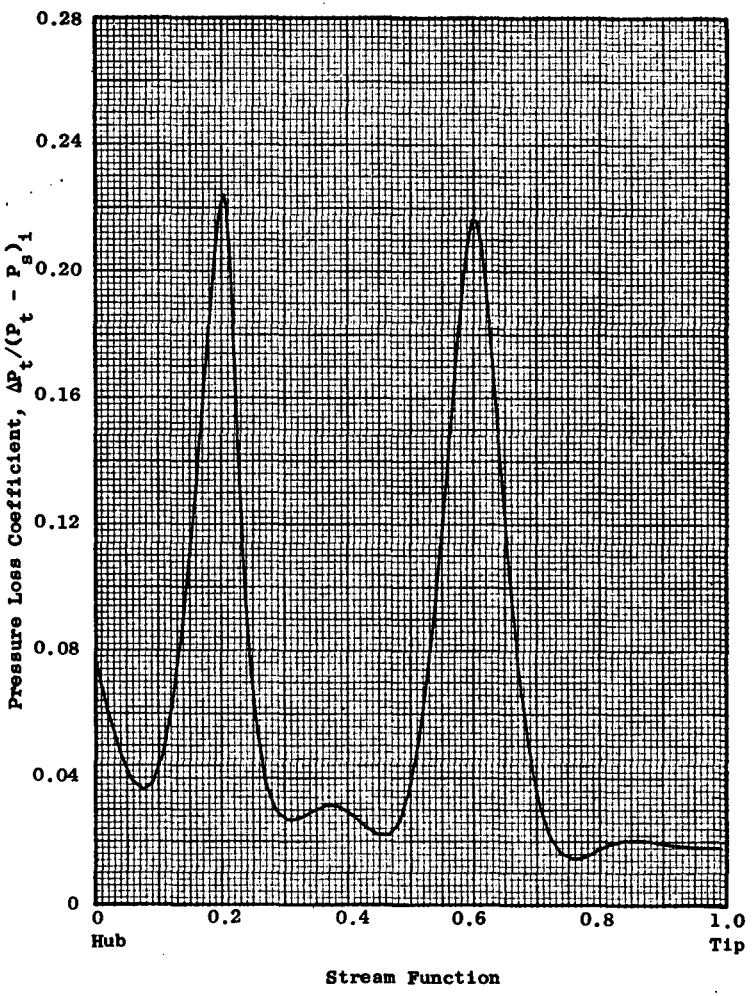

Figure 47 - LF460 Stator Total Pressure Loss Coefficients

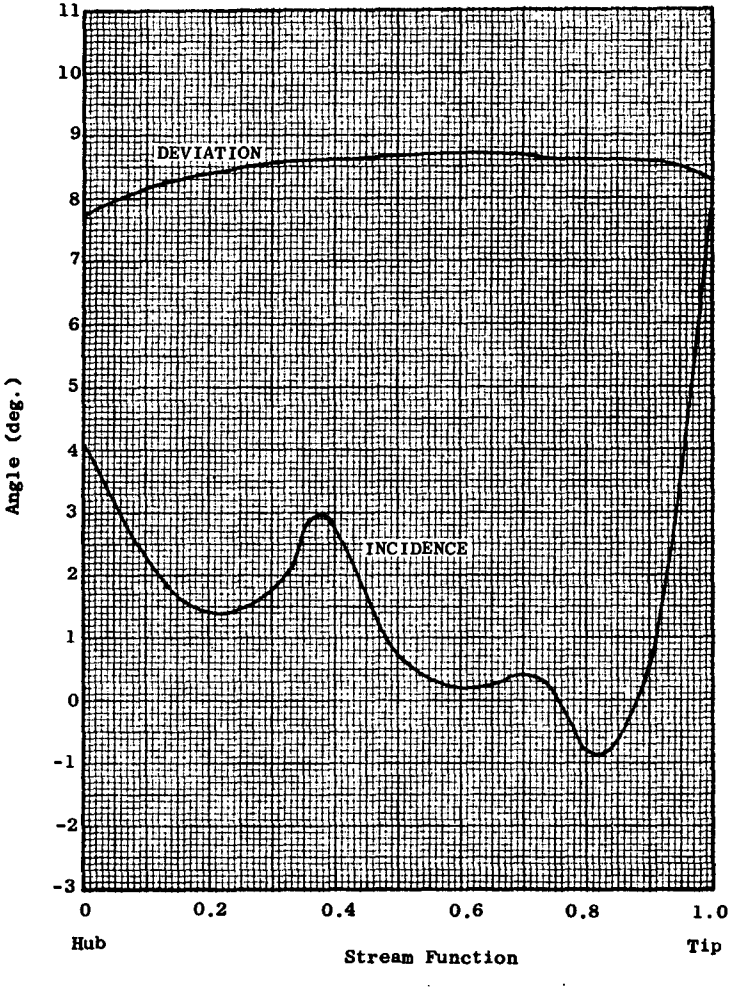

Figure 48 - LF460 Stator Incidence and Deviation Angles

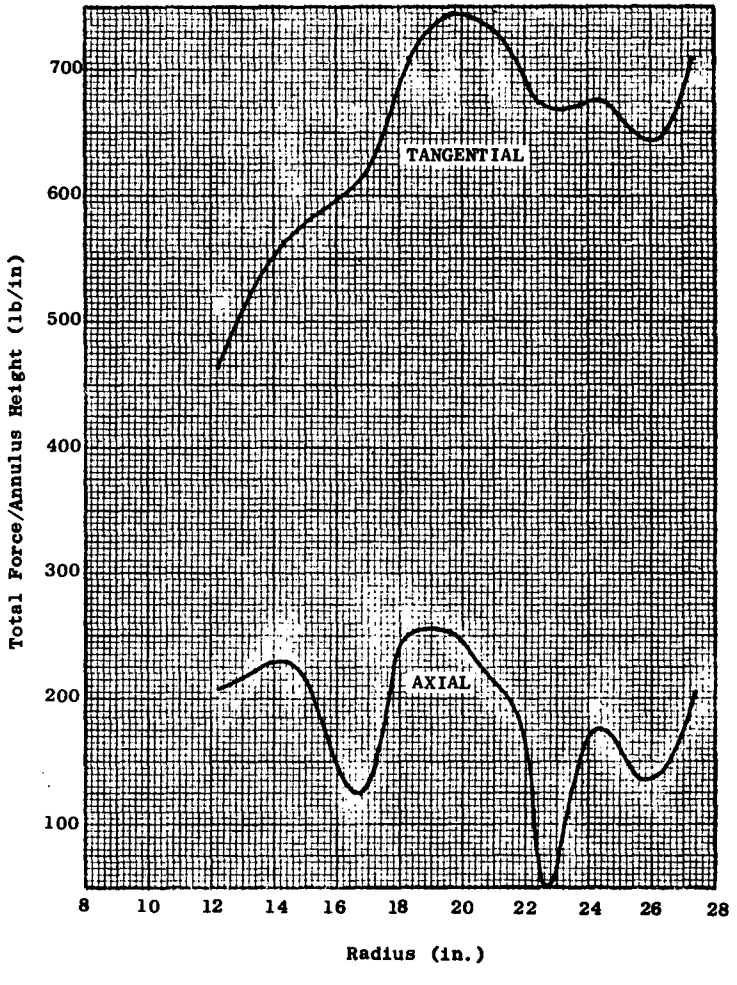

Figure 49 - Stator Vane Air Loads

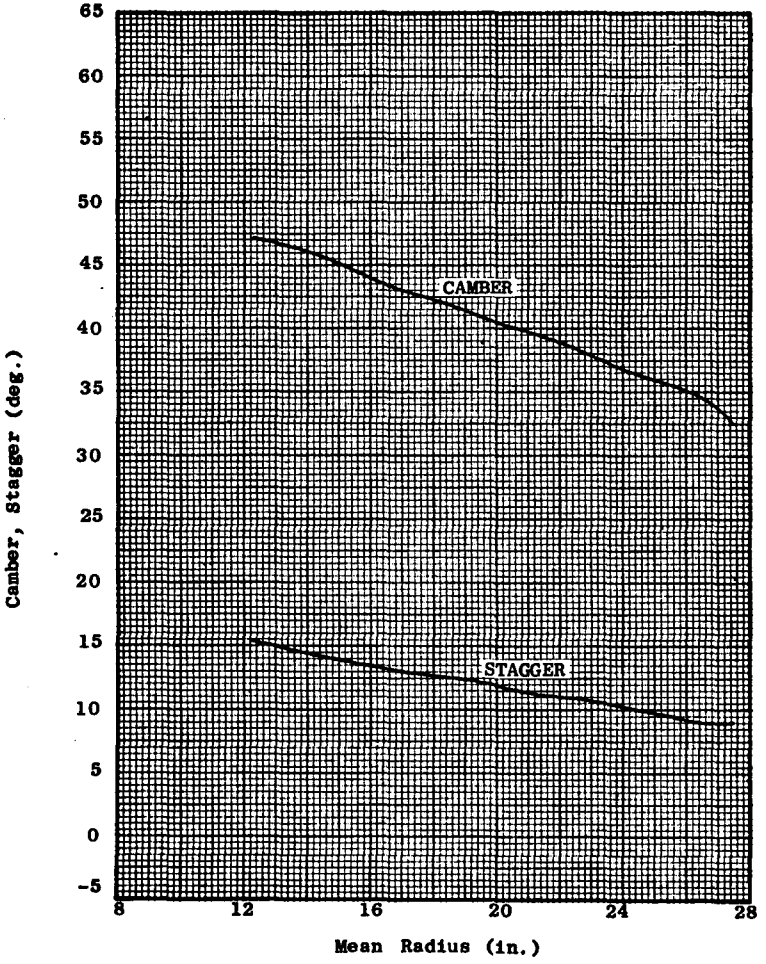

Figure 50 - LF460 Stator Vane Aerodynamic Geometry

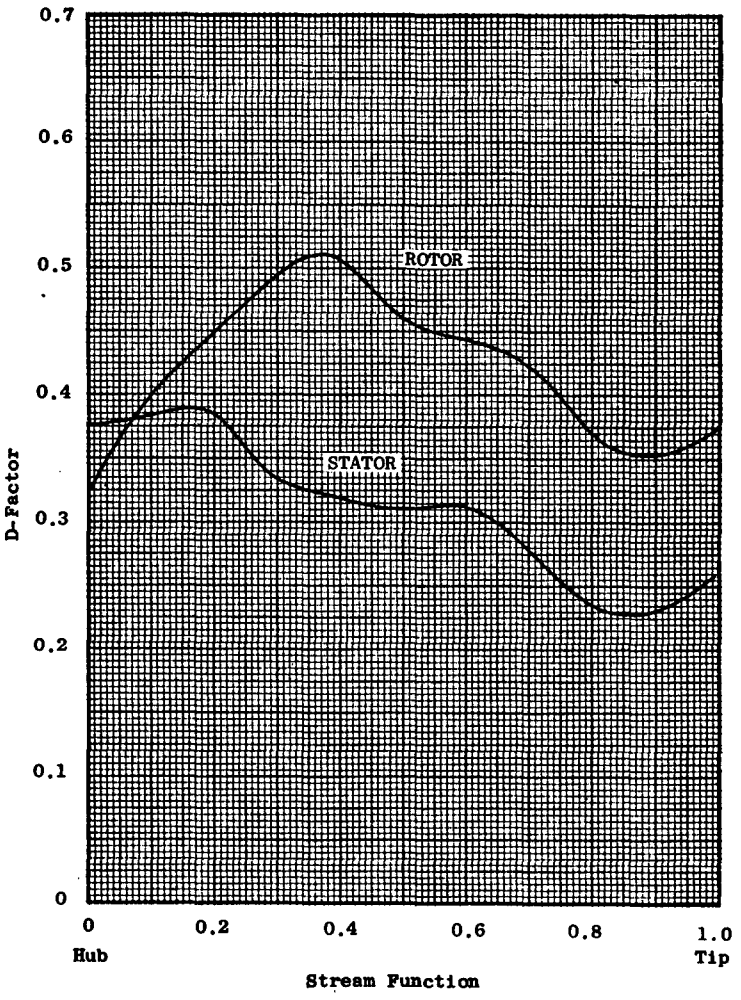

Figure 51 - LF460 Rotor and Stator D-Factors

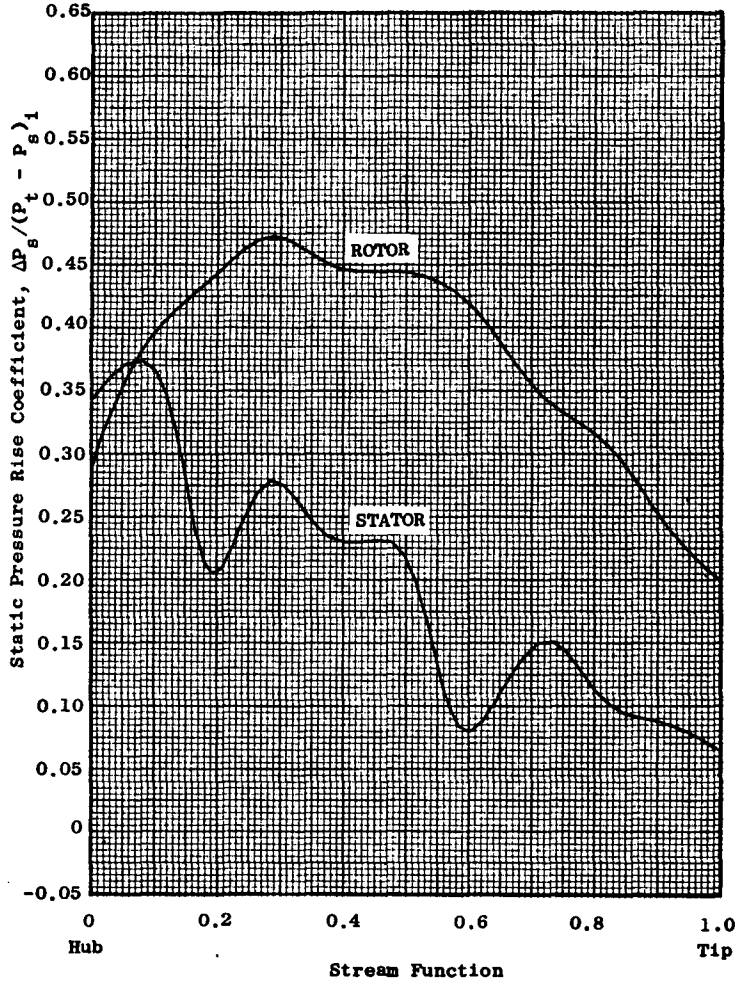

Figure 52 - LF460 Rotor and Stator
Static Pressure Rise Coefficients

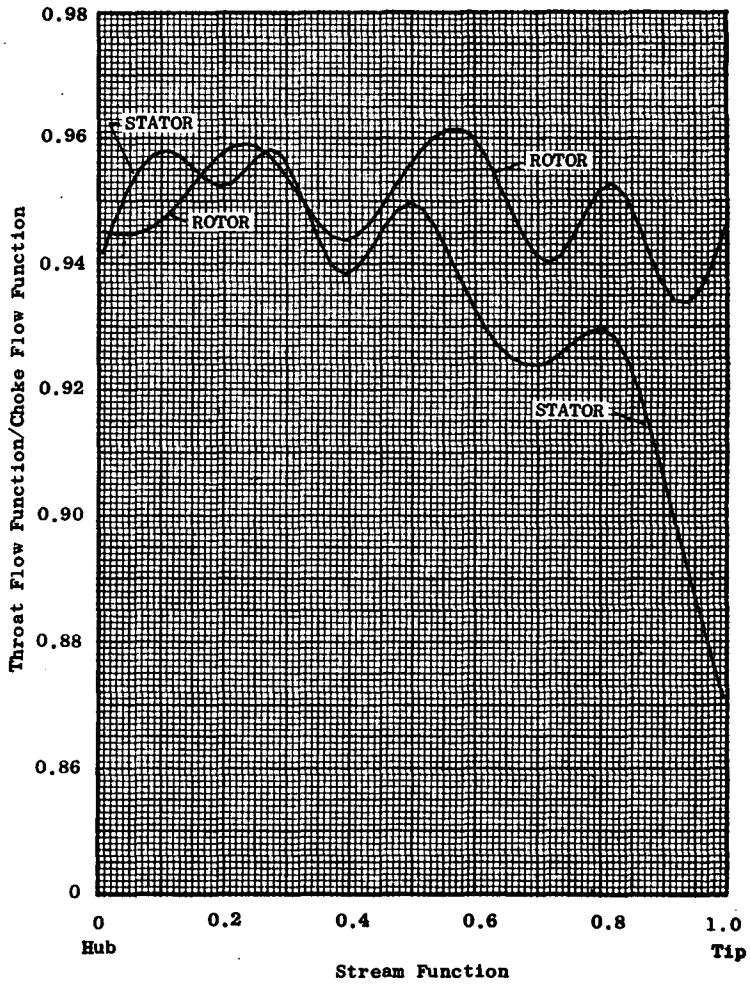

Figure 53 - LF460 Rotor and Stator
Throat-to-Critical Flow Function

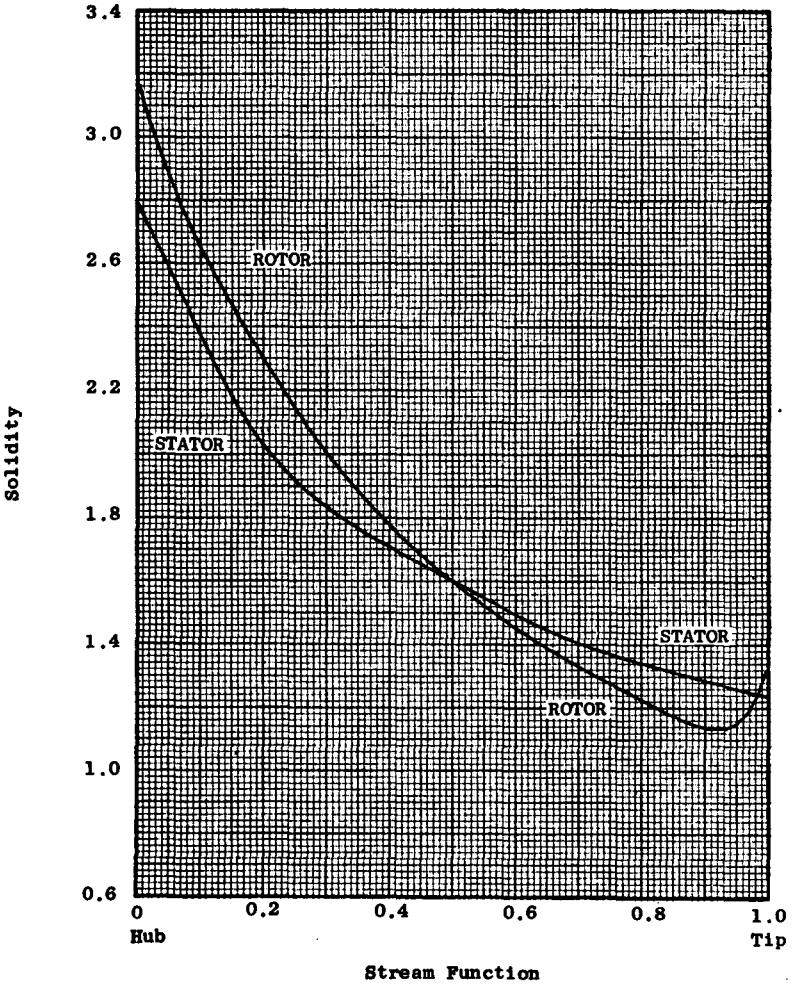

Figure 54 - LF460 Rotor and Stator Solidities

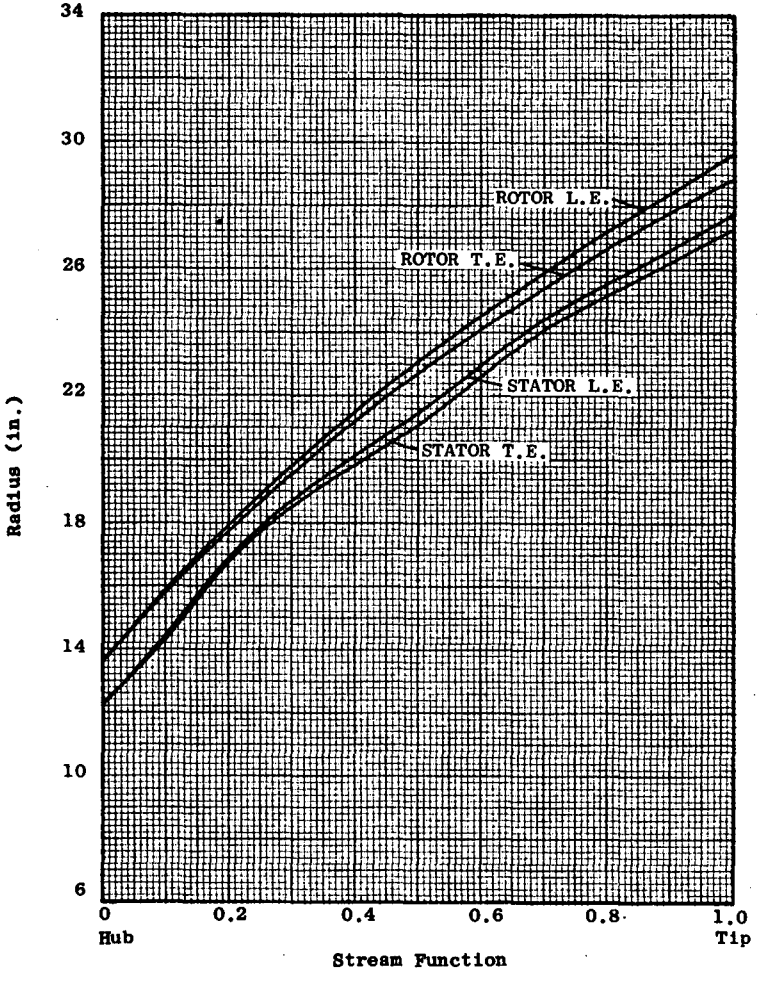

Figure 55 - LF460 Radius-Stream Function Relationship

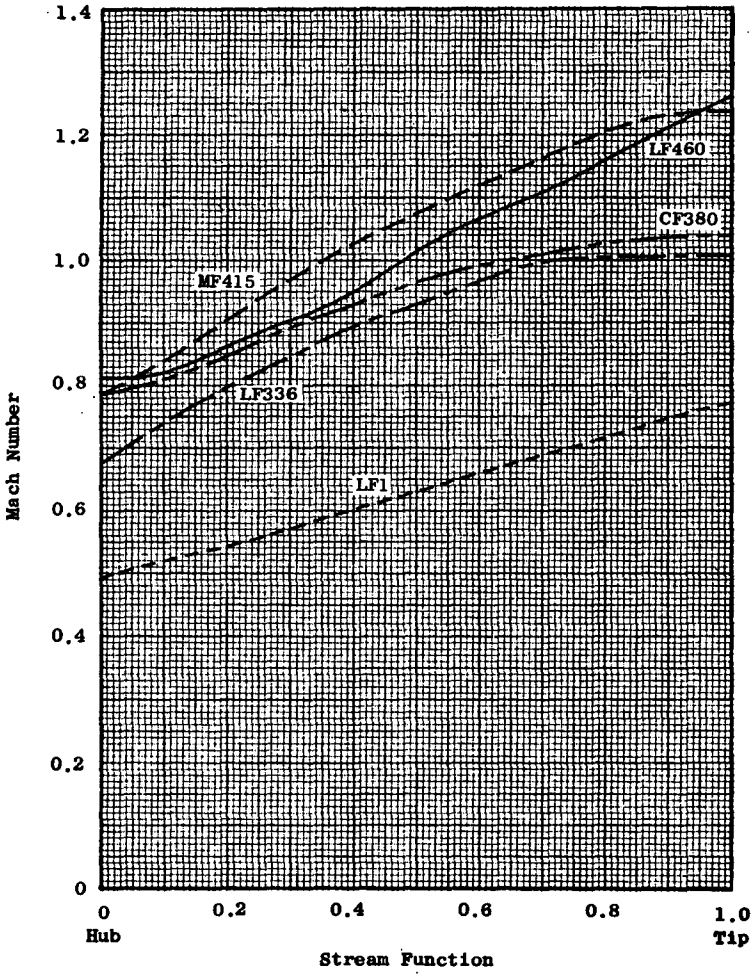

Figure 56 - Rotor Relative Mach Number Comparison

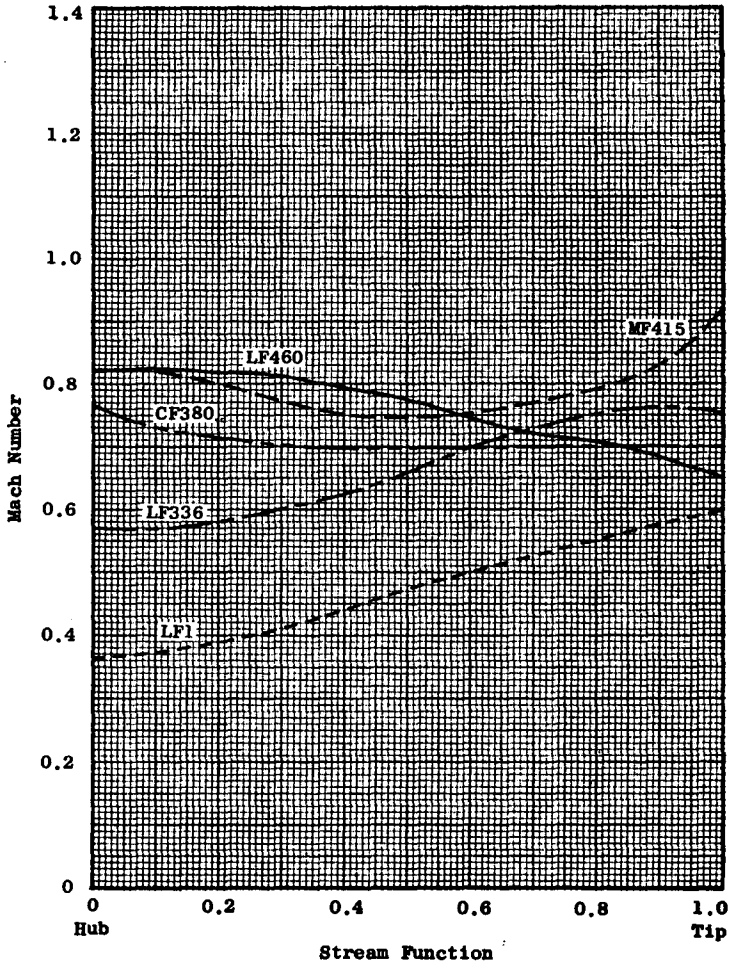

Figure 57 - Stator Relative Mach Number Comparison

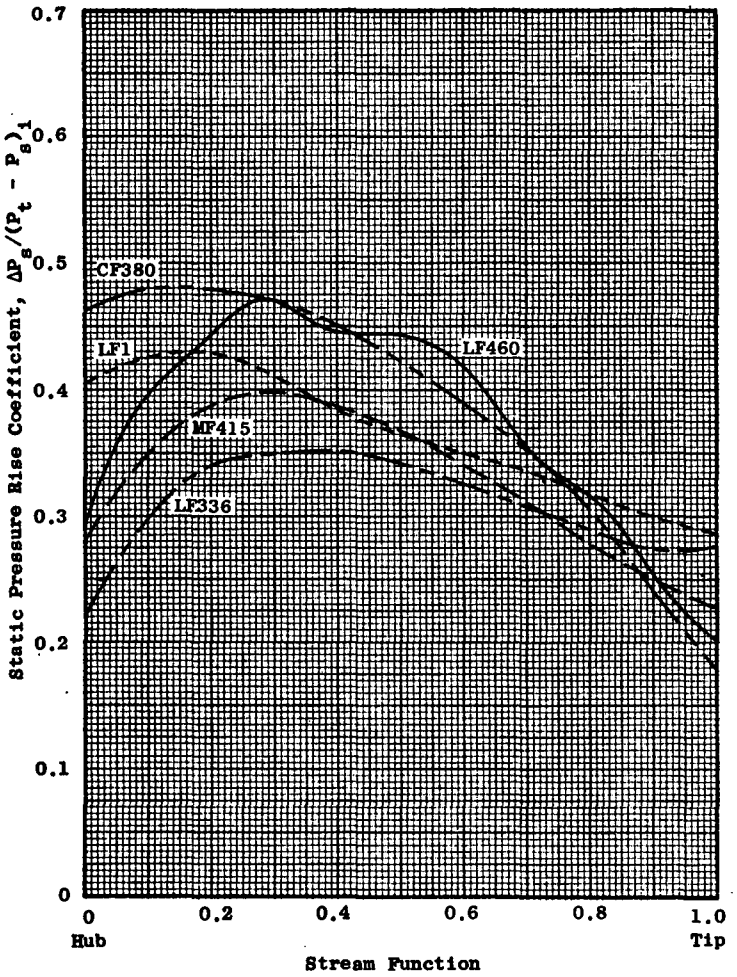

Figure 58 - Rotor Static Pressure Rise Coefficient Comparison

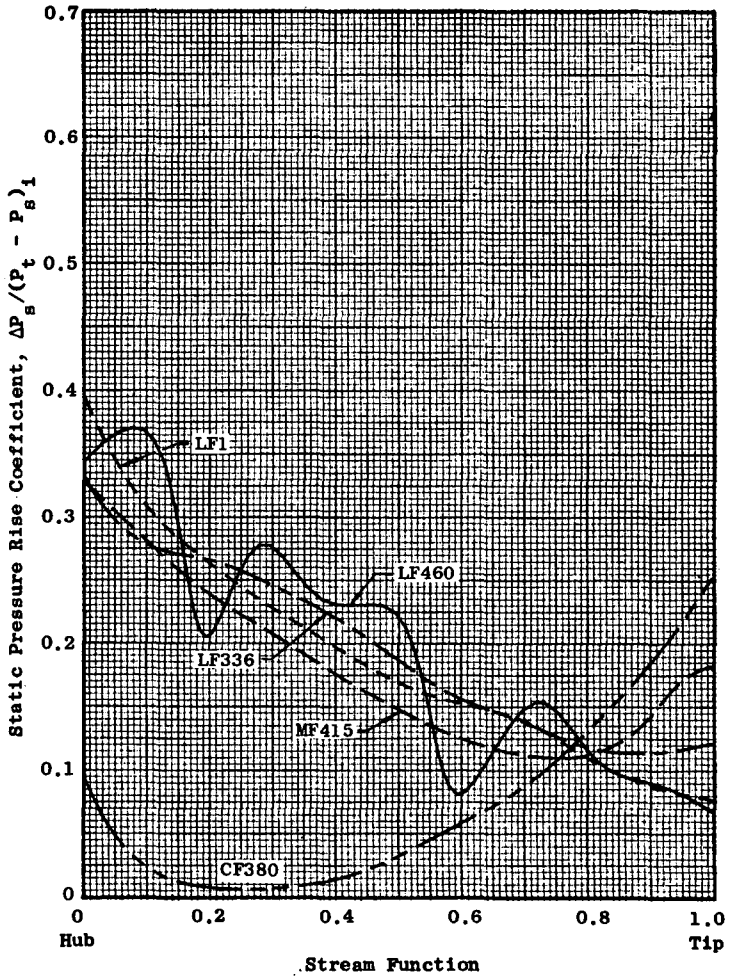

Figure 59 - Stator Static Pressure Rise Coefficient Comparison

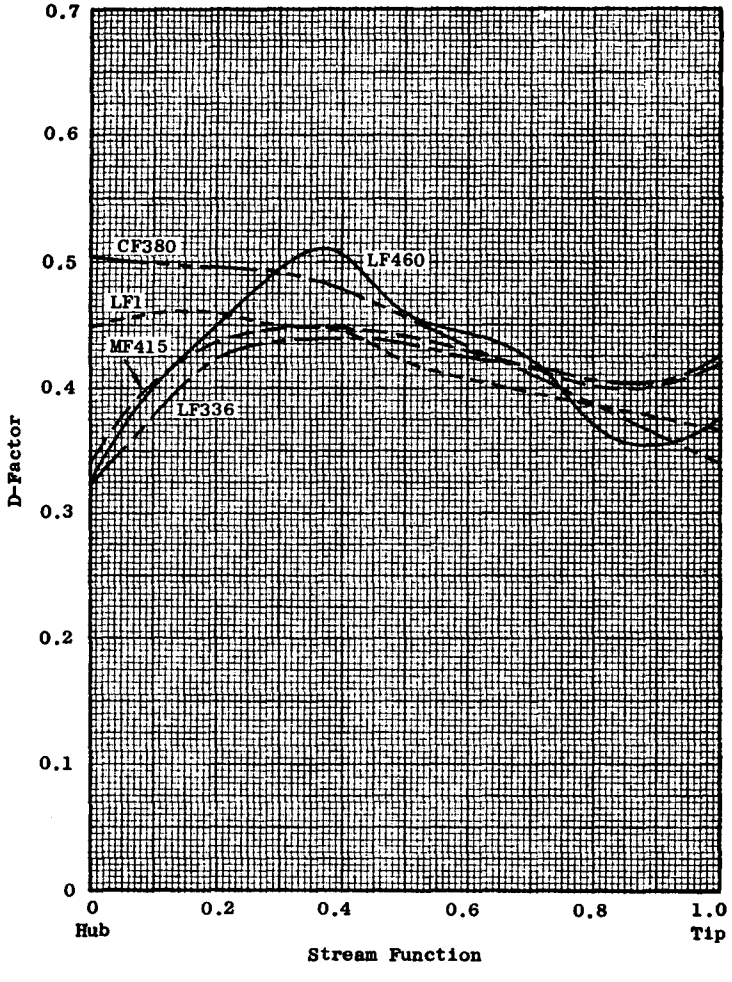

Figure 60 - Rotor D-Factor Comparison

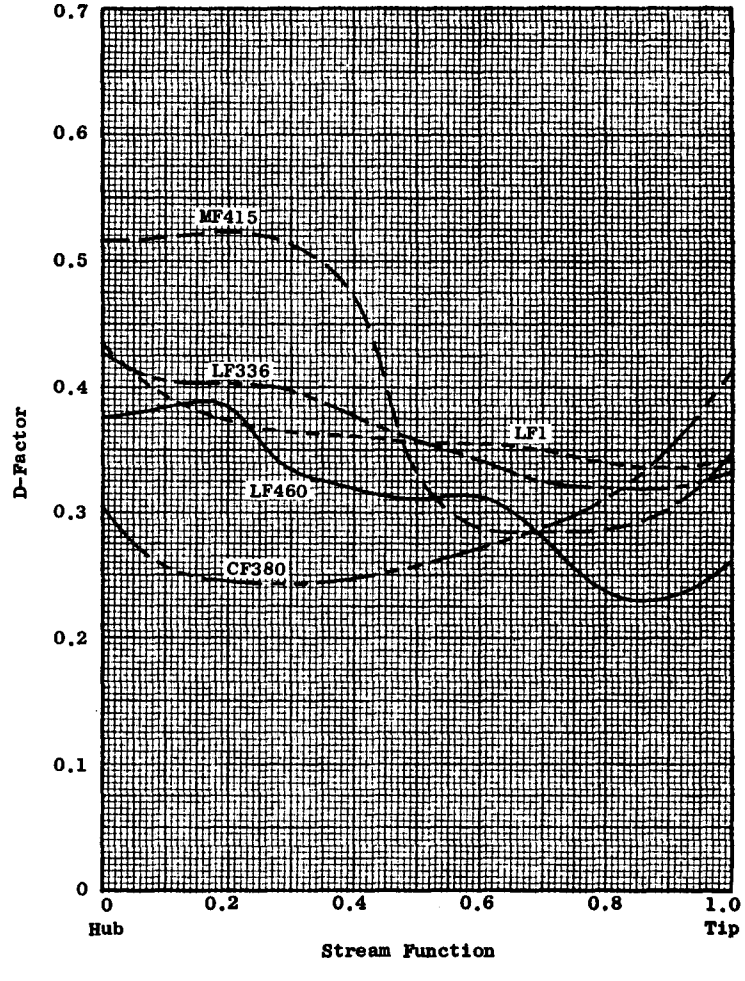

Figure 61 - Stator D-Factor Comparison

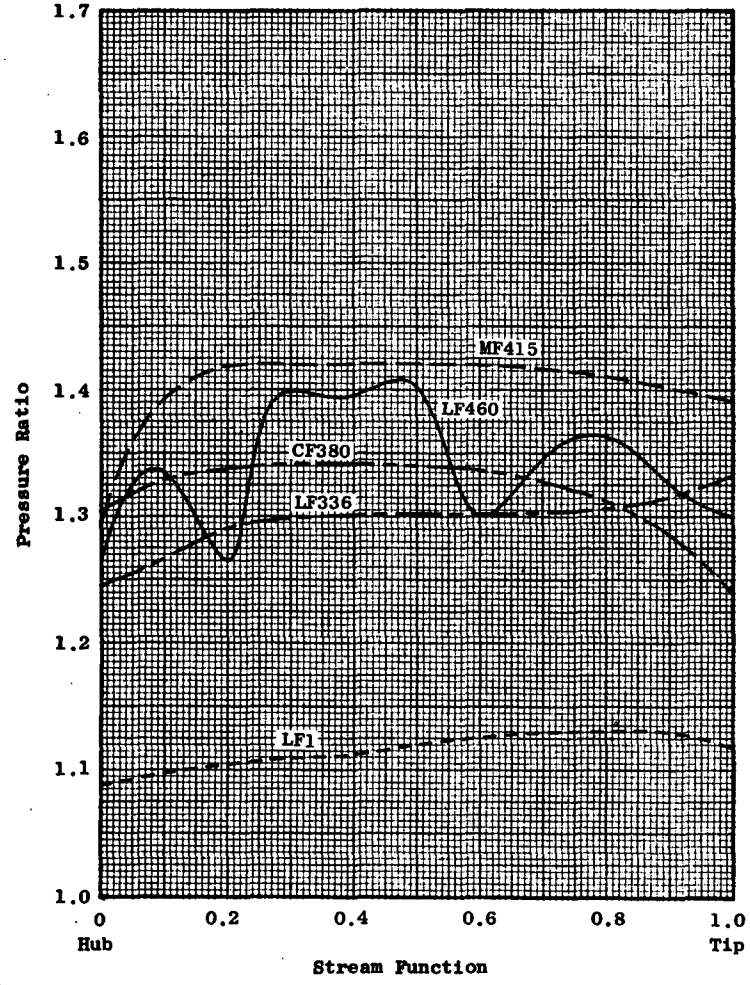

Figure 62 - Fan Pressure Ratio Comparison

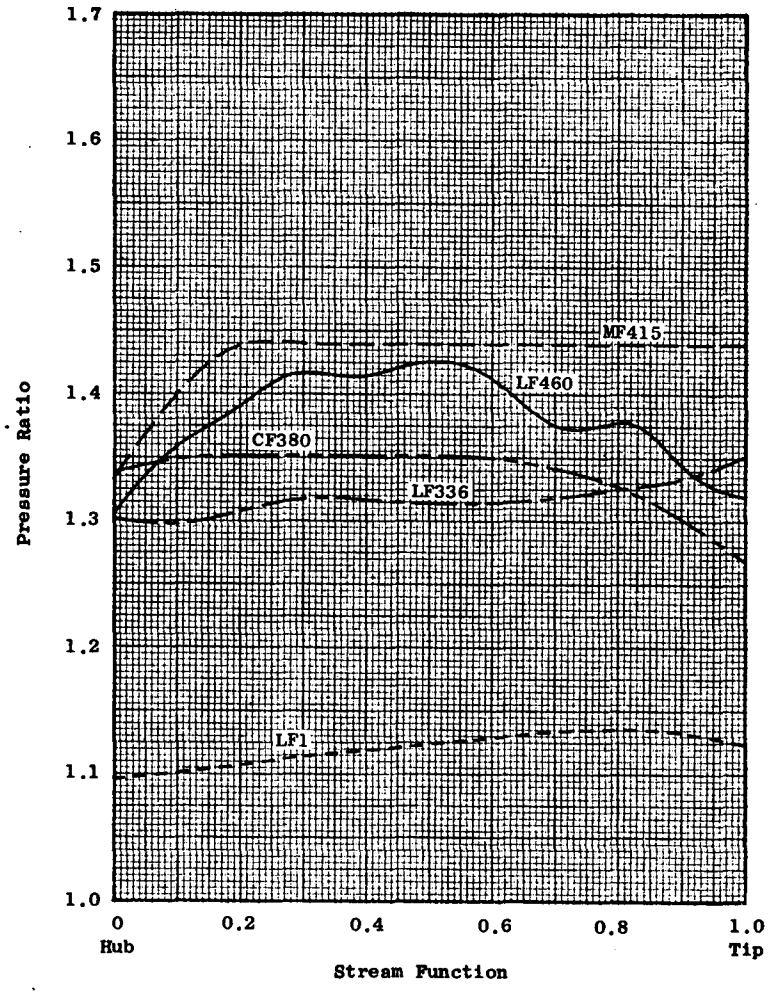

Figure 63 - Rotor Pressure Ratio Comparison

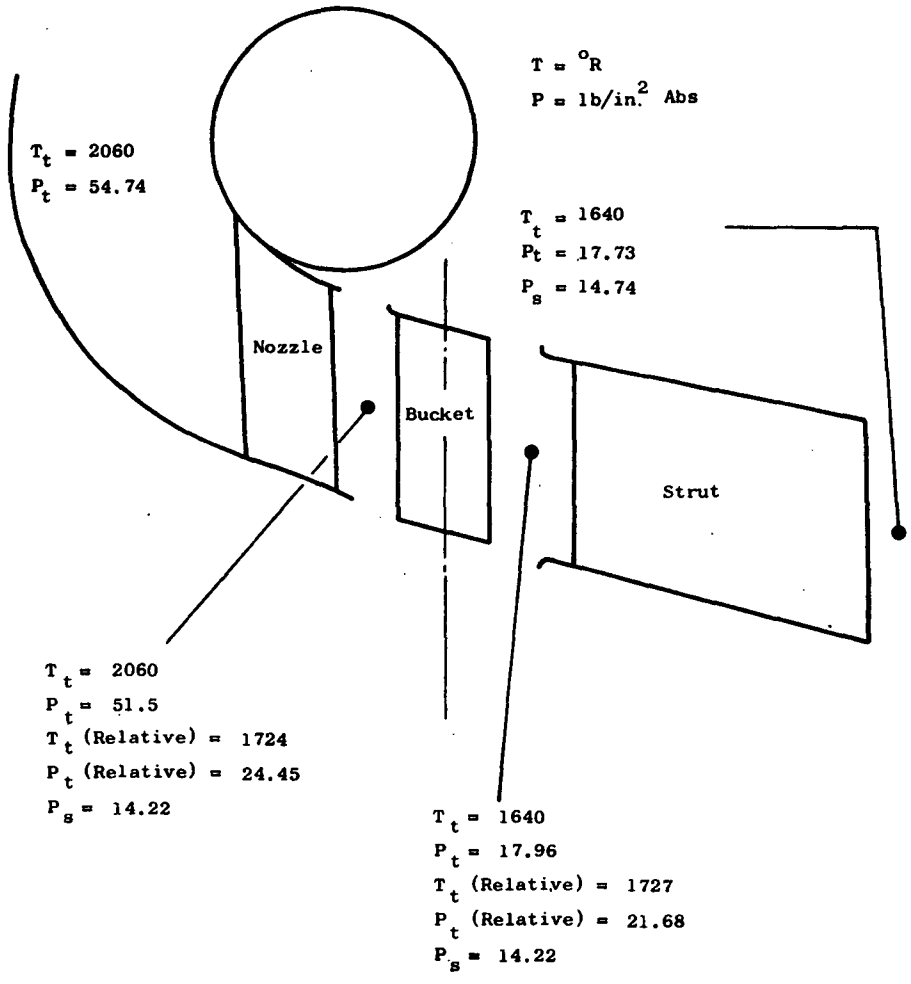

Figure 64 - Turbine Gas Conditions

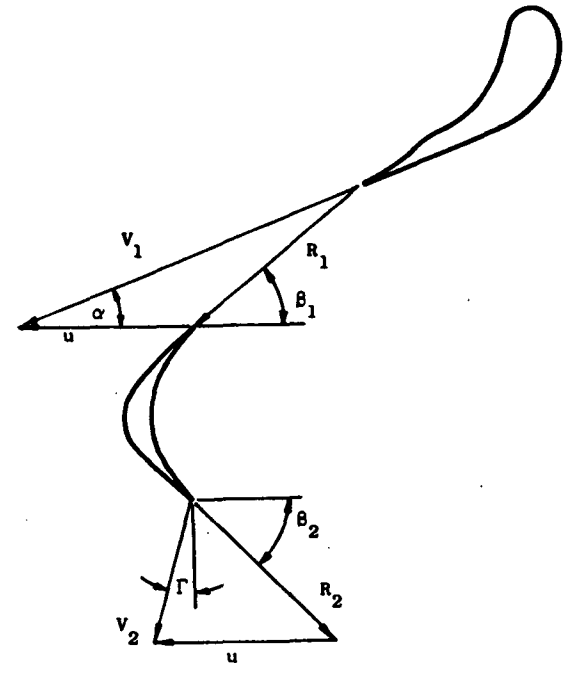

Velocities ~ ft/sec		Angle ~ degrees		Mach Number	
V_1	= 2782	α	= 23.7	M_1	= 1.50
R_1	= 1742	β_1	= 40.0	MR_1	= .94
R_2	= 1563	β_2	= 47.0	MR_2	= .82
V_2	= 1152	Γ	= 7.29	M_2	= .60
u	= 1212				

Figure 65 - Turbine Velocity Diagram

FOLDOUT FRAME 1

FOLDOUT FRAME 2

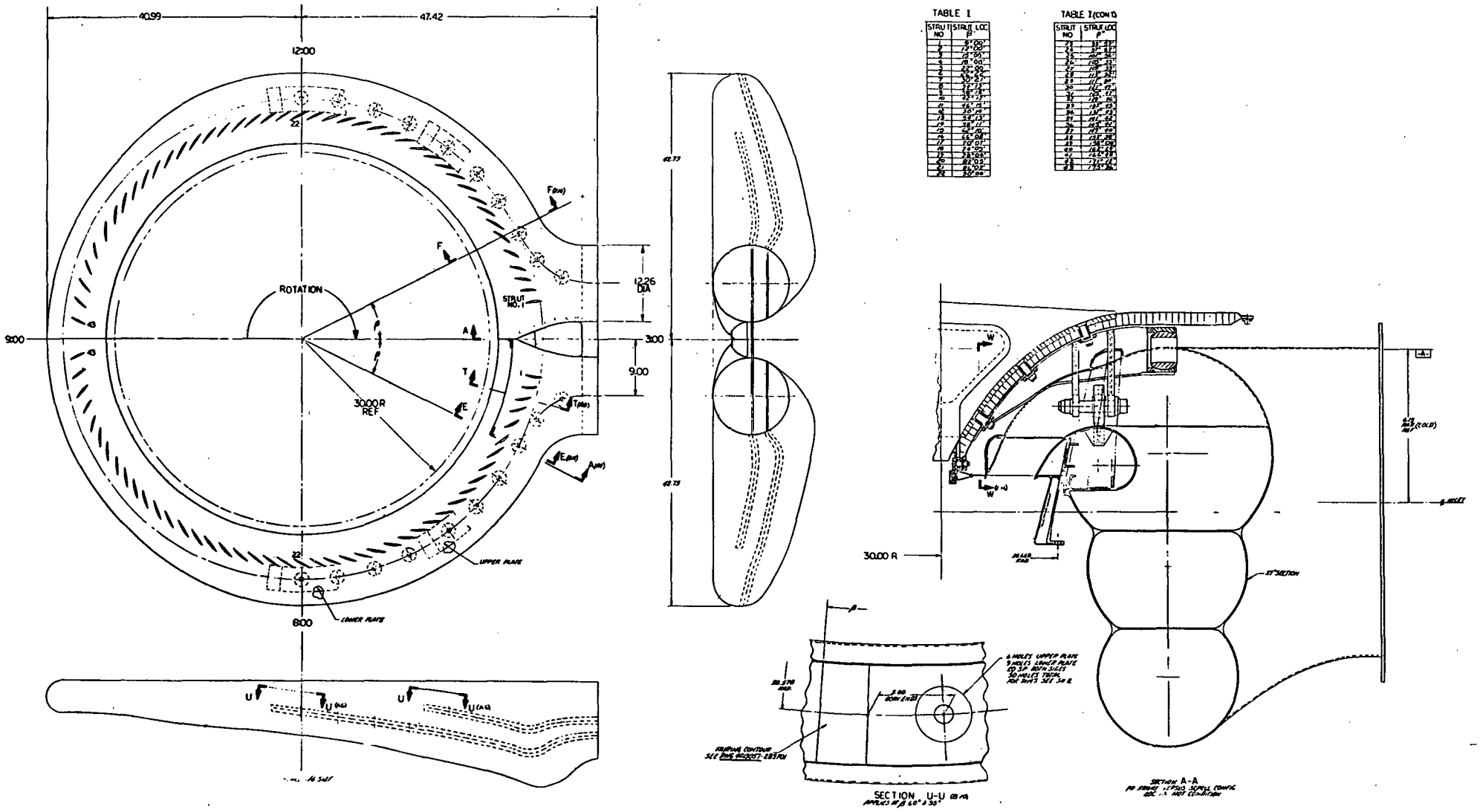

Figure 66 - LF460 Scroll Configuration

FOLDOUT FRAME 1

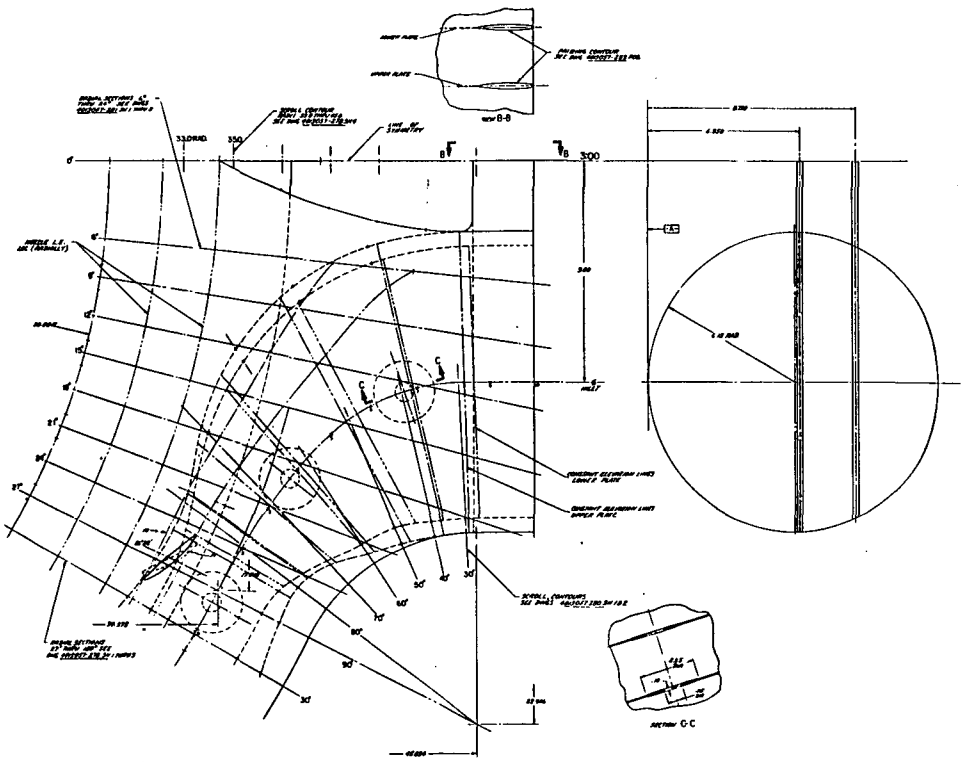

FOLDOUT FRAME 2

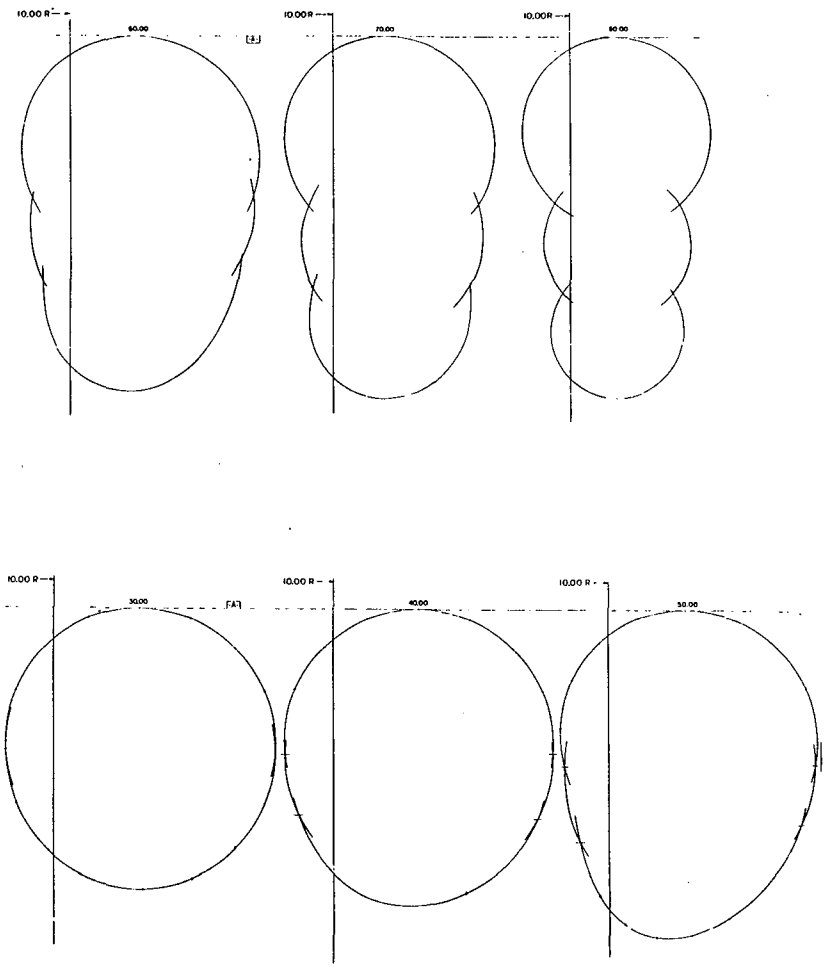

Figure 67a - LF460 Scroll Cross-Section Detail

FOLDOUT FRAME 1

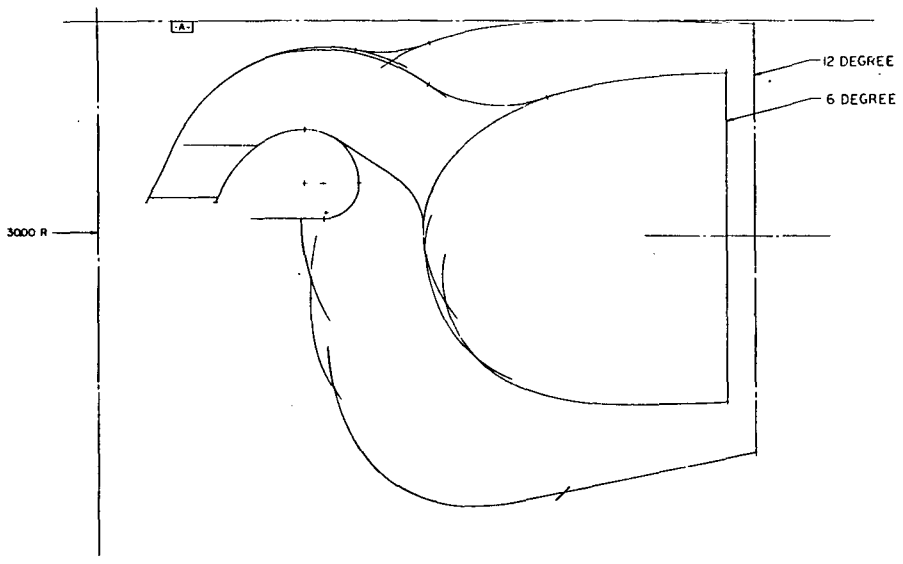

FOLDOUT FRAME 2

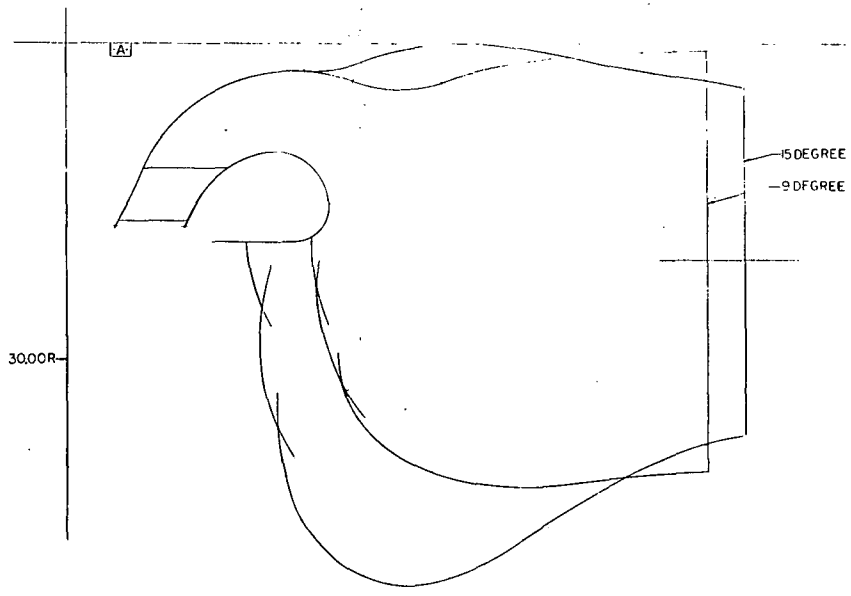

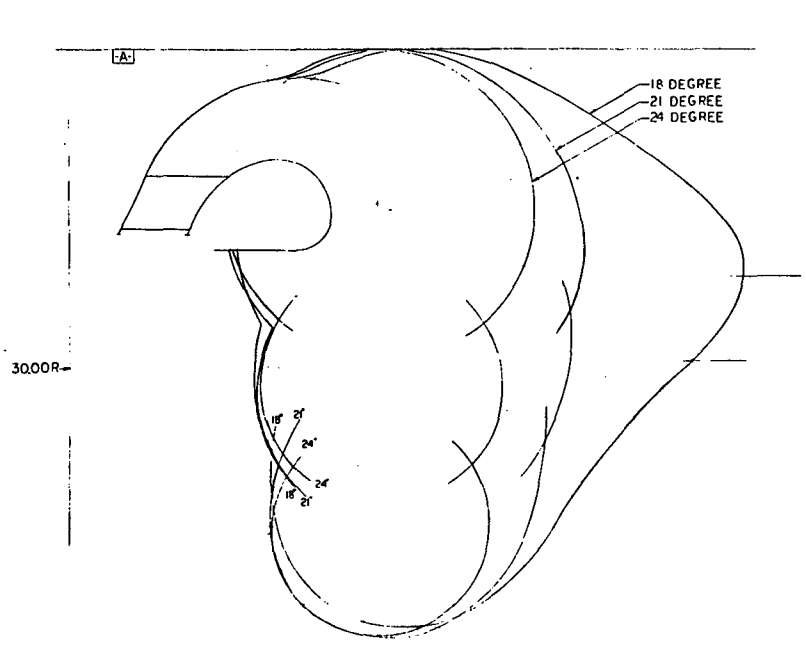

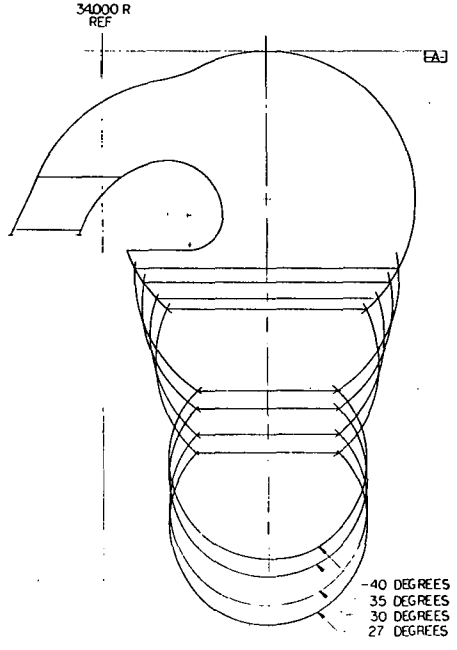

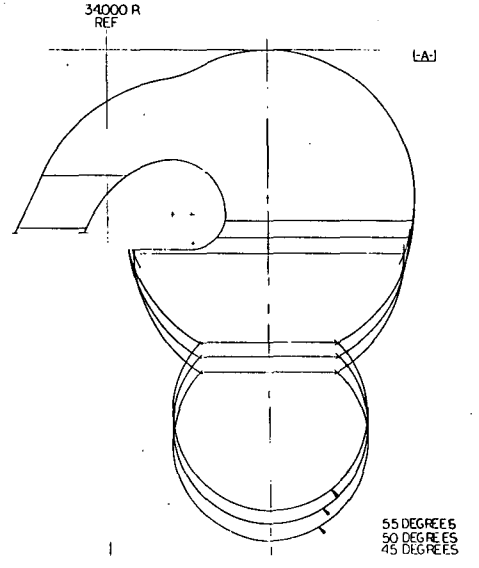

Figure 67b - LF460 Scroll Cross-Section Detail

FOLDOUT FRAME 1

FOLDOUT FRAME 2

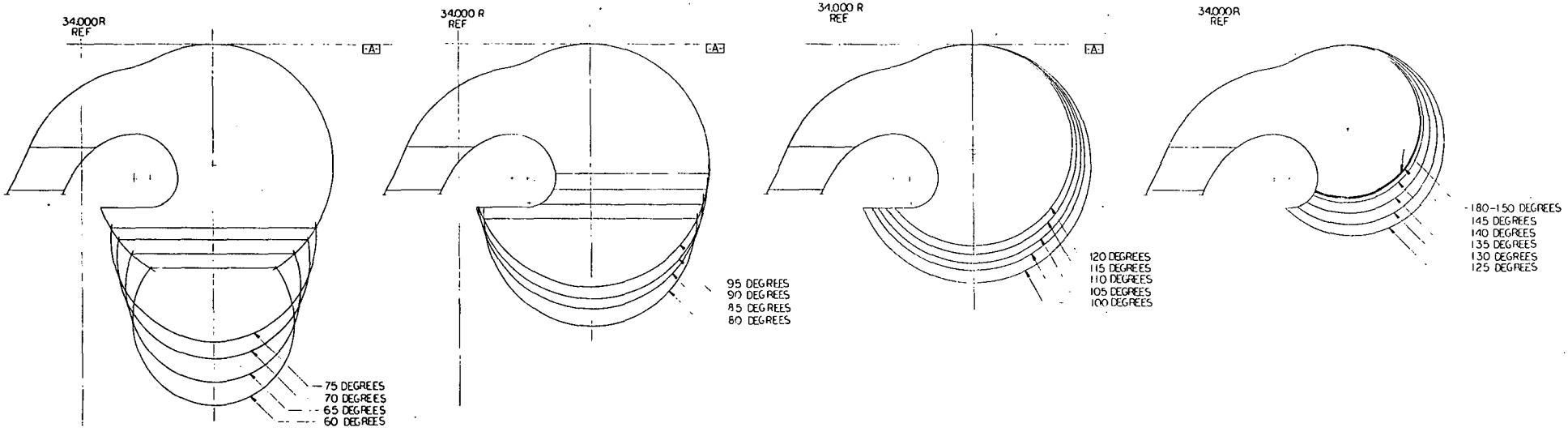

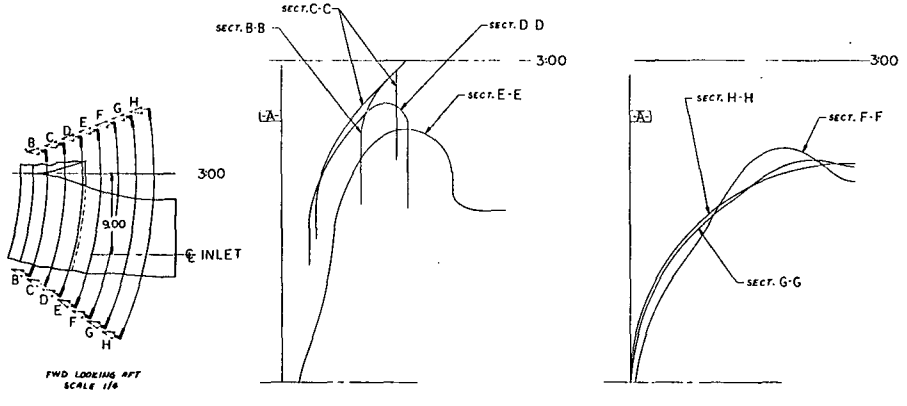

SECT.	RAD.
B-B	33.00
C-C	35.00
D-D	37.00
E-E	39.00
F-F	41.00
G-G	43.00
H-H	45.00

Figure 67c - LF460 Scroll Cross-Section Detail

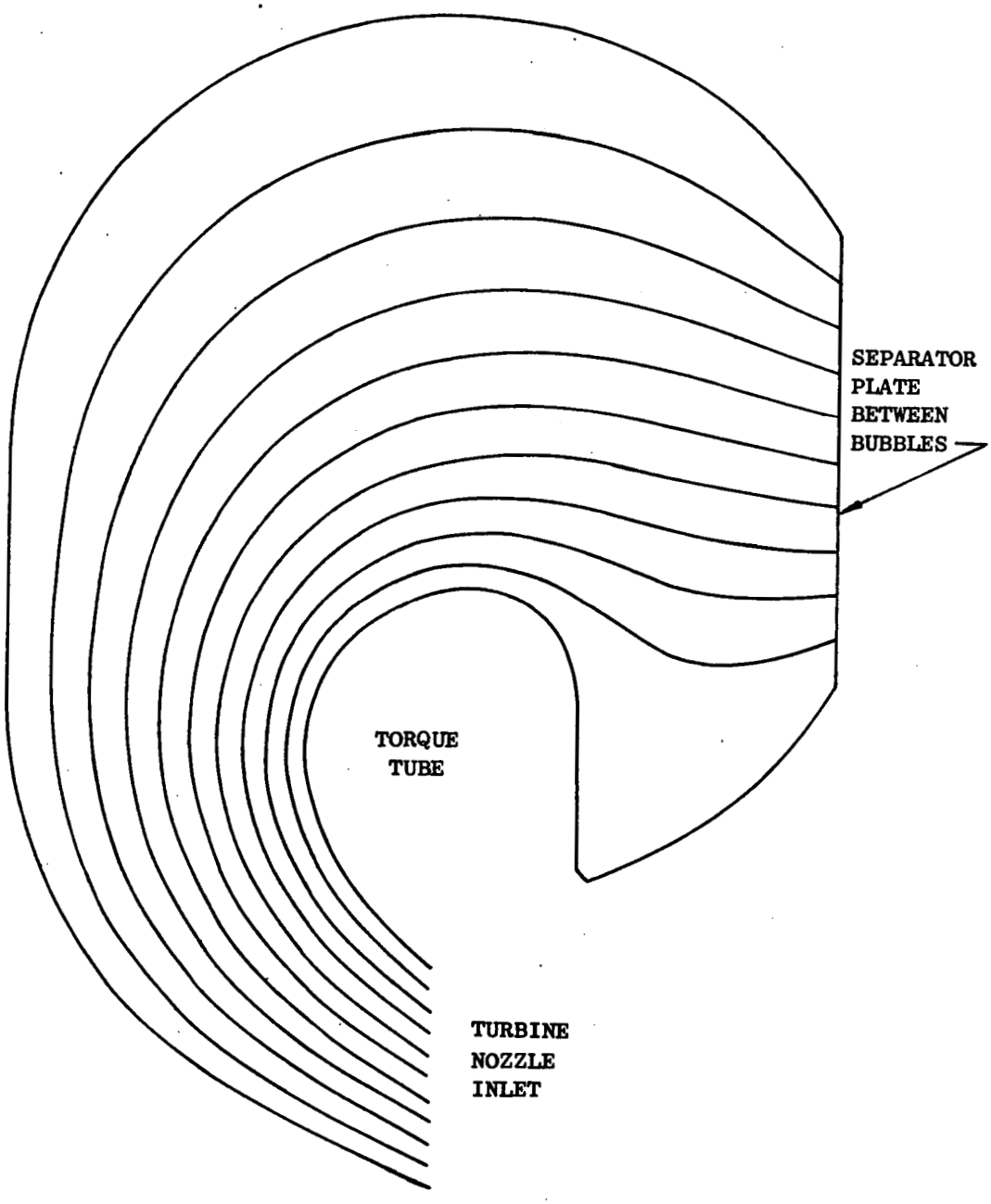

Figure 68 - Scroll Streamline Pattern in Radial Plane

FOLDOUT FRAME 1

FOLDOUT FRAME 2

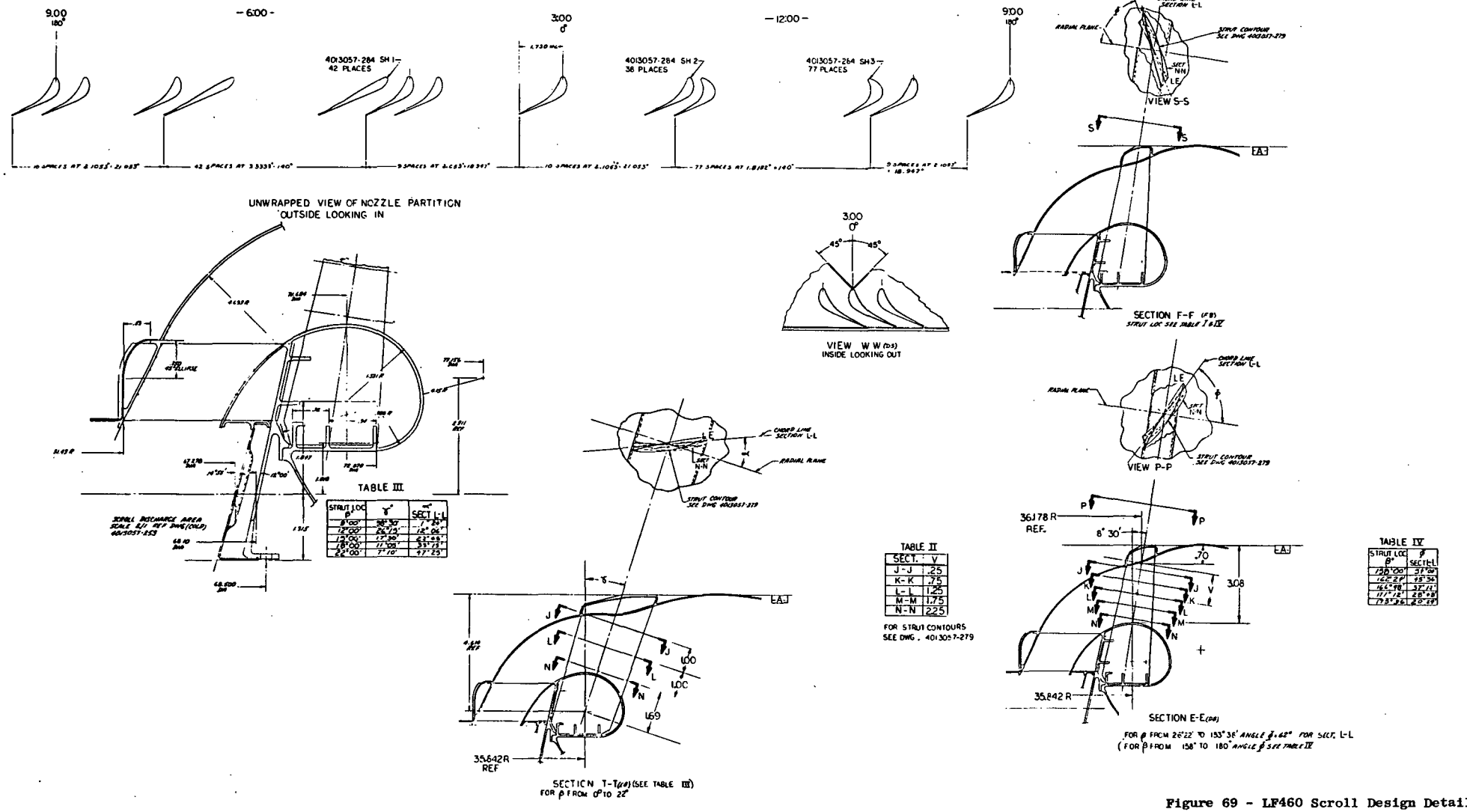

Figure 69 - LF460 Scroll Design Detail

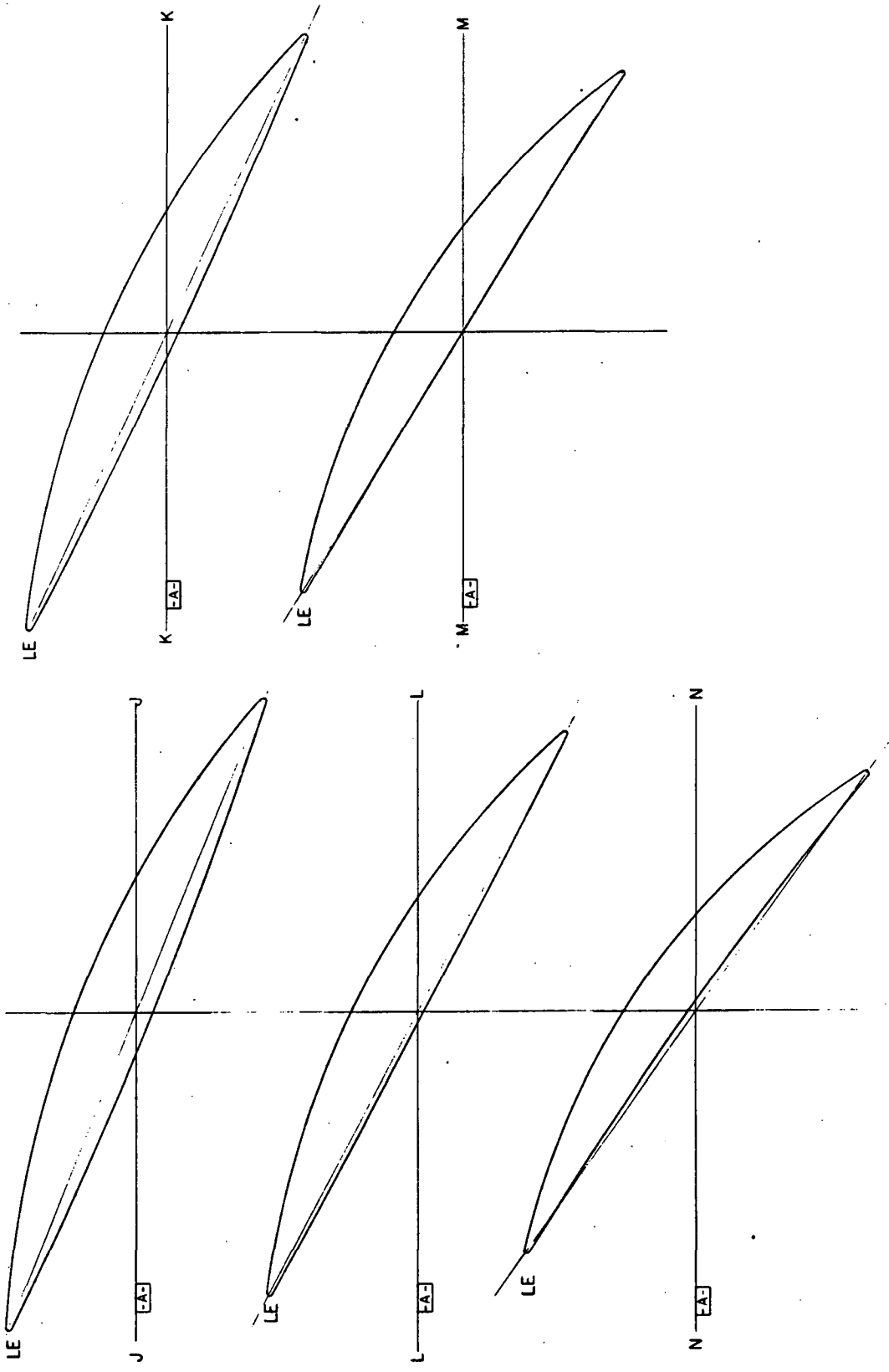

Figure 70 - Strut Contours

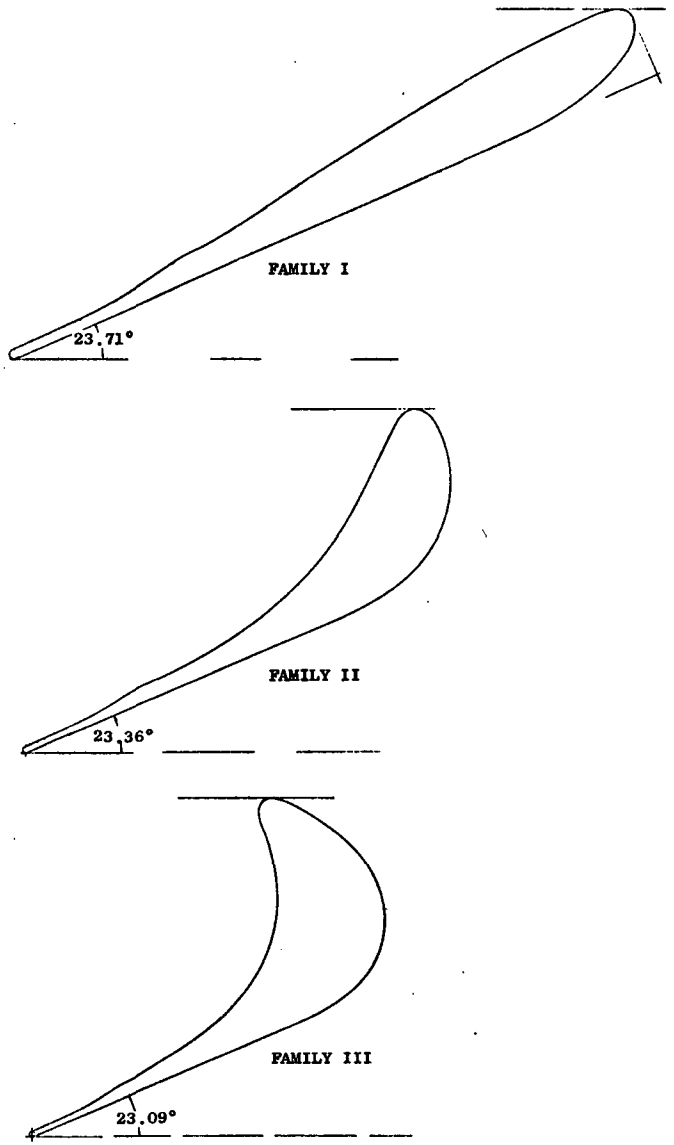

Figure 71 - Turbine Nozzle Vane Profiles

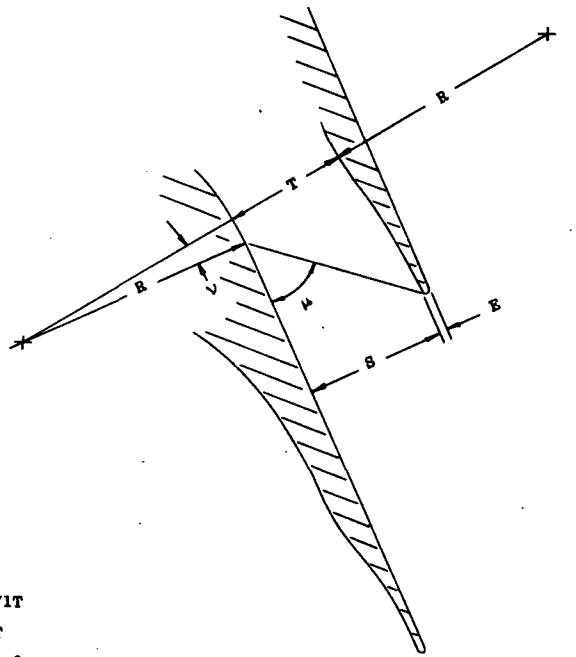

R = 2T
S = 1.071T
E = .06T
μ = 50.05°
ν = 6.57°

Figure 72 - Design of Divergent Portion of Nozzle Passages

FAMILY I

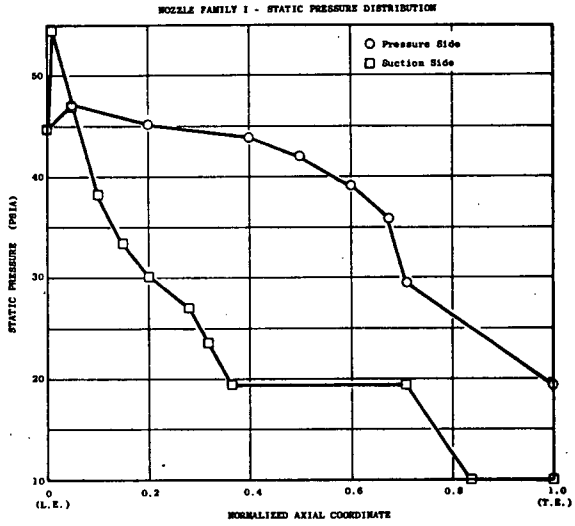

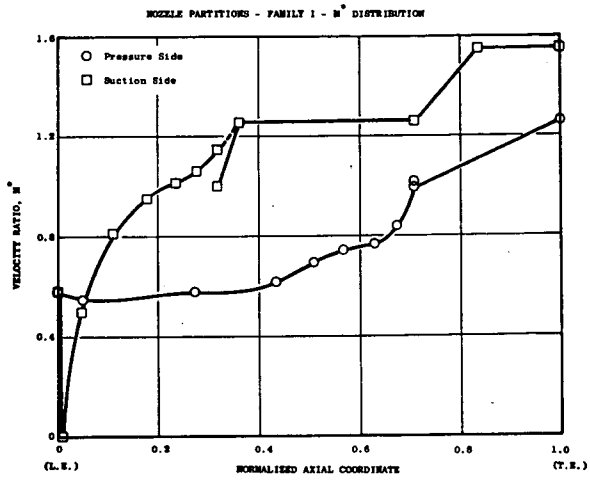

FAMILY II

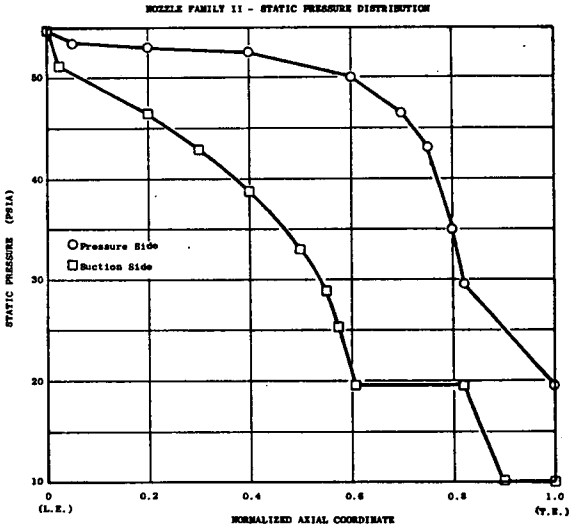

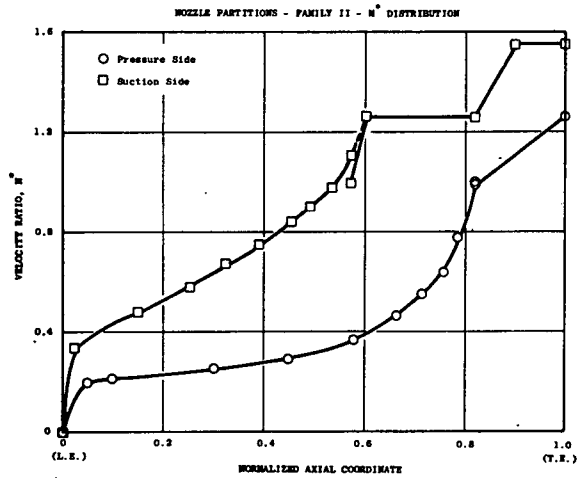

FAMILY III

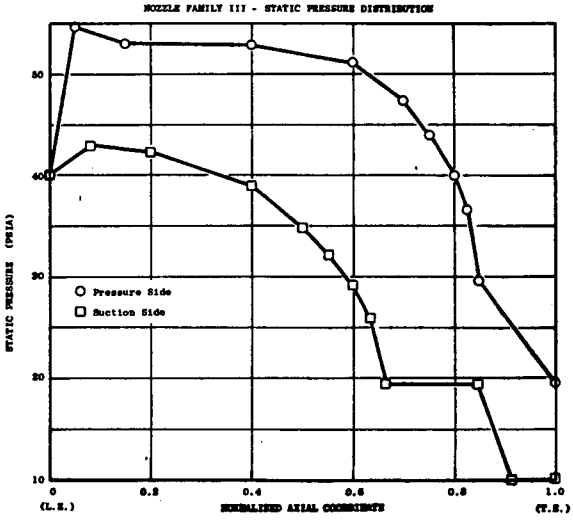

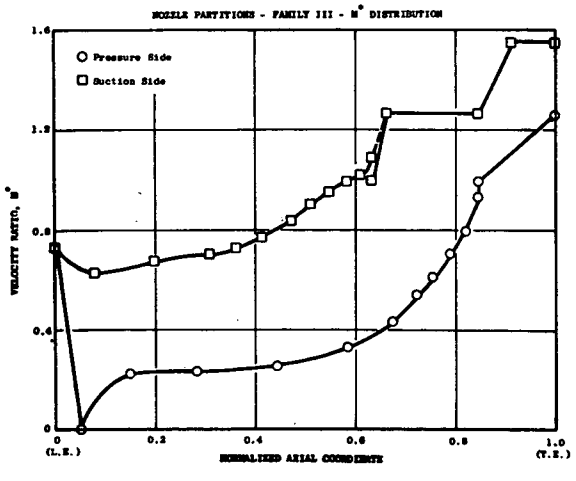

Figure 73 - Turbine Nozzle Static Pressure and Velocity Ratio Distributions

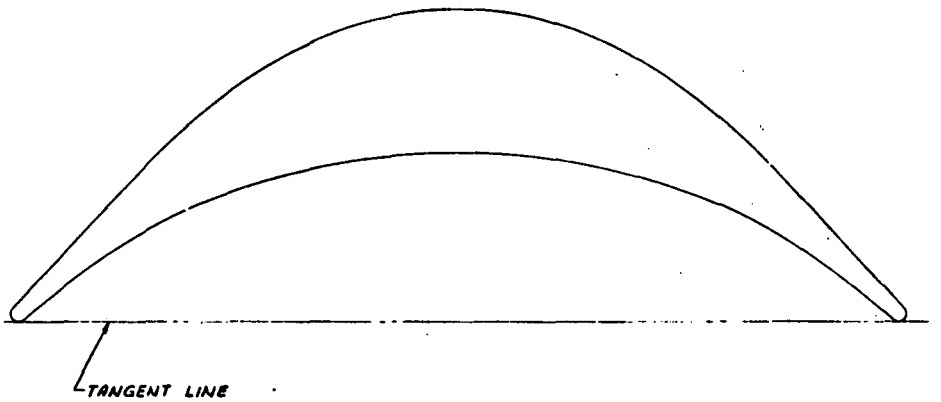

Figure 74 - Turbine Bucket Profile

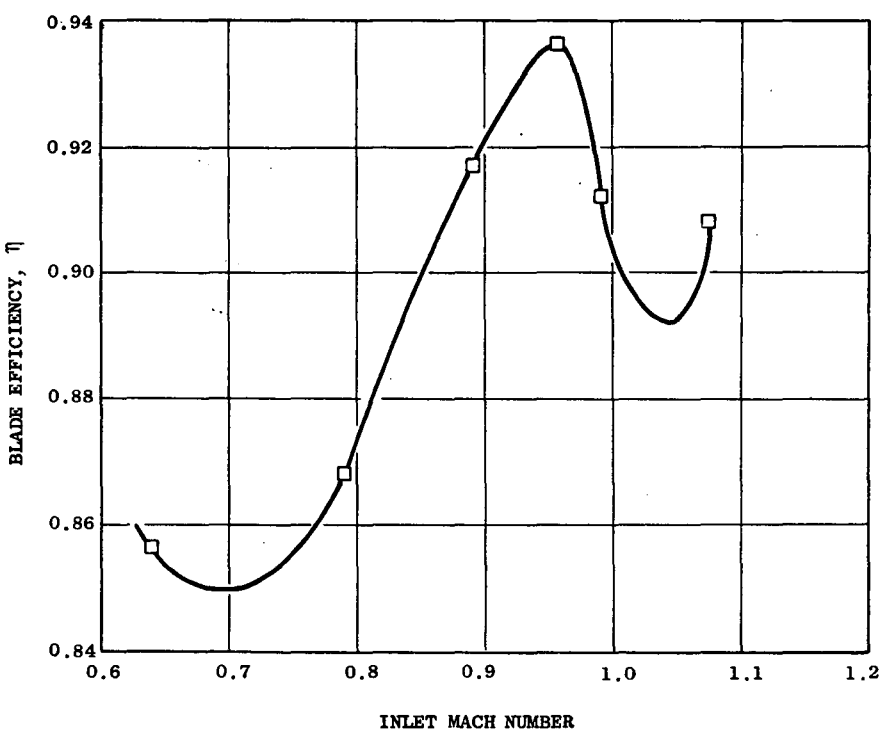

Figure 75 - Blade Efficiency from Cascade Test

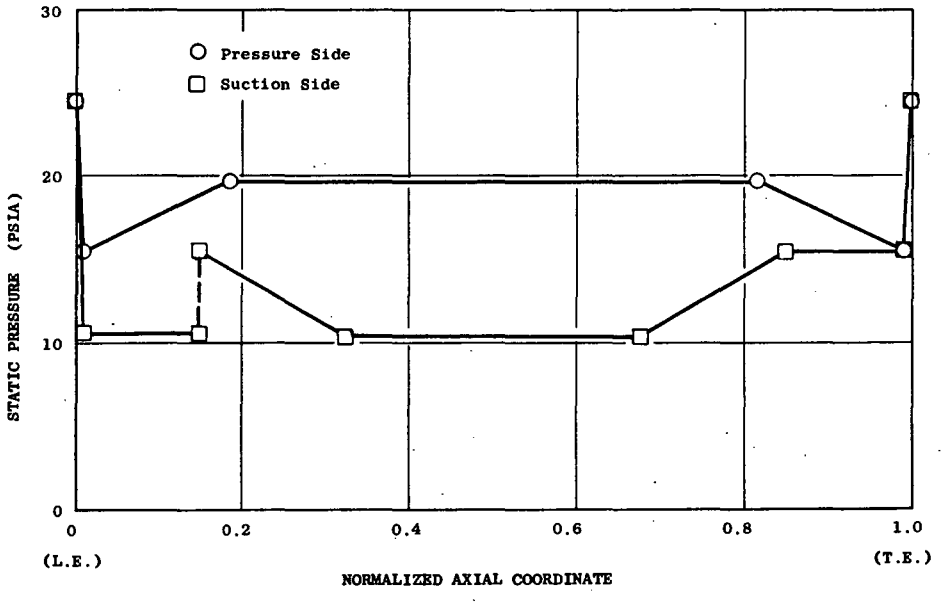

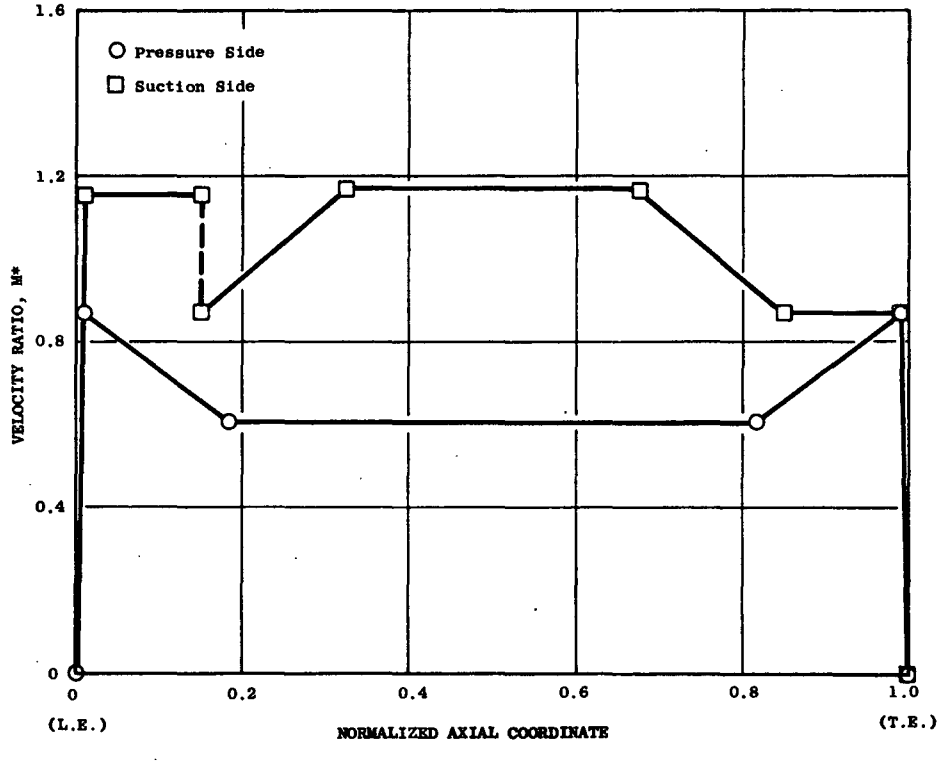

Figure 76 - Turbine Bucket Static Pressure and Velocity Ratio Distributions

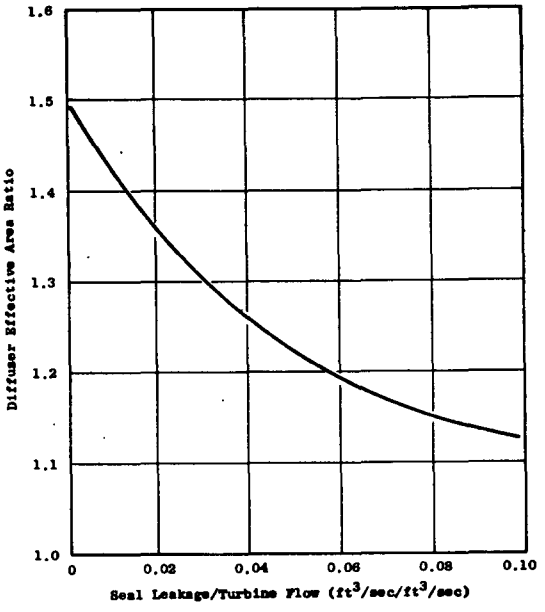

Figure 77 - Fan Turbine Diffuser Performance With Leakage

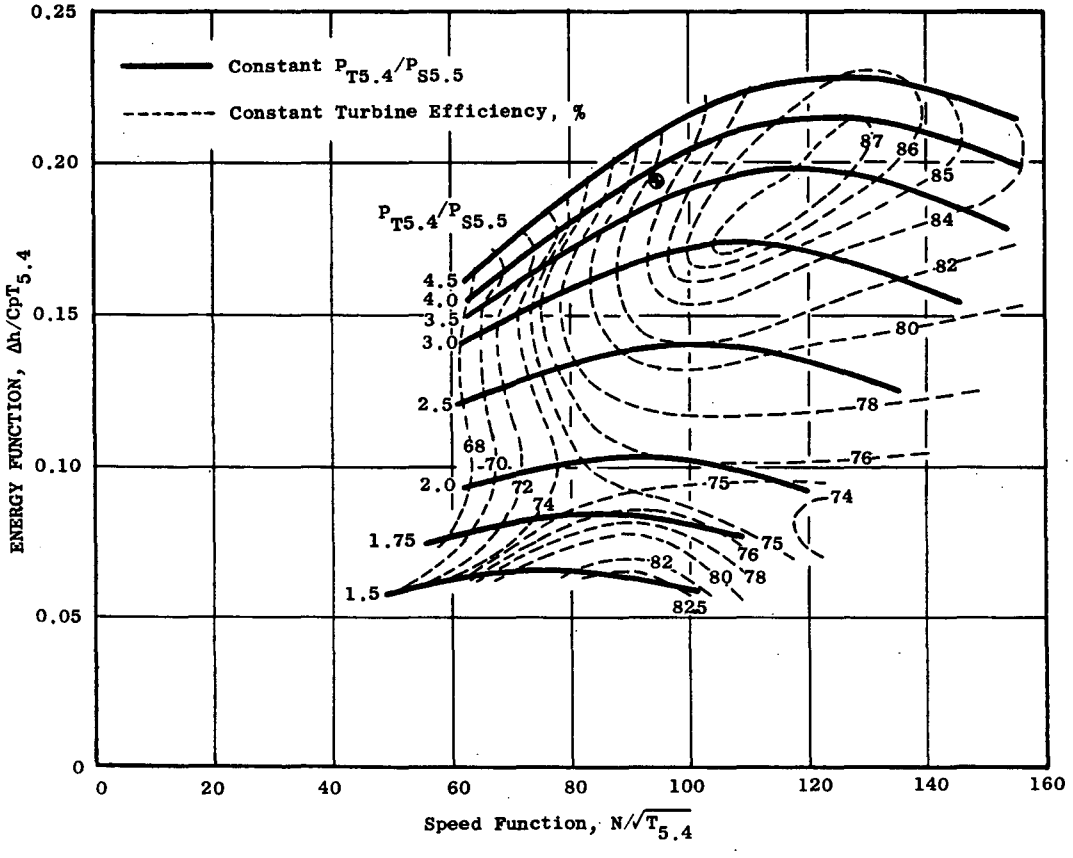

Figure 78 - LF460 Estimated Turbine Map

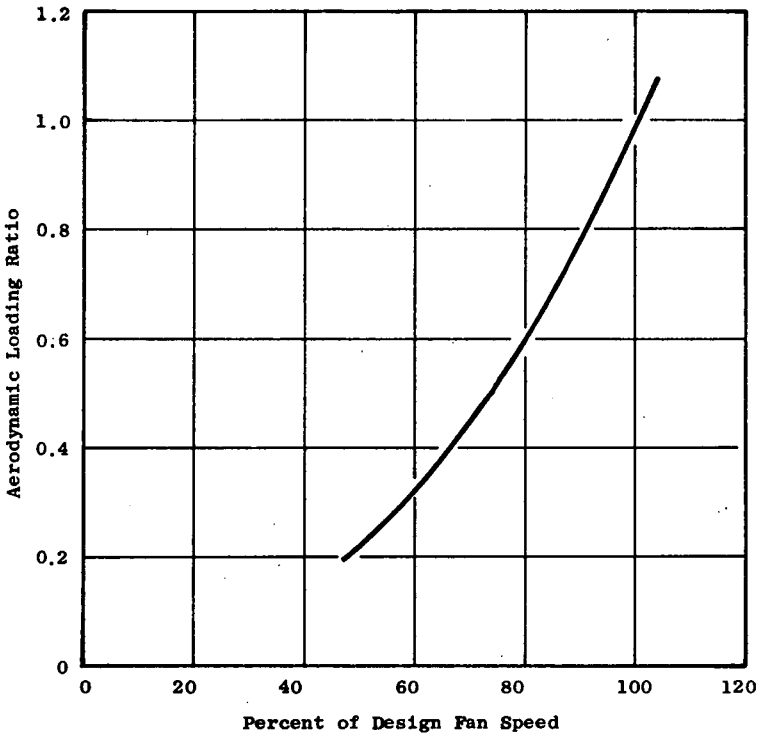

Figure 79 - Aerodynamic Loading Ratio at Less Than Design Rotational Speed

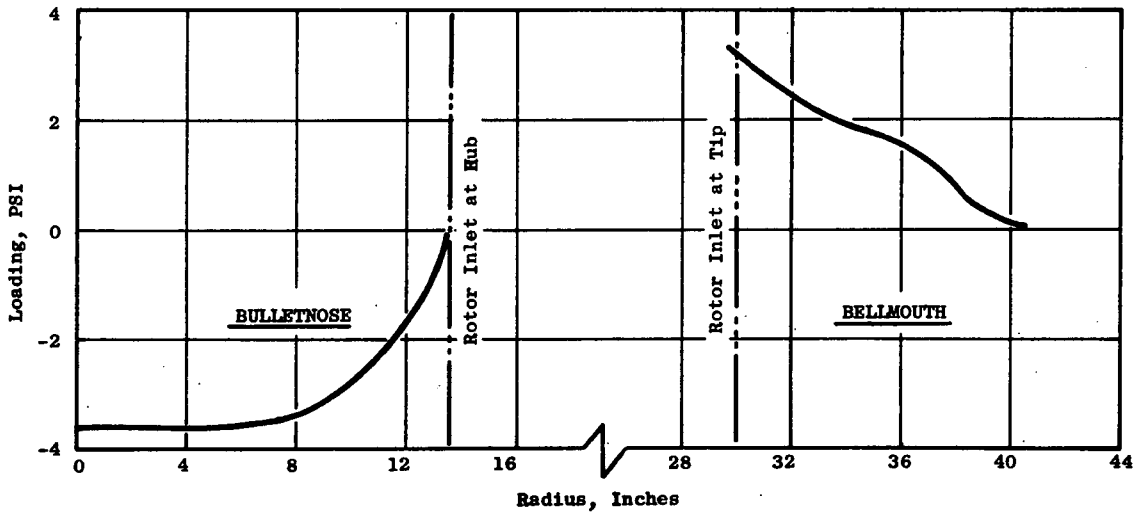

Figure 80 - Inlet System Air Loads at Static Operation, Design Speed

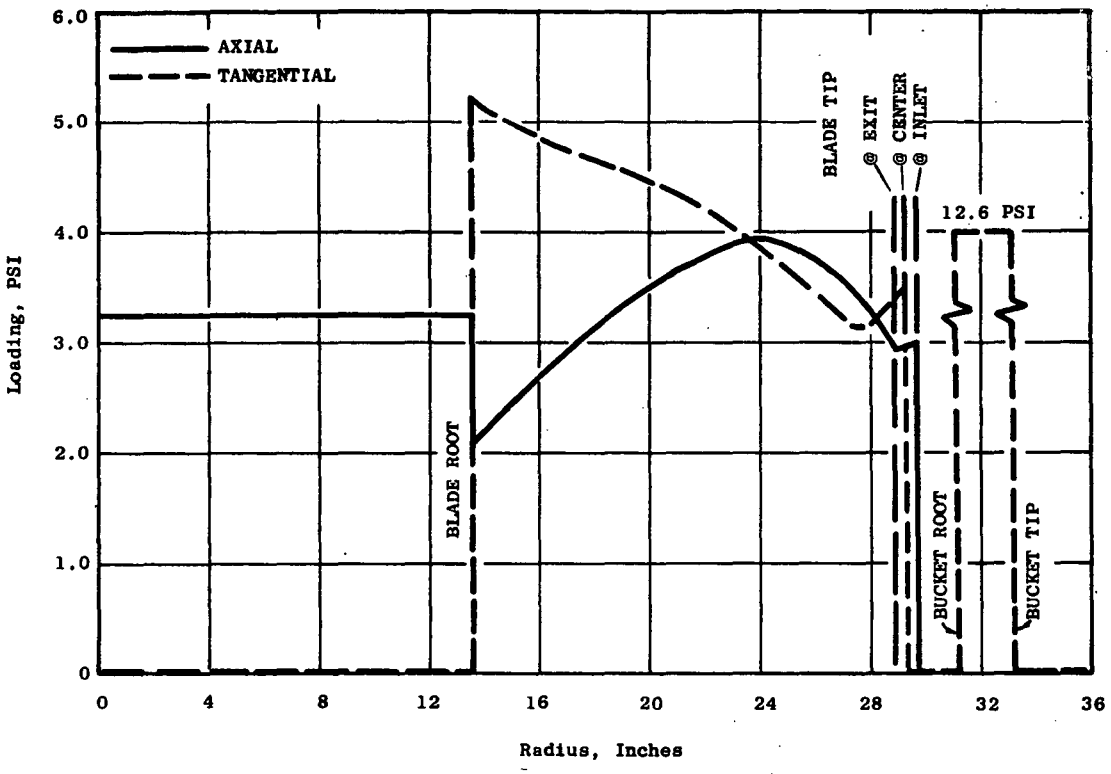

Figure 81 - Rotor System Axial and Tangential Load Distribution

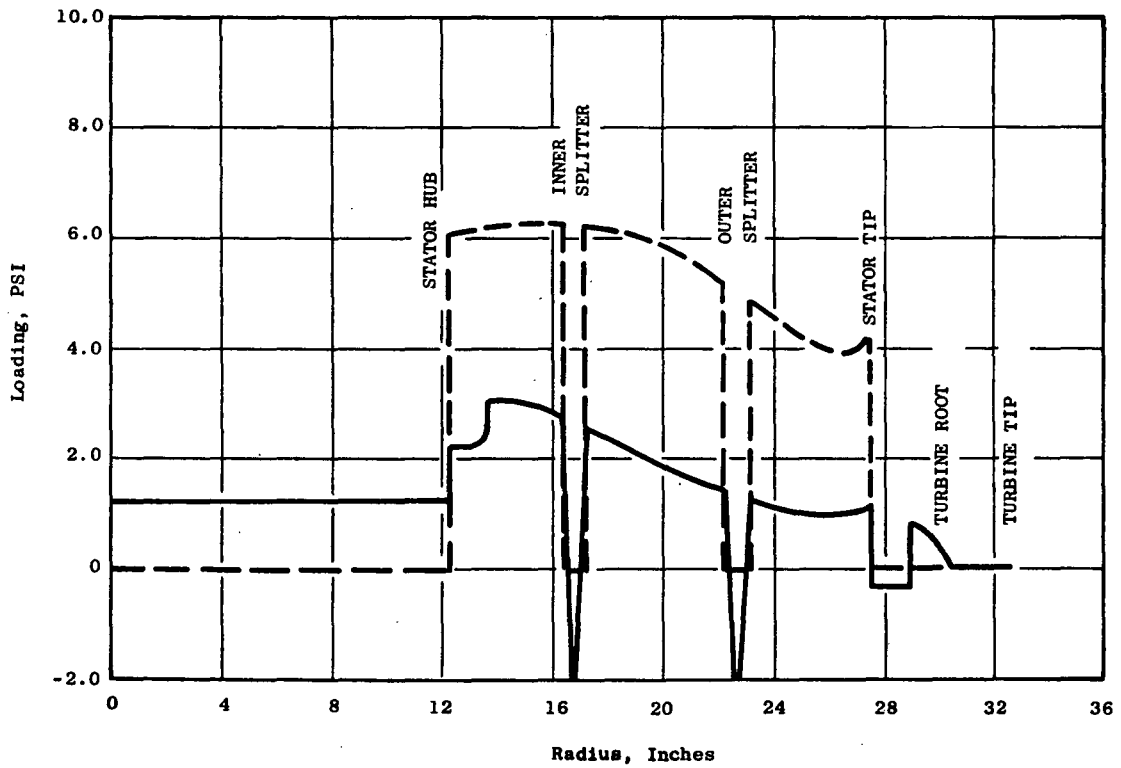

Figure 82 - Rear Frame Axial and Tangential Load Distribution

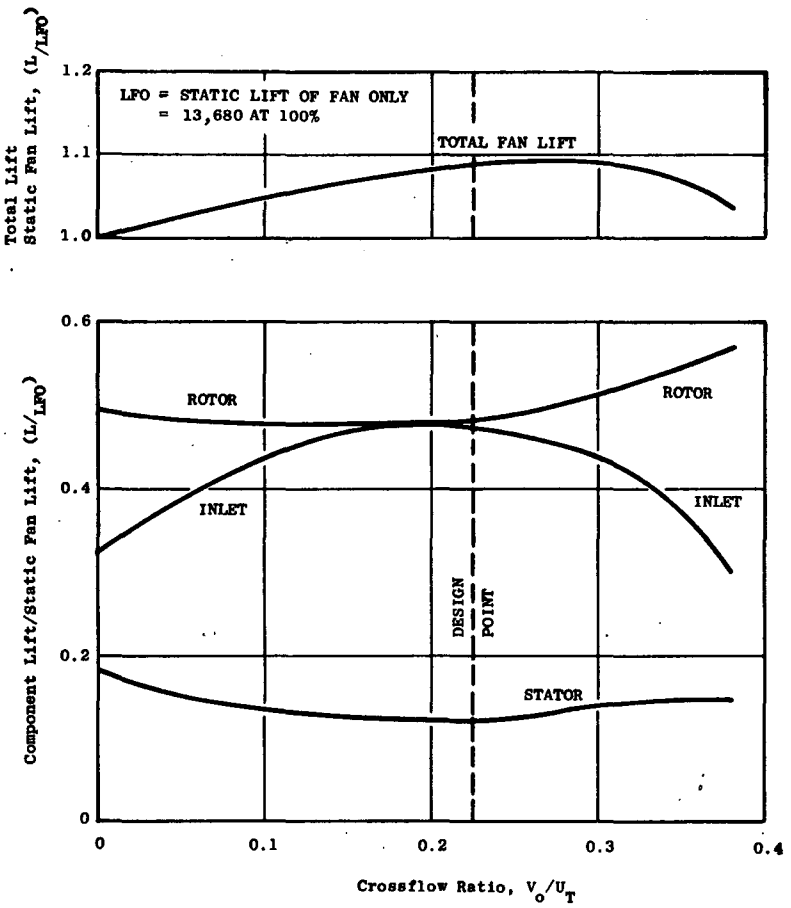

Figure 83 - Variation of Fan Component Lift in Crossflow

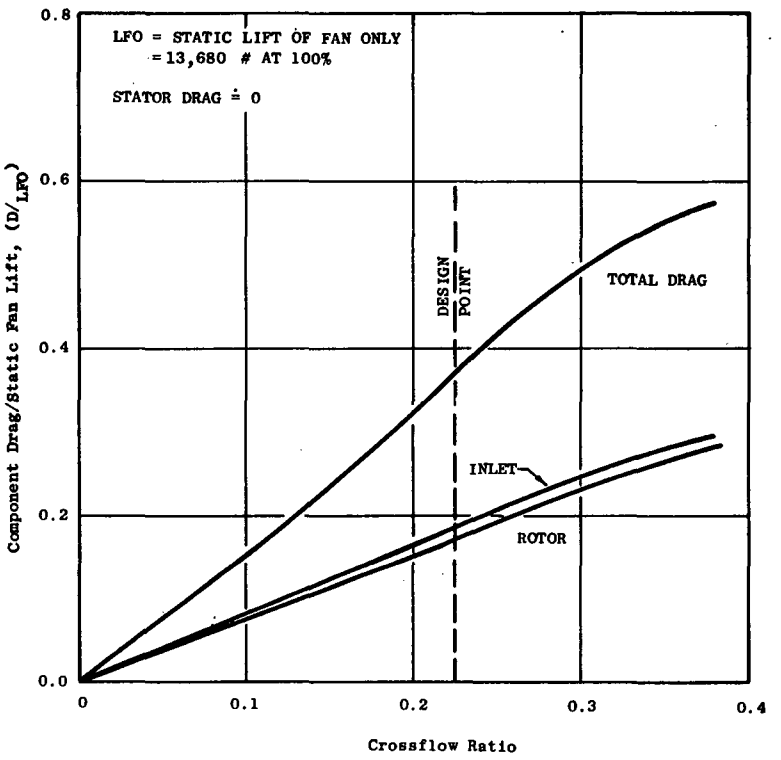

Figure 84 - Variation of Fan Component Drag in Crossflow

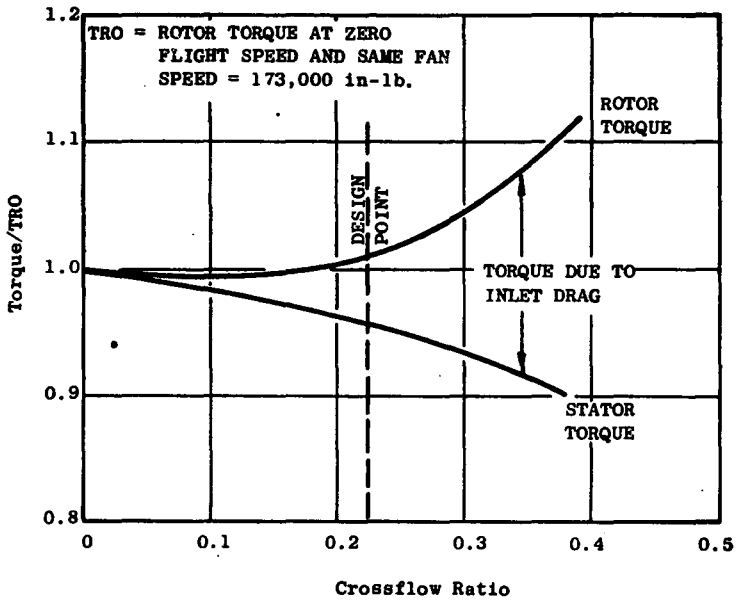

Figure 85 - Variation of Rotor and Stator Torque with Crossflow

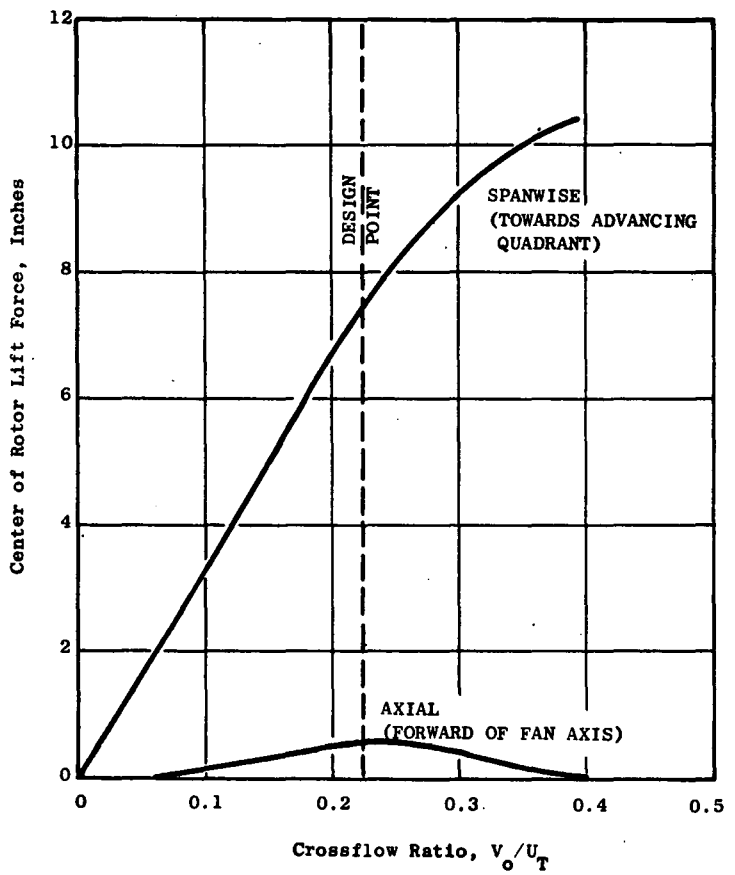

Figure 86 - Variation of Effective Center of Rotor Lift with Crossflow

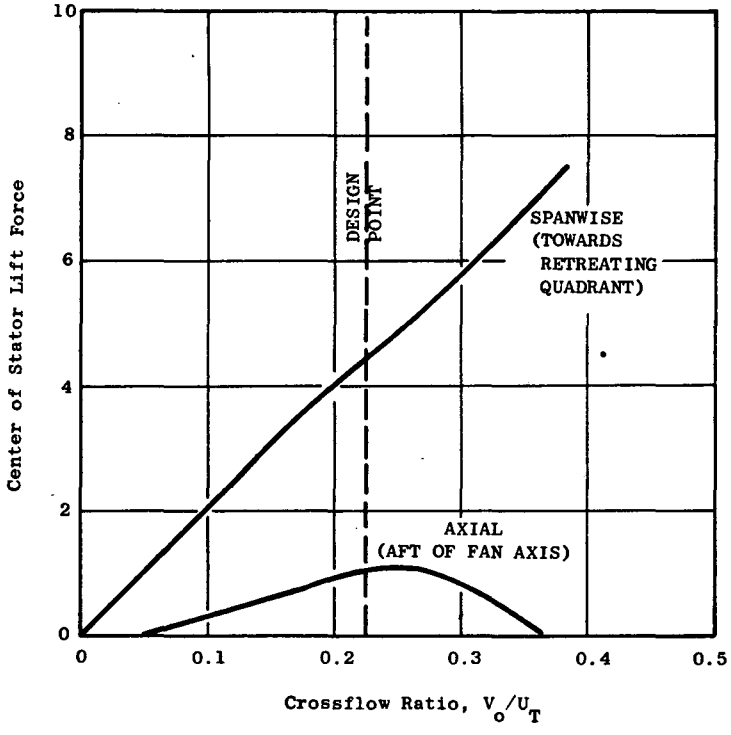

Figure 87 - Variation of Effective Center of Stator Lift with Crossflow

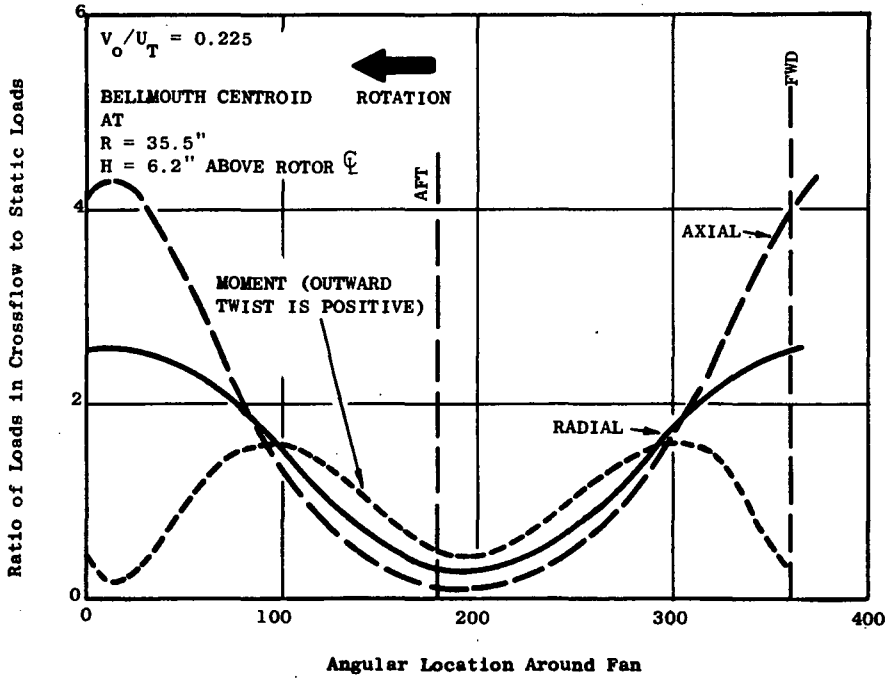

Figure 88 - Estimated Bellmouth Airloads During Crossflow

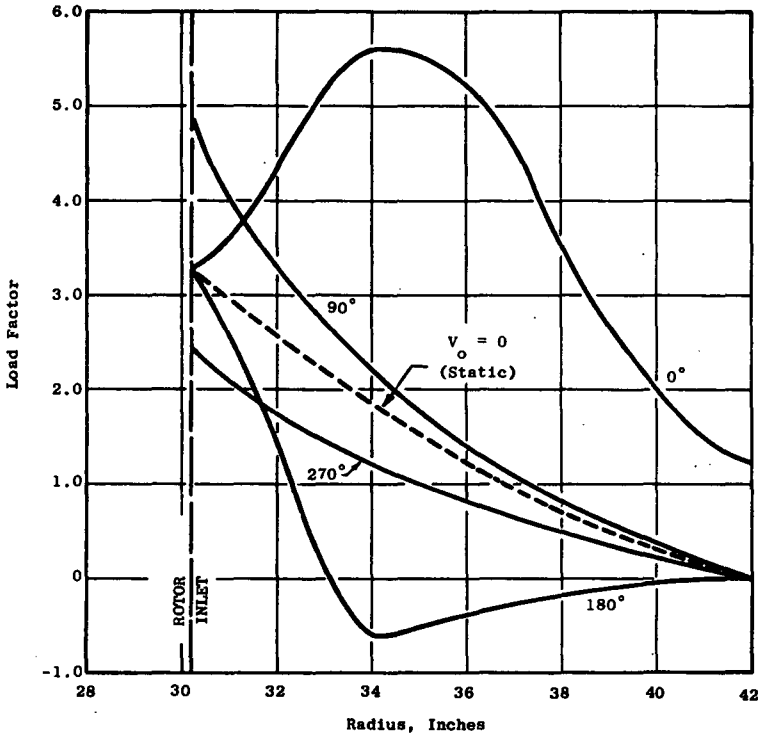

Figure 89 - Estimated Bellmouth Airloads in Crossflow, V_o/U_T = 0.225

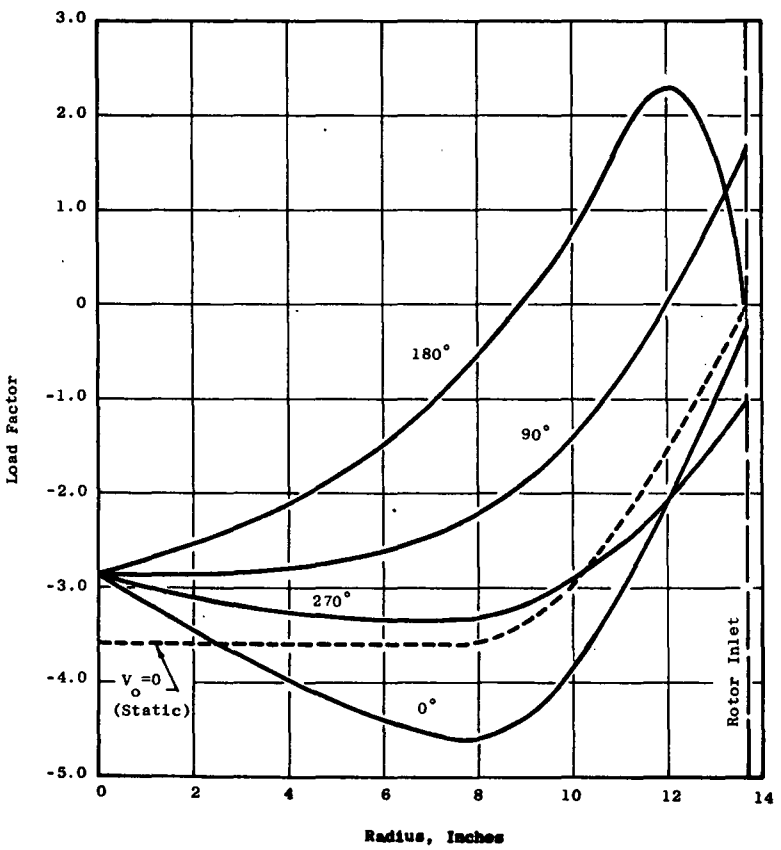

Figure 90 - Estimated Bulletnose Airloads in Crossflow, V_o/U_T = 0.225

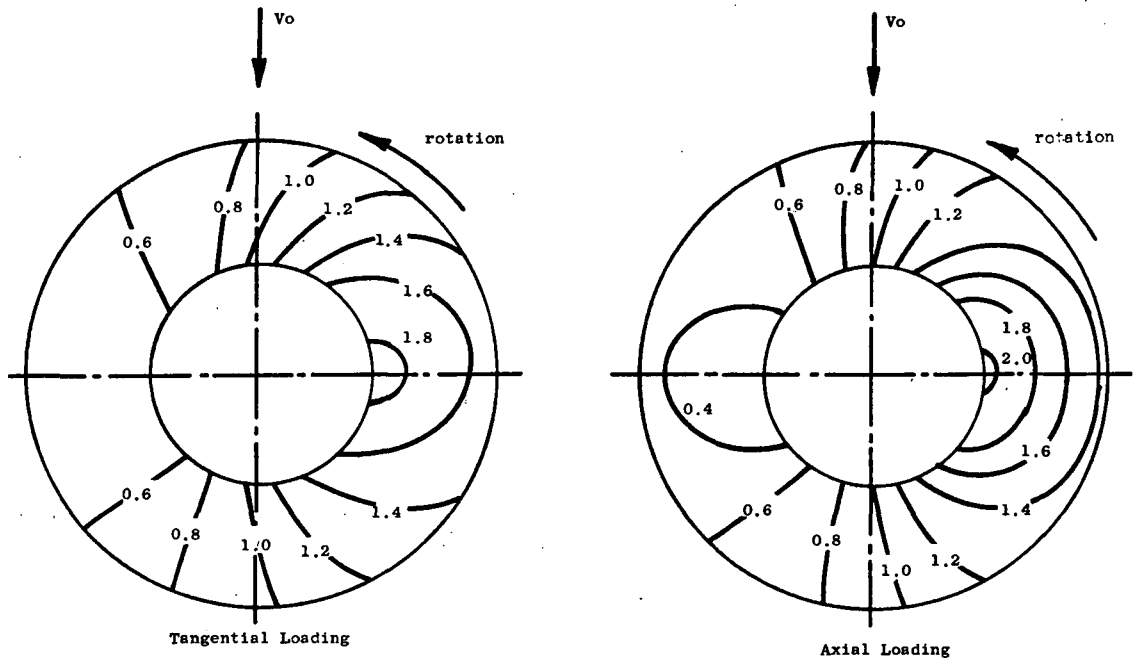

NOTE: Loading is given as ratio of loads in cross-flow to loads at static conditions and same rotational speed

Figure 91 - Rotor Airload Distributions in Crossflow, $V_o/U_T = 0.225$

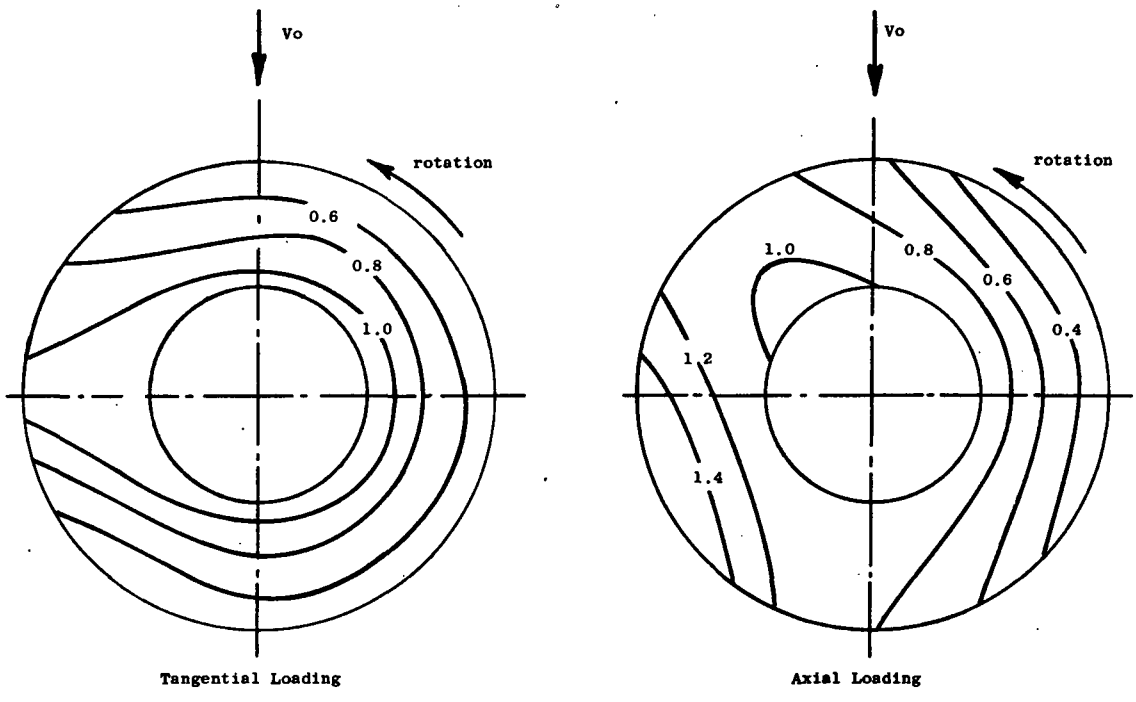

NOTE: Loading is given as ratio of loads in cross-flow to loads at static conditions and same rotational speed

Figure 92 - Stator Airload Distributions in Crossflow, $V_o/U_T = 0.225$

FOLDOUT FRAME 1

PRECEDING PAGE BLANK NOT FILMED

FOLDOUT FRAME 2

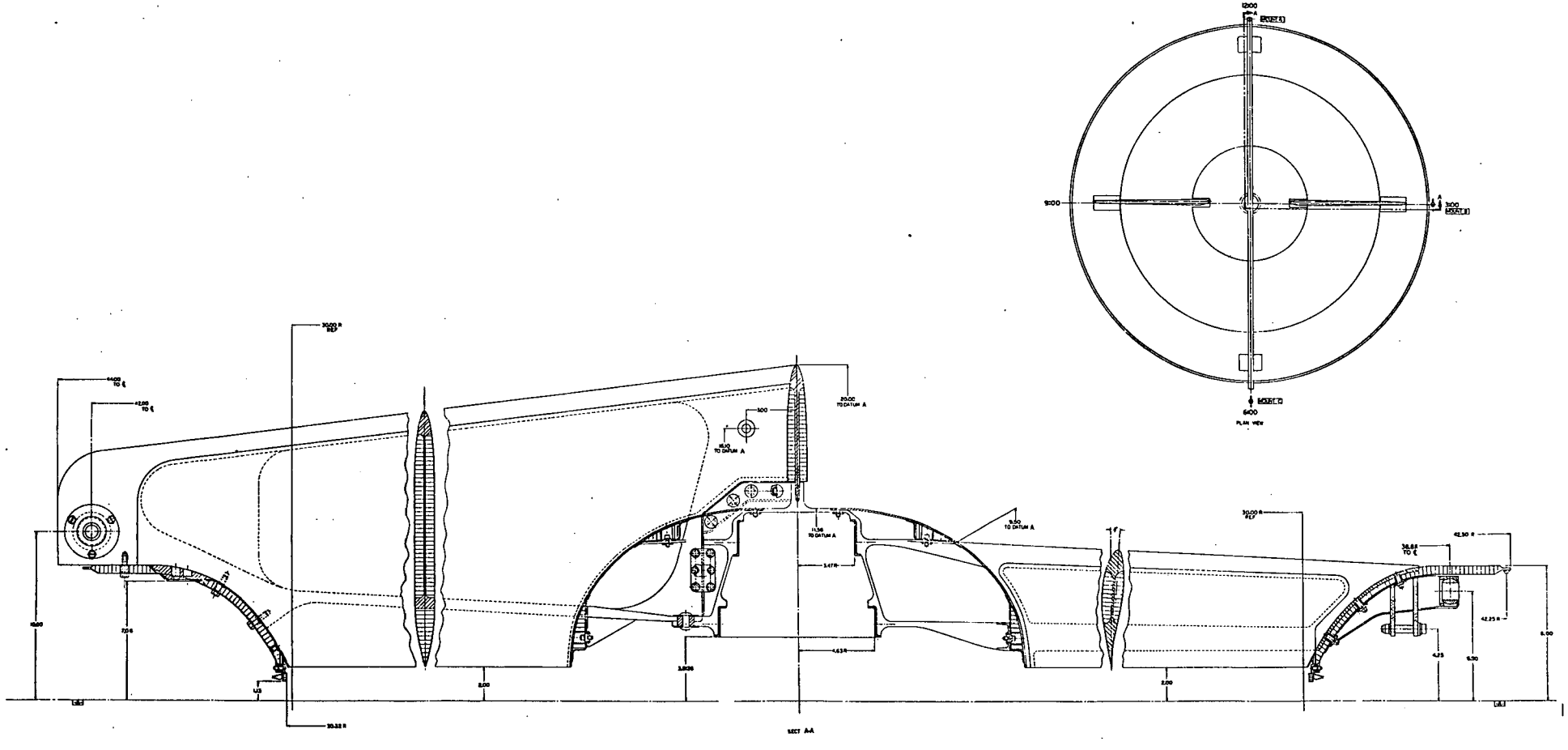

Figure 93 - LF460 Front Frame Layout

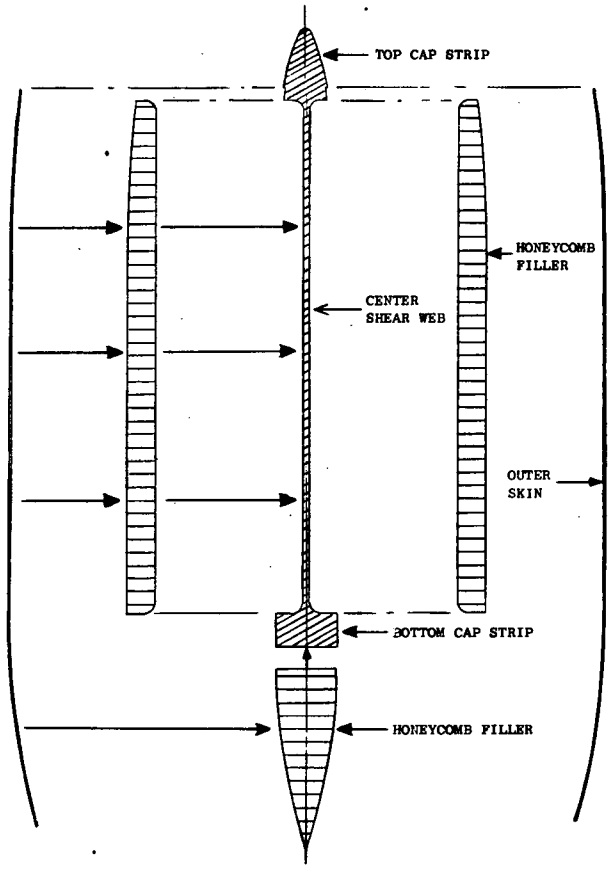

Figure 94 - Major Strut Construction

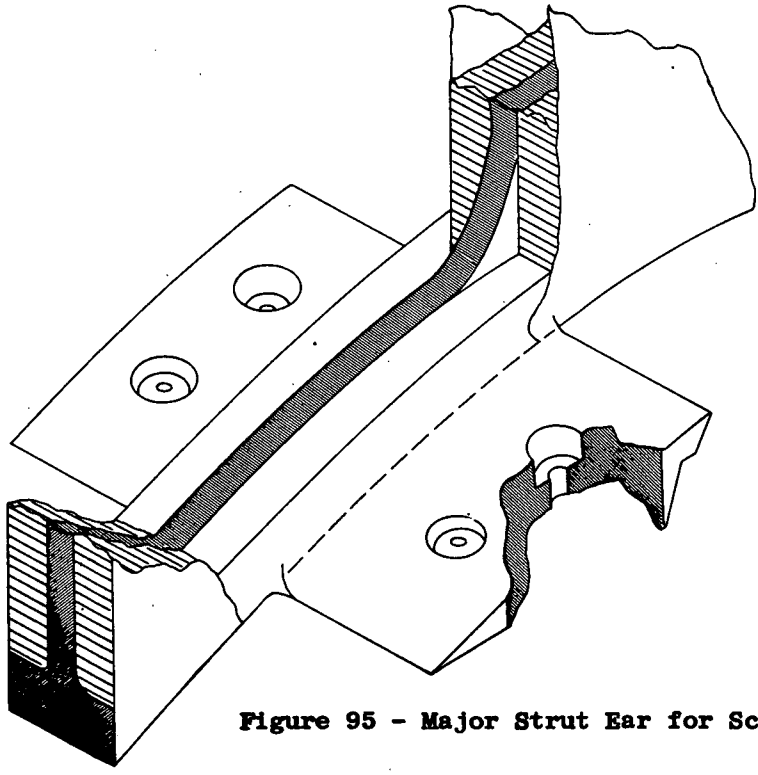

Figure 95 - Major Strut Ear for Scroll Attachment

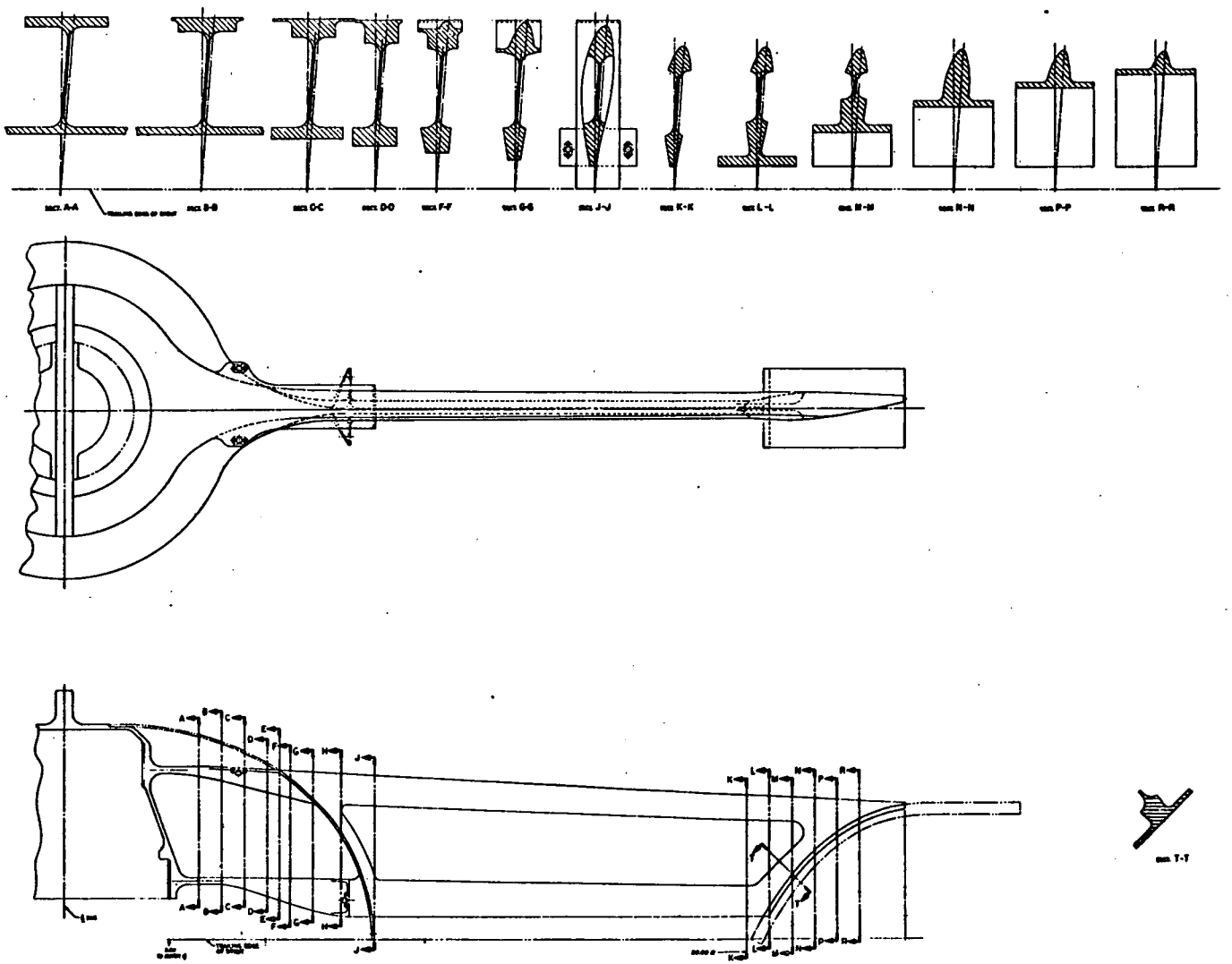

Figure 96 - Minor Strut Transition to Hub

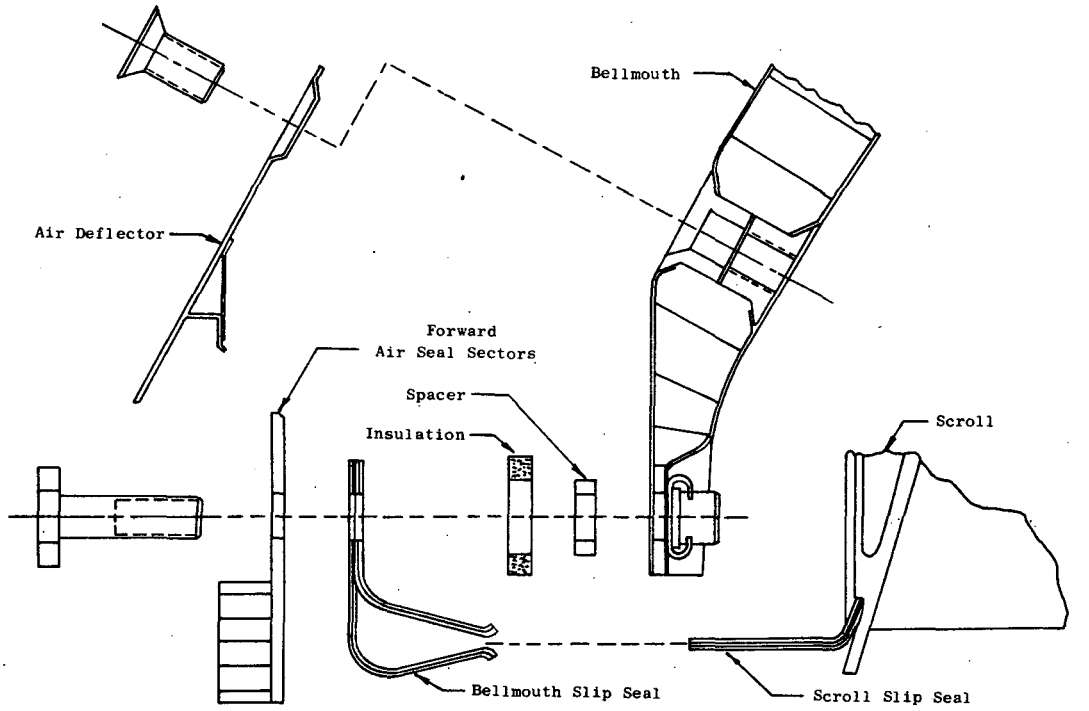

Figure 97 - Forward Air Seal Assembly

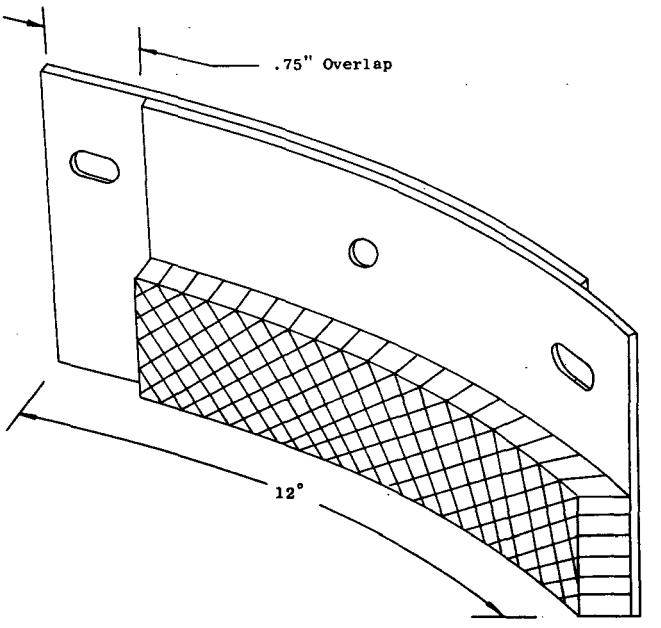

Figure 98 - Forward Air Seal Sector

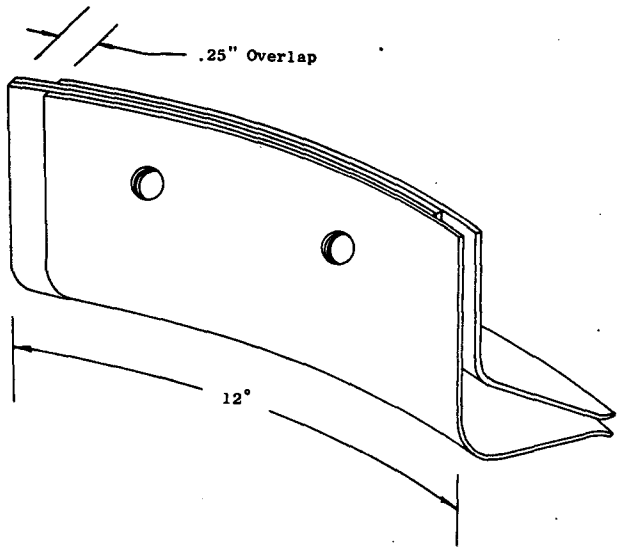

Figure 99 - Bellmouth Slip Seal Sector

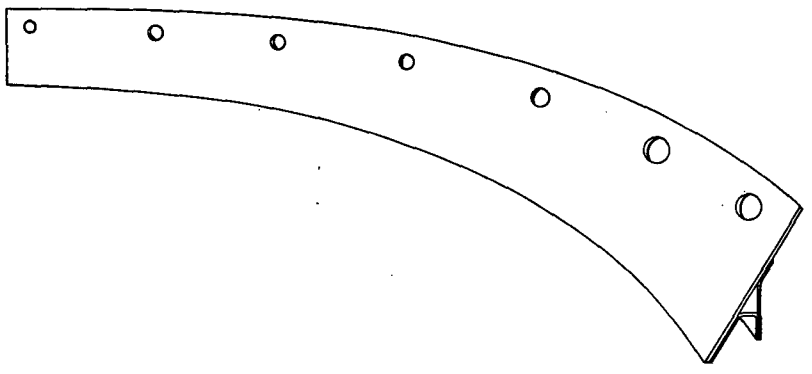

Figure 100 - Air Deflector

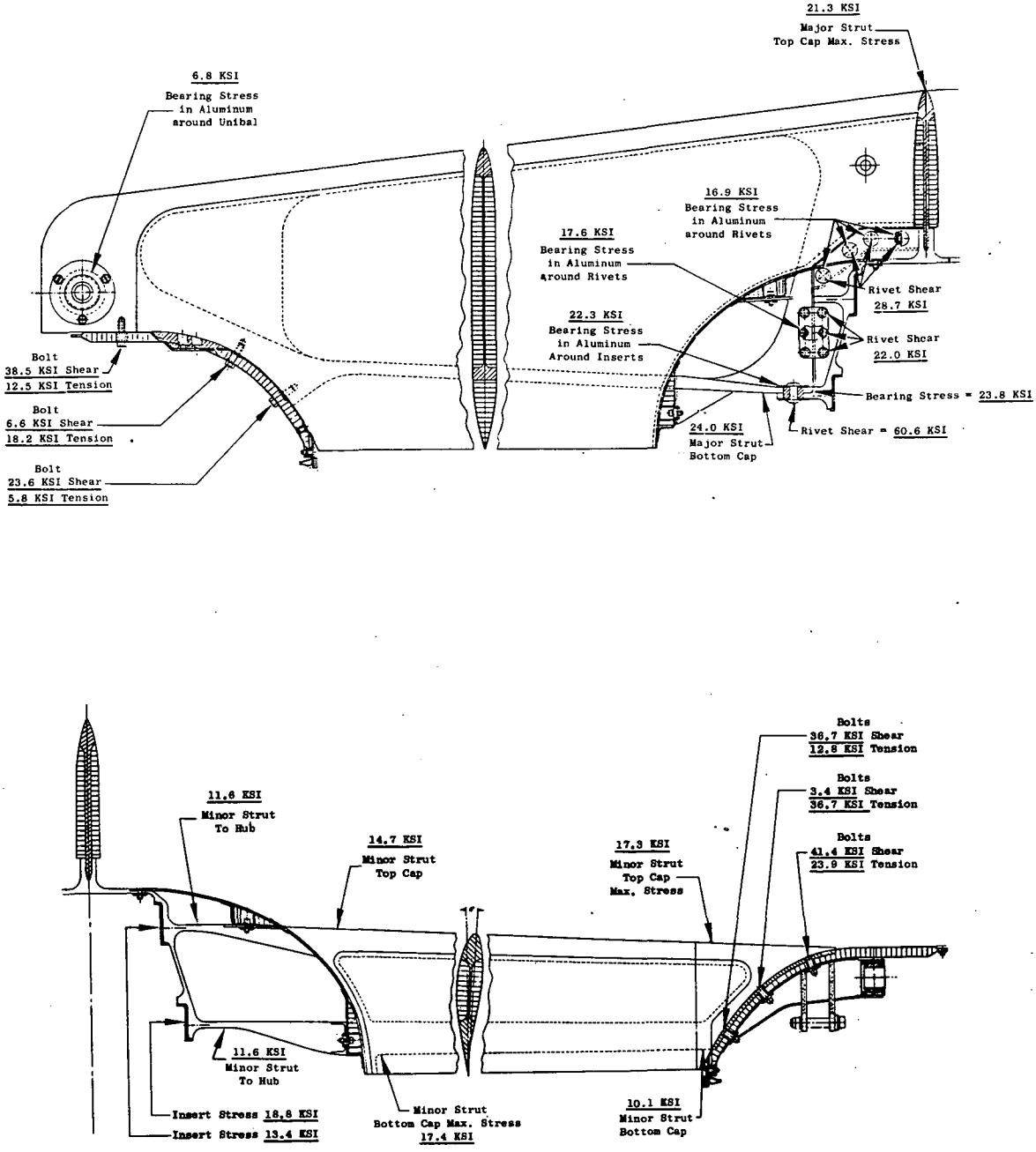

Figure 101 - Front Frame Stresses

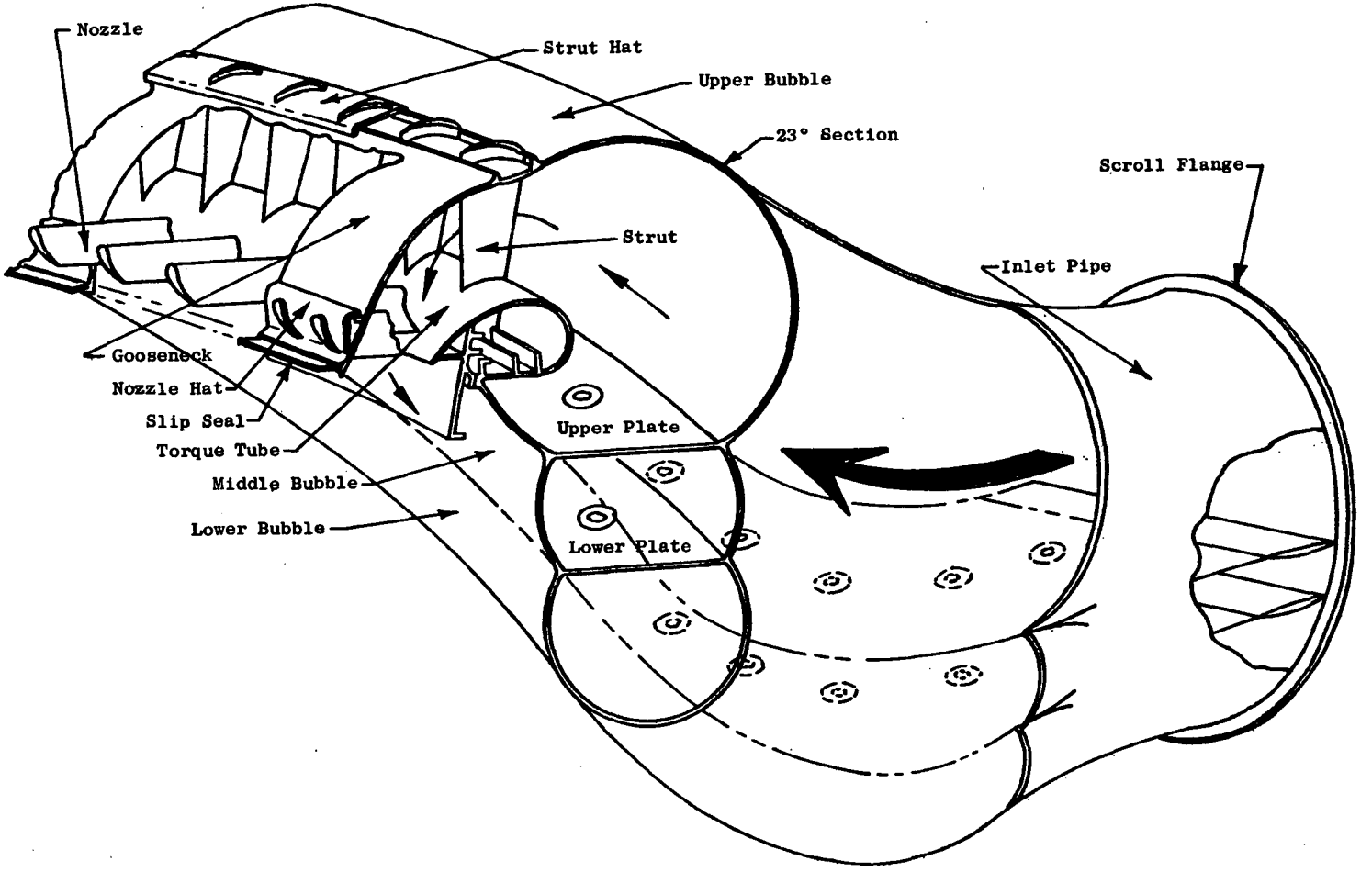

Figure 102 - Scroll Cross-Section at Inlet

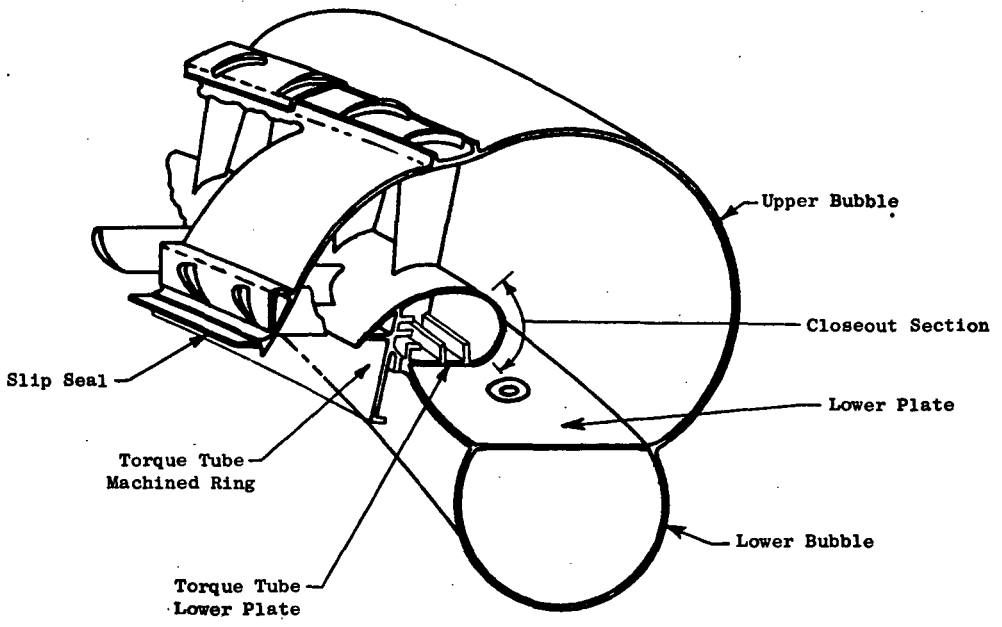

Figure 103 - Scroll Cross-Section, 60 Degrees

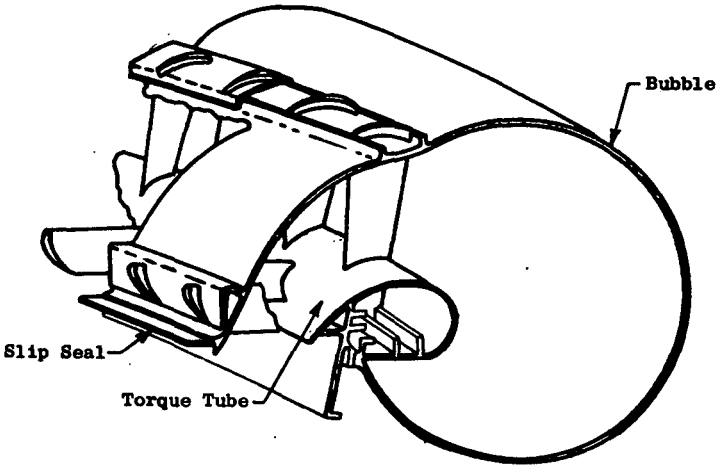

Figure 104 - Scroll Cross-Section, 98 Degrees

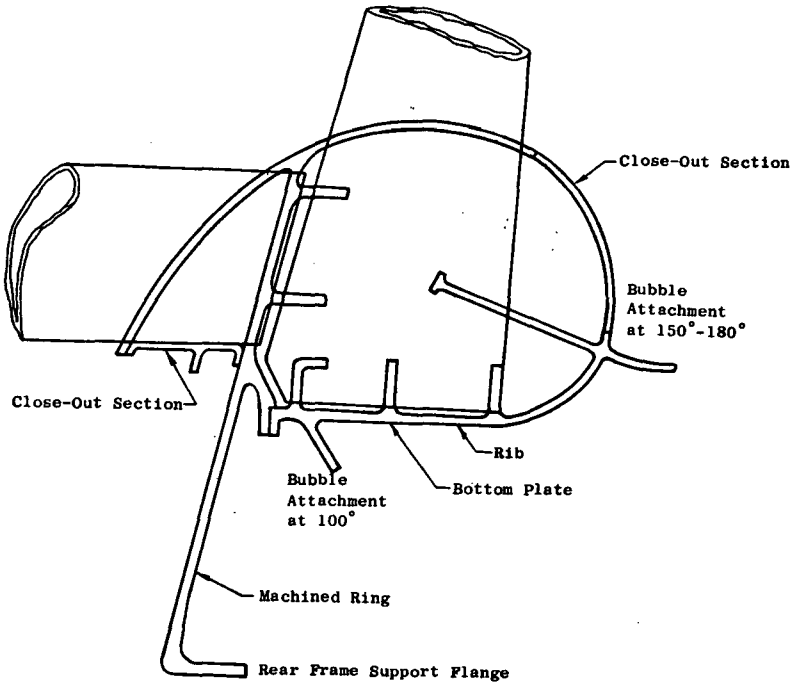

Figure 105 - Torque Tube with Bubble Attachment (100-180°)

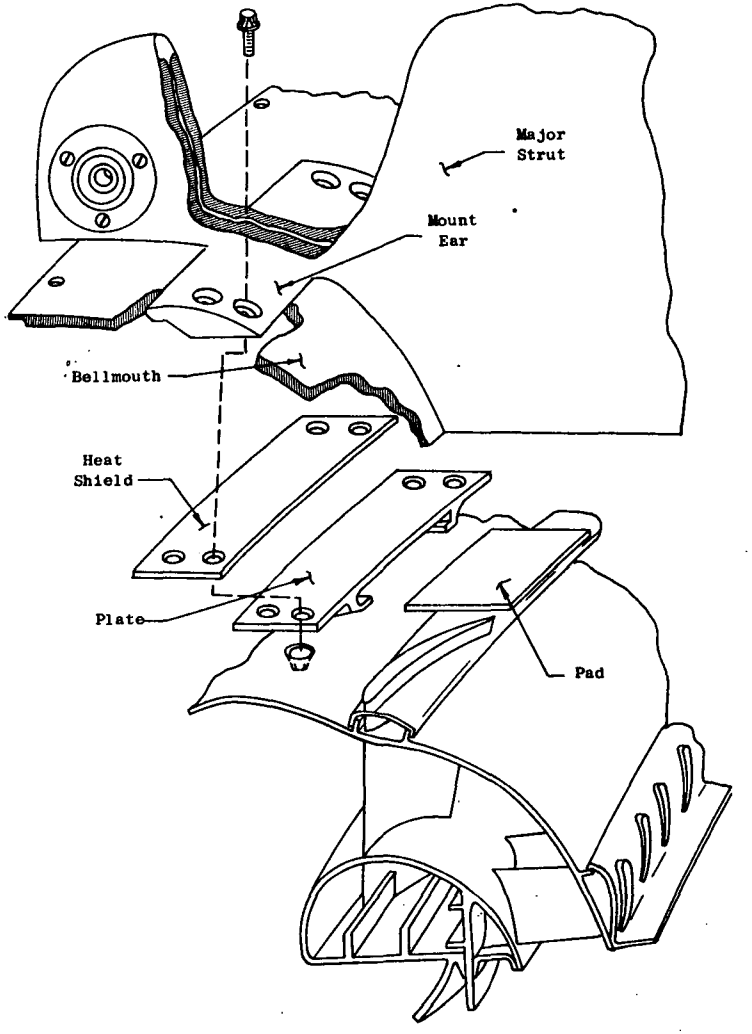

Figure 106 - Mount - Scroll to Front Frame Major Strut

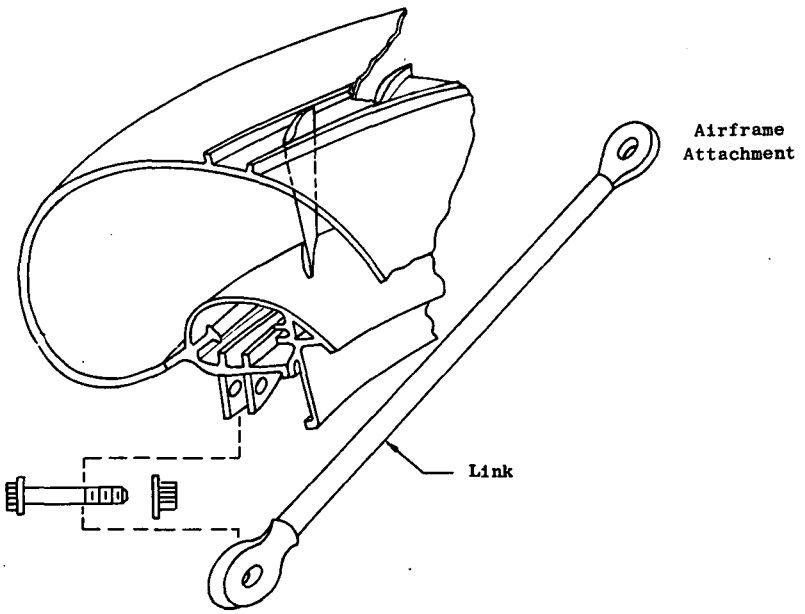

Figure 107 - Mount - Outboard Scroll to Airframe

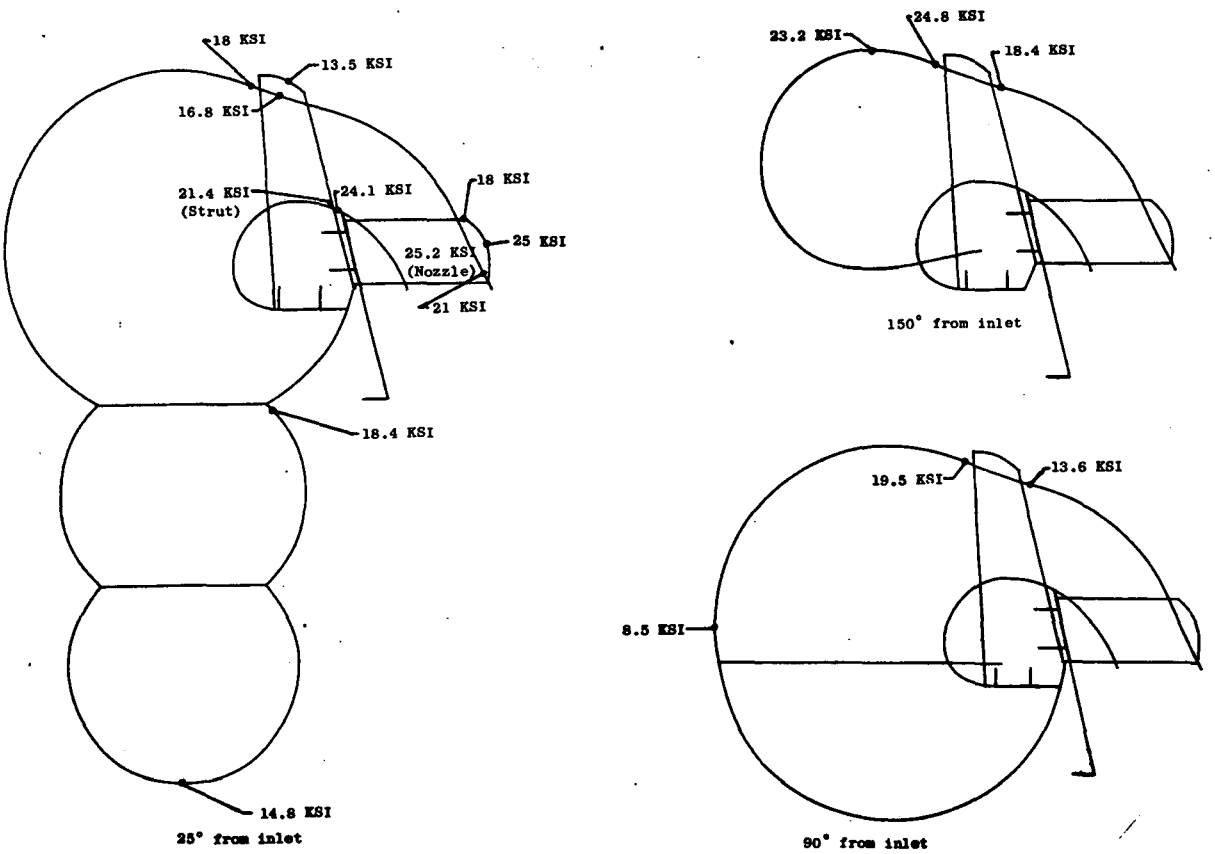

Figure 108 - Stresses in Scroll Sections

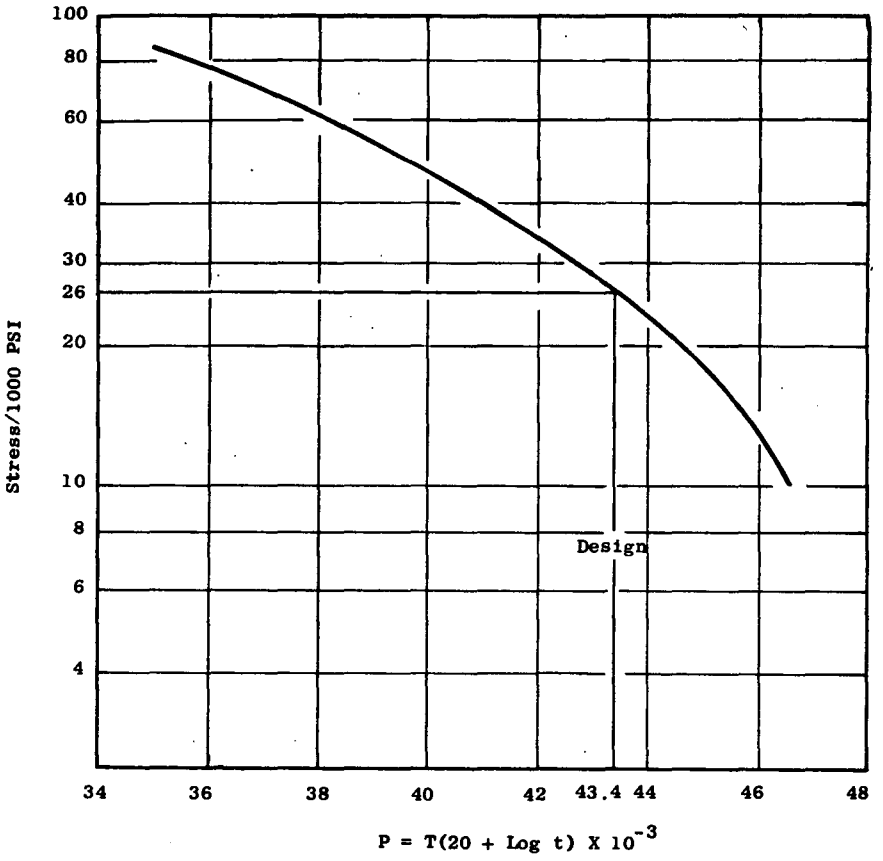

Figure 109 - René 41 0.20 Percent Plastic Creep

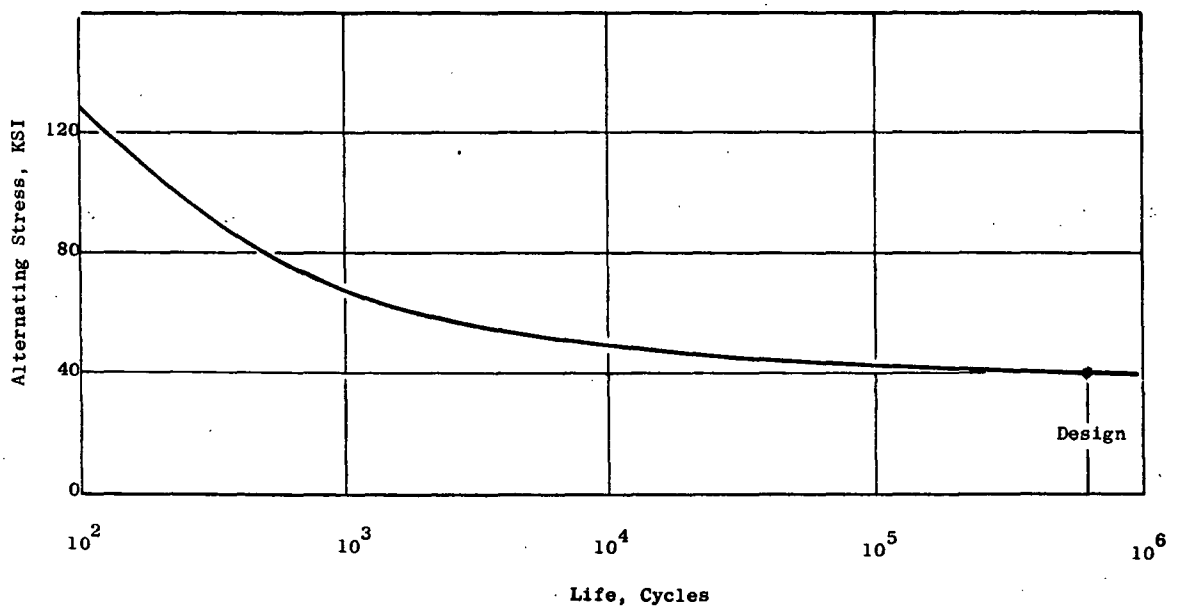

Figure 110 - René 41 Fatigue Life at 1450° Fahrenheit

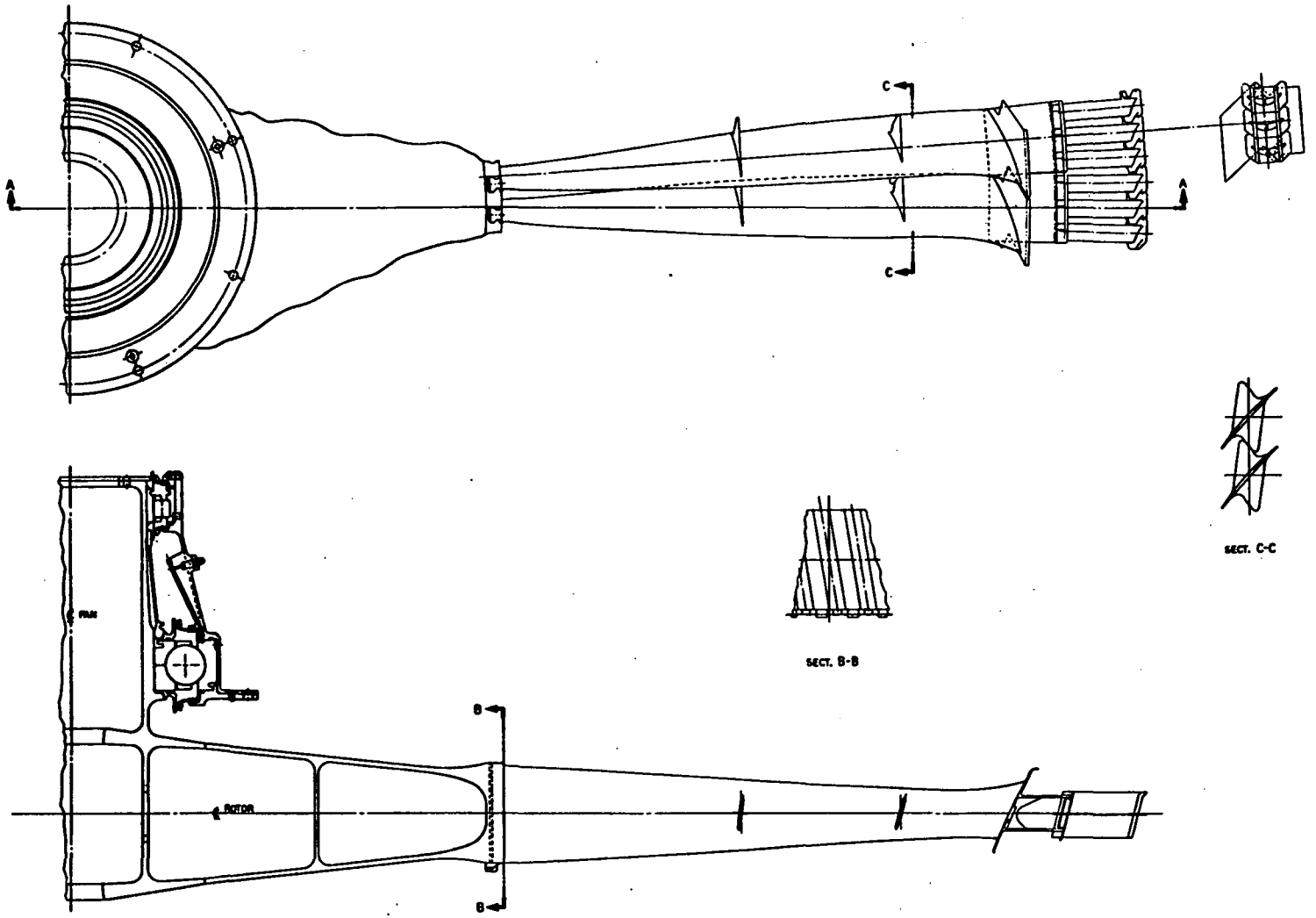

Figure 111 - LF460 Rotor Layout Drawing

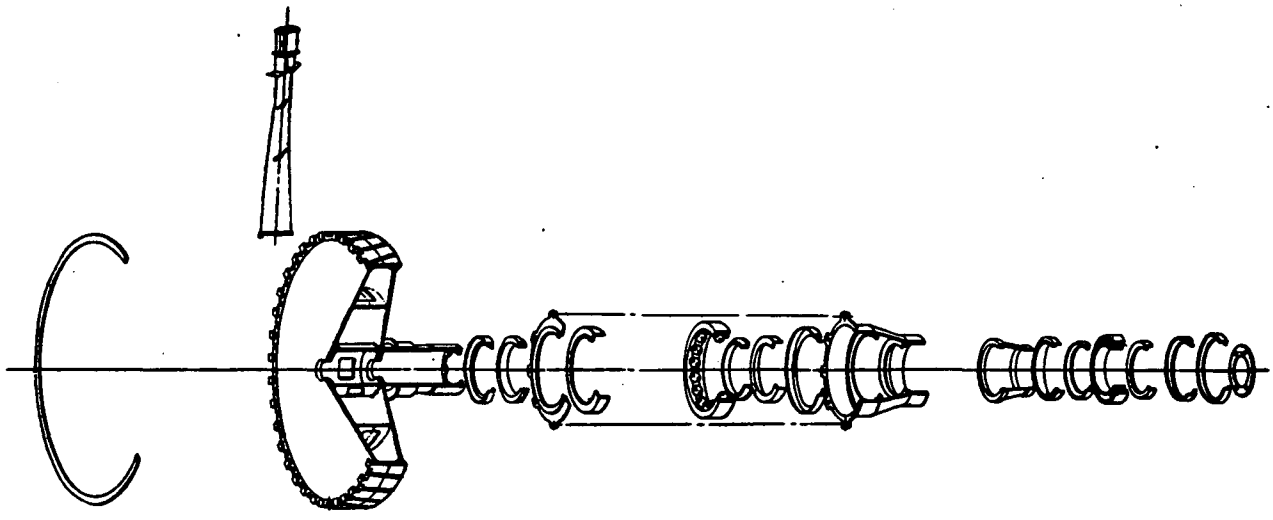

Figure 112 - Rotor Assembly Drawing

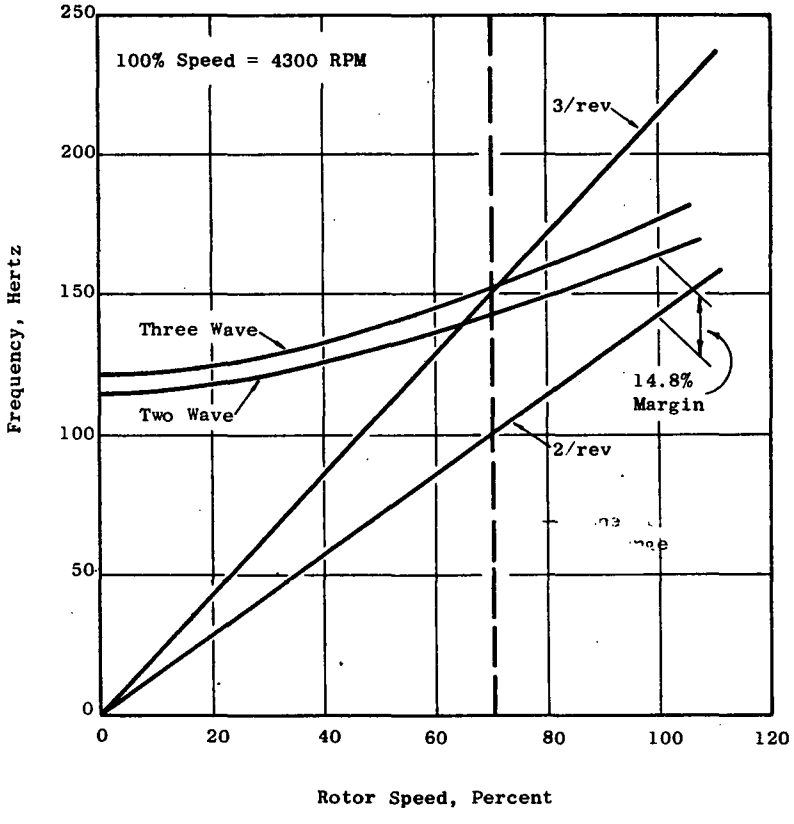

Figure 113 - Rotor Frequency-Speed Diagram

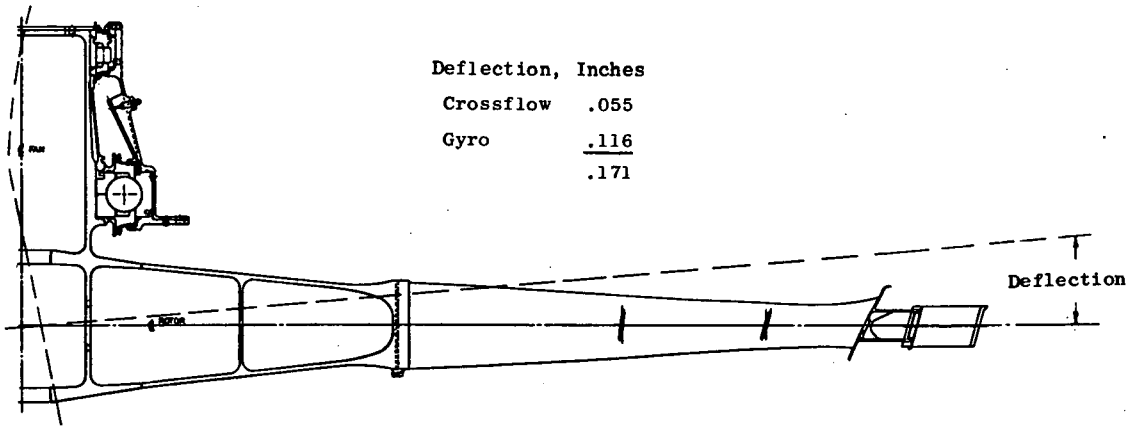

Figure 114 - Rotor Deflection Under Crossflow and Gyro

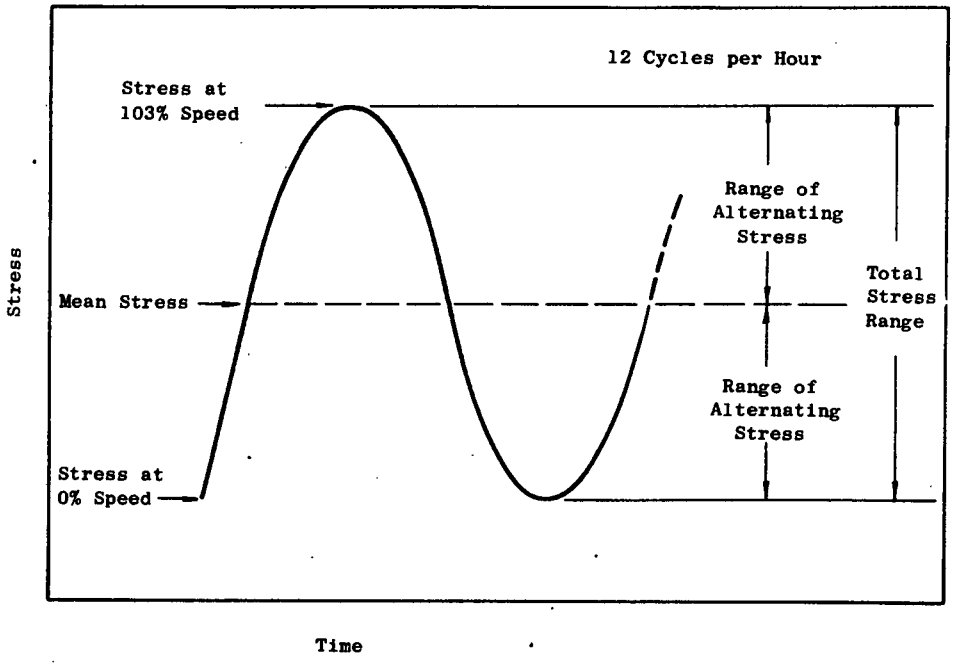

Figure 115 - Rotor Low-Cycle Fatigue Analysis

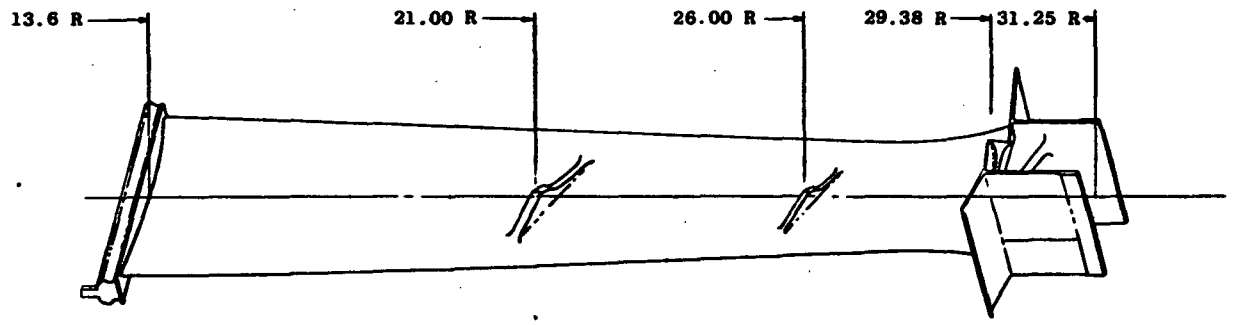

Figure 116 - Fan Blade

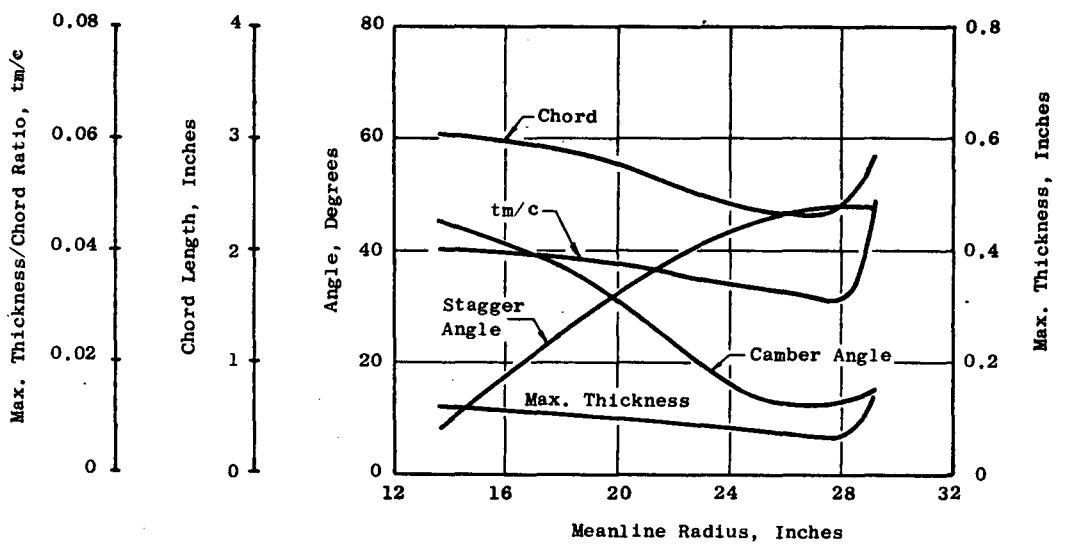

Figure 117 - Blade Airfoil Geometry

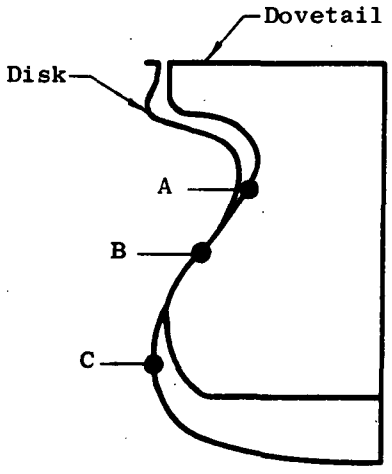

Stress at 100% Speed:

A. Blade Fillet Stress
45.2 KSI

B. Face Crush Stress
31.9 KSI

C. Disk Fillet Stress
42.6 KSI

Figure 118 - Dovetail Steady State Stress

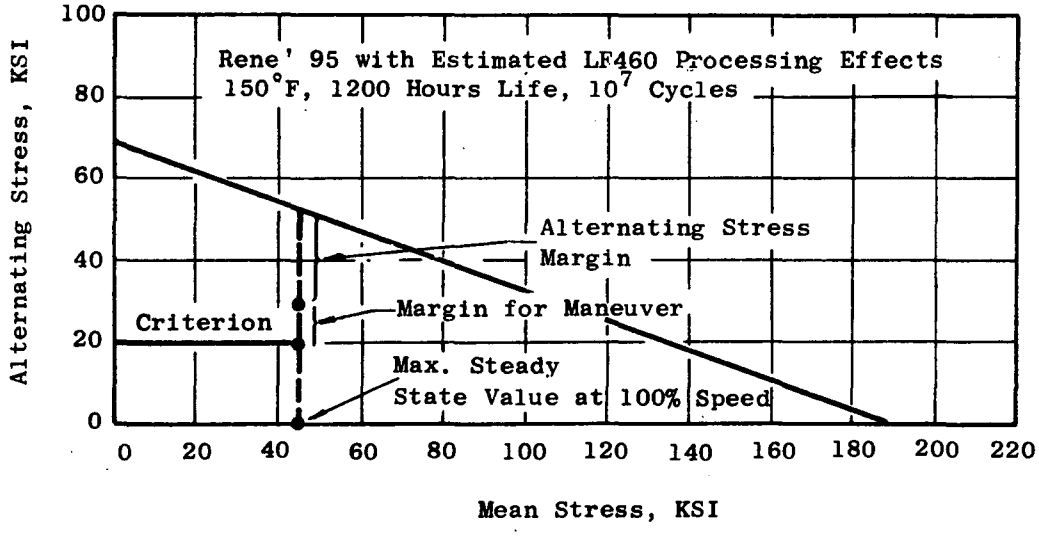

Figure 119 - Dovetail Stress Range Diagram

5Φ

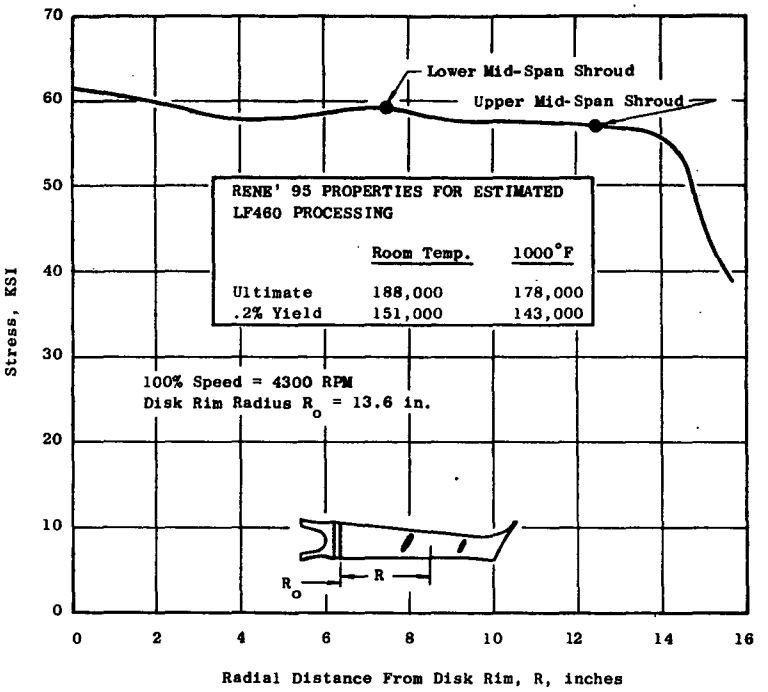

Figure 120 - Blade Average Steady State Stress

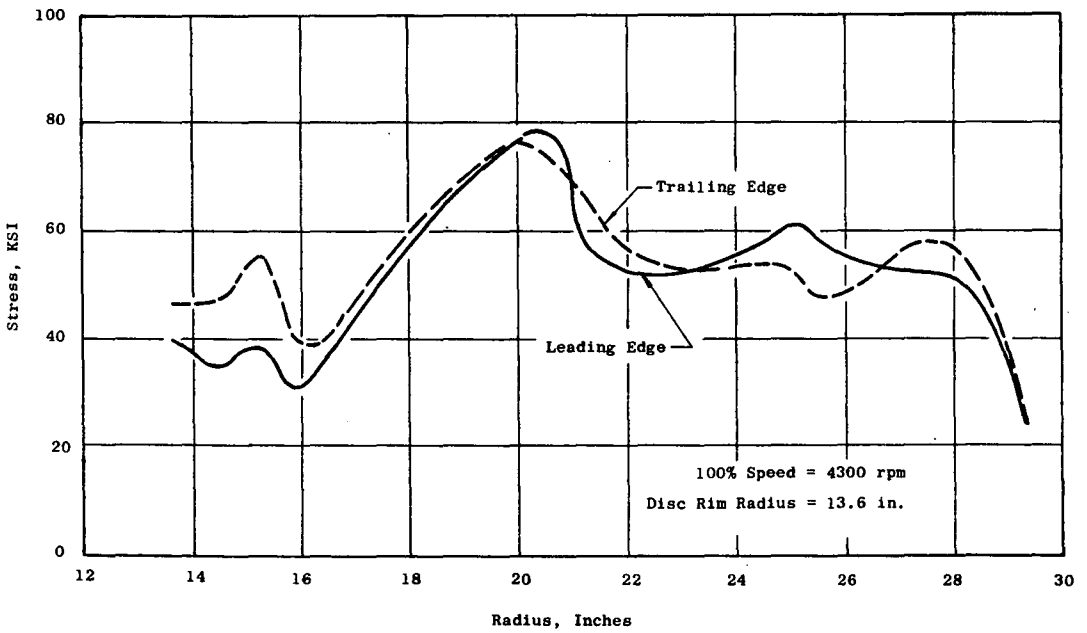

Figure 121 - Blade Airfoil Steady State Resultant Spanwise Stress

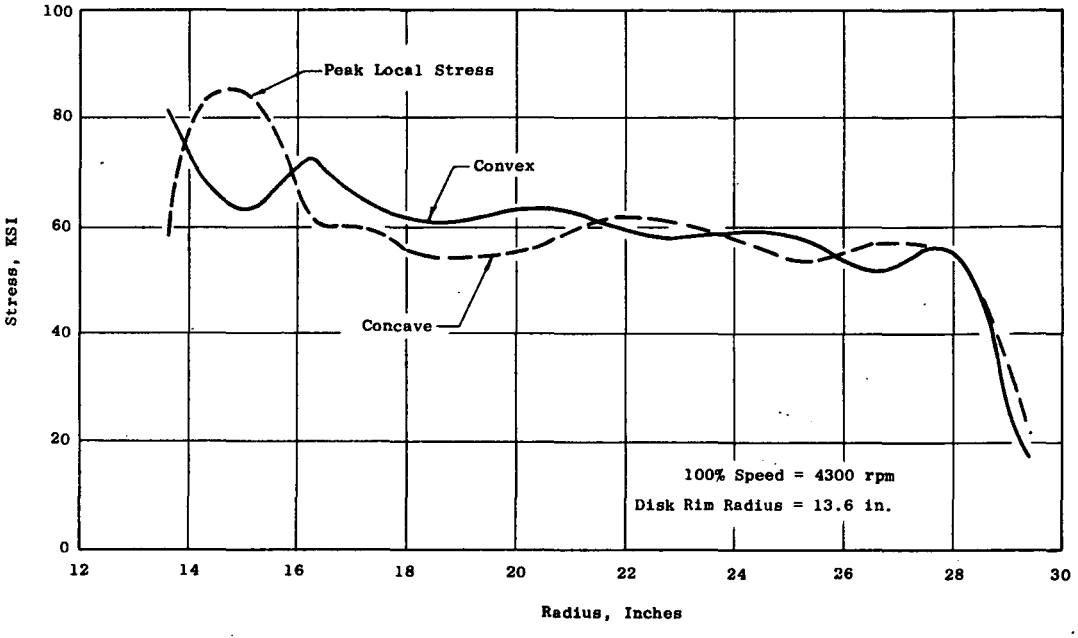

Figure 122 - Blade Airfoil Steady State Mises-Hencky Stress

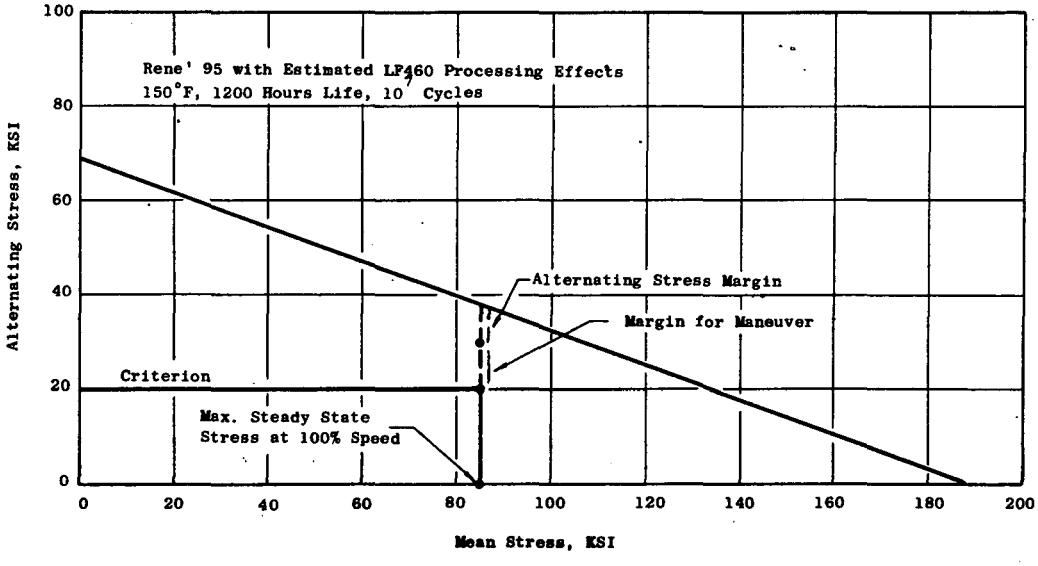

Figure 123 - Blade Airfoil Stress Range Diagram

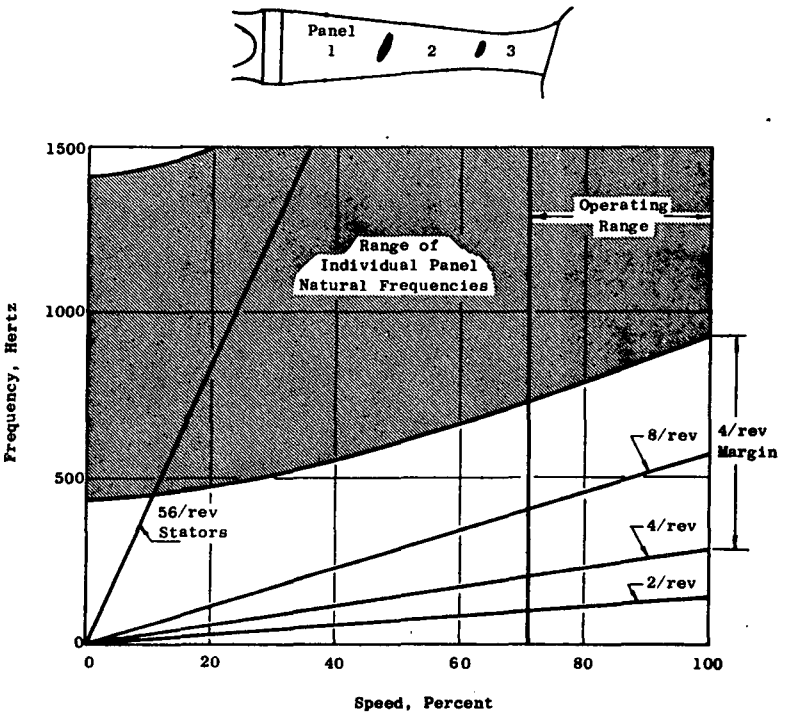

Figure 124 - Blade Frequency - Speed Diagram

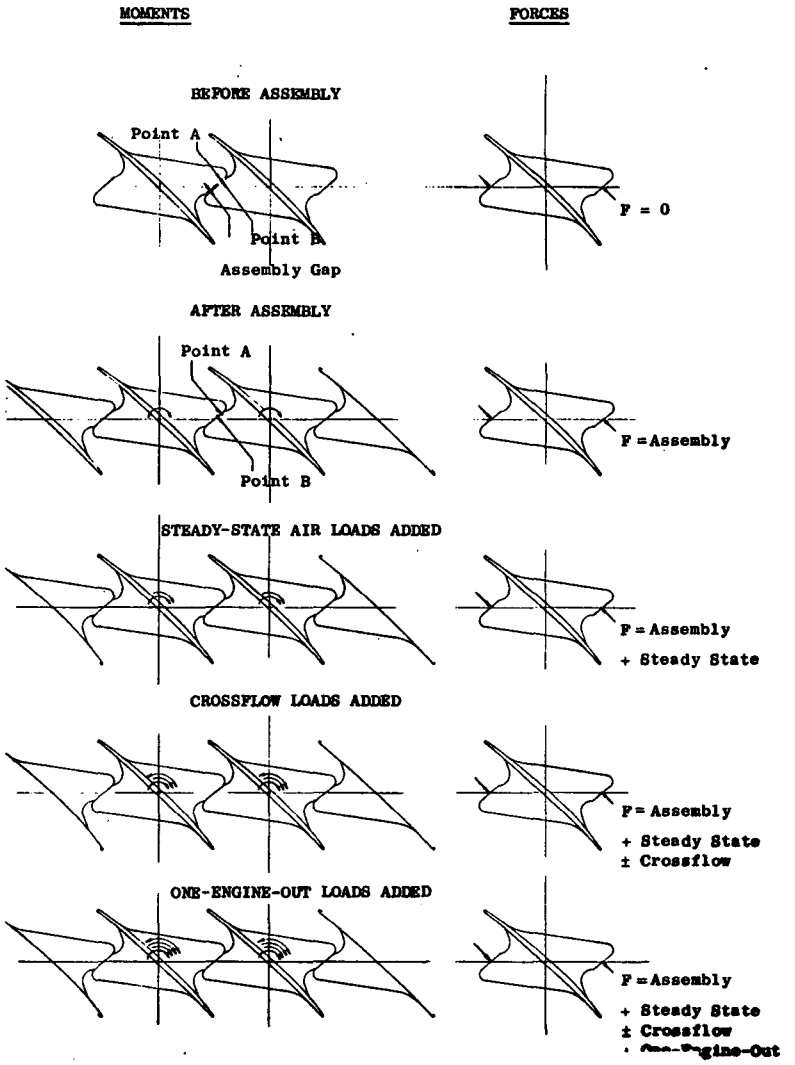

Figure 125 - Part-Span Shroud Loading

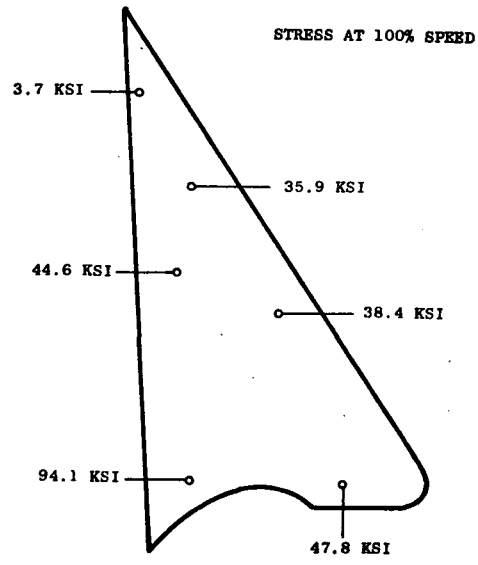

Figure 126 - Upper Part-Span Shroud Steady State Stress

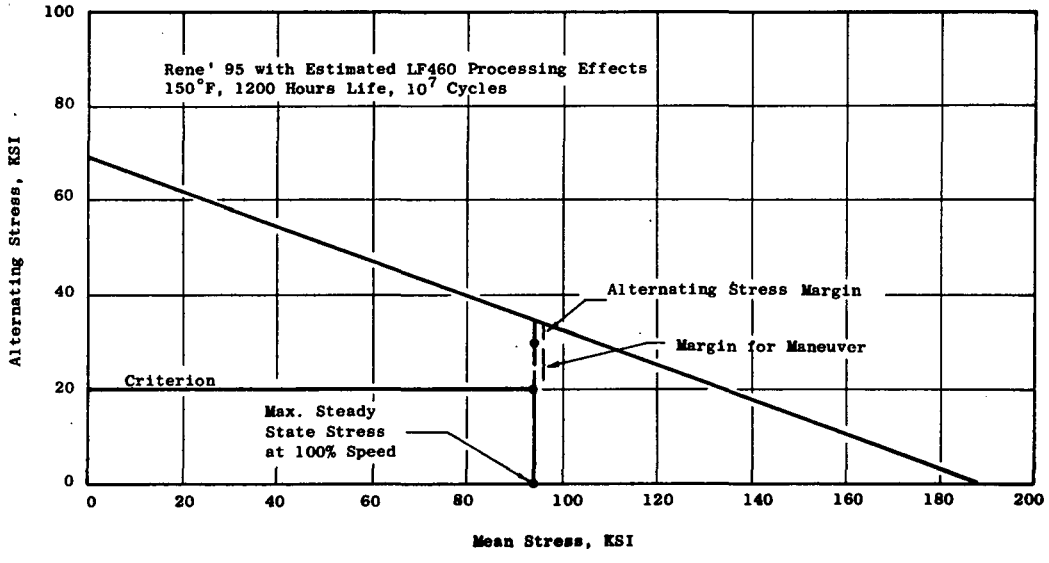

Figure 127 - Blade Upper Part-Span Shroud Stress Range Diagram

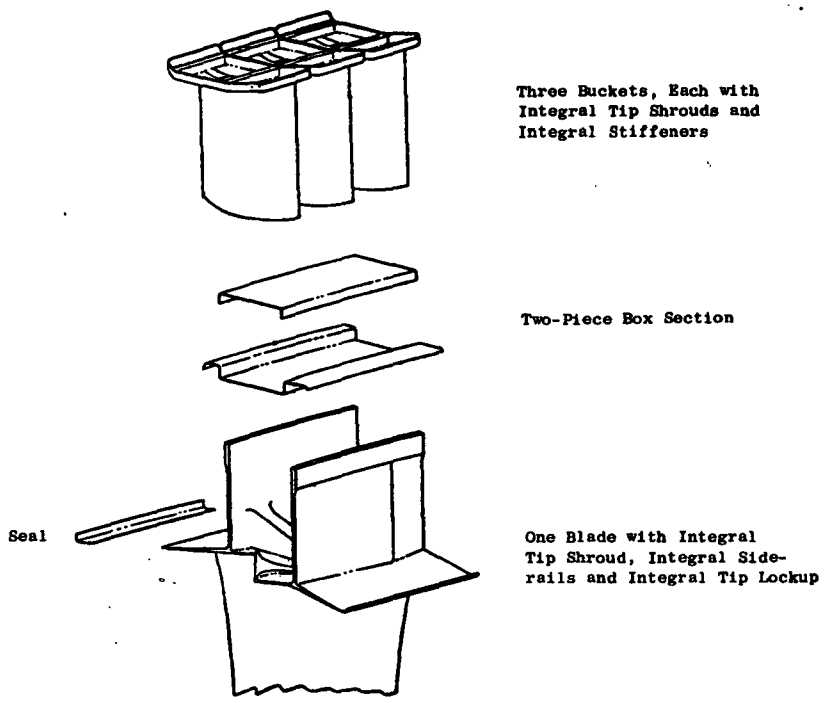

Figure 128 - Blade-Turbine Sector

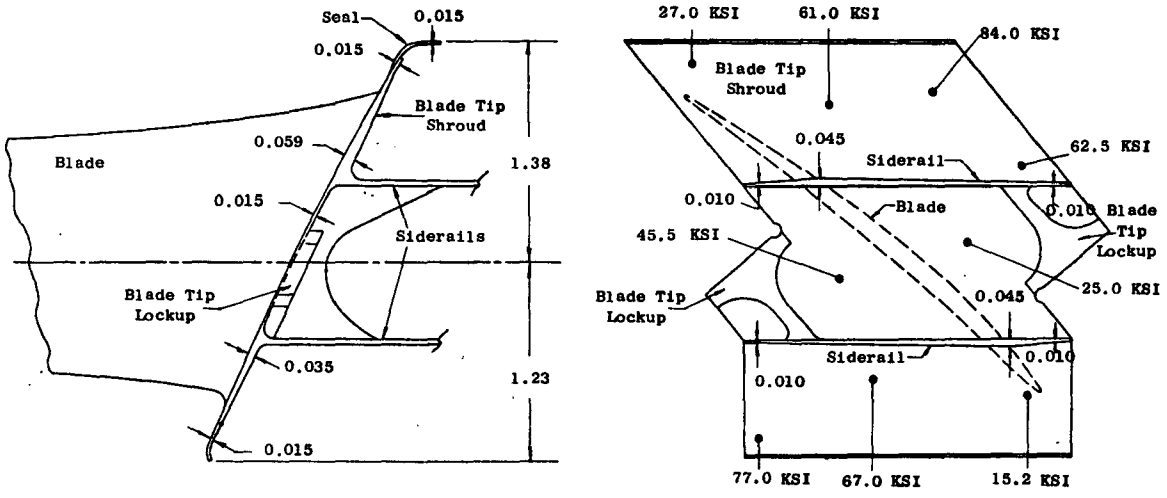

Figure 129 - Blade Tip Shroud Steady State Stress

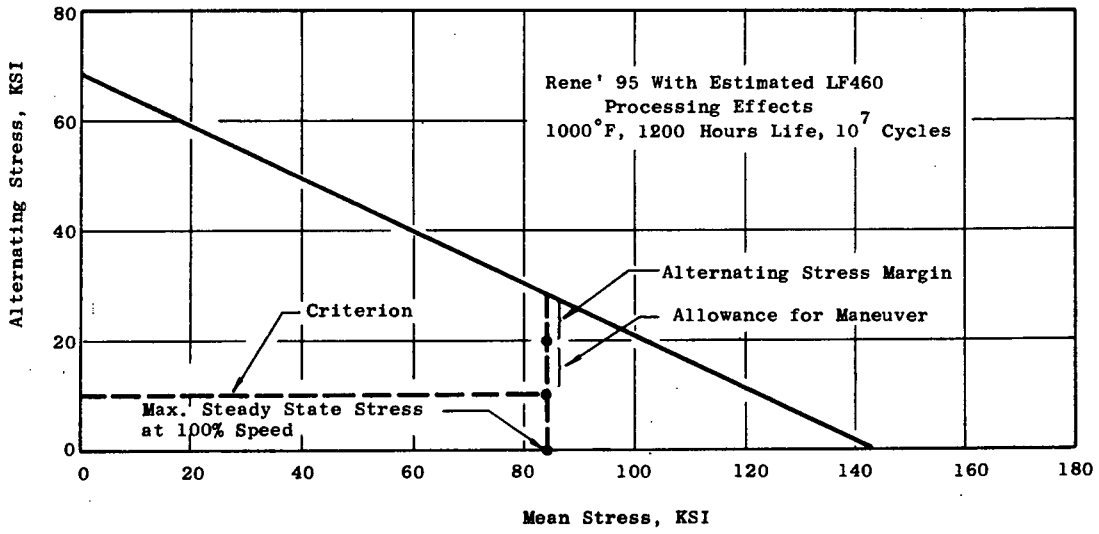

Figure 130 - Blade Tip Shroud Stress Range Diagram

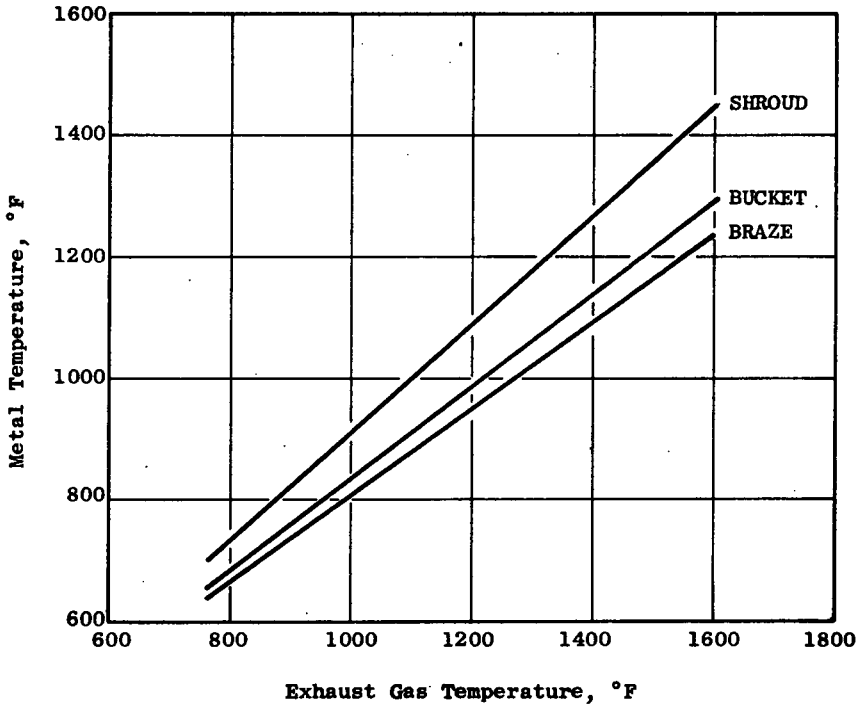

Figure 131 - Turbine Metal Design Temperatures

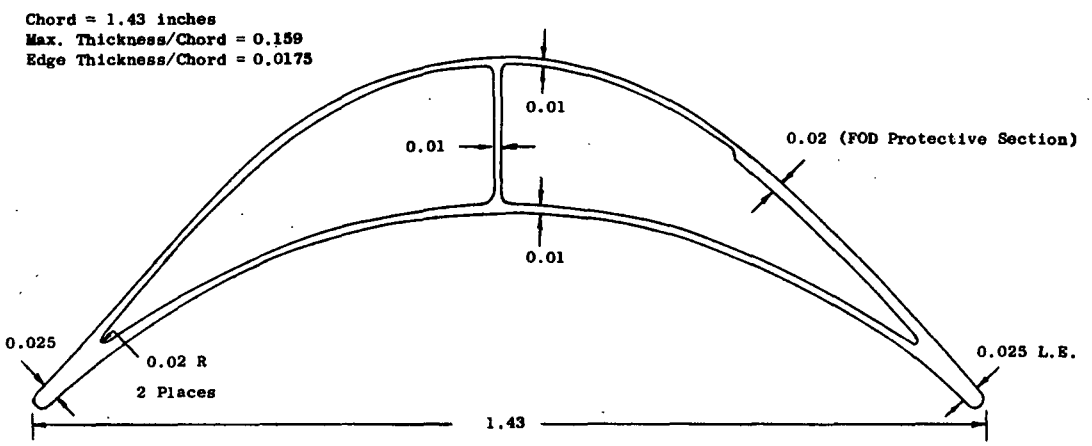

Figure 132 - Bucket Cross-Section

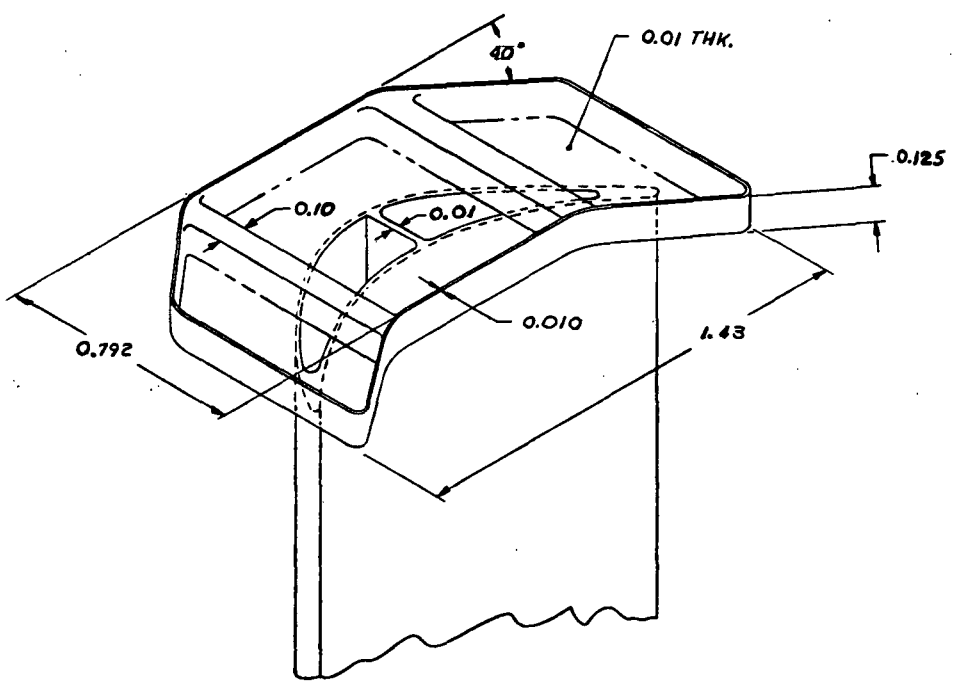

Figure 133 - Integral Bucket and Tip Shroud

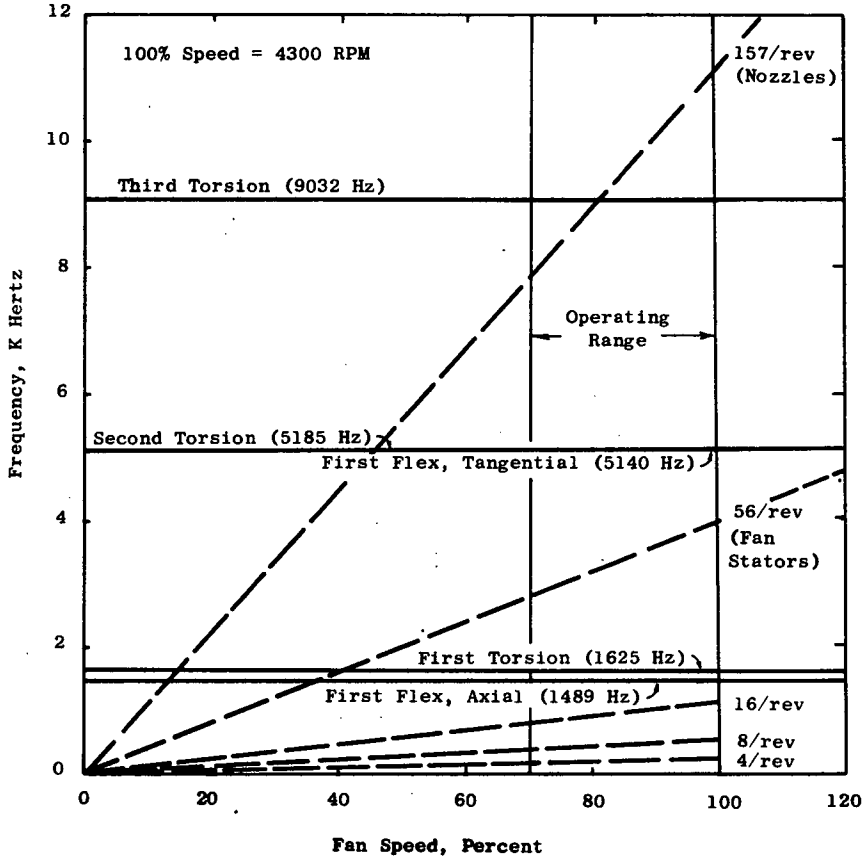

Figure 134 - Turbine Bucket Frequency-Speed Diagram

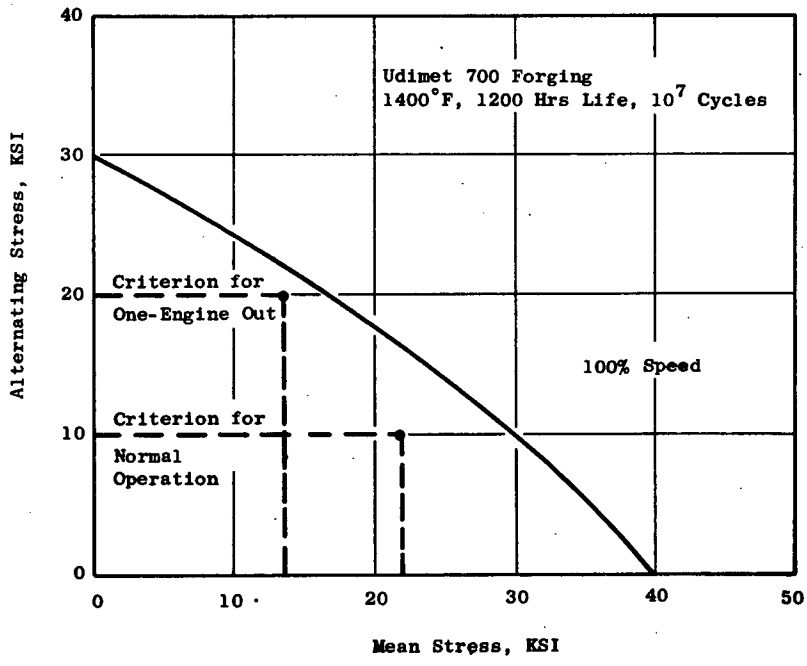

Figure 135 - Bucket Stress Range Diagram

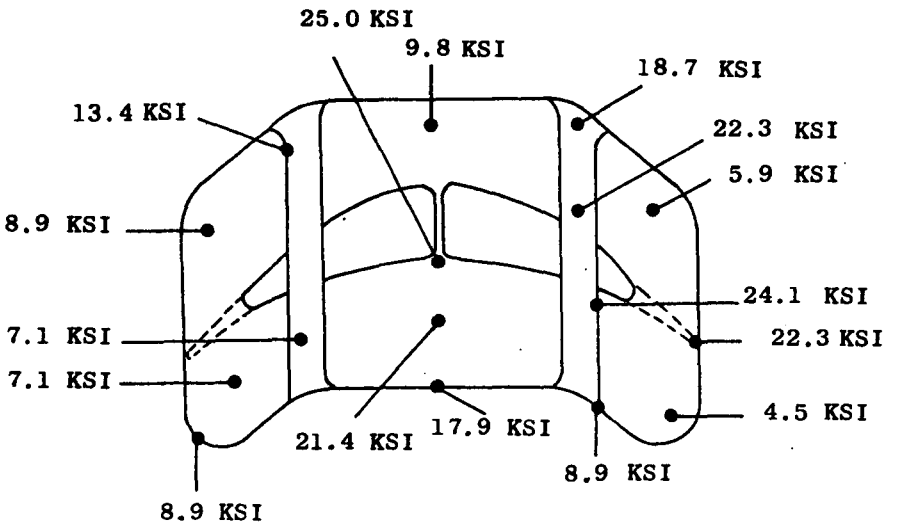

Figure 136 - Bucket Tip Shroud Stress

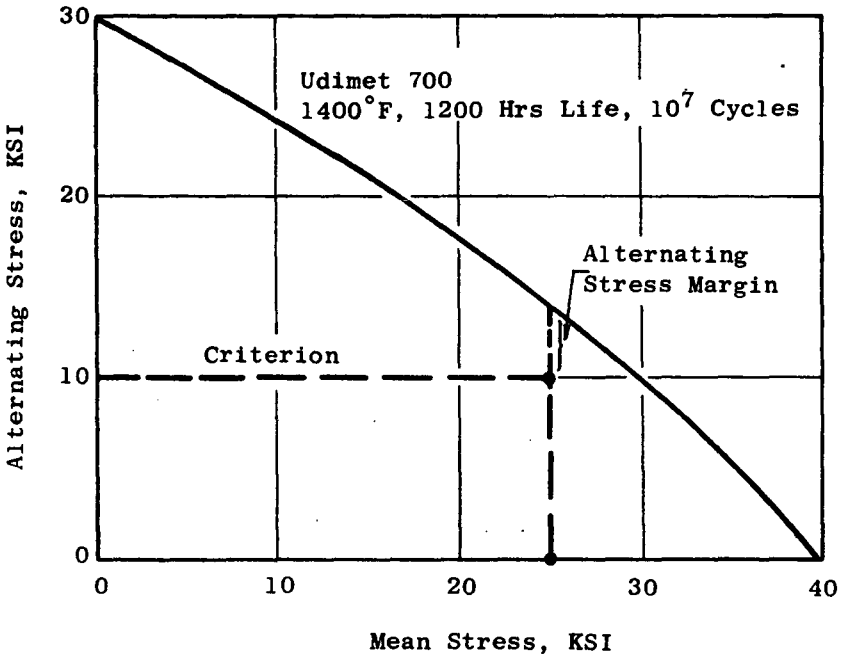

Figure 137 - Bucket Tip Shroud Stress Range Diagram

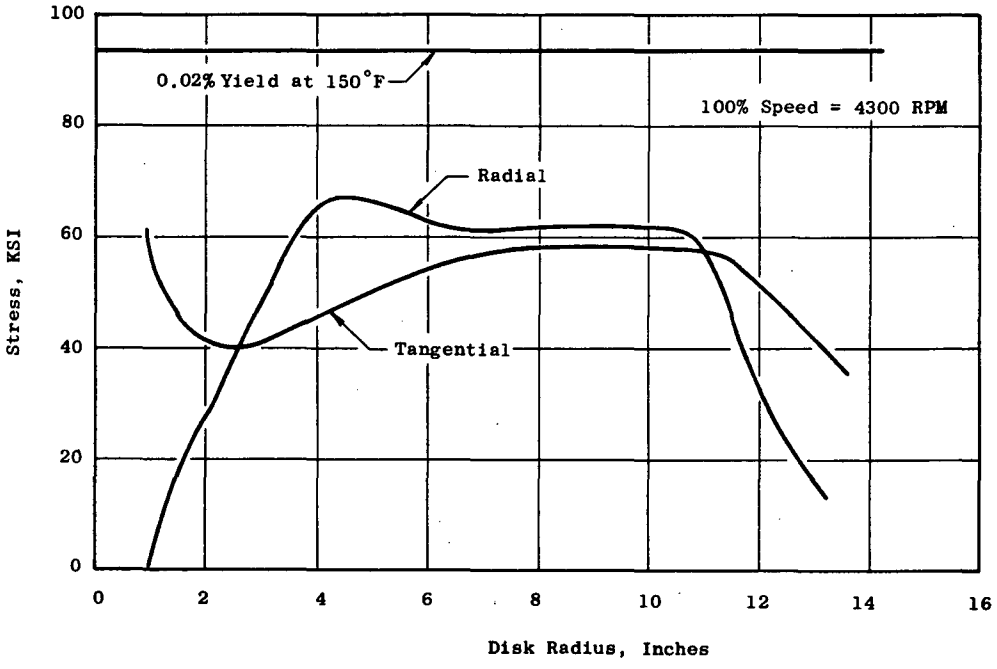

Figure 138 - Disk Forward Web Meanline Centrifugal Stress

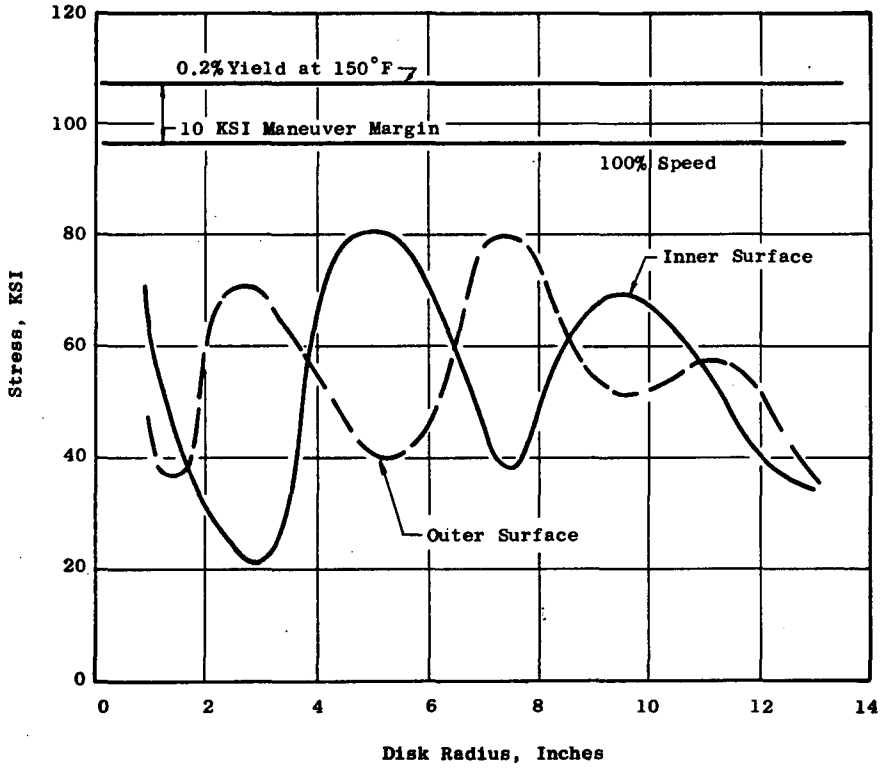

Figure 139 - Disk Forward Web Surface Centrifugal Stress

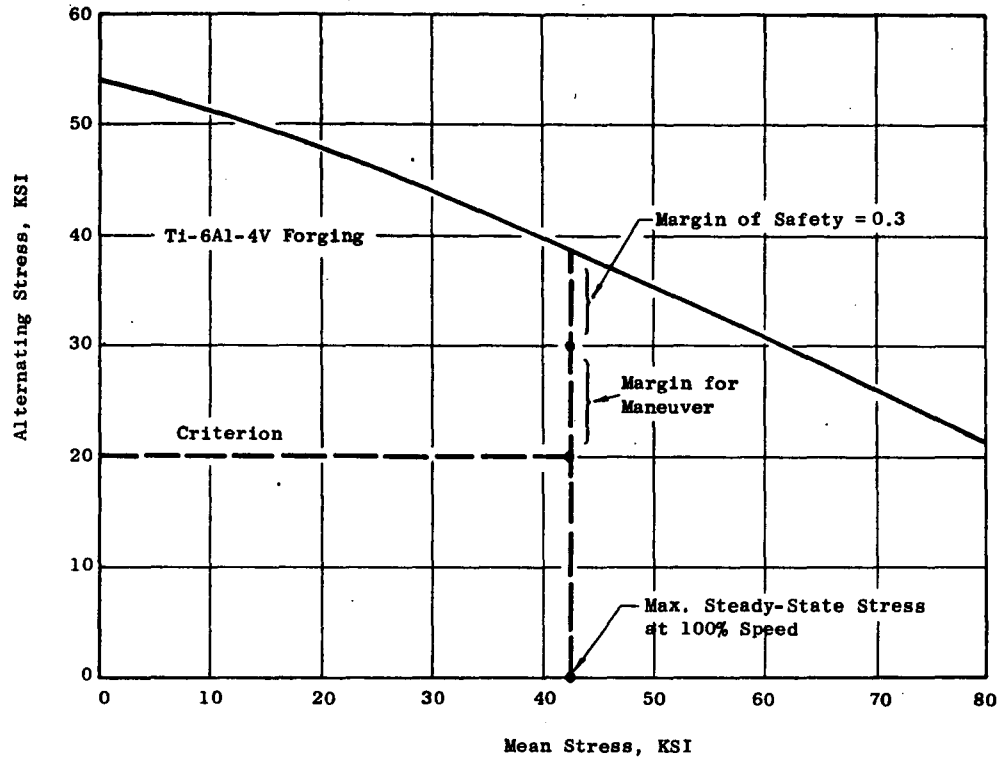

Figure 140 - Disk Dovetail Stress Range Diagram

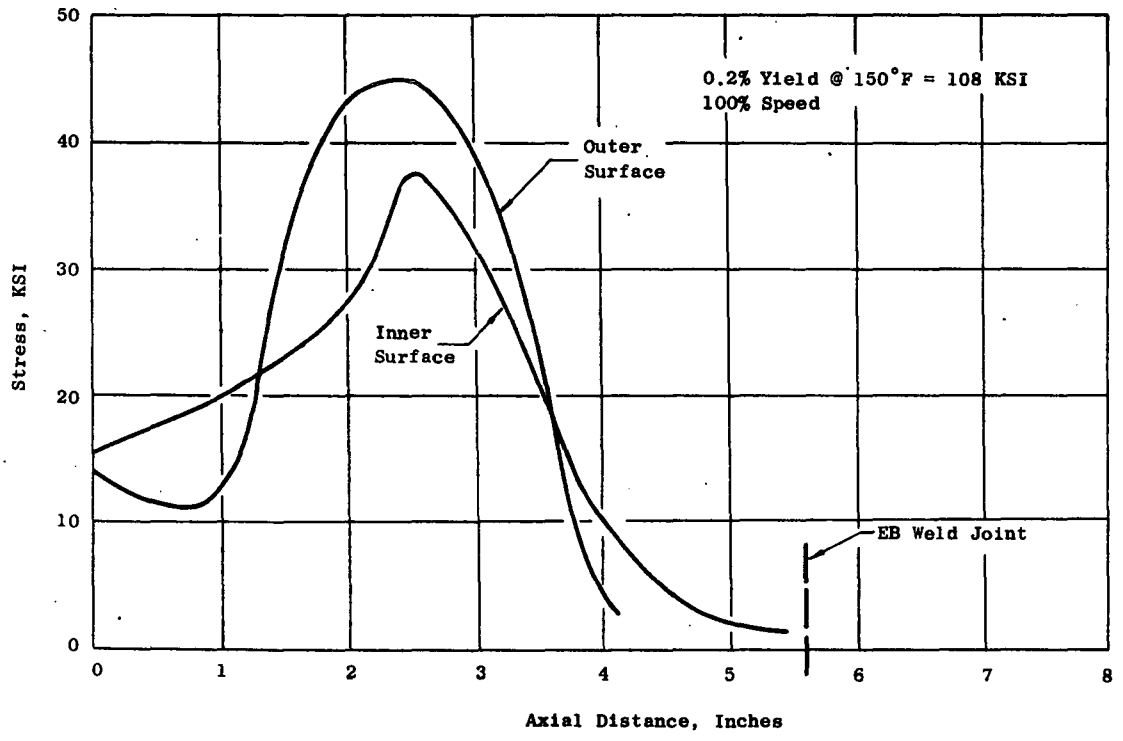

Figure 141 - Shaft Steady State Stress

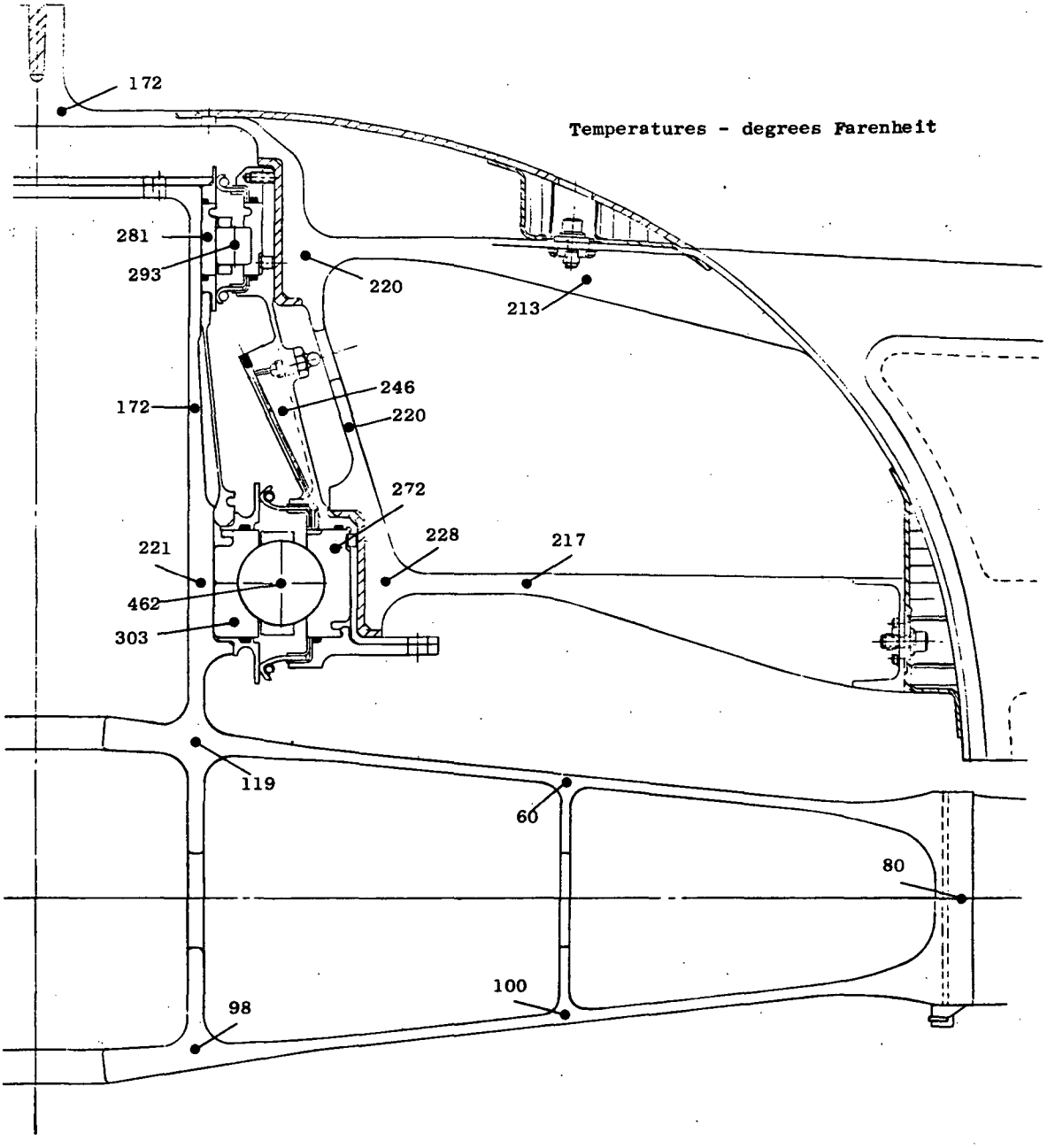

Figure 142 - Disk and Sump Steady State Temperatures During Hover

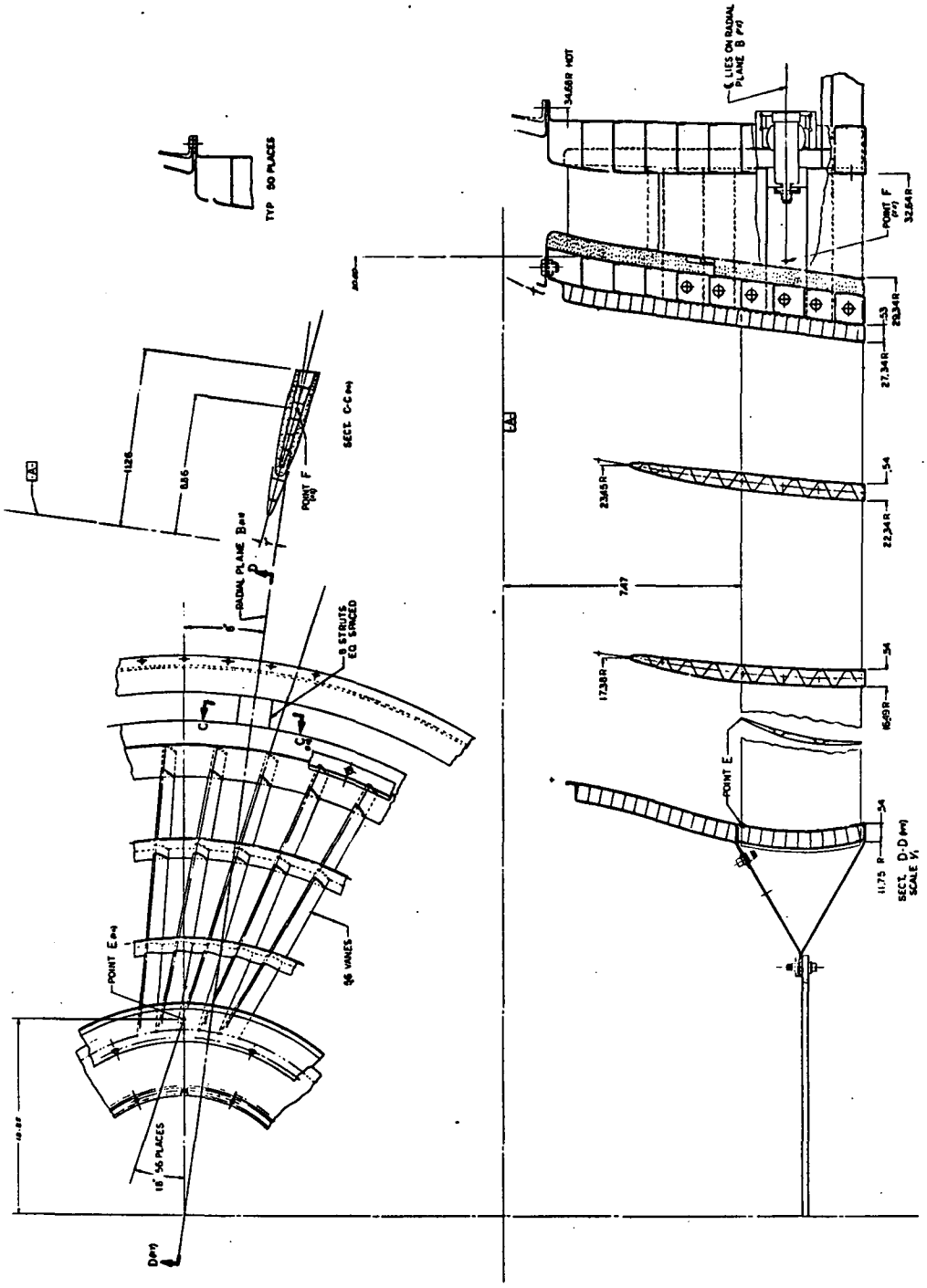

Figure 143 - LF460 Rear Frame

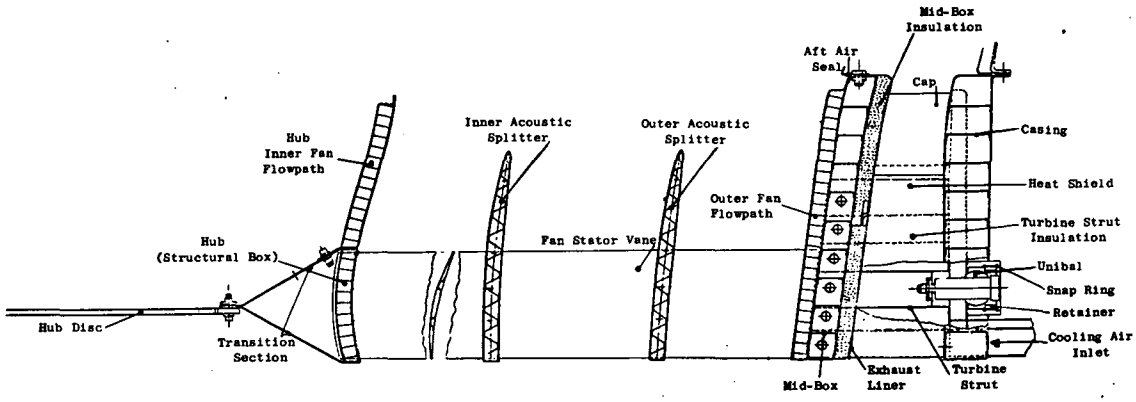

Figure 144 - Rear Frame Nomenclature

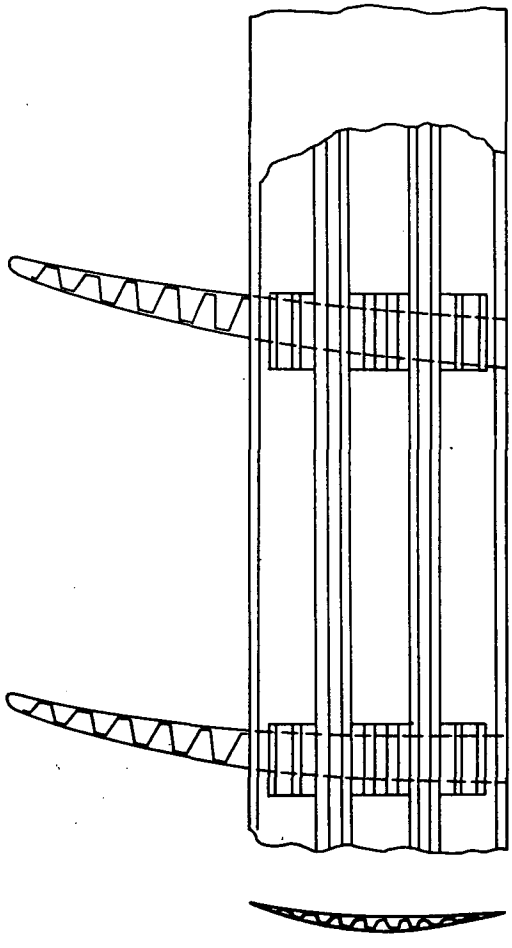

Figure 145 - Stator Vane Insert

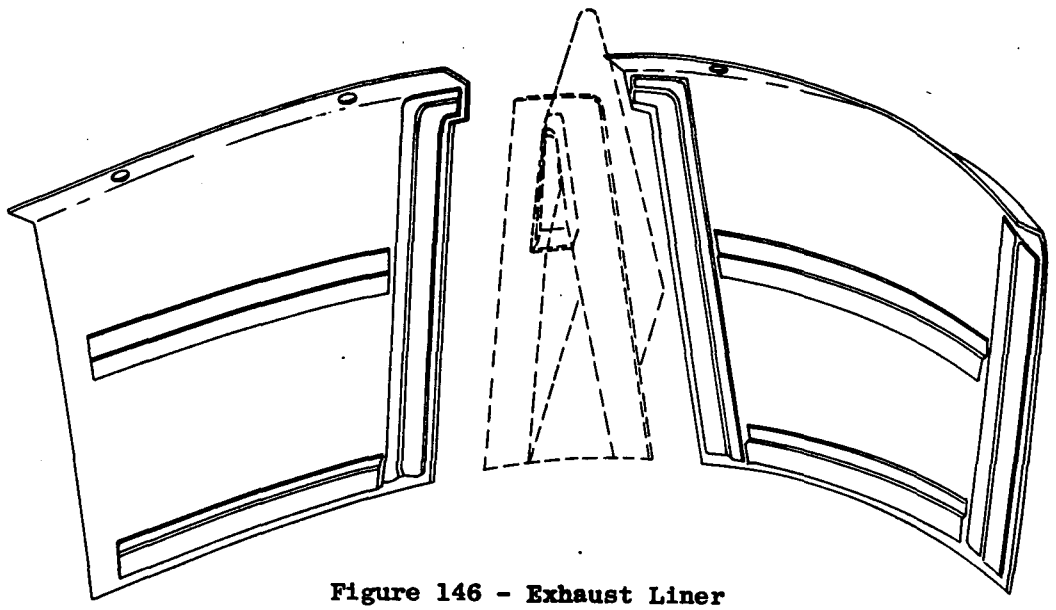

Figure 146 - Exhaust Liner

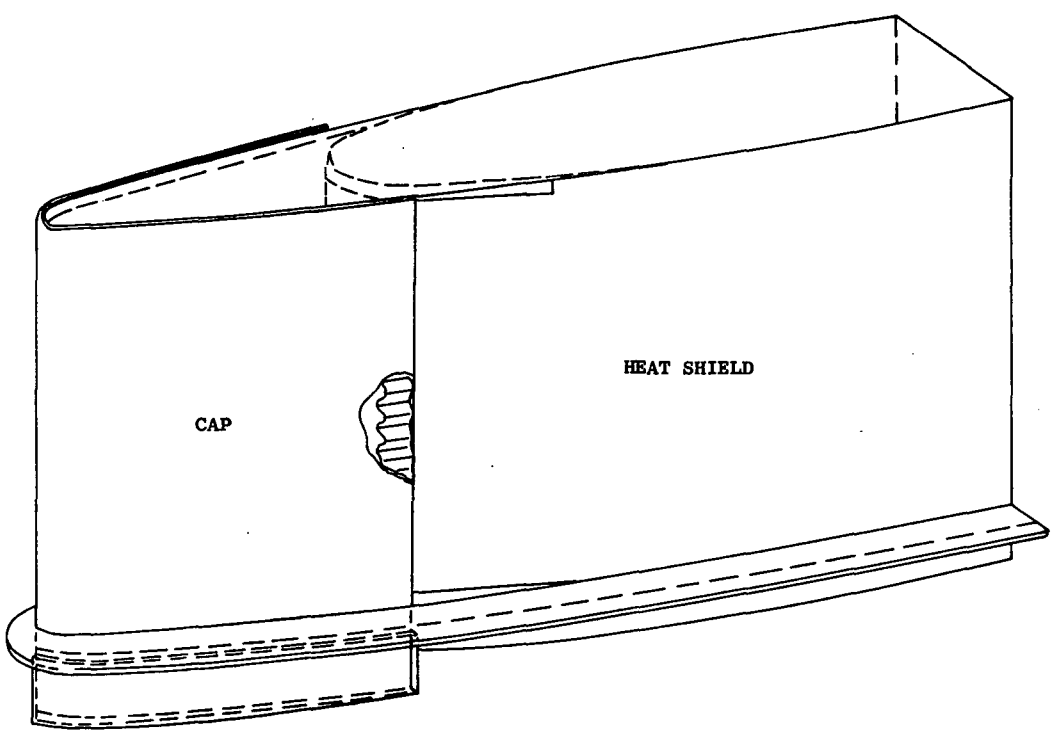

Figure 147 - Strut Heat Shield

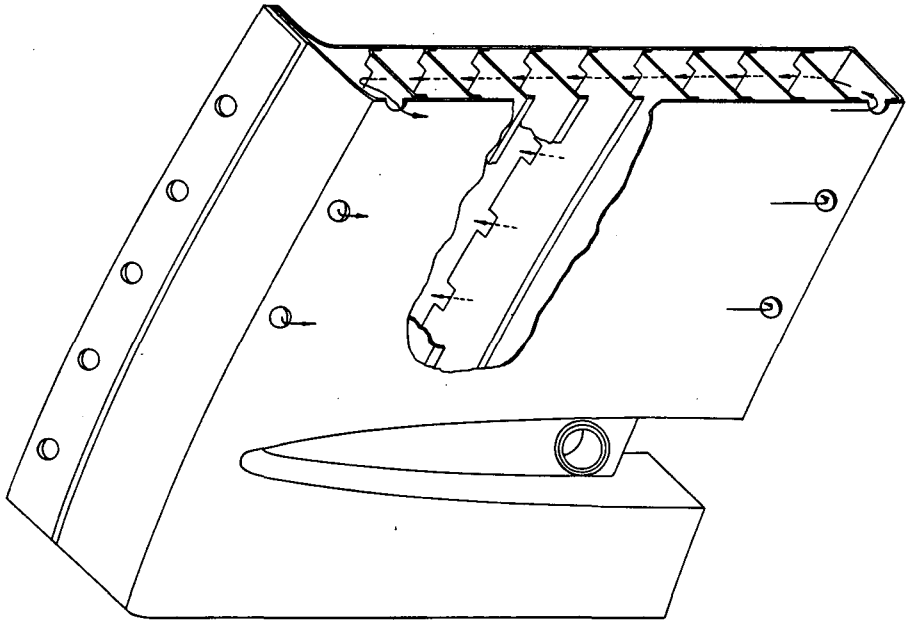

Figure 148 - Rear Frame Casing

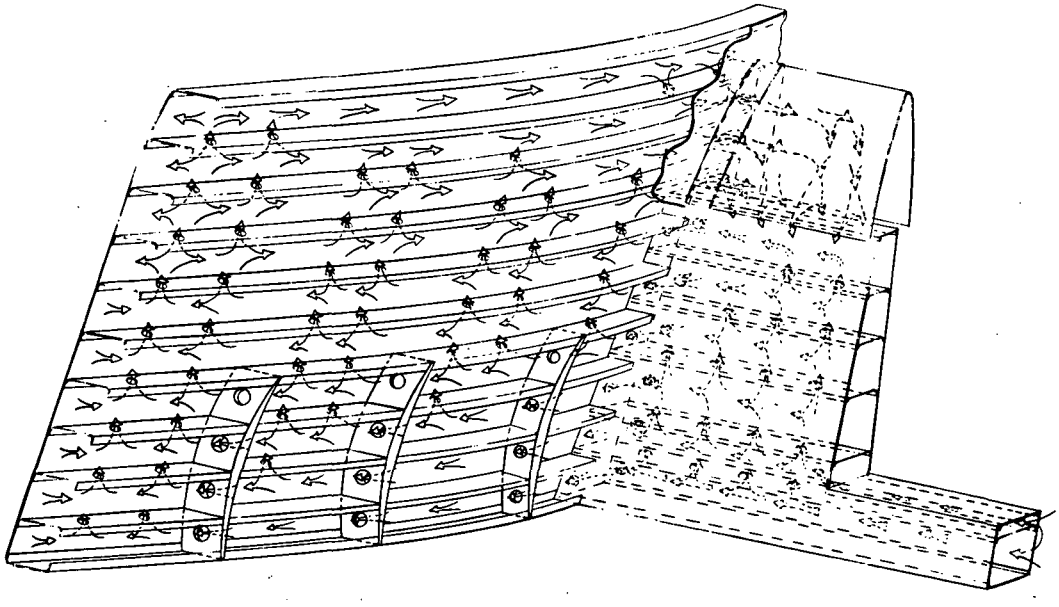

Figure 149 - Rear Frame Midbox Cooling

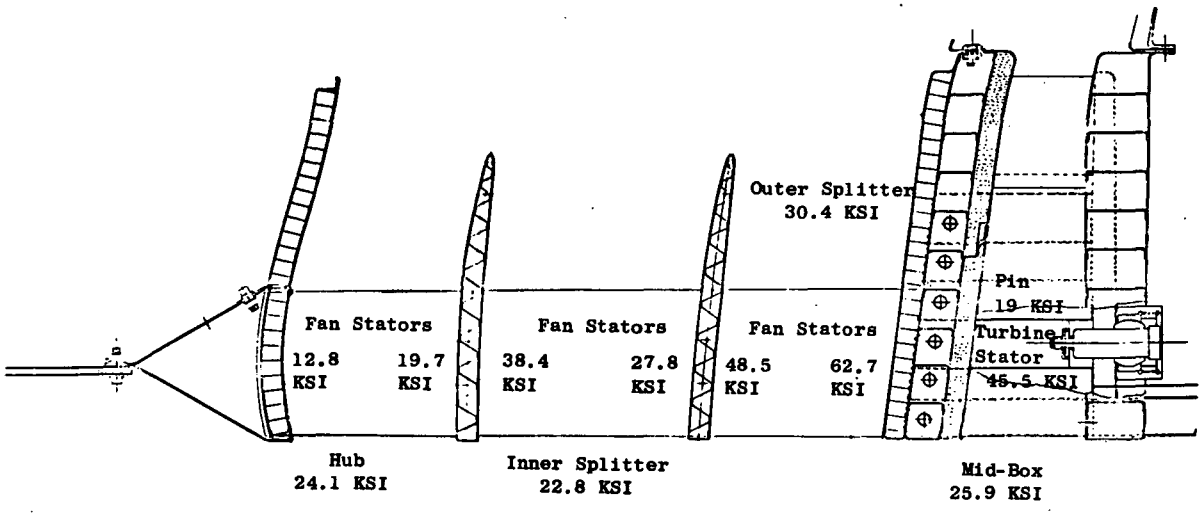

Figure 150 - Rear Frame Stresses

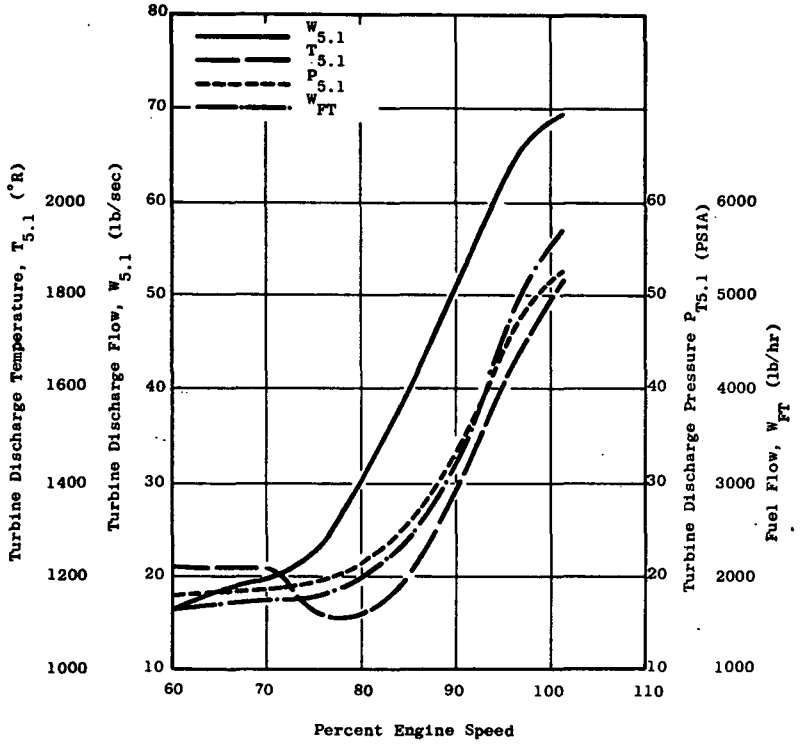

Figure 151 - Estimated YJ97 Discharge Conditions at Sea Level Static Standard Day Conditions

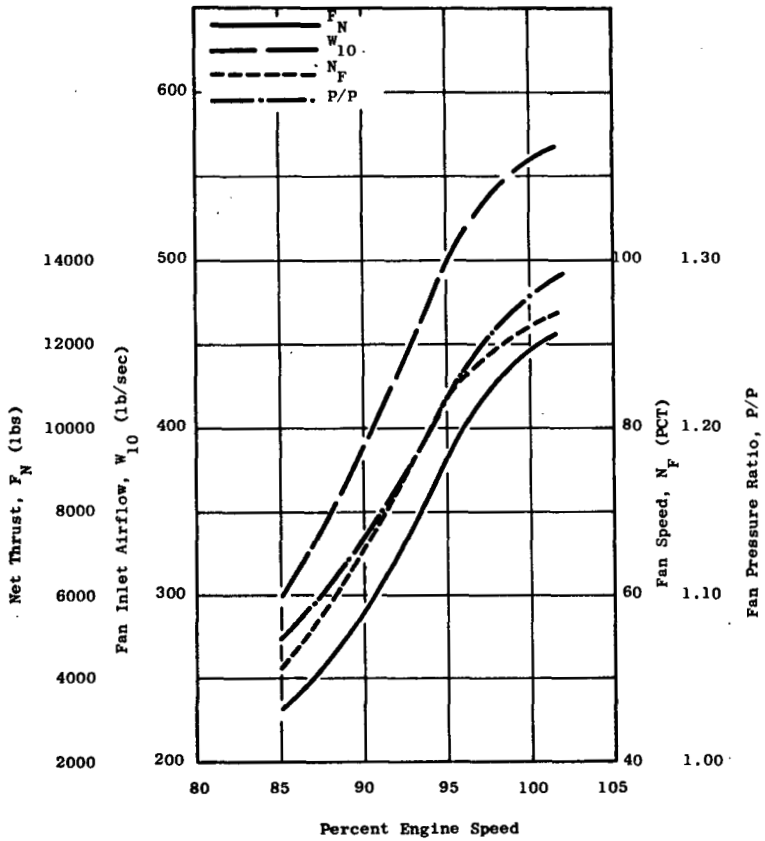

Figure 152 - Estimated LF460 Performance at Sea Level Static Standard Day Conditions

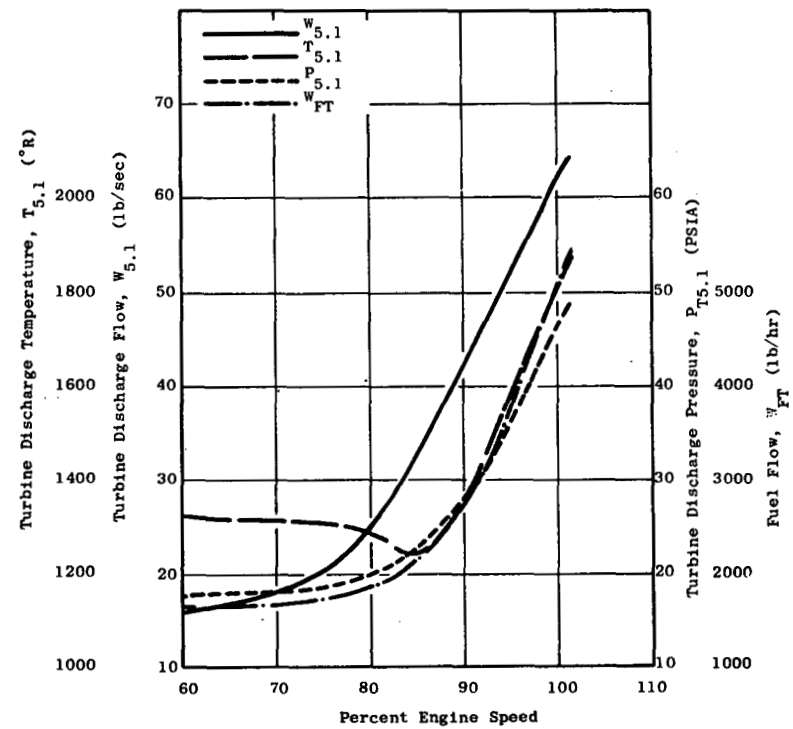

Figure 153 - Estimated YJ97 Discharge Conditions at Sea Level Statio 90°F Day Conditions

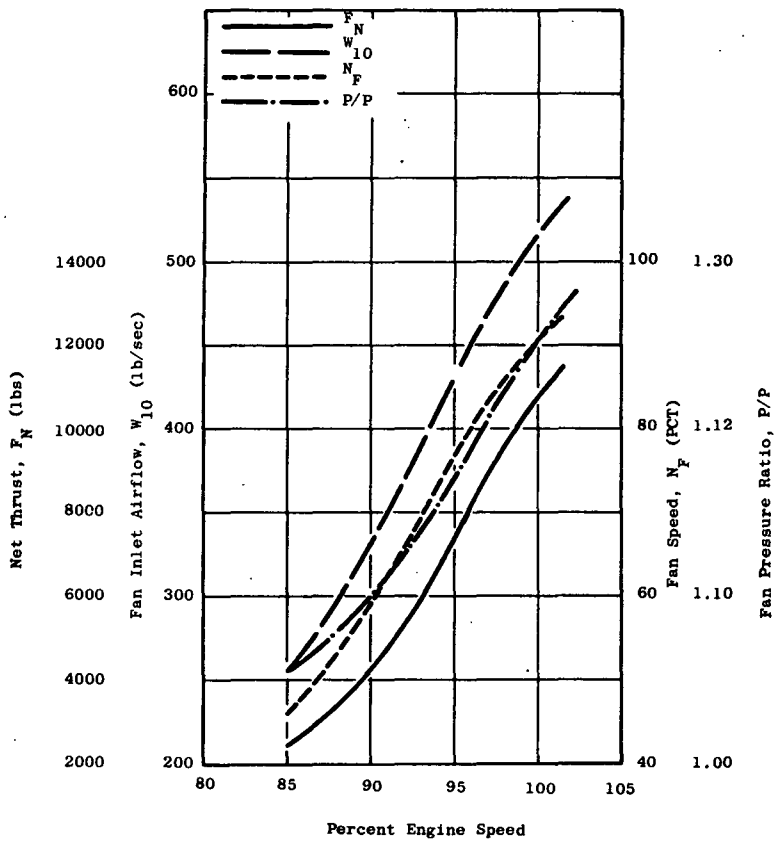

Figure 154 - Estimated LF460 Performance at Sea Level Static, 90°F Conditions

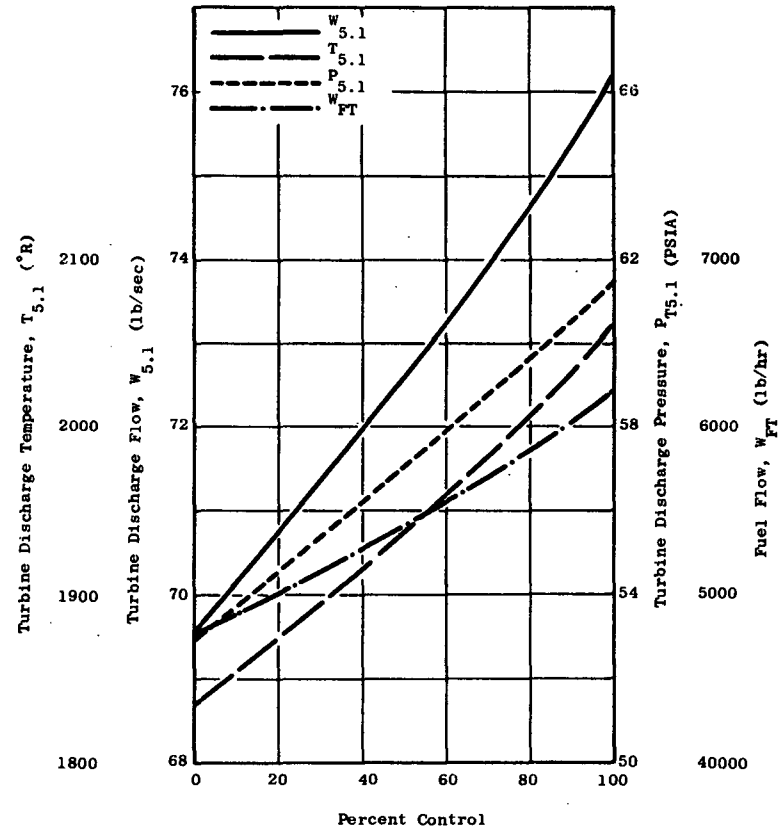

Figure 155 - Estimated YJ97 Discharge Parameters with Control at Sea Level Static Standard Day Condition, 101.5 Percent Speed

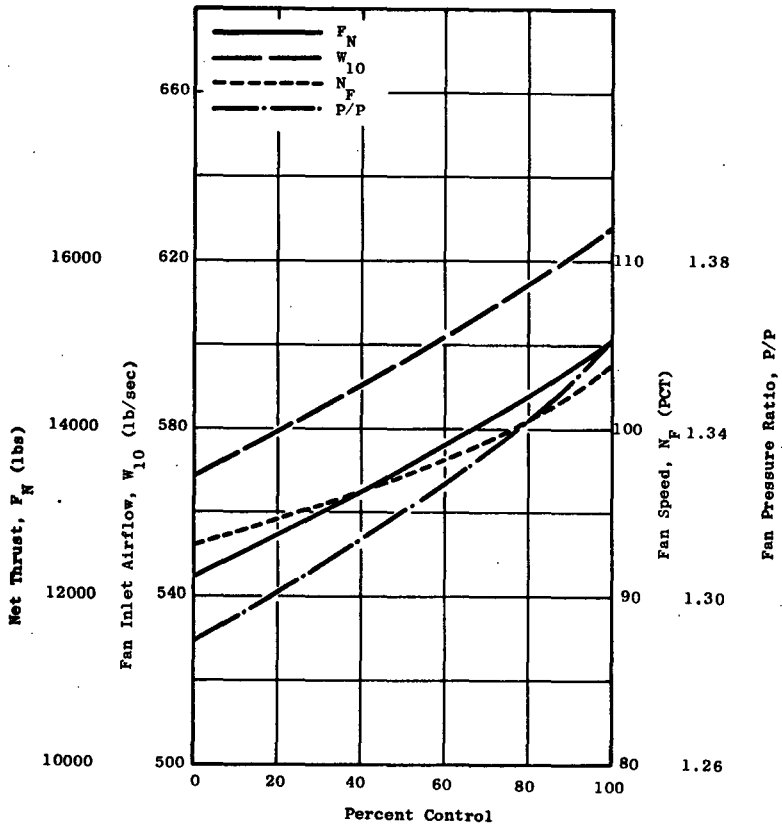

Figure 156 - Estimated LF460 Performance with Control at Sea Level Static Standard Day Condition, 101.5 Percent Engine Speed

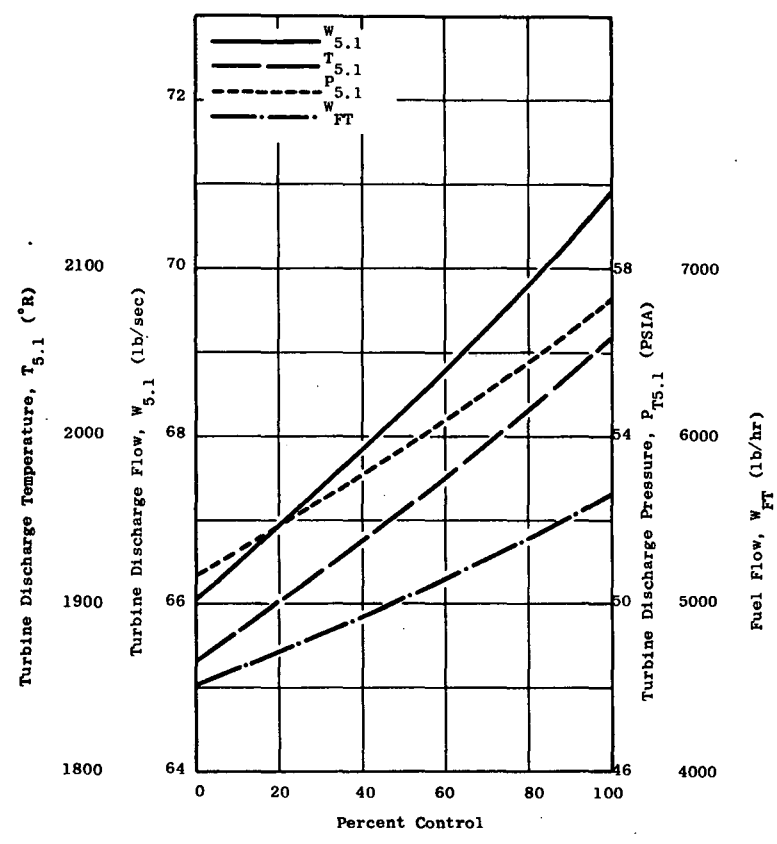

Figure 157 - Estimated YJ97 Discharge Parameters with Control at Sea Level Static, 90°F Conditions, 101.5 Percent Speed

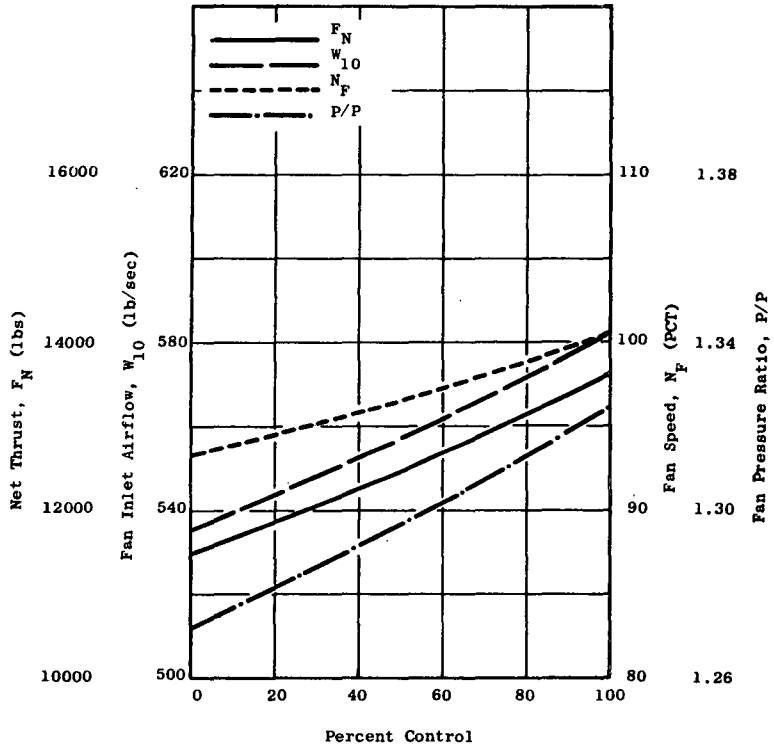

Figure 158 - Estimated LF460 Performance with Control at Sea Level Static, 90°F, 101.5 Percent Engine Speed

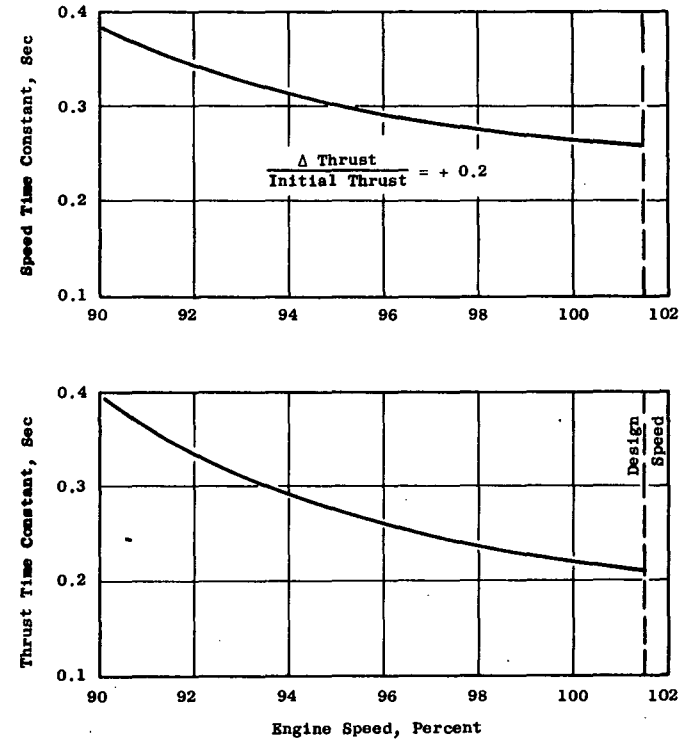

Figure 159 - LF460 Estimated Thrust and Speed Time Constants

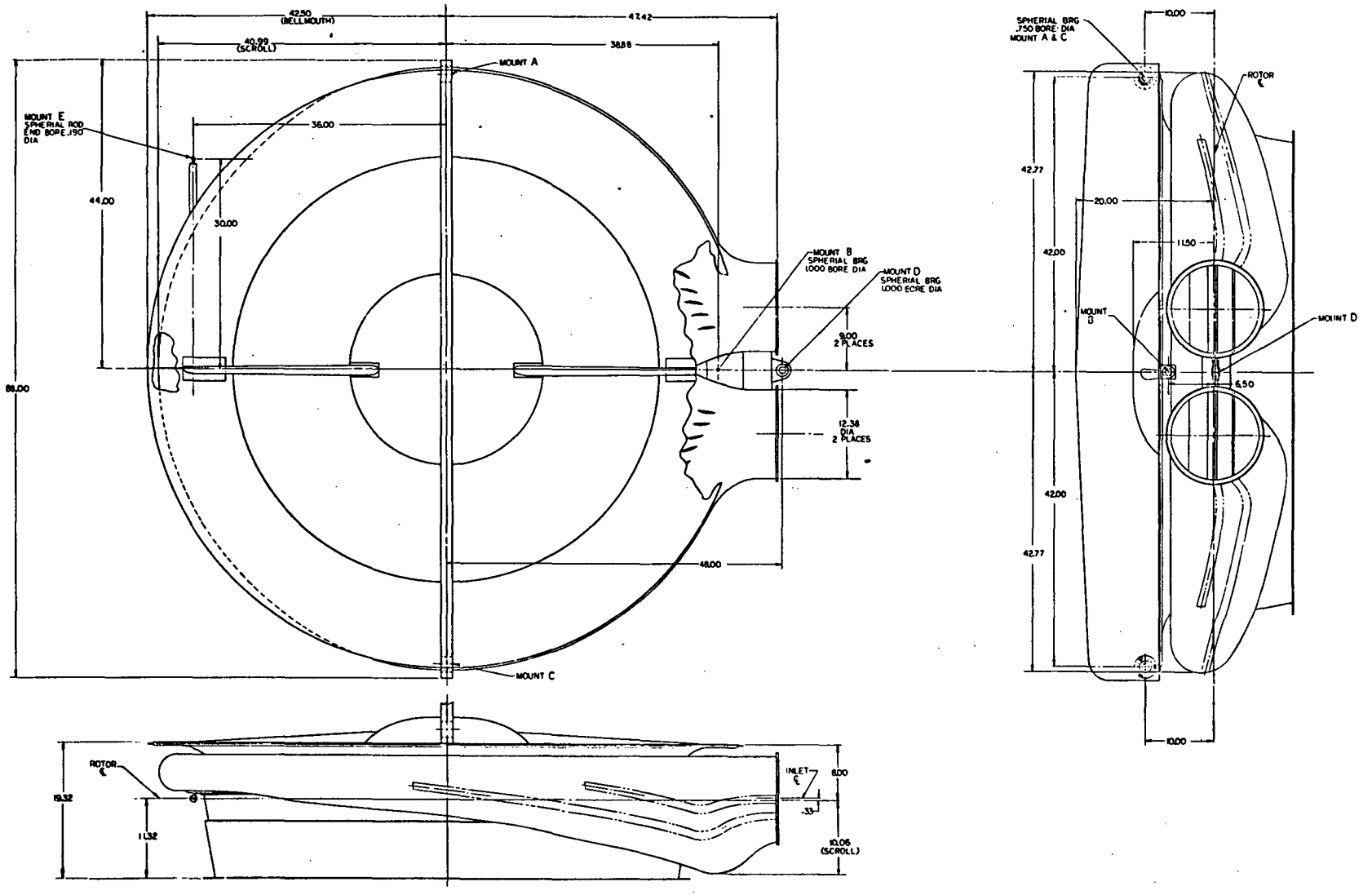

Figure 160 - LF460 Installation Drawing

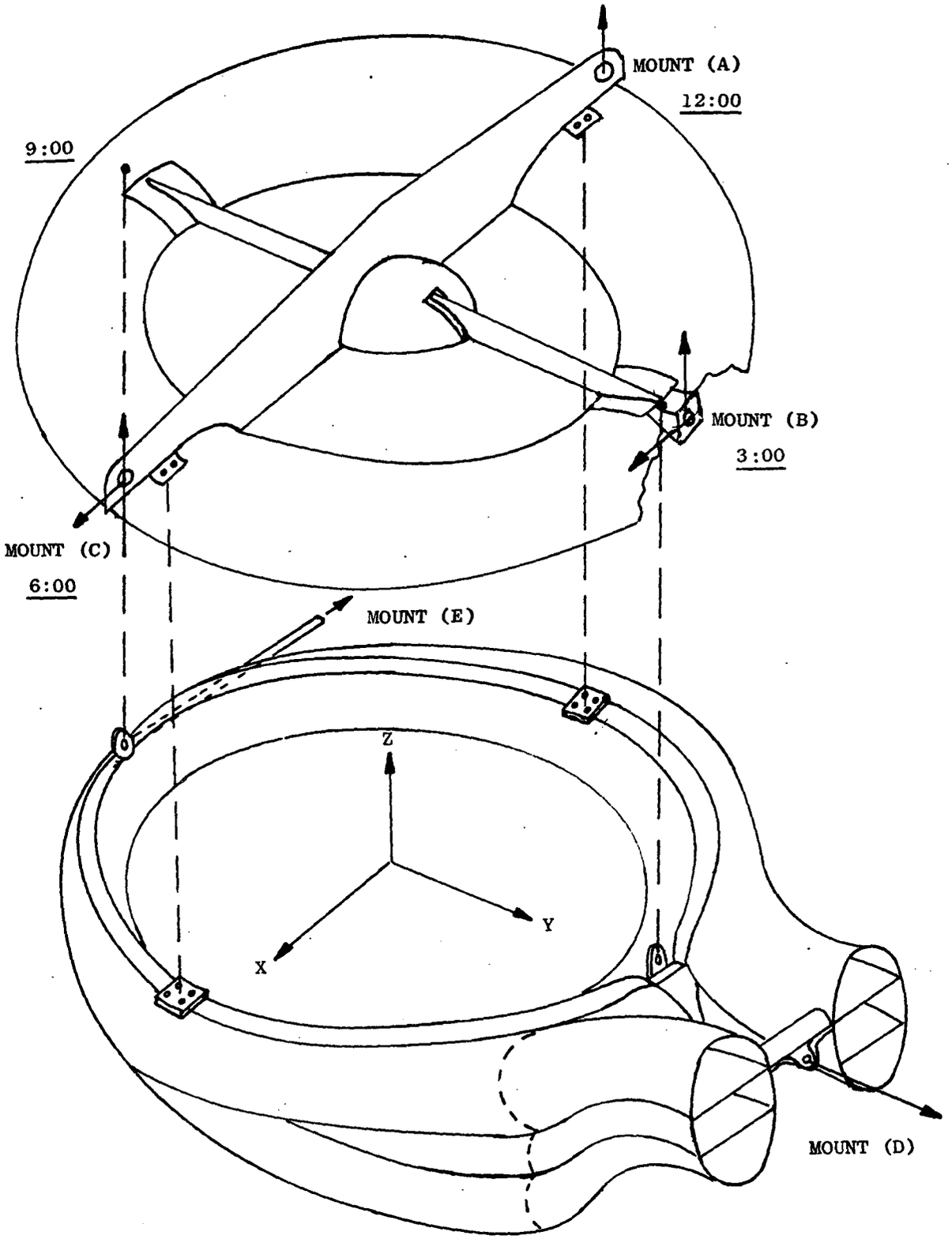

Figure 161 - Lift Unit Mounting Schematic